Smooth Muscle Cell Death, Inflammation, and Macrophage Phenotypes in the Progression of Abdominal Aortic Aneurysm

By

Stephanie E. Morgan

A dissertation submitted in partial fulfillment of

the requirements for the degree of

Doctor of Philosophy

(Cellular and Molecular Pathology)

At the

UNIVERSITY OF WISCONSIN-MADISON

2013

Date of final oral examination: 6/24/13

The dissertation is submitted for approval by the following members of the Final Oral Committee:

William J. Burlingham, Professor, Division of Transplantation

Anna Huttenlocher, Professor of Medical Microbiology and Immunology and Pediatrics

John Mansfield, Professor of Bacteriology

Wan-Ju Li, Assistant Professor, Department of Orthopedics and Rehabilitation

Matyas Sandor, Professor, Department of Pathology and Laboratory Medicine

Bo Liu, Professor, Division of Vascular Surgery

TABLE OF CONTENTS

FIGURE LIST

ACKNOWLEDGEMENTS

First and foremost, I would like to acknowledge my mentor, Dr. Bo Liu. Without Bo's patience, wisdom, and guidance, I would not have been able to produce the work that follows. Bo has been a phenomenal teacher and influence in my life and I could never provide adequate words to express my gratitude.

I would like to thank my committee members, William Burlingham, Anna Huttenlocher, Wan-Ju Li, John Mansfield, and Matyas Sandor for taking time out of your schedules to meet with me to discuss my progress over the years. Your guidance and suggestions have been highly valuable in shaping my graduate career.

Next I would like to acknowledge my colleagues and co-workers. When I first joined the lab, Dr. Dai Yamanouchi spent valuable time and energy to work with me to develop a valuable arsenal of lab techniques and to get me acquainted with the vascular biology field. His enthusiasm was contagious and I can only hope that my work does his teaching justice. Calvin Harberg and Qiwei Wang are current lab members who have been indispensable in the design and execution of several of the experiments that follow. Calvin joined our lab as a freshman and will graduate this year, and every person in our lab is sad to see him go.

Last but not least, I would be remiss not to mention my family. Their love and support is unending, and their willingness to listen to me drone on about whatever it is I'm doing at lab is admirable. They have been with me every step of the way and I couldn't have done it without them.

SMOOTH MUSCLE CELL DEATH, MACROPHAGE PHENOTYPES, and INFLAMMATION IN THE PROGRESSION OF ABDOMINAL AORTIC ANEURYSM

Stephanie E. Morgan

Under the supervision of Professor Bo Liu at the University of Wisconsin-Madison

Apoptosis or programed cell death plays an important role in development, homeostasis, and disease. In most cases, apoptosis removes excessive or damaged cells without eliciting immune responses. However, in certain disease conditions, apoptosis has been shown to stimulate inflammation. The goal of my thesis work is to determine whether and how apoptosis interacts with inflammation in a common and potentially lethal disease called abdominal aortic aneurysm (AAA).

AAA is an age-related vascular disease characterized by progressive aortic dilation. Histologic examination of AAA tissue shows the presence of significant apoptosis, inflammation, and elastin degradation; events which cumulatively result in the weakening of the arterial wall and expansion of arterial circumference. Currently, the only treatment options for aneurysm are surgical or endovascular procedures, and the limitation is due to an incomplete understanding of the biological mechanisms initiating and underlying the disease. The role of apoptosis in aneurysm pathogenesis and progression has not been directly studied. Since vascular smooth muscle cells (VSMCs) are the major source of extracellular matrix (ECM), it was conventionally assumed that apoptosis of VSMCs would contribute to tissue destruction by reducing ECM synthesis. While VSMCs are vital to vascular repair, data generated in our lab suggest another role of apoptosis, i.e. forming an amplification loop with inflammation.

In my thesis work, I explore two related hypotheses. First, chapters 1-4 focus on the idea that ***SMC apoptosis in aneurysmal tissue drives the infiltration of inflammatory cells and the subsequent development of aneurysm.*** In Chapters 1 and 2, we use a pan-caspase inhibitor to prevent apoptosis in three different aneurysm models. In Chapter 3, we show that a modified murine AAA model drives not only an advanced apoptotic and inflammatory response, but also a faster expanding and more severe aneurysm. In Chapter 4, we manipulated apoptosis through Protein Kinase C-delta (PKCδ), a signaling protein our own group has shown to be associated with SMC apoptosis. Once again, we demonstrated the link between SMC apoptosis and pro-inflammatory signaling.

In Chapter 5, I explored mechanism(s) underlying the apoptosis-inflammation interaction. Specifically, we hypothesized that ***the micro-environment within aneurysm tissues causes a shift in monocyte differentiation that results in a reduction in M2 macrophage polarization and diminished M2-mediated clearance of apoptotic cells.*** Furthermore, I tested whether manipulation of macrophage phenotype slows aneurysm progression. In conclusion, the work described here may shed some light on potential therapeutic targets for treatment of human AAA.

INTRODUCTION

Abdominal aortic aneurysm (AAA) is an age-related, chronic inflammatory vascular disease characterized by a loss of arterial wall integrity with extracellular matrix (ECM) remodeling, vascular smooth muscle cell (VSMC) apoptosis, and the infiltration of inflammatory cells. Recent large screening studies have shown AAA to have a prevalence of approximately 5% in men 65 years of age or older[1, 2], and the disease accounts for roughly 4 to 5% of sudden deaths in men over the age of 60[3]. Early aneurysm in patients has been identified as an aortic diameter between 3.0 and 5.5 cm. Once the aneurysm reaches a size of 4.5 or 5.5cm in women or men, respectively, surgical intervention methods are implemented[4, 5]. Patients with an established small aneurysm are provided only behavioral modification options such as smoking cessation or additional lifestyle changes that may lower cardiovascular risks, but current therapies have proven minimally effective in preventing the progressive growth and eventual rupture of small aneurysm[5].

Current studies in AAA are primarily aimed at establishing more effective therapeutic targets and methods for early aneurysm intervention. Due to the nature of human aneurysm disease, early-stage tissues are essentially unavailable for research purposes. Rather, tissues collected from patients tend to be almost exclusively in late-stages of the disease which limits the insight(s) made available by these studies. In order to study early pathological events, then, researchers turn to animal models of the disease. Several mouse models of AAA exist, including genetic manipulations such as those that alter ECM proteins[6], manipulate the matrix metalloproteinase (MMP) system[7, 8], or promote hyperlipidemia[9]. Additionally, several models

of AAA rely on chemical-induction methodologies. The Angiotensin II model (AngII) is created by infusing AngII at a dose of 500 to 1000 ng/kg/minue via a subcutaneous implanted mini-pump to either LDL receptor -/- or apoE -/- mice to produce a suprarenal aneurysm over a 28 day period[10]. In the calcium chloride (CaCl2) model, CaCl2 solution is applied using periaortic placement of a soaked gauze piece to the abdominal aorta between the renal artery and the iliac bifurcation. This model produces arterial wall thickening and diameter expansion with a substantial inflammatory response[11]. A model related to the CaCl2 model, the calcium phosphate (CaPO4) model, is induced in much the same way, but the application of CaCl2 solution is followed immediately by a similar application of a phosphor-buffered saline (PBS)-soaked gauze piece. This method creates CaPO4 crystal precipitate which induces significant aortic expansion, cell death, and inflammation[12]. Finally, the Elastase Infusion model requires the luminal infusion of elastase to the infrarenal segment of mouse aorta. This is achieved by first isolating the infrarenal aorta from the iliac bifurcation to the renal artery and using silk ligatures to stop blood flow through the region. A catheter can then be inserted above the iliac bifurcation to introduce elastase at a constant pressure for 5 minutes, after which the catheter is removed, the arteriotomy closed, and blood flow restored. This model creates immediate aortic expansion which grows minimally through day 7 and robust aneurysm by day 14. Pathologically this model creates significant elastin fragmentation and inflammatory infiltrate[13]. In my thesis work, I have utilized these four models of chemically-induced AAA.

Studies conducted using animal models of aneurysm have revealed several pathophysiological events that appear to be crucial for aneurysm formation and progression. One of the most prominent features of human and experimental aneurysms is substantial

inflammatory cell infiltration. Various work has suggested roles for specialized T lymphocytes[14, 15], mast cells[16, 17], and neutrophils[18]. However, macrophages have arisen as one of the most common, numerous, and significant players in aneurysm pathology. Macrophages are believed to be attracted to the aneurysmal wall partially through fragmented elastin products[19] as well as cytokines and chemokines such as monocyte chemoattractant 1 (MCP-1), RANTES (regulated on activation, normal T cell expressed and secreted), interleukin 6 (IL-6), interferon gamma (IFNγ), and tumor necrosis factor alpha (TNFα)[20-22]. Once recruited to the site of aneurysm, macrophages produce nitric oxide (NO), matrix metalloproteinases (MMPs), cathepsins, and additional cytokines and chemokines to further the inflammatory state. Using CD11b-diphtheria toxin receptor (DTR) transgenic mice, Xu B et al. demonstrated that depletion of macrophages prior to perfusion with elastase could ameliorate aortic expansion. Further, eliminating these cells 4 days after elastase treatment could promote aneurysm regression[23].

Vascular smooth muscle cells (SMCs) are a large component of the arterial wall. SMCs possess significant plasticity in their expression profiles, a feature which allows them to participate in a large number of functions[24]. Studies using human AAA tissue have shown a reduced medial content of medial SMCs, SMC apoptosis, and reduced propagation capability in SMCs cultured from human tissues[25-28]. Additionally, protease expression by SMCs has been shown to be crucial to human AAA as well as some experimental models[29, 30]. Though the true role of SMCs in AAA is undefined, conventional knowledge suggests that it is in fact the lack of SMCs in AAA tissue that most dramatically contributes to the disease. SMCs are a population of cells uniquely equipped to produce ECM components, and thus the depletion of this population

through cell death events has been thought to contribute to the continued deterioration of aortic tissue in AAA[25].

Cell death evens have for many years been described as either programed (apoptosis) or incidental (necrosis) – a dichotomous categorization that has proven far too simplistic. Apoptosis is a tightly regulated form of "programmed cell death" – a distinction indicating that the genetic information and many enzymes involved in the process(es) pre-exist within the cell[31] - mediated through activation of apoptotic caspases 3, 6, and 8[32]. Apoptotic cells are characterized by a shrinkage of cell membrane and condensation of nuclear chromatin, and are ultimately engulfed by neighboring cells in an anti-inflammatory manner[33]. Necrosis is a more general term used to describe the postmortem morphological characteristics or events of passive or 'accidental' cell death processes. Though necrosis can be the endpoint of various accidental death events, it is characterized by a loss of membrane integrity and release of intracellular contents, including 'damage associated molecular patterns (DAMPs)[34]. A large number of studies have led to an increasing awareness of the true complexity of cell death processes. While the full description of each of these processes is beyond the scope of my thesis, I have provided a very brief description as well as literature for reference.

Recent literature has expanded the category of 'programmed cell death' to include pyroptosis, oncosis, and autophagy. Pyroptosis is mediated by caspase-1, occurs independently of apoptotic caspases, and results in the rupture of cell membrane and the spillage of cellular contents[35]. Oncosis occurs in a process opposite of apoptosis in that cells and cellular organelles swell and bleb, and the membrane permeability increases as the ionic pumps in the

plasma membrane(s) fail[36]. Autophagy is a process by which a cell degrades its own components using autophagic vacuoles within the cell[37]. More recently, evidence has suggested a convergence of programmed cell death and necrosis in a process termed necroptosis. In necroptosis, cell death appears to occur in defined steps in a pathway dependent upon the receptor-interacting protein kinase 1 (RIP1)-RIPK3 complex[38]. It is important to point out that while each of these processes is talked about as discrete entities, it is more likely that various cell death processes occur simultaneously within tissue or even within a single cell. For example, a process known as secondary necrosis occurs when an apoptotic cell is not successfully cleared, and instead proceeds to a autolytic necrotic process which is highly inflammatory[39]. Although the above information is superficial, it suggests a highly complex and interesting subject of study. In the context of aneurysm, much work remains to be done regarding the type(s) of cell death present and the downstream consequences of these events.

For the purpose of my thesis, I will be focusing mainly on the role of SMC apoptosis as well as a somewhat limited view of necrosis, including secondary necrosis. I will describe the use of the pan-caspase inhibitor Q-VD-OPh, which has been shown to be an effective and non-toxic method for inhibiting apoptosis in vitro and in vivo[40-42]. Further, I will explore the potential role for protein kinase C-delta (PKCδ), a member of the PKC family of serine and threonine kinases. Evidence produced by our lab as well as others has shown PKCδ to have a wide range of actions in vascular disease. Specifically, PKCδ has been shown to be a crucial mediator for SMC apoptosis[43-45], and has also been shown to have a role in SMC migration[46, 47] and production of inflammatory cytokines specifically monocyte chemoattractant protein 1

(MCP1)[48, 49]. This information led us to believe that PKCδ would likely play a role in aneurysm formation through regulation of apoptosis and/or inflammation in the vascular wall.

Consequences of apoptotic events depend largely upon the clearance of dead cells or cell debris from tissues. In healthy tissues, apoptotic cells rarely trigger an inflammatory response due to the robust phagocytotic mechanism that swiftly removes the dying cells before their membrane disintegrates. Macrophages are well known as phagocytes, responsible for clearing microbes and/or dead cells and tissues. While this clearance mechanism is often sufficient and beneficial for the healing of tissue injuries or infections, its clearance capability could be overwhelmed or defected in certain disease states, which consequently leaves apoptotic cells to linger and undergo secondary necrosis thus creates a severe inflammatory state. In atherosclerosis, it has been shown that macrophages found in the plaque have diminished engulfment capability, which leads to a growing population of dead cells in the region[50]. The altered engulfment capability of plaque macrophages has been attributed to the cholesterol-laden state of these cells, and it has been shown that oxidized low-density lipoproteins (oxLDL) can effectively inhibit macrophage phagocytosis in vitro and in vivo[51, 52]. Macrophages have somewhat recently been shown to exist along a spectrum of phenotypes, each phenotype possessing unique characteristics that dictate their actions or role within a tissue[53]. In a simplified depiction of these phenotypes, I will describe two extreme phenotype categories designated as M1 inflammatory macrophages or M2 anti-inflammatory macrophages. M1 and M2 macrophages are the two macrophage types that have been most thoroughly explored and defined both in vitro and in vivo. In atherosclerosis, it has been shown that M1 and M2 macrophages localize differentially within the atherosclerotic plaque, with M1

cells residing mainly in the necrotic core and M2 cells localize to the fibrous cap[54]. Further, Cardilo-Reis L et al. showed that promoting an M2 dominant environment in atherosclerosis favorably modulated morphology of established atherosclerotic plaques in mice[55].

Although much evidence regarding macrophage phenotypes in vascular diseases has been gathered, there are still many questions that remain. Definition of these macrophage phenotypes was originally established using in vitro work, and transition of these data to in vivo models has proved to be far from simple[56]. In vivo, dynamic changes in the phenotype profile has been observed, with tissues displaying a coexistence of macrophages in different activation states and mixed phenotype populations[57]. Additionally, recent evidence has shown the existence of additional macrophage phenotypes outside of the simplistic M1 and M2 characterization. For example, M2 macrophages have can be subdivided to M2a (alternatively activated), M2b (regulatory), and M2c (immunosuppressive)[58-60]. In 2010, Kadl et al described the novel macrophage phenotype Mox which is driven following exposure to phospholipids[61]. Then, in 2012 a M4 macrophage was described as a unique macrophage phenotype driven by CXCL4 and possessing pro-atherogenic qualities[62]. However, no studies have been performed to evaluate the potential role(s) for this array of macrophage phenotypes in aneurysm.

In my thesis, I will bring together the above described topics to explore the two-related hypotheses. First, I will examine a unique and novel role for SMCs in aneurysm as an inflammatory signal. Specifically, I propose that ***SMC apoptosis in aneurysmal tissue drives the infiltration of inflammatory cells and the subsequent development of aneurysm.*** Secondly, I will evaluate the potential contribution of macrophage phenotypes by proposing that ***the***

micro-environment within aneurysm tissues causes a shift in monocyte differentiation that results in a reduction in M2 macrohpage polarization and diminished M2-mediated clearance of apoptotic cells.

1. Group. MASS. The multicentre aneurysm screening study (mass) into the effect of abdominal aortic aneurysm screening on mortality in men: A randomized controlled trial. . *Lancet*. 2002;360:1531-1539
2. Lederle FA, Johnson GR, Wilson SE, Acher CW, Ballard DJ, Littooy FN, Messina LM. Quality of life, impotence, and activity level in a randomized trial of immediate repair versus surveillance of small abdominal aortic aneurysm. *Journal of Vascular Surgery*. 2003;38:745-752
3. Cowan JA, Dimick JB, Henke PK, Rectenwald J, Stanley JC, Upchurch GR. Epidemiology of aortic aneurysm repair in the united states from 1993 to 2003. *Annals of the New York Academy of Sciences*. 2006;1085:1-10
4. Baxter BT, Terrin MC, Dalman RL. Medical management of small abdominal aortic aneurysms. *Circulation*. 2008;117:1883-1889
5. Brewster DC, Cronenwett JL, Hallett Jr JW, Johnston KW, Krupski WC, Matsumura JS. Guidelines for the treatment of abdominal aortic aneurysms: Report of a subcommittee of the joint council of the american association for vascular surgery and society for vascular surgery. *Journal of Vascular Surgery*. 2003;37:1106-1117
6. Reilly Jm SEBBCMTM. Hydrocortisone rapidly induces aortic rupture in a genetically susceptible mouse. *Archives of Surgery*. 1990;125:707-709
7. Silence J, Collen D, Lijnen HR. Reduced atherosclerotic plaque but enhanced aneurysm formation in mice with inactivation of the tissue inhibitor of metalloproteinase-1 (timp-1) gene. *Circulation Research*. 2002;90:897-903
8. Silence J, Lupu F, Collen D, Lijnen HR. Persistence of atherosclerotic plaque but reduced aneurysm formation in mice with stromelysin-1 (mmp-3) gene inactivation. *Arteriosclerosis, Thrombosis, and Vascular Biology*. 2001;21:1440-1445
9. Tangirala RK, Rubin EM, Palinski W. Quantitation of atherosclerosis in murine models: Correlation between lesions in the aortic origin and in the entire aorta, and differences in the extent of lesions between sexes in ldl receptor-deficient and apolipoprotein e-deficient mice. *Journal of Lipid Research*. 1995;36:2320-2328
10. Daugherty A, Rateri DL, Charo IF, Owens AP, Howatt DA, Cassis LA. Angiotensin ii infusion promotes ascending aortic aneurysms: Attenuation by ccr2 deficiency in apoe-/- mice. *Clinical Science*. 2010;118:681-689
11. Wang Y, Krishna S, Golledge J. The calcium chloride-induced rodent model of abdominal aortic aneurysm. *Atherosclerosis*. 2013;226:29-39
12. Yamanouchi D, Morgan S, Stair C, Seedial S, Lengfeld J, Kent KC, Liu B. Accelerated aneurysmal dilation associated with apoptosis and inflammation in a newly developed calcium phosphate rodent abdominal aortic aneurysm model. *Journal of Vascular Surgery*. 2012;56:455-461
13. Pyo R, Lee JK, Shipley JM, Curci JA, Mao D, Ziporin SJ, Ennis TL, Shapiro SD, Senior RM, Thompson RW. Targeted gene disruption of matrix metalloproteinase-9 (gelatinase b) suppresses development of experimental abdominal aortic aneurysms. *The Journal of Clinical Investigation*. 2000;105:1641-1649

14. Xiong W, Zhao Y, Prall A, Greiner TC, Baxter BT. Key roles of cd4+ t cells and ifn-{gamma} in the development of abdominal aortic aneurysms in a murine model. *J Immunol*. 2004;172:2607-2612
15. Romain M, Taleb S, Dalloz M, Ponnuswamy P, Esposito B, Pérez N, Wang Y, Yoshimura A, Tedgui A, Mallat Z. Overexpression of socs3 in t lymphocytes leads to impaired interleukin-17 production and severe aortic aneurysm formation in mice—brief report. *Arteriosclerosis, Thrombosis, and Vascular Biology*. 2013;33:581-584
16. Sun J, Sukhova GK, Yang M, Wolters PJ, MacFarlane LA, Libby P, Sun C, Zhang Y, Liu J, Ennis TL, Knispel R, Xiong W, Thompson RW, Baxter BT, Shi G-P. Mast cells modulate the pathogenesis of elastase-induced abdominal aortic aneurysms in mice. *The Journal of Clinical Investigation*. 2007;117:3359-3368
17. Sun J, Zhang J, Lindholt JS, Sukhova GK, Liu J, He A, Abrink M, Pejler G, Stevens RL, Thompson RW, Ennis TL, Gurish MF, Libby P, Shi G-P. Critical role of mast cell chymase in mouse abdominal aortic aneurysm formation. *Circulation*. 2009;120:973-982
18. Eliason JL, Hannawa KK, Ailawadi G, Sinha I, Ford JW, Deogracias MP, Roelofs KJ, Woodrum DT, Ennis TL, Henke PK, Stanley JC, Thompson RW, Upchurch GR, Jr. Neutrophil depletion inhibits experimental abdominal aortic aneurysm formation. *Circulation*. 2005;112:232-240
19. Maeda I, Mizoiri N, Briones MPP, Okamoto K. Induction of macrophage migration through lactose-insensitive receptor by elastin-derived nonapeptides and their analog. *Journal of Peptide Science*. 2007;13:263-268
20. Colonnello JS, Hance KA, Shames ML, Wyble CW, Ziporin SJ, Leidenfrost JE, Ennis TL, Upchurch Jr GR, Thompson RW. Transient exposure to elastase induces mouse aortic wall smooth muscle cell production of mcp-1 and rantes during development of experimental aortic aneurysm. *Journal of Vascular Surgery*. 2003;38:138-146
21. Middleton RK, Lloyd GM, Bown MJ, Cooper NJ, London NJ, Sayers RD. The pro-inflammatory and chemotactic cytokine microenvironment of the abdominal aortic aneurysm wall: A protein array study. *Journal of Vascular Surgery*. 2007;45:574-580
22. Middleton RK, Bown MJ, Lloyd GM, Jones JL, London NJ, Sayers RD. Characterisation of interleukin-8 and monocyte chemoattractant protein-1 expression within the abdominal aortic aneurysm and their association with mural inflammation. *European Journal of Vascular and Endovascular Surgery*. 2009;37:46-55
23. Xu B XH, Tanaka H, Glover K, Nagai T, Fujimura N, Iida Y, Wang W, Furusho Y, Miyata M, Michie SA, Matsuyama T, Dalman RL. Macrophage depletion limits experimental aneurysm progression. *ATVB Abstract*. 2013
24. Li S, Sims S, Jiao Y, Chow LH, Pickering JG. Evidence from a novel human cell clone that adult vascular smooth muscle cells can convert reversibly between noncontractile and contractile phenotypes. *Circulation Research*. 1999;85:338-348
25. Lopez-Candales A, Holmes D, Liao S, Scott M, Wickline S, Trompson R. Decreased vascular smooth muscle cell density in medial degeneration of human abdominal aortic aneurysms. *Am J Pathol*. 1997;150:993-1007
26. Henderson EL, Geng Y-J, Sukhova GK, Whittemore AD, Knox J, Libby P. Death of smooth muscle cells and expression of mediators of apoptosis by t lymphocytes in human abdominal aortic aneurysms. *Circulation*. 1999;99:96-104

27. Holmes DR, LÓPez-Candales A, Liao S, Thompson RW. Smooth muscle cell apoptosis and p53 expression in human abdominal aortic aneurysmsa. *Annals of the New York Academy of Sciences*. 1996;800:286-287
28. Jacob T, Hingorani A, Ascher E. Examination of the apoptotic pathway and proteolysis in the pathogenesis of popliteal artery aneurysms. *European Journal of Vascular and Endovascular Surgery*. 2001;22:77-85
29. Sinha I, Hannawa KK, Eliason JL, Ailawadi G, Deogracias MP, Bethi S, Ford JW, Roelofs KJ, Grigoryants V, Henke PK, Stanley JC, Upchurch Jr GR. Early mt-1 mmp expression following elastase exposure is associated with increased cleaved mmp-2 activity in experimental rodent aortic aneurysms. *Surgery*. 2004;136:176-182
30. Goodall S, Porter KE, Bell PR, Thompson MM. Enhanced invasive properties exhibited by smooth muscle cells are associated with elevated production of mmp-2 in patients with aortic aneurysms. *European Journal of Vascular and Endovascular Surgery*. 2002;24:72-80
31. Golstein P KG. Cell death by necrosis: Towards a molecular definition. *TRENDS in Biochemical Sciences*. 2007;32:37-43
32. Thornberry NA, Lazebnik Y. Caspases: Enemies within. *Science*. 1998;281:1312-1316
33. Kockx MM, Herman AG. Apoptosis in atherosclerosis: Beneficial or detrimental? *Cardiovascular Research*. 2000;45:736-746
34. Fink SL, Cookson BT. Apoptosis, pyroptosis, and necrosis: Mechanistic description of dead and dying eukaryotic cells. *Infection and Immunity*. 2005;73:1907-1916
35. Fink SL, Cookson BT. Caspase-1-dependent pore formation during pyroptosis leads to osmotic lysis of infected host macrophages. *Cellular Microbiology*. 2006;8:1812-1825
36. Weerasinghe P, Buja LM. Oncosis: An important non-apoptotic mode of cell death. *Experimental and Molecular Pathology*. 2012;93:302-308
37. Fimia G, Piacentini M. Regulation of autophagy in mammals and its interplay with apoptosis. *Cell. Mol. Life Sci.* 2010;67:1581-1588
38. Kaczmarek A, Vandenabeele P, Krysko Dmitri V. Necroptosis: The release of damage-associated molecular patterns and its physiological relevance. *Immunity*. 2013;38:209-223
39. Silva MT. Secondary necrosis: The natural outcome of the complete apoptotic program. *FEBS Letters*. 2010;584:4491-4499
40. Caserta TM SA, Gultice AD, Reedy MA, Brown TL. Q-vd-oph, a broad spectrum caspase inhibitor with potent antiapoptotic properties. *Apoptosis*. 2003;8:345-352
41. DeBiasi RL, Robinson BA, Sherry B, Bouchard R, Brown RD, Rizeq M, Long C, Tyler KL. Caspase inhibition protects against reovirus-induced myocardial injury in vitro and in vivo. *J. Virol.* 2004;78:11040-11050
42. Renolleau S, Fau S, Goyenvalle C, Joly L-M, Chauvier D, Jacotot E, Mariani J, Charriaut-Marlangue C. Specific caspase inhibitor q-vd-oph prevents neonatal stroke in p7 rat: A role for gender. *Journal of Neurochemistry*. 2007;100:1062-1071
43. Kato K, Yamanouchi D, Esbona K, Kamiya K, Zhang F, Kent KC, Liu B. Caspase-mediated protein kinase c-{delta} cleavage is necessary for apoptosis of vascular smooth muscle cells. *Am J Physiol Heart Circ Physiol*. 2009;297:H2253-2261

44. Ryer EJ, Sakakibara K, Wang C, Sarkar D, Fisher PB, Faries PL, Kent KC, Liu B. Protein kinase c delta induces apoptosis of vascular smooth muscle cells through induction of the tumor suppressor p53 by both p38-dependent and p38-independent mechanisms. *Journal of Biological Chemistry*. 2005;280:35310-35317
45. Schubl S, Tsai S, Ryer EJ, Wang C, Hu J, Kent KC, Liu B. Upregulation of protein kinase c[delta] in vascular smooth muscle cells promotes inflammation in abdominal aortic aneurysm. *Journal of Surgical Research*. 2009;153:181-187
46. Li C, Wernig F, Leitges M, Hu Y, Xu Q. Mechanical stress-activated pkcδ regulates smooth muscle cell migration. *FASEB J.* 2003:03-0150fje
47. Liu B, Ryer EJ, Kundi R, Kamiya K, Itoh H, Faries PL, Sakakibara K, Kent KC. Protein kinase c-[delta] regulates migration and proliferation of vascular smooth muscle cells through the extracellular signal-regulated kinase 1/2. *Journal of Vascular Surgery*. 2007;45:160-168
48. Liu B, Dhawan L, Blaxall B, Taubman M. Protein kinase cδ mediates mcp-1 mrna stabilization in vascular smooth muscle cells. *Molecular and Cellular Biochemistry*. 2010;344:73-79
49. Si Y, Ren J, Wang P, Rateri DL, Daugherty A, Shi XD, Kent KC, Liu B. Protein kinase c-delta mediates adventitial cell migration through regulation of monocyte chemoattractant protein-1 expression in a rat angioplasty model. *Arterioscler Thromb Vasc Biol*. 2012;32:943-954
50. Schrijvers DM, De Meyer GR, Kockx MM, Herman AG, Martinet W. Phagocytosis of apoptotic cells by macrophages is impaired in atherosclerosis. *Arterioscler Thromb Vasc Biol*. 2005;25:1256-1261
51. Clarke MC, Littlewood TD, Figg N, Maguire JJ, Davenport AP, Goddard M, Bennett MR. Chronic apoptosis of vascular smooth muscle cells accelerates atherosclerosis and promotes calcification and medial degeneration. *Circ Res*. 2008;102:1529-1538
52. Clarke MCH, Talib S, Figg NL, Bennett MR. Vascular smooth muscle cell apoptosis induces interleukin-1-directed inflammation. Effects of hyperlipidemia-mediated inhibition of phagocytosis. *Circ Res*. 2009:CIRCRESAHA.109.208389
53. Gordon S, Taylor PR. Monocyte and macrophage heterogeneity. *Nat Rev Immunol*. 2005;5:953-964
54. Ley K, Miller YI, Hedrick CC. Monocyte and macrophage dynamics during atherogenesis. *Arterioscler Thromb Vasc Biol*. 2011;31:1506-1516
55. Cardilo-Reis L, Gruber S, Schreier SM, Drechsler M, Papac-Milicevic N, Weber C, Wagner O, Stangl H, Soehnlein O, Binder CJ. Interleukin-13 protects from atherosclerosis and modulates plaque composition by skewing the macrophage phenotype. *EMBO Molecular Medicine*. 2012;4:1072-1086
56. Koh TJ, DiPietro LA. Inflammation and wound healing: The role of the macrophage. *Expert Reviews in Molecular Medicine*. 2011;13:null-null
57. Sica A, Mantovani A. Macrophage plasticity and polarization: In vivo veritas. *The Journal of Clinical Investigation*. 2012;122:787-795
58. Martinez FO SA, Mantovani A, Locati M. Macrophage activation and polarization. *Frontiers in Bioscience*. 2008;13:453-461

59. Liu G, Yang H. Modulation of macrophage activation and programming in immunity. *Journal of Cellular Physiology*. 2013;228:502-512
60. Gordon S. Alternative activation of macrophages. *Nat Rev Immunol*. 2003;3:23-35
61. Kadl A, Meher AK, Sharma PR, Lee MY, Doran AC, Johnstone SR, Elliott MR, Gruber F, Han J, Chen W, Kensler T, Ravichandran KS, Isakson BE, Wamhoff BR, Leitinger N. Identification of a novel macrophage phenotype that develops in response to atherogenic phospholipids via nrf2. *Circulation Research*. 2010;107:737-746
62. Gleissner CA. Macrophage phenotype modulation by cxcl4 in vascular disease. *Frontiers in Physiology*. 2012;3

Chapter 1: "Effects of caspase inhibitor on angiotensin II-induced abdominal aortic aneurysm in apolipoprotein E-deficient mice"

Published in Arteriosclerosis Thrombosis and Vascular Biology 2010; 30:702-707

Effects of Caspase Inhibitor on Angiotensin II-Induced Abdominal Aortic Aneurysm in Apolipoprotein E Deficient Mice

Dai Yamanouchi, Stephanie Morgan, Kaori Kato, Justin Lengfeld, Fan Zhang and Bo Liu

Division of Vascular Surgery, Department of Surgery, School of Medicine and Public Health, University of Wisconsin-Madison, Madison, WI, USA

Keywords: apoptosis; aneurysms; angiotensin II; MCP-1; migration

Abstract

Objective:

The presence of apoptotic markers is a prominent histological feature of abdominal aortic aneurysm. To understand the role of apoptosis in the pathogenesis of this common vascular disease, we tested the effect of pan caspase inhibitor, Quinoline-Val-Asp-Difluorophenoxymethylketone (Q-VD-OPh) on aneurysm formation using mouse angiotensin II (AngII) model.

Methods and results:

AngII in ApoE-deficient mice significantly induced medial cell apoptosis 3 days after infusion at the aortic region eventually becoming aneurismal. A daily administration of 20 mg/kg/day of Q-VD-OPh starting 6 hours prior to AngII-infusion reduced aneurysm incidence from 83.3% to 16.7% and maximal aortic diameter from 2.43 ± 0.29 mm to 1.58 ± 0.18 mm. The caspase inhibitor treated mice showed profoundly diminished levels of medial apoptosis and inflammation. In contrast, administration of Q-VD-OPh starting 7 days after AngII infusion had no significant impact on aneurysm development. In vitro, media conditioned by AngII-treated SMCs stimulated macrophage chemotaxis in a caspase dependent manner. Inhibition of monocyte chemoattractant protein-1 (MCP-1) in the conditioned media via a neutralizing antibody completely blocked the ability of conditioned media to attract macrophages.

Conclusions:

These results indicate that medial SMC apoptosis may contribute to vascular inflammation and thus aneurysm formation in part through production of MCP-1.

Introduction

Abdominal aortic aneurysm (AAA) is a common age-related degenerative disease associated with high mortality. Histologically, AAA is characterized by destruction of the extracellular matrix (ECM) accompanied by a depletion in medial vascular smooth muscle cells (SMCs), infiltration of lymphocytes and macrophages, and neovascularization.[1, 2] Selective depletion of neutrophils[3], lymphocytes[4], matrix metalloproteinases (MMPs)[5, 6], or pro-inflammatory cytokines[7] have all been found to impair aneurysm formation in experimental models of AAAs, demonstrating the multi-factoral nature of this disease.

Histological examinations of both animal and human experimental AAAs have revealed a paucity of medial SMCs in these specimens.[8-10] Additionally, many medial SMCs in human AAA specimens bear markers of apoptosis and demonstrate upregulation of pro-apoptotic initiators such as FAS/FASL.[9] As medial SMCs are major sources of ECM proteins, it was postulated that depletion of medial SMCs may also make an important contribution to aneurysm by eliminating a cell population capable of directing connective tissue repair.

Apoptosis, the ordered dismantling of cells, is a multi-step process that is centered by the activation of caspases, a group of structurally related cysteine proteases. Caspases can be divided into three groups based on their biological functions: apoptosis initiation, apoptosis execution, or cytokine activation. All caspases are synthesized and maintained as zymogens, which give rise to the active forms through limited proteolysis.[11] In mammalian cells, apoptosis can be initiated through two main pathways. The extrinsic pathway involves the activation of transmembrane death receptors such as Fas or TNF-α receptor by their respective ligands

leading to activation of caspase 8. The intrinsic pathway, secondary to DNA damage or oxidative stress, involves mitochondrial depolarization that leads to the release of cytochrome c and activation of caspase 9. Both pathways ultimately result in activation of caspase 3, which then leads to the execution of apoptosis including the cleavage of cell proteins, subsequent DNA fragmentation, and cell death.[12]

Multiple factors identified in human aneurismal tissues can potentially activate the extrinsic pathway (FasL and TNF-α)[9] or the intrinsic pathway (oxidative stress)[13]. In addition, activated caspase-9, the key initiator of the intrinsic pathway, was documented in experimental aneurysm[14], further supporting the presence of mitochondrial-dependent apoptosis during aneurysm development. The integral relationship between SMC apoptosis and aneurysm is further demonstrated by studies in which apoptosis was attenuated by experimental approaches such as the removal of mast cells[14], blockage of the angiotensin II (AngII) signaling,[15] and inhibition of Rho GTPase[16]. However, whether and how SMC apoptosis contributes to aneurysm formation has not been directly addressed.

In the present study, we inhibit apoptosis with a broad spectrum caspase inhibitor Quinoline-Val-Asp-Difluorophenoxymethylketone (Q-VD-OPh), in the AngII infusion model of aneurysm. Using a combination of in vitro and in vivo approaches, we examined the potential interplay between SMC apoptosis and aneurysm formation.

Materials and Methods.

General Materials

Dulbecco's Modified Eagles Medium (DMEM) and cell culture reagents were from Gibco BRL Life Technologies. Chemicals, if not specified, were purchased from Sigma Chemical Co.

Animal model

Male, 24-week-old, apoE-deficient mice with a C57BL/6 background were obtained from Jackson Laboratories (Bar Harbor, ME, USA). All mice had free access to a normal diet and water. Angiotensin II (1000 ng/kg/min) or saline was administered subcutaneously by Alzet osmotic minipump (model 2004; Alzet, CA) up to 4 weeks.[17] In the caspase inhibitor, Q-VD-OPh (BioVision, CA) study, mice were randomized to receive either the inhibitor or DMSO. Q-VD-OPh at 20 mg/kg/day or DMSO was administered daily via intraperitoneal injection to the AngII-treated mice 6 hours before the beginning of, or 7 days after, the AngII infusion. The external aortic diameter was measured at the region showing maximum dilatation with a digital caliper (VWR, PA). Aneurysm incidence is defined as an external width of the suprarenal aorta that was increased by 50% or greater compared with aorta from the infrarenal region. At selective time points, mice were killed by an overdose of pentobarbital and were perfusion-fixed with a mixture of 4% formaldehyde in PBS at physiological perfusion pressure. The observers were blinded to treatment allocation. All experiments were conducted in accordance with experimental protocols that were approved by the Institutional Animal Care and Use Committee at the University of Wisconsin Madison (Protocol M02284).

Histology and Immunohistochemistry

Morphological and Immunohistochemical analysis was performed as described previously.[18] In brief, paraffin embedded aortas were cut into 6 µm sections for morphological and immunohistochemical analysis. The aortas of Q-VD-OPh or DMSO administered mice were embedded and frozen in OCT compound, and cut into 6µm sections. Morphometric analysis was carried out on elastic-stained arteries by elastic-Van Gieson staining. Immunostaining for IL-6, CD3 antibody (17A2) (Santa Cruz Biotechnology, CA), alpha-smooth muscle actin (DAKO, CA), MCP-1 using rabbit polyclonal anti-MCP-1 antibody (Santa Cruz Biotechnology, CA) and macrophage using monoclonal anti-Mac3 antibody (Santa Cruz Biotechnology, CA) was performed as described previously.[19] TUNEL staining was performed according to manufacturer's protocol (Roche Applied Science, IN). Immunofluorescent staining was performed with donkey anti-rat Alexa 488 (Invitrogen, CA). 4',6-diamidino-2-phenylindole dihydrochloride (DAPI) was used as a nuclear counterstain. Slides were then visualized with a Nikon Eclipse E800 upright microscope with equipped with appropriate filters. Digital images were acquired using a RetigaEXi CCD digital camera and processed and analyzed using IPLab software.[20] TUNEL index was calculated as (number of TUNEL positive cells/number of total nuclei) per section by identifying TUNEL positive cells out of DAPI positive cells from at least 5 independent high power fields in each sample on NIH image software (ImageJ 1.36b).

In situ Zymography

For in situ zymography, freshly cut frozen aortic sections (8 µm) were incubated at 37°C with a fluorogenic elastin substrate (DQ elastin, Invitrogen, CA) according to the manufacturer's

protocol. Proteolytic activity represented by green fluorescence was measured after 48 h of incubation under a Nikon Eclipse E800 upright microscope. Fluorescent images were also acquired immediately after the addition of substrate (0 hour) and served as controls for tissue autofluorescence. Digital images were acquired using a RetigaEXi CCD digital camera.[21]

Cell Culture

Mouse aortic SMCs from the thoracic aorta of C57BL/6 mouse were isolated based on a protocol described by Clowes et al.[22] The isolated cells and RAW 264.7 cells (ATCC, VA) were maintained in DMEM containing 10% FBS at 37°C with 5% CO2 and antibiotics.

DNA Fragmentation ELISA (Apoptosis Assay)

DNA fragmentation ELISA was performed according to manufacturer's instruction using the Cell Death Detection ELISA system (Roche Applied Science, IN)

Monocyte chemoattractant Protein-1 (MCP-1) ELISA

ELISA for MCP-1-ELISA to detect MCP-1 secreted by SMC was performed using mouse MCP-1 ELISA kit (BD Biosciences, CA). Conditioned media of SMCs were collected by culturing SMCs at a density of 1×10^5/ml in 1 ml of complete medium in the presence or absence of AngII in 6-well plates. After incubation for specified periods of time at 37 °C, cell-free culture supernatants were obtained. The concentrations of MCP-1 were then measured according to the manufacturer's instructions.[23]

Chemotaxis Assay

Chemotaxis assay was performed as described previously.[23] 2×10^5 macrophages (RAW 264.7) were placed in the upper chamber of Costar 24-well transwell plates with 5-µm pore filters (Corning, Inc., Corning, NY). Cultured conditioned medium or control media was placed into the lower chambers or wells. Anti-MCP-1 antibody (Biolegend, CA) was used for neutralization of MCP-1. After incubating plates for 6 h at 37 °C, migrated cells were collected from the lower chambers and on the bottom of the filters were counted.[23]

RNA Isolation and Quantification

RNA was isolated from mouse aortic smooth muscle cells (SMCs) stimulated with 10 µM of angiotensin II (AngII) for 24 hours using an adaptation of the Trizol method (Invitrogen, CA) and the RNeasy mini column method (Qiagen) as previously described.[24, 25] RNA quality was assessed using Nano Drop 1000 (Thermo Scientific, DE).

Expression Analysis by Real-Time PCR

The expression of selected genes was assessed independently by quantitative real-time PCR. Total RNA was reverse-transcribed using High Capacity cDNA Reverse Transcription Kit (Applied Biosystems, CA) and real-time PCR amplification was performed using the SYBR® Green PCR Master Mix (Applied Biosystems, CA) on 7500 Real-time PCR System (Applied Biosystems, CA). Gene expression was normalized against GAPDH. Relative gene expression (RQ) was calculated using the ΔΔCt. Data was expressed as fold increase of RQ. n = 3, $*P<0.05$.

Statistical Analysis

Values were expressed as means ± standard error. Experiments were repeated at least three times unless stated otherwise. Differences between 2 groups were analyzed by Student's *t* test, and one- or two-way analysis of variance (ANOVA) followed by Scheffe's test was used for multiple comparisons. Values of $P<0.05$ were considered significant.

Results

Apoptosis in Angiotensin II induced aneurysm

To characterize apoptotic events during the development of aneurysm, we conducted a time course study using an AngII induced AAA model. Apolipoprotein E-deficient (ApoE KO) mice were implanted with osmotic pumps containing either AngII (1000 $ng.kg^{-1}.min^{-1}$) or saline, and were sacrificed at selected time points. In contrast to the saline control, infusion of AngII led to rapid changes in the suprarenal region of abdominal aorta that subsequently became aneurismal (Fig. 1A). At day 3, our earliest time point, most AngII-treated mice showed grossly visible vascular hematomas, presumably resulting from medial dissection.[26] Seven days after AngII infusion, the maximal external diameter of suprarenal aorta became significantly larger than saline-treated controls (saline: 1.1 ± 0.1 at 28days; AngII: 1.6 ± 0.44, 2.2 ± 0.28*, 2.5 ± 0.24* mm at 3, 7 and 28 days, respectively. *P<0.05). By 28 days, 80% of AngII-treated mice showed aneurysm formation, which was defined as a ≥50% increase in external aortic diameter compared to that of the infra-renal region (Fig. 1B). Immunohistological analysis showed a profound presence of TUNEL positivity in aortic media at day 3 in AngII infused mice (Fig. 1C). Although a significant amount of TUNEL signal persisted to day 7, most of the apoptotic cells were localized in adventitia at this point. The detection of TUNEL positivity was not restricted to the region of aortic dissection. To confirm that the TUNEL positivity detected in tunic medium resulted from apoptosis of vascular SMCs, we co-stained the tissue sections for smooth muscle specific α-actin. As shown in Supplemental Figure 1, TUNEL staining colocalized with α-actin positivity. Furthermore, immunostaining for a macrophage marker (Mac3) showed a

remarkable increase in the number of infiltrated macrophages in the aortic wall 3 and 7 days after pump implantation (Figure 1D).

In vivo inhibition of apoptosis

Since robust apoptosis occurs during the early phase of aneurysm development, we hypothesized that blockage of apoptosis may attenuate pathogenesis of this disease process. To test this hypothesis, we employed Q-VD-OPh, a broad spectrum inhibitor of caspases known to block apoptosis mediated by both extrinsic and intrinsic pathways.[27] Indeed, an in vitro apoptosis assay using cultured mouse aortic SMCs stimulated with hydrogen peroxide (H_2O_2), a well known apoptotic stimulus, confirmed the potency of this inhibitor in vascular SMCs (Supplemental Figure 2). Next, we administered Q-VD-OPh (20 mg/kg/day) or DMSO via daily intraperitoneal injection to ApoE KO mice starting 6 hours before AngII infusion. Mice were sacrificed 3, 7 or 28 days after. Compared to DMSO-injected mice, Q-VD-OPh-treated mice showed remarkably impaired aneurysm formation (Fig. 2A) reflected by a reduced AAA incidence (from 50% to 0% at day 7 and from 83.3% to 16.7% at day 28, respectively) (Figure 2B & Supplemental Figure 3). Consistently, the maximal diameter of the suprarenal aorta was also significantly decreased by Q-VD-OPh (Figure 2B and 2C). At day 7, vascular hematoma was only noticed in 1 out of the 6 Q-VD-OPh-treated mice while 4 out of 6 mice in the DMSO group showed substantial aortic hemorrhage (Supplemental Figure 3). In tissue cross sections, the AngII-induced expansion of both luminal area and external diameter of the aorta were completely eliminated by Q-VD-OPh at day 7 and greatly reduced at day 28 (Figure 2D).

To test whether the pan caspase inhibitor affects aneurysm growth, we began the Q-VD-OPh treatment 7 days after AngII infusion, a time point at which TUNEL positivity had begun to subside. In contrast to what we observed with the early drug application, the delayed administration of Q-VD-OPh had no significant impact on aneurismal expansion measured at day 28 (Figure 2E).

Caspase inhibitor diminishes both aortic apoptosis and macrophage filtration

Further immunohistological analyses of the aortic tissues harvested after 3, 7 or 28 days of AngII infusion confirmed that Q-VD-OPh significantly inhibited apoptosis (Figure 3A). At day 3, the percentage of TUNEL positive cells detected in the aortic wall was reduced from 14.8 ± 5.4% in the DMSO control group to 0.8 ± 0.1% in the inhibitor group ($P < 0.01$; n = 6). Furthermore, Q-VD-OPh profoundly reduced the level of macrophage infiltration, evident by the nearly undetectable positivity of Mac3 in mice treated with this inhibitor (Figure 3A). Immunostaining with an anti-CD3 antibody suggests that infiltration of T cells was also decreased by the Q-VD-OPh treatment (Supplemental Figure 4). In agreement with the diminished inflammation, arteries derived from the Q-VD-OPh treated mice showed profound reduction in immunostaining to IL-6 as compared to arteries from the DMSO-treated mice (Supplemental Figure 5).

We also examined the effect of the caspase inhibitor on neutrophil infiltration. At the time points of our study (days 3, 7 and 28 post AngII infiltration), we did not detect the

significant presence of neutrophils (data not shown). It is likely that the influx of neutrophils occurs at earlier time points.

Since infiltrated macrophages are thought to be the major source of elastase activity in aneurismal tissues, we next performed an in situ zymography assay using aortic samples harvested from mice treated with AngII for 7 days. Freshly frozen aortic sections were incubated with DQ-Elastin. Elastase activity, reflected by the fluorescence signal generated during substrate degradation, was recorded before (0 h) or after incubation (48 h, 37^{o}C). Arteries derived from DMSO-injected, AngII infused mice showed a noticeable induction of elastase activity (Figure 3B). In contrast, elastase activity was barely detectable in Q-VD-OPh-injected, AngII-infused mice (Figure 3B).

The effect of pan caspase inhibitor on macrophage migration

The diminished macrophage infiltration resulting from the Q-VD-OPh treatment suggests that aortic SMC apoptosis may actively contribute to vascular inflammation by attracting macrophage or monocytes to the site where active apoptosis takes place. To test this hypothesis, we turned to cultured mouse aortic SMCs. We found that AngII dose-dependently induced SMC apoptosis (Figure 4A), an effect that was completely eliminated by Q-VD-OPh (Figure 4B). Next, we tested the effect of AngII on migration of RAW264.7 cells, a monocyte/ macrophage cell line. As shown in Fig. 4C, AngII alone had little chemotactic effect on RAW264.7 cell migration. In contrast, media conditioned by AngII-treated SMCs prompted a significant number of RAW264.7 to migrate through a porous membrane (Figure 4C). Inhibition

of caspase activity in SMCs by Q-VD-OPh blocked this chemotactic effect of the conditioned media, suggesting an involvement of apoptosis (Figure 4D).

To identify the potential chemoattractant factors released by apoptotic SMCs, we examined the expression of pro-inflammatory mediators in AngII-treated SMCs by real-time PCR. Among the five inflammatory cytokines we examined, only the expression of MCP-1 was significantly induced by AngII in a caspase-dependent manner (Supplemental Figure 6). Subsequently, we confirmed an enhanced level of MCP-1 protein in media conditioned by AngII-treated SMCs (Figure 4E). Similar to the mRNA induction, the accumulation of MCP-1 protein from the conditioned media was significantly reduced by Q-VD-OPh (Figure 4E). To further show that MCP-1 released by AngII-treated SMCs is responsible for attracting monocyte/macrophages, we incubated the conditioned media with a neutralizing antibody to MCP-1 prior to the chemotaxis assay. The migration of macrophages was significantly blocked by neutralization of MCP-1 (Figure 4F).

Based on the above in vitro study, we speculate that apoptotic SMCs in the aortic wall recruit inflammatory cells by producing MCP-1. To test this hypothesis, we performed additional immunohistological analyses of the aortic tissues harvested after 3 days of AngII infusion. As previously reported by Ishibashi et al., AngII infusion led to a significant elevation of MCP-1 expression in the aortic wall (Figure 4G).[28] Such induction was profoundly impaired in mice treated with Q-VD-OPh (Figure 4G).

Discussion

The presence of apoptotic markers is a major pathological feature associated with abdominal aortic aneurysm.[1, 8] Many experimental manipulations that have been shown to impair aneurysm formation have also caused a significant reduction in the number of apoptotic cells detected in the aortic wall.[3, 14-16] However, it has not been possible to determine whether apoptotic cell death is merely a result of vascular inflammation or/and matrix destruction or if apoptosis is a contributing cellular event necessary for the development of aneurysm. In order to determine whether there is a causal relationship between apoptotic death and the pathogenesis of aneurysm, we employed a new caspase inhibitor Q-VD-OPh, which inhibits apoptosis by blocking activation of caspases. In the AngII-induced aneurysm model, administration of Q-VD-OPh at the time of aneurysm induction profoundly reduced both the incidence and severity of aneurysm in ApoE deficient mice. To the best of our knowledge, this is the first report that directly links apoptosis to the pathogenesis of abdominal aortic aneurysm.

Histological analyses of aortic tissues removed from Q-VD-OPh-treated mice showed a remarkable reduction in the number of infiltrated macrophages and CD3+ T cells. Associated with diminished inflammation, the aortic wall of Q-VD-OPh-treated mice displayed significantly decreased accumulation IL-6 as well as elastase activity. These findings suggest that inhibition of apoptosis may attenuate aneurysm formation not only by preventing SMC depletion but also by affecting vascular inflammation and matrix degradation. The potential interplay between the apoptotic event and vascular inflammation is also supported by our time course study. We showed that apoptotic SMCs were prominent throughout the tunic media 3 days after AngII

infusion, a time point at which infiltrated macrophages were most prominent in the media. We think that this early phase of apoptosis is critical to aneurysm formation, at least in the AngII model, since application of the pan caspase inhibitor after this window of apoptotic event had little effect on AngII-induced aortic expansion.

Unlike necrosis, apoptosis is classically considered to be self-contained and non-inflammatory. However, this conventional view has recently been challenged. Using a rat carotid angioplasty model, Schaub et al. showed that activation of apoptosis in SMCs resulted in a massive inflammatory response consisting almost entirely of macrophages.[29] Using a genetic approach, Clarke and colleagues showed that acute induction of vascular SMC apoptosis in atherosclerotic plaques leads to intense intimal inflammation associated with thinning of fibrous caps and a loss of matrix proteins.[30] More recently, this same investigative group showed that chronic low-level SMC apoptosis during either atherogenesis or within established plaques of Apo-E deficient mice accelerates plaque growth by two-fold and is associated with enhanced macrophage infiltration.[31] By demonstrating that the inhibition of apoptosis prevented the extensive vascular inflammation normally associated with aneurysm development, our current data further supports the pro-inflammatory potential of apoptosis. The inhibitory effect of Q-VD-OPh on inflammation was substantial. The immunostaining of Mac3, CD3 or IL-6 was nearly undetectable in Q-VD-OPh mice, a great contrast to the extensive inflammation observed in DMSO-treated controls.

The accumulation of macrophages in aortic media during the period of SMC apoptosis (~3 day after AngII infusion) could be caused by active recruitment via release of monocyte

chemoattractants, including MCP-1. Data generated from our in vitro chemotaxis studies and from the immunohistochemical analysis support this notion. Media conditioned by AngII-treated SMCs attracted monocytes/macrophages in a caspase-dependent manner. This chemoattractant property of apoptotic SMCs is mediated by MCP-1, as the release of MCP-1 is also sensitive to caspase inhibition. Neutralizing MCP-1 activity with an anti-MCP-1 antibody in the conditioned media diminished the chemotactic ability of apoptotic SMCs. Finally, in vivo administration of Q-VD-OPh profoundly decreased the level of MCP-1 in AngII infused ApoE deficient mice. MCP-1 mediated infiltration of monocytes and other inflammatory cells has been previously shown to underlie AngII induced vascular inflammation.[28] Of note, MCP-1 was also identified by Schaub et al as an important chemoattractant released by Fas-induced apoptosis of SMC.[29] We have recently reported that protein kinase C-delta (PKCδ) mediates the expression of MCP-1 in vascular SMCs in response to another proinflammatory or apoptotic factor TNFα.[32] PKCδ, a well established mediator for apoptosis,[33, 34] is also found to be upregulated in human aneurysm tissues.[32] Whether PKCδ is the molecular link between SMC apoptosis and the production of monocyte chemoattractants remains to be tested.

In addition to a reduction in the number of apoptotic SMCs and infiltrated macrophages, Q-VD-OPh resulted in dramatically diminished elastase activity thought to be responsible for arterial matrix destruction and loss of tissue integrity. Our observed link between SMC apoptosis and elastin degradation is supported by Clarke's finding in atherosclerotic plaque. Also using Apo E deficient mice, Clarke and colleagues showed that chronic induction of SMC apoptosis leads to medial expansion accompanied by increased elastic lamina breaks.[31] Since macrophages are the major source of proteases, we attribute the reduced elastase activity to

the diminished macrophage invasion. However, our studies do not exclude the possibility that caspase inhibition may directly influence the synthesis, secretion, or activation of proteases.

A potential limitation of our study is the use of AngII to induce aneurysm development. This is a unique model characterized by the initial formation of dissection followed by dilatation of the suprarenal aorta. The exact cause of medial dissection in this model is not well elucidated. Our observation of reduced vascular hematoma in Q-VD-OPh treated mice suggests that cell apoptosis may contribute to medial dissection. Although Q-VD-OPh is highly specific to caspases and no toxic effect associated with this inhibitor has been reported in vivo[35-37], our data do not exclude the possible that Q-VD-OPh might affect other classes of proteases involved in arterial wall remodeling. We do not know whether Q-VD-OPh affected the lipid profile of Apo E mice that were maintained on normal diet in our experiments. It is also possible that AngII-induced aneurysm is more dependent upon apoptosis and thus more sensitive to the caspase inhibitor as compared to other animal models of AAA, though this is unlikely since upregulated apoptosis has been detected in all experimental models of aneurysms.[14, 16, 38]

In summary, our results demonstrate that the incidence and severity of Angiotensin II induced aneurysm in ApoE deficient mice was remarkably reduced by the blockage of apoptosis with a pan caspase inhibitor, Q-VD-OPh. The recruitment of macrophage measured by immunohistochemistry, chemotaxis assay, and in situ zymography was also blocked by this inhibitor at least in part through the reduction of MCP-1 production. These results suggest that apoptosis may be an early cellular event during aneurysm development that contributes to tissue destruction by stimulating macrophage infiltration and depletion of residential SMCs.

Acknowledgements

The authors like to thank Dr. K. Craig Kent of University of Wisconsin for intellectual inputs, Dr. Brad Herman of Weill Cornell Medical College for constructive discussion, and Karla Esbona for technical assistance.

Source of Funding

This work was supported by a Start-up Fund of Department of Surgery, University of Wisconsin, School of Medicine and Public Health.

Disclosures

None.

References

1. Ailawadi G, Eliason JL, Upchurch GR, Jr. Current concepts in the pathogenesis of abdominal aortic aneurysm. *J Vasc Surg*. 2003;38:584-588
2. Wassef M, Upchurch GR, Jr., Kuivaniemi H, Thompson RW, Tilson MD, 3rd. Challenges and opportunities in abdominal aortic aneurysm research. *J Vasc Surg*. 2007;45:192-198
3. Eliason JL, Hannawa KK, Ailawadi G, Sinha I, Ford JW, Deogracias MP, Roelofs KJ, Woodrum DT, Ennis TL, Henke PK, Stanley JC, Thompson RW, Upchurch GR, Jr. Neutrophil depletion inhibits experimental abdominal aortic aneurysm formation. *Circulation*. 2005;112:232-240
4. Xiong W, Zhao Y, Prall A, Greiner TC, Baxter BT. Key roles of cd4+ t cells and ifn-gamma in the development of abdominal aortic aneurysms in a murine model. *J Immunol*. 2004;172:2607-2612
5. Pyo R, Lee JK, Shipley JM, Curci JA, Mao D, Ziporin SJ, Ennis TL, Shapiro SD, Senior RM, Thompson RW. Targeted gene disruption of matrix metalloproteinase-9 (gelatinase b) suppresses development of experimental abdominal aortic aneurysms. *The Journal of clinical investigation*. 2000;105:1641-1649
6. Longo GM, Xiong W, Greiner TC, Zhao Y, Fiotti N, Baxter BT. Matrix metalloproteinases 2 and 9 work in concert to produce aortic aneurysms. *The Journal of clinical investigation*. 2002;110:625-632
7. Shimizu K, Shichiri M, Libby P, Lee RT, Mitchell RN. Th2-predominant inflammation and blockade of ifn-gamma signaling induce aneurysms in allografted aortas. *The Journal of clinical investigation*. 2004;114:300-308
8. Lopez-Candales A, Holmes DR, Liao S, Scott MJ, Wickline SA, Thompson RW. Decreased vascular smooth muscle cell density in medial degeneration of human abdominal aortic aneurysms. *Am J Pathol*. 1997;150:993-1007
9. Henderson EL, Geng YJ, Sukhova GK, Whittemore AD, Knox J, Libby P. Death of smooth muscle cells and expression of mediators of apoptosis by t lymphocytes in human abdominal aortic aneurysms. *Circulation*. 1999;99:96-104
10. Walton LJ, Franklin IJ, Bayston T, Brown LC, Greenhalgh RM, Taylor GW, Powell JT. Inhibition of prostaglandin e2 synthesis in abdominal aortic aneurysms: Implications for smooth muscle cell viability, inflammatory processes, and the expansion of abdominal aortic aneurysms. *Circulation*. 1999;100:48-54
11. Stennicke HR, Salvesen GS. Caspases - controlling intracellular signals by protease zymogen activation. *Biochim Biophys Acta*. 2000;1477:299-306
12. Stennicke HR, Salvesen GS. Properties of the caspases. *Biochim Biophys Acta*. 1998;1387:17-31
13. Miller FJ, Jr. Aortic aneurysms: It's all about the stress. *Arteriosclerosis, thrombosis, and vascular biology*. 2002;22:1948-1949
14. Sun J, Sukhova GK, Yang M, Wolters PJ, MacFarlane LA, Libby P, Sun C, Zhang Y, Liu J, Ennis TL, Knispel R, Xiong W, Thompson RW, Baxter BT, Shi GP. Mast cells modulate the

pathogenesis of elastase-induced abdominal aortic aneurysms in mice. *The Journal of clinical investigation*. 2007;117:3359-3368

15. Kaschina E, Schrader F, Sommerfeld M, Kemnitz UR, Grzesiak A, Krikov M, Unger T. Telmisartan prevents aneurysm progression in the rat by inhibiting proteolysis, apoptosis and inflammation. *J Hypertens*. 2008;26:2361-2373
16. Wang YX, Martin-McNulty B, da Cunha V, Vincelette J, Lu X, Feng Q, Halks-Miller M, Mahmoudi M, Schroeder M, Subramanyam B, Tseng JL, Deng GD, Schirm S, Johns A, Kauser K, Dole WP, Light DR. Fasudil, a rho-kinase inhibitor, attenuates angiotensin ii-induced abdominal aortic aneurysm in apolipoprotein e-deficient mice by inhibiting apoptosis and proteolysis. *Circulation*. 2005;111:2219-2226
17. Daugherty A, Manning MW, Cassis LA. Angiotensin ii promotes atherosclerotic lesions and aneurysms in apolipoprotein e-deficient mice. *The Journal of clinical investigation*. 2000;105:1605-1612
18. Tsai S, Hollenbeck ST, Ryer EJ, Edlin RS, Yamanouchi D, Wang C, Liu B, Kent KC. Tgf-{beta} through smad3 signaling stimulates vascular smooth muscle cell proliferation and neointimal formation. *Am J Physiol Heart Circ Physiol*. 2009
19. Silence J, Lupu F, Collen D, Lijnen HR. Persistence of atherosclerotic plaque but reduced aneurysm formation in mice with stromelysin-1 (mmp-3) gene inactivation. *Arteriosclerosis, thrombosis, and vascular biology*. 2001;21:1440-1445
20. Edlin RS, Tsai S, Yamanouchi D, Wang C, Liu B, Kent KC. Characterization of primary and restenotic atherosclerotic plaque from the superficial femoral artery: Potential role of smad3 in regulation of smc proliferation. *J Vasc Surg*. 2009;49:1289-1295
21. Satoh K, Nigro P, Matoba T, O'Dell MR, Cui Z, Shi X, Mohan A, Yan C, Abe J, Illig KA, Berk BC. Cyclophilin a enhances vascular oxidative stress and the development of angiotensin ii-induced aortic aneurysms. *Nat Med*. 2009;15:649-656
22. Clowes AW, Reidy MA, Clowes MM. Mechanisms of stenosis after arterial injury. *Lab Invest*. 1983;49:208-215
23. Zhang F, Tsai S, Kato K, Yamanouchi D, Wang C, Rafii S, Liu B, Kent KC. Transforming growth factor-{beta} promotes recruitment of bone marrow cells and bone marrow-derived mesenchymal stem cells through stimulation of mcp-1 production in vascular smooth muscle cells. *J Biol Chem*. 2009;284:17564-17574
24. Papaspyridonos M, Smith A, Burnand KG, Taylor P, Padayachee S, Suckling KE, James CH, Greaves DR, Patel L. Novel candidate genes in unstable areas of human atherosclerotic plaques. *Arteriosclerosis, thrombosis, and vascular biology*. 2006;26:1837-1844
25. Papaspyridonos M, McNeill E, de Bono JP, Smith A, Burnand KG, Channon KM, Greaves DR. Galectin-3 is an amplifier of inflammation in atherosclerotic plaque progression through macrophage activation and monocyte chemoattraction. *Arteriosclerosis, thrombosis, and vascular biology*. 2008;28:433-440
26. Saraff K, Babamusta F, Cassis LA, Daugherty A. Aortic dissection precedes formation of aneurysms and atherosclerosis in angiotensin ii-infused, apolipoprotein e-deficient mice. *Arteriosclerosis, thrombosis, and vascular biology*. 2003;23:1621-1626
27. Caserta TM, Smith AN, Gultice AD, Reedy MA, Brown TL. Q-vd-oph, a broad spectrum caspase inhibitor with potent antiapoptotic properties. *Apoptosis*. 2003;8:345-352

28. Ishibashi M, Egashira K, Zhao Q, Hiasa K, Ohtani K, Ihara Y, Charo IF, Kura S, Tsuzuki T, Takeshita A, Sunagawa K. Bone marrow-derived monocyte chemoattractant protein-1 receptor ccr2 is critical in angiotensin ii-induced acceleration of atherosclerosis and aneurysm formation in hypercholesterolemic mice. *Arterioscler Thromb Vasc Biol*. 2004;24:e174-178
29. Schaub FJ, Han DK, Liles WC, Adams LD, Coats SA, Ramachandran RK, Seifert RA, Schwartz SM, Bowen-Pope DF. Fas/fadd-mediated activation of a specific program of inflammatory gene expression in vascular smooth muscle cells. *Nat Med*. 2000;6:790-796
30. Clarke MC, Figg N, Maguire JJ, Davenport AP, Goddard M, Littlewood TD, Bennett MR. Apoptosis of vascular smooth muscle cells induces features of plaque vulnerability in atherosclerosis. *Nat Med*. 2006;12:1075-1080
31. Clarke MC, Littlewood TD, Figg N, Maguire JJ, Davenport AP, Goddard M, Bennett MR. Chronic apoptosis of vascular smooth muscle cells accelerates atherosclerosis and promotes calcification and medial degeneration. *Circ Res*. 2008;102:1529-1538
32. Schubl S, Tsai S, Ryer EJ, Wang C, Hu J, Kent KC, Liu B. Upregulation of protein kinase cdelta in vascular smooth muscle cells promotes inflammation in abdominal aortic aneurysm. *J Surg Res*. 2009;153:181-187
33. Ryer EJ, Sakakibara K, Wang C, Sarkar D, Fisher PB, Faries PL, Kent KC, Liu B. Protein kinase c delta induces apoptosis of vascular smooth muscle cells through induction of the tumor suppressor p53 by both p38-dependent and p38-independent mechanisms. *J Biol Chem*. 2005;280:35310-35317
34. Leitges M, Mayr M, Braun U, Mayr U, Li C, Pfister G, Ghaffari-Tabrizi N, Baier G, Hu Y, Xu Q. Exacerbated vein graft arteriosclerosis in protein kinase cdelta-null mice. *The Journal of clinical investigation*. 2001;108:1505-1512
35. Renolleau S, Fau S, Goyenvalle C, Joly LM, Chauvier D, Jacotot E, Mariani J, Charriaut-Marlangue C. Specific caspase inhibitor q-vd-oph prevents neonatal stroke in p7 rat: A role for gender. *J Neurochem*. 2007;100:1062-1071
36. Yang L, Sugama S, Mischak RP, Kiaei M, Bizat N, Brouillet E, Joh TH, Beal MF. A novel systemically active caspase inhibitor attenuates the toxicities of mptp, malonate, and 3np in vivo. *Neurobiol Dis*. 2004;17:250-259
37. DeBiasi RL, Robinson BA, Sherry B, Bouchard R, Brown RD, Rizeq M, Long C, Tyler KL. Caspase inhibition protects against reovirus-induced myocardial injury in vitro and in vivo. *J Virol*. 2004;78:11040-11050
38. Yoshimura K, Aoki H, Ikeda Y, Fujii K, Akiyama N, Furutani A, Hoshii Y, Tanaka N, Ricci R, Ishihara T, Esato K, Hamano K, Matsuzaki M. Regression of abdominal aortic aneurysm by inhibition of c-jun n-terminal kinase. *Nat Med*. 2005;11:1330-1338

Figure Legends

Figure 1. Medial apoptosis occurs early during the development of experimental aneurysm.

A: Representative pictures of aortas removed from AngII- or saline-infused mice 3, 7 and 28 days after pump implantation in ApoE deficient mice. Scale bar = 2 mm. B: Maximum diameter of the suprarenal aorta of AngII-infused or saline infused mice after 3, 7 and 28 days. The rate of AAA formation, defined as a ≥100% increase in external aortic diameter compared to that of the infra-renal region, is also shown. n = 5, **P*<0.05 compared to saline. C: Representative micrographs of TUNEL staining (red), and nuclei (blue) of aortic sections. Merged images are shown in lower panels. Scale bar = 500 μm. D: Representative pictures of immunostaining using an anti-Mac3 antibody of aortic sections from saline- (28 days) or AngII-infused (3, 7 and 28 days) ApoE deficient mice. Scale bar = 250 μm.

Figure 2. Inhibitor of caspase attenuates aneurysm formation induced by AngII.

A: Representative pictures of the aortas removed from AngII infused mice treated with Q-VD-OPh or DMSO. Scale bar = 2 mm. B-C: Morphological analyses. Aortic expansion, expressed as a ratio of the maximum diameter of the supra-renal aorta to the infra-renal aorta (B) and rate of aneurysm (C) of each group are shown. n = 6, **P*<0.05. D: Representative pictures of elastin staining of Q-VD-OPh or DMSO injected AngII infused ApoE mice at 7 or 28 days. Scale bar = 500 μm.

Figure 3. Q-VD-OPh blocks aortic SMC apoptosis, macrophage invasion and elastase activation.

A: Representative pictures of TUNEL staining and immunostaining for Mac3. Aortic sections of Q-VD-OPh or DMSO treated AngII infused ApoE KO mice at 3, 7 and 28 days were stained for TUNEL or anti-Mac3. Scale bar = 50 μm. n = 6. B: Representative pictures of in situ zymography. Aortic sections of Q-VD-OPh or DMSO treated AngII infused ApoE KO mice at 7 days were freshly frozen and incubated with DQ-elastin for 48 hours. The fluorescent intensity was obtained before and after incubation. Scale bar = 200 μm. n = 6.

Figure 4. Apoptotic SMCs attract monocytes through release of MCP-1.

A: Mouse aortic SMCs were stimulated with 0 to 10 μM of AngII for 48 hours. Apoptosis was evaluated though ELISA measured DNA fragmentation. *P<0.05. B: Mouse aortic SMCs were stimulated with 10 μM of AngII in the presence of 20 μM of Q-VD-OPh or DMSO. Apoptosis was evaluated though ELISA-measured DNA fragmentation. *P<0.05. C&D: Migration of macrophages was evaluated by chemotaxis assay. Fresh media containing AngII or media-conditioned by aortic SMCs underwent treatment as indicated was used as chemoattractants. n = 6. *P<0.05. E: Aortic SMCs were stimulated with 10 μM of AngII in the presence of 20 μM of Q-VD-OPh for 48 hours. The amount of MCP-1 in media was evaluated by ELISA for MCP-1. n= 6, *P<0.05. F: Conditioned media was treated with a neutralizing antibody to MCP-1 (1 μg/ml) prior to the chemotaxis assay of monocytes. n = 6, *P<0.05. G: Representative pictures of

immunostaining for MCP-1. Aortic sections of Q-VD-OPh or DMSO treated AngII infused ApoE KO mice at 3 days were stained for anti-MCP-1. Scale bar = 100 µm. n = 3.

Figure 1.

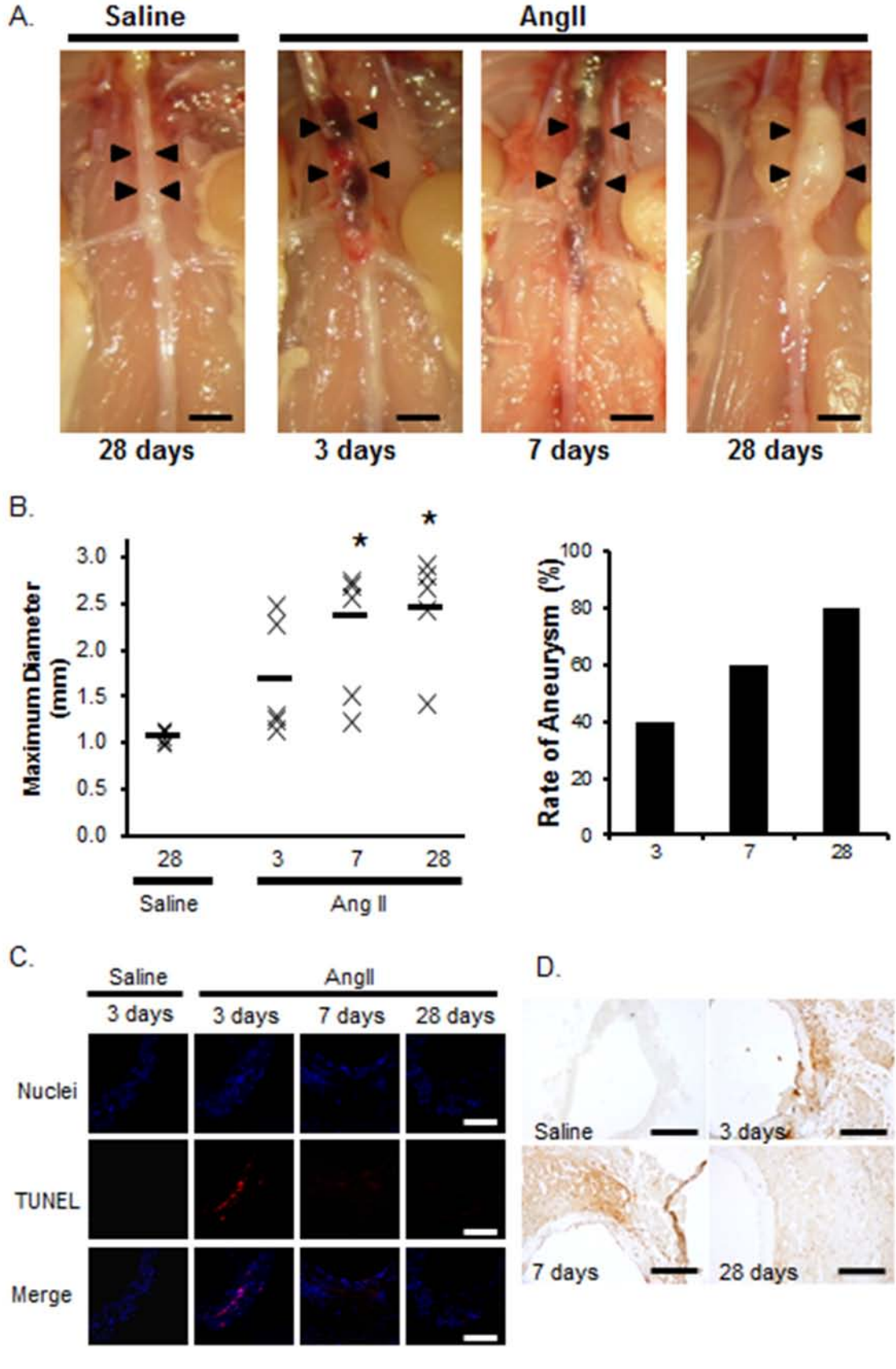
A.
Saline
AngII
28 days
3 days
7 days
28 days
B.
Maximum Diameter (mm)
3.0
2.5
2.0
1.5
1.0
0.5
0.0
28
3
7
28
Saline
Ang II
Rate of Aneurysm (%)
100
80
60
40
20
0
3
7
28
C.
Saline
AngII
3 days
3 days
7 days
28 days
Nuclei
TUNEL
Merge
D.
Saline
3 days
7 days
28 days

Figure 2.

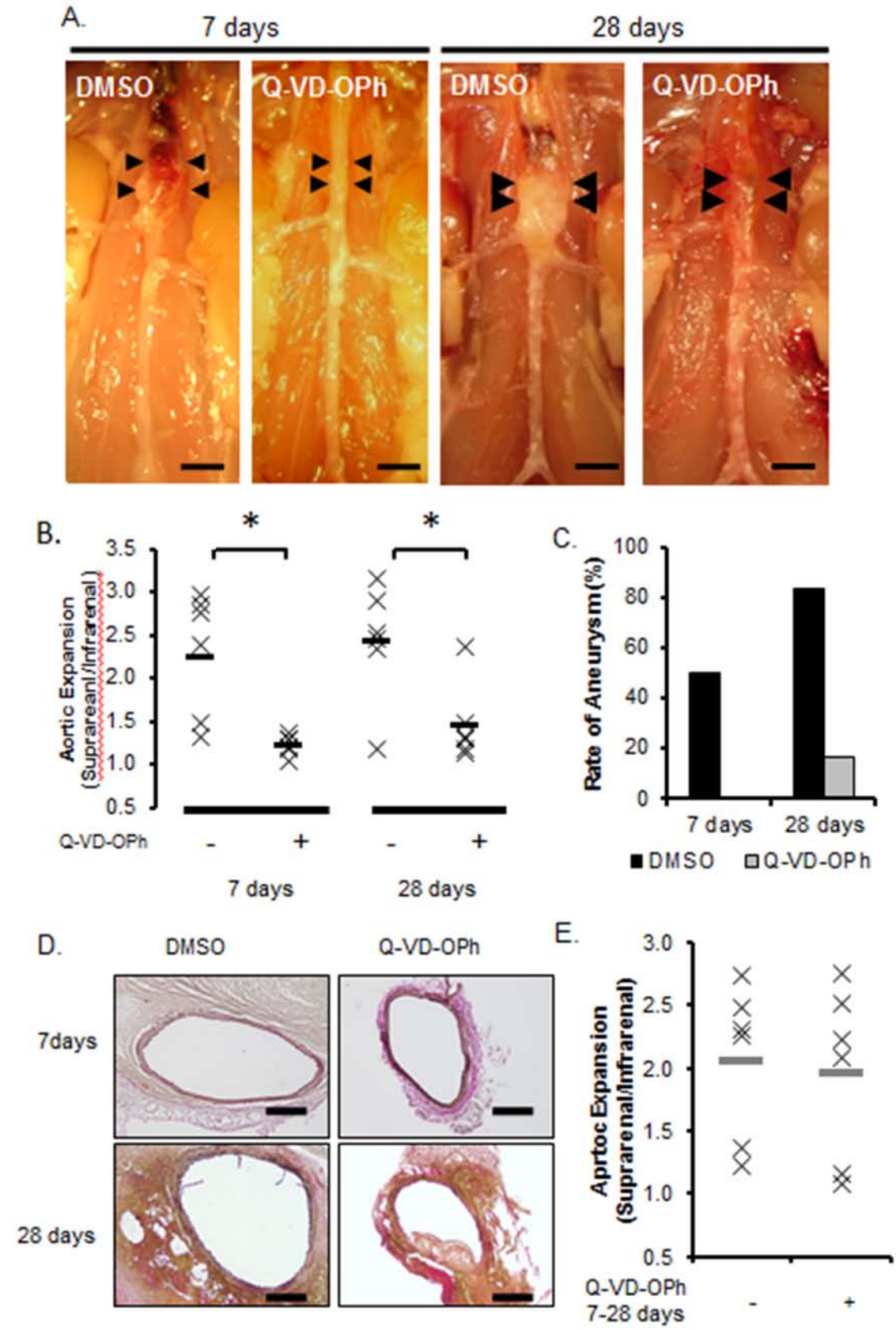
A.
7 days
28 days
DMSO
Q-VD-OPh
DMSO
Q-VD-OPh
B.
*
*
Aortic Expansion (Suprarenal/Infrarenal)
3.5
3.0
2.5
2.0
1.5
1.0
0.5
Q-VD-OPh
-
+
-
+
7 days
28 days
C.
Rate of Aneurysm (%)
100
80
60
40
20
0
7 days
28 days
DMSO
Q-VD-OPh
D.
DMSO
Q-VD-OPh
7days
28 days
E.
Aprtoc Expansion (Suprarenal/Infrarenal)
3.0
2.5
2.0
1.5
1.0
0.5
Q-VD-OPh
7-28 days
-
+

Figure 3.

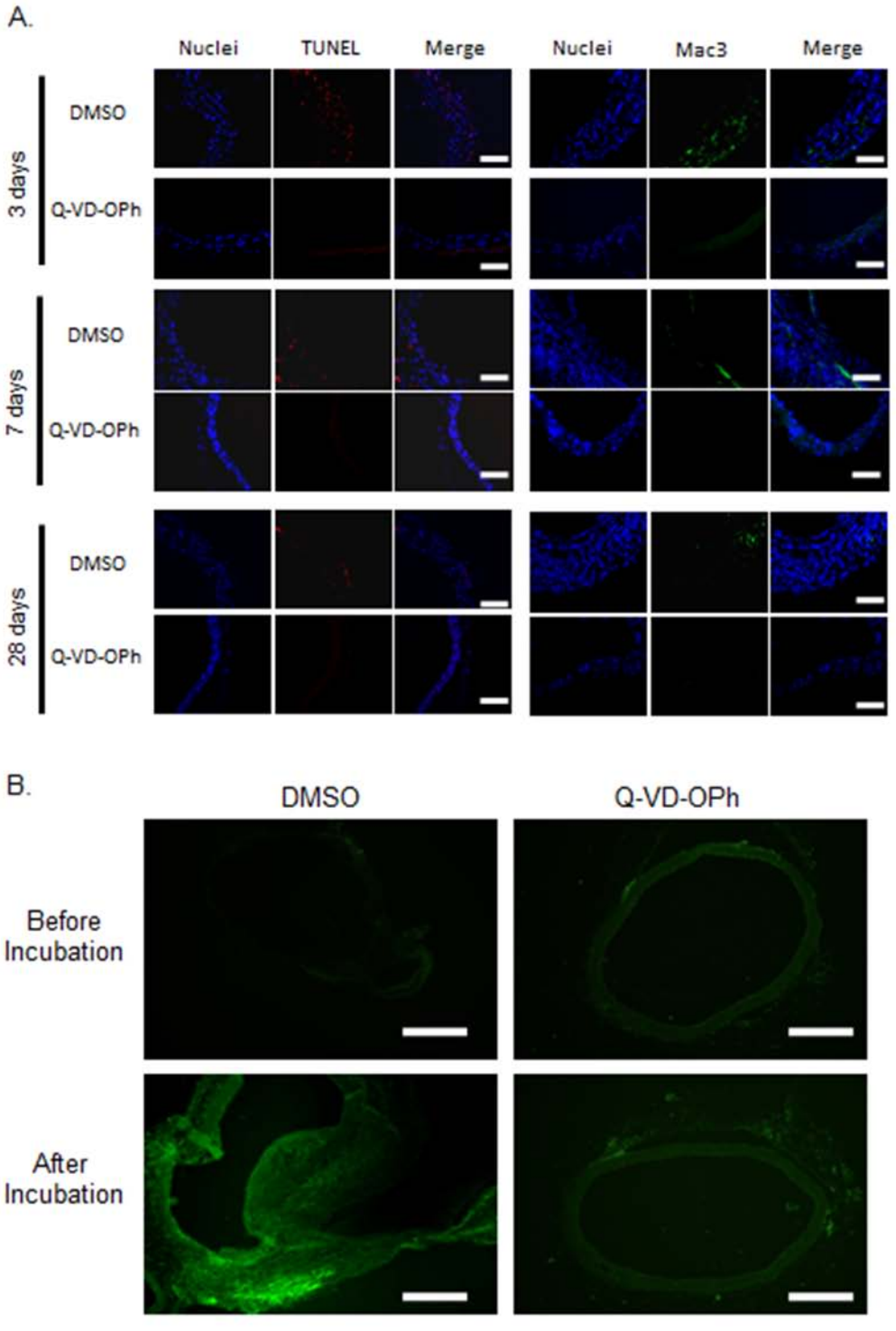
A.
Nuclei
TUNEL
Merge
Nuclei
Mac3
Merge
3 days
DMSO
Q-VD-OPh
7 days
DMSO
Q-VD-OPh
28 days
DMSO
Q-VD-OPh
B.
DMSO
Q-VD-OPh
Before Incubation
After Incubation

Figure 4.

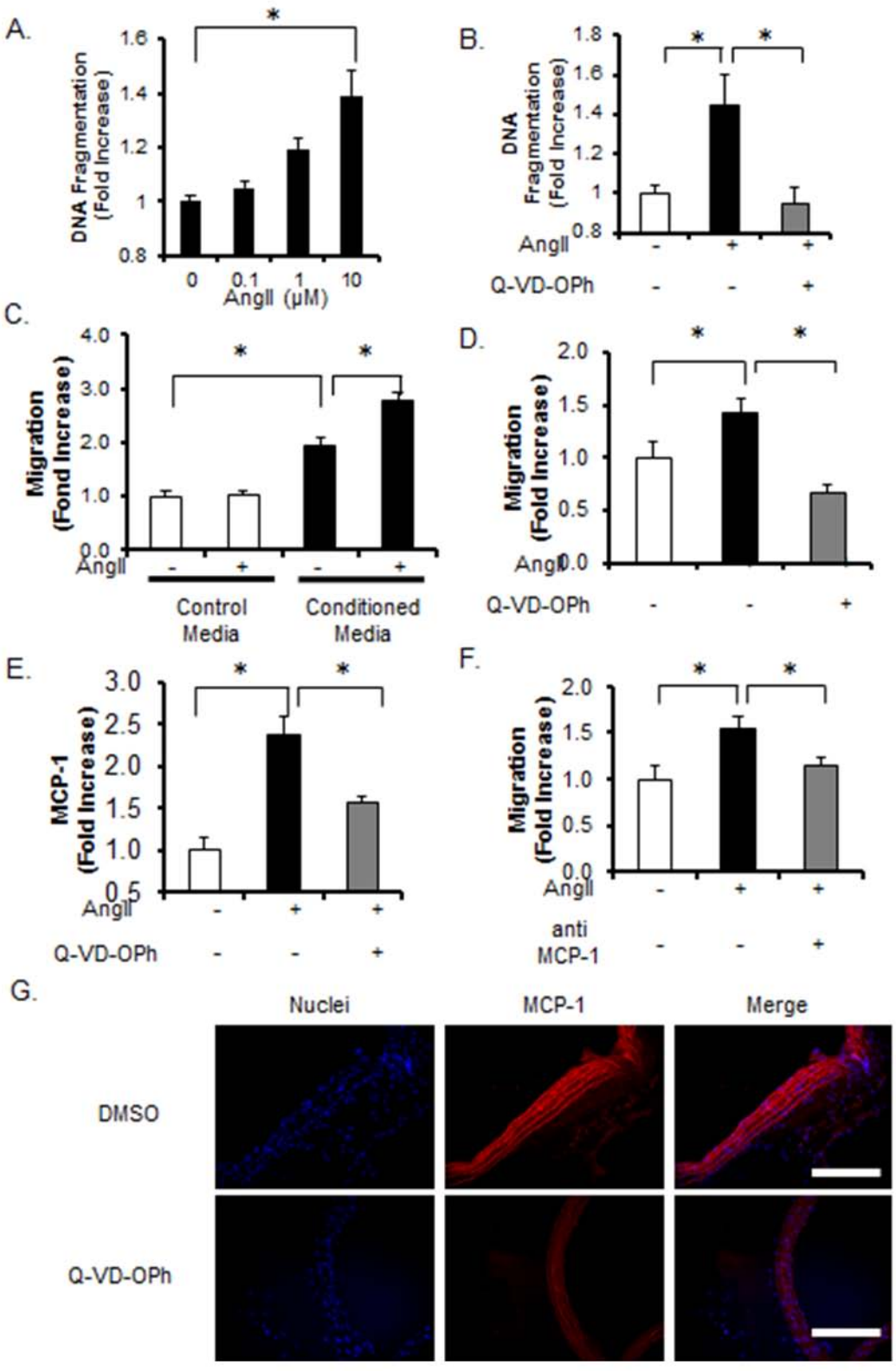
A.
DNA Fragmentation (Fold Increase)
1.6
1.4
1.2
1
0.8
0
0.1
1
10
AngII (μM)
*
B.
DNA Fragmentation (Fold Increase)
1.8
1.6
1.4
1.2
1
0.8
*
*
AngII
-
+
+
Q-VD-OPh
-
-
+
C.
Migration (Fond Increase)
4.0
3.0
2.0
1.0
0.0
*
*
AngII
-
+
-
+
Control Media
Conditioned Media
D.
Migration (Fold Increase)
2.0
1.5
1.0
0.5
0.0
*
*
AngII
Q-VD-OPh
-
-
+
E.
MCP-1 (Fold Increase)
3.0
2.5
2.0
1.5
1.0
0.5
*
*
AngII
-
+
+
Q-VD-OPh
-
-
+
F.
Migration (Fold Increase)
2.0
1.5
1.0
0.5
0.0
*
*
AngII
-
+
+
anti MCP-1
-
-
+
G.
Nuclei
MCP-1
Merge
DMSO
Q-VD-OPh

Supplemental Figure 1.

Representative pictures of immunostaining for alpha-smooth muscle actin (SMA) and TUNEL. Aortic sections of Q-VD-OPh or DMSO treated AngII infused ApoE KO mice at 3 days were co-stained for SMA and TUNEL. Scale bar = 50 μm, n = 3.

Supplemental Figure 2.

A: Effect of Q-VD-OPh on hydrogen peroxide (H_2O_2) induced apoptosis of SMCs.

SMCs were stimulated with 0 to 500 μM H_2O_2 for 24 hours. Apoptosis was evaluated though ELISA measured DNA fragmentation. n = 3. *P<0.05.

B: Effect of pan caspase inhibitor, Q-VD-OPh, on H_2O_2 induced apoptosis of SMCs. SMCs were stimulated with 500 μM of H2O2 in the presence of 20 μM of Q-VD-OPh or DMSO. Apoptosis was evaluated though ELISA-measured DNA fragmentation. n = 3. *P<0.05.

Supplemental Figure 3.

Pictures of the aortas of removed from ApoE deficient mice treated with Q-VD-OPh or DMSO 7 and 28 days after AngII infusion. Scale bar = 2 mm**.**

Supplemental Figure 4.

Representative pictures of immunostaining for CD3. Aortic sections of Q-VD-OPh or DMSO treated AngII infused ApoE KO mice at 3 days were stained for CD3. Scale bar = 50 μm, n = 3.

Supplemental Figure 5.

Representative pictures of immunostaining for IL-6. Aortic sections of Q-VD-OPh or DMSO treated AngII infused ApoE KO mice at 3 days were stained for IL-6. Scale bar = 50 μm, n = 3.

Supplemental Figure 6.

Effect of AngII cytokine/chemokine expression in SMCs. SMCs were stimulated with 10 μM of AngII for 24 hours with or without 20 μM of Q-VD-OPh. The relative gene expression (RQ) of tumor necrosis factor-α (TNFα), interleukin-1β (IL1β), interleuskin-6 (IL6), interferon γ (IFNγ) or MCP-1 was determined using the ΔΔCt. GAPDH was used as an internal control. n = 3. $P<0.05$.

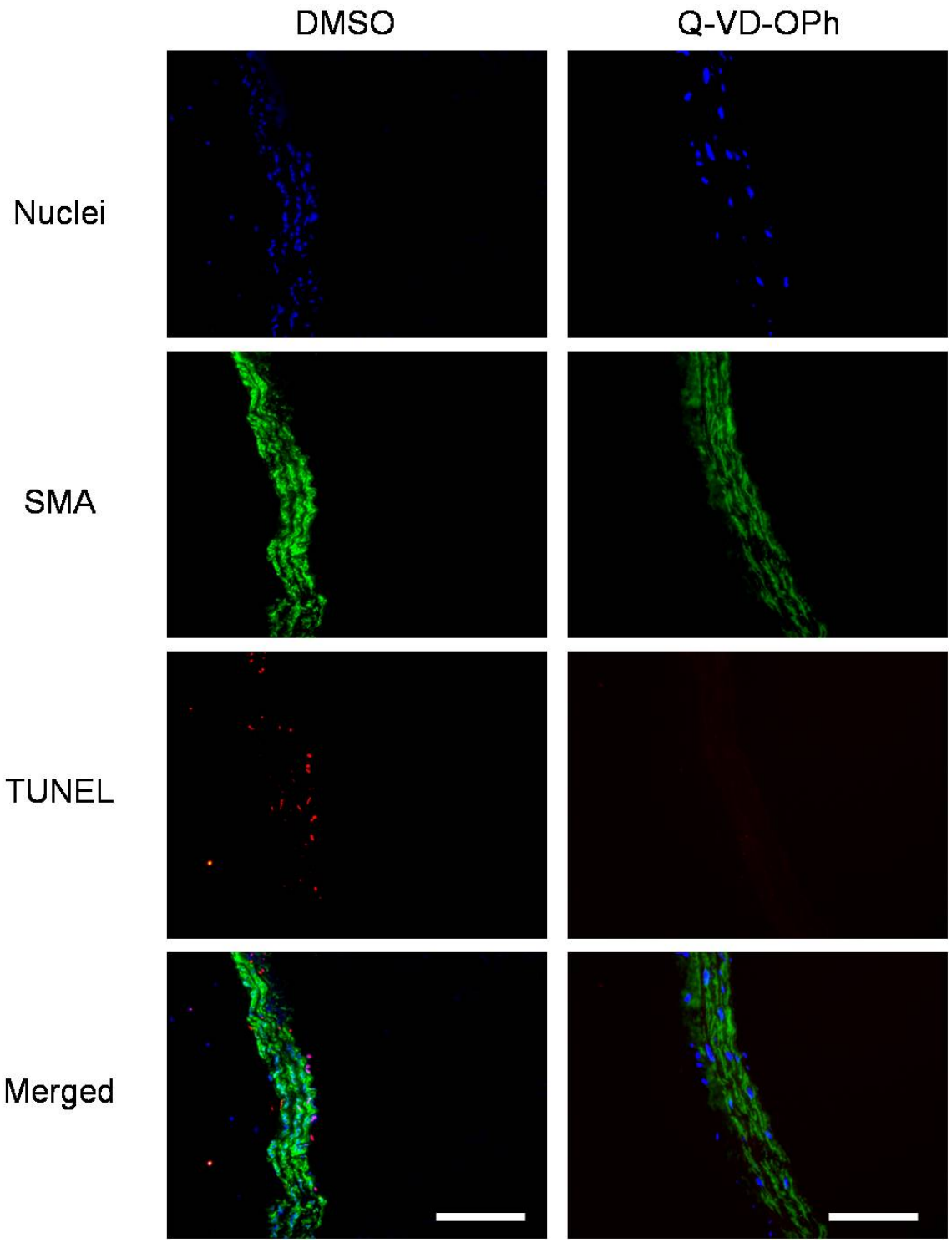
DMSO
Q-VD-OPh
Nuclei
SMA
TUNEL
Merged

A.

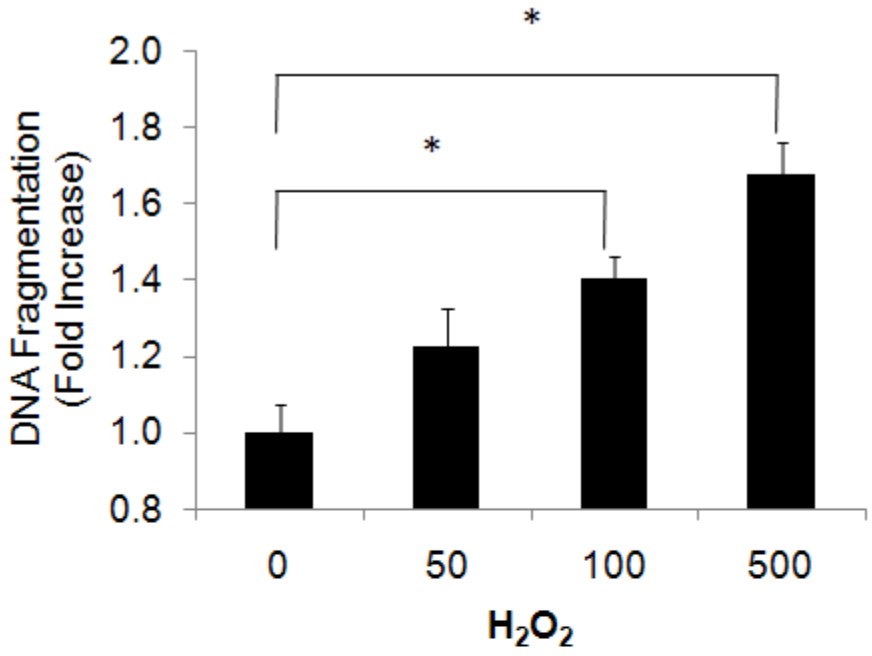
*
*
2.0
1.8
1.6
1.4
1.2
1.0
0.8
DNA Fragmentation
(Fold Increase)
0
50
100
500
H2O2

B.

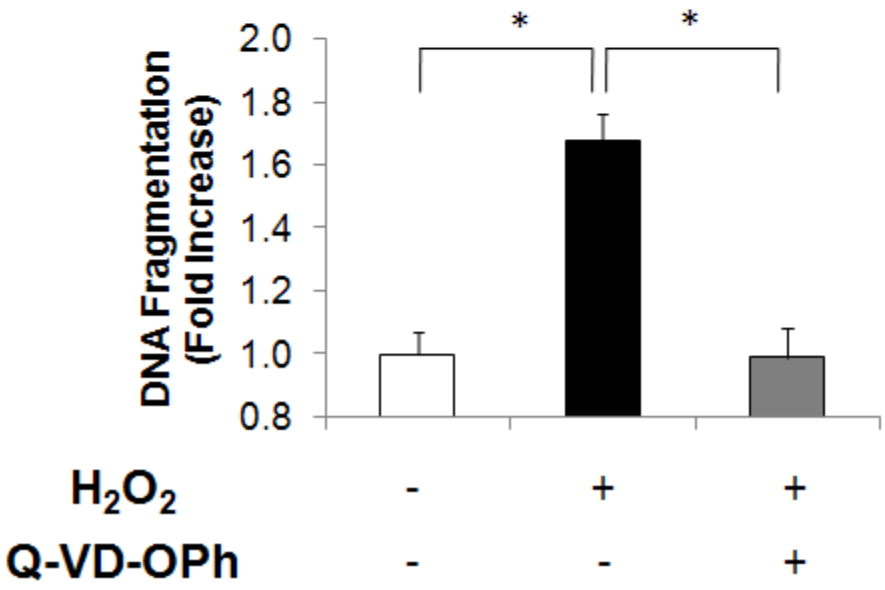
*
*
2.0
1.8
1.6
1.4
1.2
1.0
0.8
DNA Fragmentation
(Fold Increase)
H2O2
-
+
+
Q-VD-OPh
-
-
+

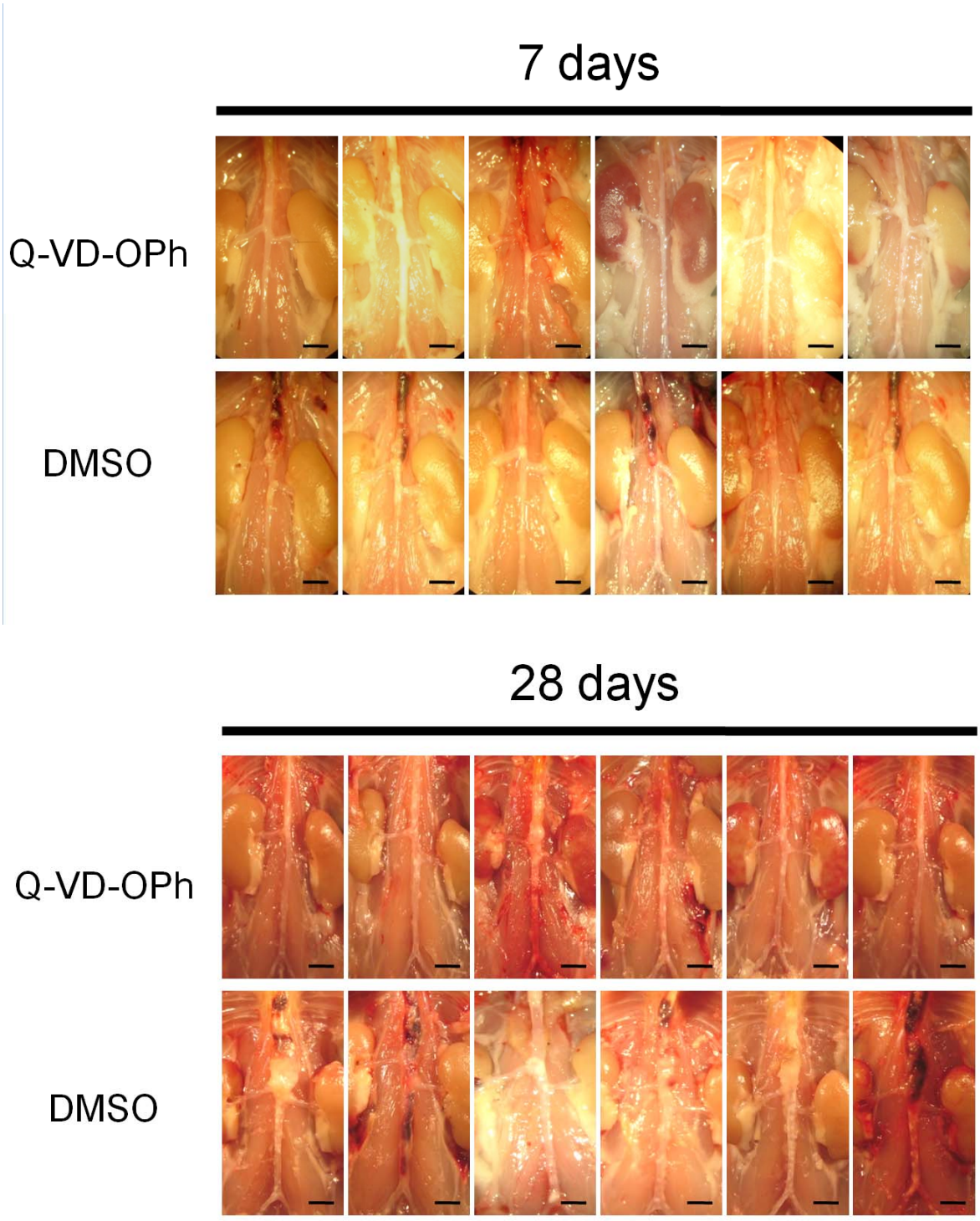
7 days
Q-VD-OPh
DMSO
28 days
Q-VD-OPh
DMSO

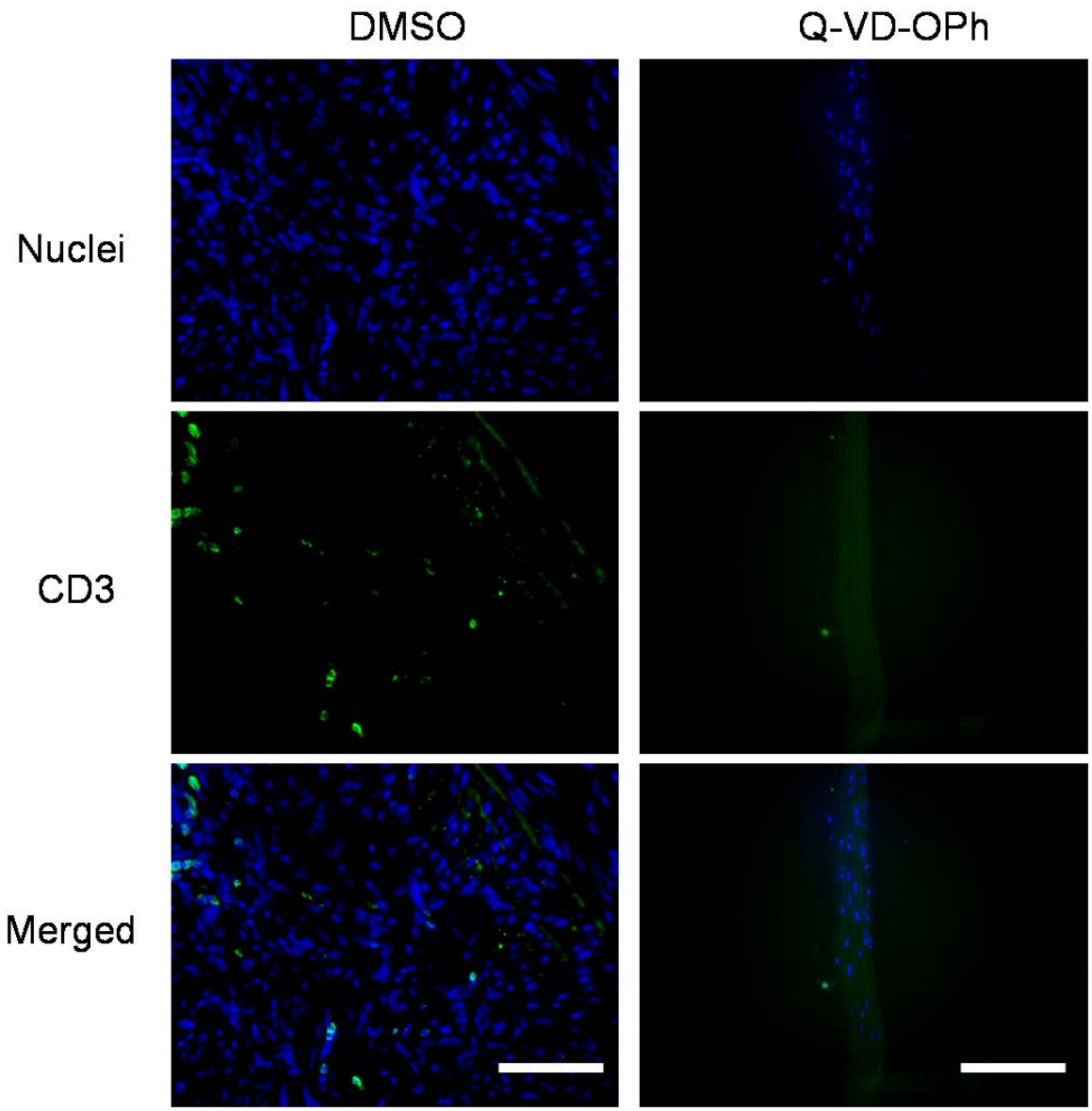
DMSO
Q-VD-OPh
Nuclei
CD3
Merged

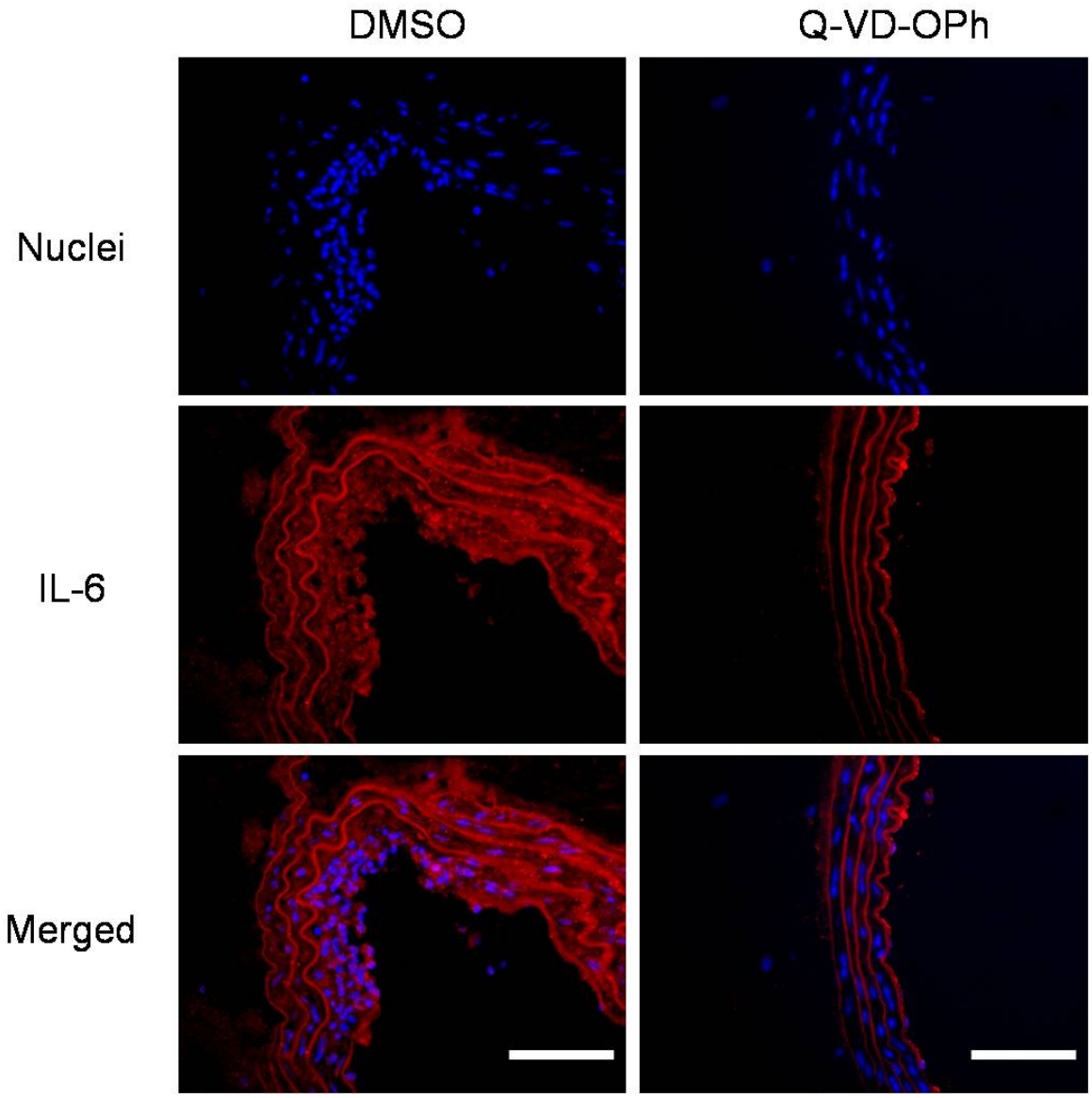
DMSO
Q-VD-OPh
Nuclei
IL-6
Merged

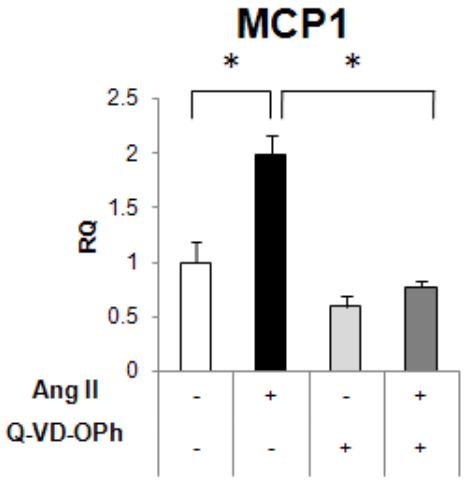
MCP1
*
*
2.5
2
1.5
1
0.5
0
RQ
Ang II
Q-VD-OPh
- + - +
- - + +

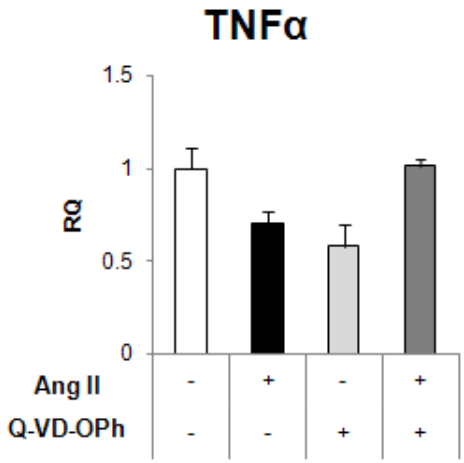
TNFα
1.5
1
0.5
0
RQ
Ang II
Q-VD-OPh
- + - +
- - + +

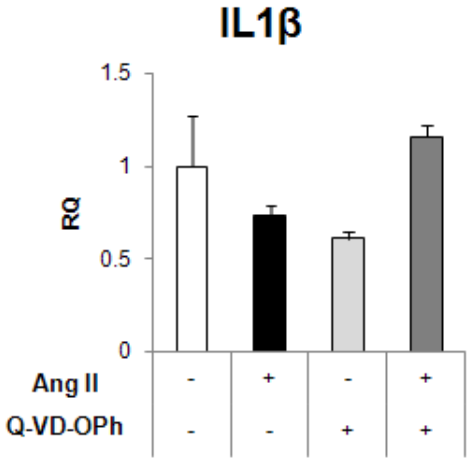
IL1β
1.5
1
0.5
0
RQ
Ang II
Q-VD-OPh
- + - +
- - + +

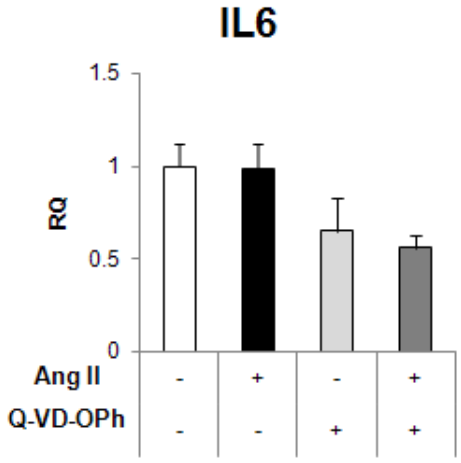
IL6
1.5
1
0.5
0
RQ
Ang II
Q-VD-OPh
- + - +
- - + +

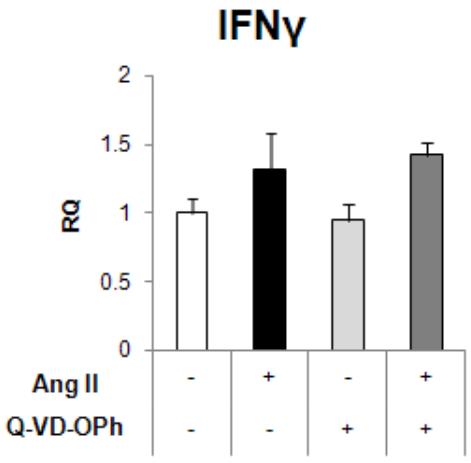
IFNγ
2
1.5
1
0.5
0
RQ
Ang II
Q-VD-OPh
- + - +
- - + +

Transition

The nature of aneurysm makes their study highly difficult. Since biopsy is not a valid option in AAA, the only human tissues available for research are obtained during open-surgery repair. Thus, tissues harvested from human subjects are almost invariably end-stage tissue. Additionally, patients and care-providers are increasingly choosing an endovascular approach to open-surgery repair, which prevents the harvest of tissue. These facts limit not only tissue quantity, but the points of disease progression from which data can be gathered. While efforts are being made toward data gathering in patients with small aneurysm, animal modeling is an invaluable approach allowing us to gain insight to the biological events that initiate and potentiate the disease.

For small aneurysm, there are four major murine models of aneurysm available, and each works through distinct mechanisms. The Angiotensin II (AngII) model, as described in Chapter 1, works by activation of the inflammatory response, proteolytic cascade, NF-kappaB, and urokinase pathways. Second, the elastase model, is a chemically induced aneurysm model that relies on the degradation of elastin layers by the elastase enzyme introduced via catheter. Next, the calcium chloride ($CaCl_2$) model, involves a peri-aortic application of $CaCl_2$ that results in structural disruption of the artery, especially elastin layers, and an immense adventitial inflammatory response with aneurysm forming after 6 weeks. Finally, the Calcium phosphate ($CaPO_4$) model is similar to the $CaCl_2$ model, but phosho-buffered saline is applied to the artery after $CaCl_2$ is removed. This creates $CaPO_4$ crystals that are believed to accelerate cellular death and inflammation, producing an aneurysm in only one week.

Each of these models produces aortic expansion and vascular destruction, similar to that seen in large human aneurysm. Due to the lack of human data on small aneurysm, it has been difficult for the field to evaluate the animal models for their respective value in studying progression of small aneurysm. Thus, any therapeutic target identified in one model warrants investigation in additional model(s). The

findings made in Chapter 1, specifically that inhibition of caspases by Q-VD-OPh prevents aneurysm expansion in the AngII model, should be repeated in additional aneurysm models. With this in mind, we decided to explore the efficacy of caspase inhibition in the CaPO4 and Elastase models.

In addition to validating the findings made in Chapter 1, Chapter 2 aims to translate. Because human aneurysms are discovered after expansion has begun, treatments that begin before formation will be nearly useless in the pursuit of therapeutic treatments. We therefore designed our study to administer Q-VD-OPh after small aneurysm has formed.

Chapter 2: A Pan-Caspase Inhibitor Successfully Prevents Abdominal Aortic Aneurysm Formation but Does Not Prevent Expansion of Established AAA in a Mouse Model.

Unpublished Work

Stephanie Morgan, Guoqing Song, Timothy Hacker, Calvin Harberg, Qiwei Wang, and Bo Liu

ABSTRACT

OBJECTIVE

Apoptosis has been shown to play an important role in murine abdominal aortic aneurysm (AAA). We have previously shown the caspase inhibitor Q-VD-OPh to effectively prevent aneurysm formation in a mouse model of AAA. Here, we sought to establish a role for apoptosis in two additional mouse models of AAA as well the progression of an established aneurysm.

METHODS

In the first experiment, murine AAA was induced by the CaPO4 model. Injection of a pan-caspase inhibitor (Q-VD-OPh, 20mg/kg) was started 6 hours before surgery, and daily through the seventh day after surgery. Aneurysm expansion was measured at 7 and 42 days after surgery. Histological analysis was performed on 7 day tissue to measure apoptosis and inflammation, and elastin degradation was measured in tissue harvested 42 days after surgery. The efficacy of early Q-VD-OPh administration was confirmed in the elastase perfusion model of AAA.

In a second experiment, Q-VD-OPh injections were started 7 days after surgery and continued once every 48 hours through day 14. Ultrasound measurements were used first to establish initial aneurysm formation at day 7, and again to measure final aneurysm expansion at day 14. Tissue was harvested at day 14 for morphological and histological analysis.

RESULTS

Early administration of Q-VD-OPh inhibited CaPO4-induced aneurysm growth in DMSO vs. Q-VD-OPh treated animals at 7 days (100.1±8.2% vs. 13.8±1.79%, respectively). Further, apoptosis was reduced from 5.8±2.1% in control to 0.5±1% in Q-VD-OPh treated animals. The inhibition of aneurysm growth was continued through 42 days, with DMSO treated mice showing aneurysmal expansion of 133.7±34.1% and Q-VD-OPh treated mice with 61.6±9.04% expansion. Early Q-VD-OPh administration in Elastase-treated arteries reduced aneurysm growth by 37%. However, administration of Q-VD-OPh to small aneurysm produced an insignificant reduction in aneurysm size as compared to DMSO treated animals (1.16±0.12mm vs. 1.21±0.08mm, respectively).

CONCLUSION

Data presented here suggests that apoptosis is an important and driving factor for events in early aneurysm, such as inflammation. However, caspase-mediated cell death appears to have a minimal role in the further growth of small aneurysm.

Introduction

Abdominal aortic aneurysm (AAA) is a lethal, age-related vascular disease in which the structural integrity of the artery is compromised and the aortic wall is segmentally weakened. Currently, the only method of treatment for AAA is surgical intervention, and no effective therapeutic targets have been identified. Histological and morphological features of human AAA have been replicated in several animal models in order to investigate the pathophysiological events that underlie AAA formation[1]. In this study, we will be utilizing two chemically-induced aneurysm models. First, the calcium phosphate (CaPO4) model is created via a periaortic application of calcium chloride followed by phospho-buffered saline. This method results in a significant amount of apoptosis, inflammation, and calcification; which ultimately leads to aneurysm formation by 7 days[2]. The second model is the elastase model, which requires luminal infusion of porcine elastase to the abdominal aorta. This method results an immediate mechanical stretching of the aorta, and continuous expansion forming aneurysm between 7 and 14 days. Here, aneurysm will be defined as a 100% increase in extraluminal diameter measurement[3].

The depletion of vascular smooth muscle cells (SMCs) in human aneurysmal tissues has been explored by several groups[4, 5]. The common hypothesis regarding this phenomenon is that the elimination of the SMC population contributes to aneurysm by removing a group of cells capable of producing extracellular matrix proteins and, possibly, repairing aneurysmal tissue. Recently, we demonstrated that the administration of a pan-caspase inhibitor can effectively inhibit aneurysm growth[6]. Further, we have shown that the acceleration of

apoptosis is linked to the inflammatory response, elastin degradation, and calcification in another aneurysm model[2]. These data, as well as those provided by several other groups, led us to hypothesize that the role for SMC apoptosis in aneurysm may expand beyond current understanding, and that it may in fact be a critical event in the formation of aneurysm.

The investigations of SMC apoptosis in aneurysm, as briefly described above, were carried out in studies in which apoptosis manipulation is enacted prior to, or in conjunction with, aneurysm induction. Given the nature of the human aneurysm disease and the necessity for therapeutic interventions, these early-administration methods make little headway in regards to translational research strategies. Rather, research must focus on methods of inhibiting or even reversing the expansion of an established aneurysm. This study addresses the role of caspase activation in later stages of the disease by administering a pan-caspase inhibitor after small aneurysm has formed.

METHODS

Mouse Models of AAA

Male C57BL/6 mice, 12 weeks of age, were purchased from Jackson Laboratory (Bar Harbor, ME). All mice had free access to a normal diet and water. $CaPO_4$ induced abdominal aortic aneurysm model were created through a method described previously[2]. Briefly, animals were placed under general anesthesia and a midline incision was made. The infrarenal region of the abdominal aorta was isolated and a small piece of gauze soaked in 0.5M $CaCl_2$ was applied perivascularly for 10 minutes. This gauze was then replaced with another piece of phosphate buffered saline (PBS)-soaked gauze for 5 minutes. Control mice received a single treatment of PBS soaked gauze for 15 minutes. The elastase-induced experimental aneurysm was created as described previously. Briefly, the aorta is isolated from the renal vein to the iliac bifurcation and occluded with silk suture proximally and distally of the isolation points. Then, an aortotomy is made with a 30-gauge needle and a catheter is used to perfuse the artery with () elastase or equal concentration heat inactivated elastase at constant pressure. Once the catheter is removed, the aortotomy is closed with 11-0 suture. All animals were treated with elastase from the same lot, and heat-inactivated (5 minutes at 100ºC) elastase served as control.

The caspase inhibitor, Q-VD-OPh (BioVision, CA) was administered at a dose of 20mg/kg, with DMSO given as control. Q-VD-OPh or DMSO was injected via intraperitoneal (IP) injection in two different injection protocols. In the first experiment, daily injections are started 6 hours before surgery. In the second experiment, injections are given every 48 hours beginning 7 days after surgery. The maximum external diameter of the infrarenal aorta was measured using a

digital caliper (VWR Scientific, Radnor, PA) prior to treatment (initial measurement) and at the time of tissue harvest (final measurement). Aortic expansion (% Aortic Dilation) was determined by first calculating the expansion (final measurement – initial measurement), and dividing that difference by the initial measurement: ((Final measurement – initial measurement)/Final measurement)*100. In the second experimental design, ultrasound images were collected on a Vevo 770 micro-unltrasound imaging system (Visualsonics Inc., Toronto, Canada).

At selected time points, mice were sacrificed and tissues were perfusion-fixed with a mixture of 4% paraformaldehyde (PFA) in PBS at physiological perfusion pressure. Harvested tissue was further fixed in 4% PFA and imbedded in O.C.T. Compound (Sakura Tissue Tek, Netherlands) or fully processed for paraffin imbedding. All O.C.T. sections were cut 6µm thick using a Leica CM3050S cryostat, and all paraffin sections were cut at 8µm thick on a Leica RM2135 rotary microtome. All animal procedures were conducted in accordance with experimental protocols that were approved by the Institutional Animal Care and Use Committee at the University of Wisconsin, Madison (Protocol M02284).

Histology and Immunohistochemistry

Van Geison stains were carried out using Chromaview Van Gieson kit (Richard Allan Scientific, Kalamazoo, MI) according to provided protocol. For additional immunohistochemistry, arterial sections were permeabilized with 0.1% TritonX for 10 minutes at room temperature. Non-specific sites were blocked using 5% bovine serum albumin (BSA), 3% normal donkey serum in Tris-buffered Saline and Tween 20 (TBS-T) for 1 hour at room temperature. Primary antibodies to CD3 and Mac3 were purchased from Santa Cruz (Santa

Cruz, CA), CD45 was purchased from BD Biosciences (San Jose, CA), Ly6G was purchased from BioLegend (San Diego, CA), CD68 was purchased from AbD Serotec (Raleigh, NC), and Smooth muscle alpha-actin (SMA) was purchased from Sigma-Aldrich (St. Louis, MO). Primary antibodies were diluted in previously described blocking solution and incubated overnight at 4°C. Apoptosis was identified through Terminal deoxynucleotidyl transferase dUTP nick end labeling (TUNEL) in an *In Situ* Cell Death Detection Kit (Roche, Indianapolis, IN), carried out according to kit directions. Fluorescent stains were completed using secondary antibodies purchased from Invitrogen Molecular Probes (Carlsbad, CA) and 4'6-diamidino-2-phenyl-indole, dihydrochloride (DAPI, Invitrogen, Carlsbad, CA) was used to detect nuclei. Staining was visualized with a Nikon Eclipse Ti inverted microscope system and digital images were acquired using a Nikon DS-Ri1 digital camera. Quantification of stains was performed in a manner to that previously described[7] using Image J Software. Data quantification was performed using at least 3 sections per artery.

Statistical analysis

Values were expressed as means ± standard error. Experiments were repeated at least three times unless stated otherwise. Differences between 2 groups were analyzed by Student's t test, and one-way analysis of variance (ANOVA) followed by Scheffe's test was used for multiple comparisons. Values of $P<0.05$ were considered significant.

RESULTS

A pan-caspase inhibitor prevents aneurysm in surgery-induced murine AAA models

To further assess the role of apoptosis in aneurysm formation, we designed two separate experiments in which the pan-caspase inhibitor Q-VD-OPh was administered prior to the surgical induction of murine AAA. In the first experiment, an intraperitoneal injection of Q-VD-OPh (20 mg/kg/day) or DMSO (as control) was given 6 hours before C57B/6 males underwent aneurysm induction by the Calcium phosphate (CaPO4), and the inhibitor was administered daily for 7 days after surgery (Figure 1A). In order to evaluate aneurysm expansion, the maximum external diameter of the abdominal aorta was measured prior to elastase perfusion and again at the time of sacrifice. Aortic expansion is expressed as a percentage describing the difference between aortic diameter measured at sacrifice and that measured immediately prior to AAA induction ((Final – Prior)/Prior)*100). Animals harvested at the end of the Q-VD-OPh treatment schedule, at day 7, displayed significantly smaller aneurysm (1.13±.02mm, 61.6±9.04%) than animals receiving DMSO injections (2±0.1mm; 139±30.9%). When examined 5 weeks after cessation of drug treatment, aortic diameter of Q-VD-OPh treated mice retained a significantly smaller aneurysm than that of DMSO-treated mice (1.61±0.11mm, 214.9±16.7% vs. 2.39±0.31mm, 362.7±65.6%, respectively; Figure 1B, C). These measurements suggest that the protective effect of early administration Q-VD-OPh remains through 42 days. However, comparison made between 42 and 7 day time points of Q-VD-OPh-treated arteries showed substantial aneurysm growth (Figure 1C). Tissues harvested 42 days after surgery were evaluated for elastin integrity, revealing that Q-VD-OPh treated aorta displayed greater

preservation of elastin (Supplemental Figure 1A). For histological analysis, tissues were harvested 7 days after surgery. Results reveal that apoptosis was reduced in Q-VD-OPh treated animals (Figure 1D). Further, administration of Q-VD-OPh successfully reduced infiltration of neutrophils (Ly6G), macrophages (CD68), and T lymphocytes (CD3) (Figure 1E, F, Supplemental Figure 1B).

To test whether the protective effect of Q-VD-OPh is specific to the CaPO4 model, we turned to a different murine AAA model that employs intraluminal perfusion of aorta with elastase. First, we tested three additional drug administration schedules by reducing injection frequency to once every 48 hours and testing two additional doses (10mg/kg/day and 15mg/kg/day). These modified methods provided results suggesting that the original dosage (20mg/kg/day) was the minimum dosage necessary for apoptosis inhibition. However, we found administration every 48 hours was sufficient to inhibit apoptosis (results not shown). Using this new drug administration schedule, we performed preliminary experiments (n=2) to test the efficacy of Q-VD-OPh to inhibit aneurysm growth in the elastase-perfusion model of murine AAA (Supplemental Figure 2A). As seen in Supplemental Figure 2B, a Q-VD-OPh administration schedule beginning 6 hours before surgery prevented aneurysmal expansion when compared to DMSO control injections (0.92, 88.7% vs. 1.09, 93.8%, respectively). Further, Q-VD-OPh treatment reduced apoptosis as measured by TUNEL (Supplemental Figure 2C) as well as infiltration of macrophages as identified by CD68 (Supplemental Figure 2D).

Pan-caspase inhibitor failed to prevent further dilation of small aneurysm

In the clinical setting, AAA is identified almost exclusively once the disease process has begun to noticeably expand the aortic diameter. Thus, in order to identify an effective translational drug therapy target, we aimed to assess the role of caspase activation in established small aneurysms. The elastase-induced AAA model drives aneurysm expansion by day 7 after surgery, with further expansion continuing through day 14 (Figure1A). In this study, we utilized the modified Q-VD-OPh administration schedule beginning 7 days after elastase induction of aneurysm and continuing every 48 hours until sacrifice (Figure 2A). We used ultrasound imaging, a routinely used imaging modality employed in clinical management of AAA patients, to monitor aneurysm growth (Figure 2B). Mice were first Imaged 7 days after elastase treatment to confirm the establishment of small aneurysm (Figure 2C, D). Mice of both elastase- and control-treated groups were then randomly assigned to subgroups receiving either Q-VD-OPh or DMSO control injections every 48 hours. Ultrasound measurements at 7 days after surgery showed treatment with inactive elastase induced smaller aortic dilation than elastase treated arteries (0.89±0.09mm vs. 1.05±0.18mm). In inactive elastase treated animals, no significant aortic expansion was seen in either DMSO or Q-VD-OPh treated mice as compared to measurements taken at 7 days (0.96±0.04mm vs. 0.97±0.11mm). Conversely, elastase induced aneurysms from both DMSO and Q-VD-OPh treated animals showed a greater expansion from measurements taken at 7 days, with aortic diameters increasing to 1.21±0.09mm and 1.15±0.12mm, respectively (Figure 2C, D). These measurements were shown to be significantly greater than their inactive elatase-treated counterparts. Although the aneurysmal measurements appear slightly reduced in Q-VD-OPh treated animals, the

differences were not statistically significant (p value 0.34). Further, no significant change was noted in inactive elastase-induced aneurysm from either treatment mice from either group.

Morphological and histological features of AAA in pan-caspase treated AAA

Morphological and histological analyses of elastase-treated tissues revealed that elastin fragmentation, a hallmark of elastase-induced aneurysm, was unchanged between Q-VD-OPh or DMSO treated animals when pan-caspase injections began 7 days after aneurysm induction (Figure 3A, B). Importantly, the efficacy of Q-VD-OPh is evidenced in Figure 3C and D by the measurement of apoptosis in aneurysmal tissue. Control tissue from Q-VD-OPh treated mice showed significantly increased infiltration of macrophages, but macrophages infiltration was not seen to be significantly regulated in other treatment groups (Figure3E, F). Additional inflammatory cell infiltrate was measured using markers for total leukocytes (CD45), neutrophils (Ly6G), and T Lymphocytes (CD3) (Figure 4A, B, C). Total leukocyte content (CD45+) was significantly reduced in elastase-induced aneurysm tissue treated with Q-VD-OPh as compared to DMSO (12.1±3.5% vs. 21.1±5.1%, respectively; p value 0.009)(Figure 4A). Interestingly, Q-VD-OPh treatment actually slightly increased T lymphocyte presence in elastase-induced aneurysm as compared to DMSO treatment (Figure 4C).

DISCUSSION

Clinically, the presence of apoptotic markers is a noted pathological feature associated with late stage abdominal aortic aneurysm. However, the role apoptosis may play in aneurysm development or progression remains poorly understood. In this study, we report that the pan-caspase inhibitor, Q-VD-OPh, successfully inhibits aneurysm formation in three different murine models when administered prior to aneurysm induction. When administered after aneurysm has formed, however, Q-VD-OPh does not significantly attenuate further aneurysm expansion. These findings suggest that caspase activation drives early pathological events in aneurysm, but does not contribute substantially to later-stage events.

Previously, our group published a study in which daily Q-VD-OPh administration, beginning 6 hours before experimental aneurysm induction, successfully reduced AAA formation in the Angiotensin II (AngII) murine model. The AngII model is one of four common murine models which, at their final stages, resemble human aneurysm disease by displaying significant reduction in smooth muscle cell (SMC) density, severe elastin degradation, and substantial inflammatory infiltrate. Each of these four models, however, produces tissue damage, inflammation, and aneurysm through distinct approaches. It is unclear which of these approaches more closely resembles human aneurysm due largely to the lack of knowledge surrounding early pathological events in human. Thus, none of the currently available methods are considered entirely accurate depictions of the human disease, and a method of aneurysm intervention tested in one model may be ineffective in another model. We postulated that although each model possesses its own unique variation, they each depend on caspase activity

to instigate common pathological events such as inflammation and SMC depletion. The findings described in this study confirm that aneurysm induction via the AngII, CaPO4, and Elastase models all require caspase activity.

Our findings from early-administration studies showed that once Q-VD-OPh administration ceases, the rate of aneurysmal expansion in the Q-VD-OPh treated animals was restored to that seen in DMSO treated animals. Further, a previous publication showed that late-stage administration of Q-VD-OPh did not successfully inhibit aneurysm growth in the AngII model. In that study, we speculated that the aortic dissection characteristic of AngII-induced aneurysm brought the aneurysm to a 'point of no return', which prevented its growth from being altered by Q-VD-OPh. Thus, we wanted to test whether a non-dissecting model, the elastase model, could be inhibited by Q-VD-OPh. Ultrasound confirmed initial aneurysm expansion 7 days after surgery, at which time Q-VD-OPh administration began. Again, our data showed that Q-VD-OPh was unable to significantly alter aneurysm growth as compared to control injections.

These results, in conjunction with those previously described in the AngII model, suggest that caspase activity may only be important in the earliest stages of aneurysm development. That is, cellular apoptosis likely plays a role in initiating inflammation and extracellular matrix destruction in early aneurysmal disease. However, evidence provided here suggests that both inflammatory responses and elastin integrity change minimally as a result of caspase inhibition in small aneurysm. We believe the differential role of caspases in early and small aneurysm can be attributed to the inflammatory response. Specifically, we believe that cellular apoptosis

drives the inflammatory response in early stages of aneurysm formation, and thus administering Q-VD-OPh prior to aneurysm induction prevents these events from occurring. Conversely, small aneurysm contains an inflammatory cell presence sufficient to potentiate the further, additional inflammatory response necessary to expand the aneurysm. Interestingly, we have previously shown that supplying the inflammatory cytokine MCP-1 at the time of aneurysm induction is sufficient to induce aneurysm formation even in the absence of apoptosis[8].

One important consideration in this study is a non-localized administration of a pan-caspase inhibitor which, as suggested, inhibits activation of all caspases. This feature dictates that the specific cells in which apoptosis is effectively altered is not definitive. The caspase inactivation in our treated animals likely promotes the survival of smooth muscle cells and inflammatory cells. Elimination of specific subsets of inflammatory cells at different stages of atherosclerosis has been shown to have different outcomes[9]. Conversely, the promotion of inflammatory cell survival is likely to produce a unique outcome in our model. Interestingly, we did see an increase in the number of T lymphocytes in the Q-VD-OPh treated group. Caspases have also been shown to play a role in the production of cytokines, such as IL1-beta. Thus, the differential effects of Q-VD-OPh administration before or after small aneurysm formation cannot be strictly attributed to apoptotic functions. Moving forward, it may be valuable to focus on a method that specifically promotes survival of SMCs or prevents production of caspase-related cytokines.

The study we have described here focuses narrowly on caspase-mediated cell death and admittedly ignores the potential contributions of one or more additional cell death forms. For example, necrosis is a disorganized form of cell death which spills cellular contents to surrounding areas, potentiating substantial inflammation and additional tissue damage. Clarke et al. explored a somewhat related process termed 'secondary necrosis' which occurs when apoptotic cells are unsuccessfully cleared from tissue. This process is shown to be highly inflammatory and proatherogenic in mice. Each of these cell death forms are caspase independent and could account for the inflammatory cytokine production and inflammatory cell infiltration seen in experimental aneurysm tissues. Thus, it is possible that early administration of Q-VD-OPh is successful in inhibiting aneurysm formation because caspase-mediated cell death is important at early stages. Conversely, administration of Q-VD-OPh to small aneurysm could be unsuccessful in aneurysm growth inhibition because alternative forms of cell death such as necrosis and/or secondary necrosis dominate later stages of aneurysm growth. Additional studies will be needed to clarify the potential role(s) for these cell death forms.

The results presented in this study suggest that caspase activity is necessary for aneurysm development in at least three distinct models of murine aneurysm. In animals treated with the pan-caspase inhibitor, total apoptosis load is reduced and the inflammatory response is attenuated. Ultimately, these same animals develop smaller aneurysm, suggesting that these pathological features are crucial for aneurysm expansion. Additionally, our results suggest that the generalized inhibition of caspases alone may not be a feasible therapeutic

strategy for the prevention of AAA progression. However, a more specific and/or effective system for the preservation of the smooth muscle cell population may still be a viable option.

One approach toward ameliorating inflammation and apoptosis is the targeting of cellular stress response pathway components, such as the inflammasome. Recent studies have explored various strategies to manipulate the inflammasome, related-caspase activity, and specific inflammasome components[10-13]. In future studies, focusing on strategies such as these could prove effective in reducing the persistent inflammatory state noted in aneurysm tissues. Further, these strategies may aid in identifying suitable therapeutic targets for aneurysm treatment.

In summary, our data show that caspase activity is a vital pathological event in early stages of aneurysm development. Casapse activity in this environment appears to drive inflammatory cell death processes which in turn promote a substantial inflammatory response characteristic of aneurysm. Further, caspase-mediated cytokine production may be at least partially responsible for inflammation at this stage in the disease. At later stages of aneurysm progression, however, caspase activity is not necessary for aneurysm expansion. Taken together, we believe our results suggest that a broad-spectrum caspase inhibitor may not be a suitable therapeutic strategy for human aneurysm treatment. Instead, methods of interfering with the inflammatory process(es) taking place in aneurysm tissue may be more effective.

1. Daugherty A, Cassis LA. Mouse models of abdominal aortic aneurysms. *Arterioscler Thromb Vasc Biol*. 2004;24:429-434
2. Yamanouchi D, Morgan S, Stair C, Seedial S, Lengfeld J, Kent KC, Liu B. Accelerated aneurysmal dilation associated with apoptosis and inflammation in a newly developed calcium phosphate rodent abdominal aortic aneurysm model. *Journal of Vascular Surgery*. 2012;56:455-461
3. Pyo R, Lee JK, Shipley JM, Curci JA, Mao D, Ziporin SJ, Ennis TL, Shapiro SD, Senior RM, Thompson RW. Targeted gene disruption of matrix metalloproteinase-9 (gelatinase b) suppresses development of experimental abdominal aortic aneurysms. *The Journal of Clinical Investigation*. 2000;105:1641-1649
4. Henderson EL, Geng Y-J, Sukhova GK, Whittemore AD, Knox J, Libby P. Death of smooth muscle cells and expression of mediators of apoptosis by t lymphocytes in human abdominal aortic aneurysms. *Circulation*. 1999;99:96-104
5. Lopez-Candales A, Holmes D, Liao S, Scott M, Wickline S, Trompson R. Decreased vascular smooth muscle cell density in medial degeneration of human abdominal aortic aneurysms. *Am J Pathol*. 1997;150:993-1007
6. Yamanouchi D, Morgan S, Kato K, Lengfeld J, Zhang F, Liu B. Effects of caspase inhibitor on angiotensin ii-induced abdominal aortic aneurysm in apolipoprotein e-deficient mice. *Arterioscler Thromb Vasc Biol*. 2010;30:702-707
7. Tang XN, Berman AE, Swanson RA, Yenari MA. Digitally quantifying cerebral hemorrhage using photoshop® and image j. *Journal of Neuroscience Methods*. 2010;190:240-243
8. Morgan S, Yamanouchi D, Harberg C, Wang Q, Keller M, Si Y, Burlingham W, Seedial S, Lengfeld J, Liu B. Elevated protein kinase c-δ contributes to aneurysm pathogenesis through stimulation of apoptosis and inflammatory signaling. *Arteriosclerosis, Thrombosis, and Vascular Biology*. 2012;32:2493-2502
9. Andrés V, Pello OM, Silvestre-Roig C. Macrophage proliferation and apoptosis in atherosclerosis. *Current Opinion in Lipidology*. 2012;23:429-438 410.1097/MOL.1090b1013e328357a328379
10. López-Castejón G, Pelegrín P. Current status of inflammasome blockers as anti-inflammatory drugs. *Expert Opinion on Investigational Drugs*. 2012;21:995-1007
11. Martinon F, Burns K, Tschopp J. The inflammasome: A molecular platform triggering activation of inflammatory caspases and processing of proil-β. *Molecular Cell*. 2002;10:417-426
12. Taxman DJ, Huang MTH, Ting JPY. Inflammasome inhibition as a pathogenic stealth mechanism. *Cell Host & Microbe*. 2010;8:7-11
13. Zheng Y, Gardner SE, Clarke MCH. Cell death, damage-associated molecular patterns, and sterile inflammation in cardiovascular disease. *Arteriosclerosis, Thrombosis, and Vascular Biology*. 2011;31:2781-2786

Figure 1. Pan-caspase inhibitor prevents formation of aneurysm in the CaPO4 model.

The pan-caspase inhibitor Q-VD-OPh was administered daily beginning 6 hours before induction of aneurysm by the CaPO4 model. Tissues were harvested at 7 and 42 days after surgery. (A) Schematic of the experimental design. (B) Representative photos of abdominal aortas from PBS (control, left) and CaPO4 (right) treated mice, taken 42 days after treatment. Scale bar = 5mm. (C) Aortic dilation measured in CaPO4 treated tissues from DMSO (control, white bar) and Q-VD-OPh (black bar) groups 7 and 42 days after surgery. % Aortic dilation is calculated as described in methods. Aneurysm is defined as a 100% increase (dashed line). (D) Co-stain TUNEL (red) and SMCs (smooth muscle actin, SMA, green), overlay with DAPI (blue). Scale bar=150µm. (E) Quantification of cell death in aortic tissue as identified by TUNEL stain, expressed as TUNEL positive(+) cells/nuclei. *$*p<0.05$* compared to DMSO treated group, n=3. (F, H) IFC for neutrophils (Ly6G, green, F) and macrophages (Mac3, green, H), overlay with DAPI (blue). Scale bar=150µm. (G, I) Quantification of neutrophil (G) or macrophage (I) content in aortic tissue as identified by Ly6G or Mac3 staining, respectively, and quantified as positive(+) cells/nuclei. *$*p<0.05$* compared to DMSO treated group, n=3.

Figure 2. Pan-caspase inhibitor does not prevent expansion of established experimental aneurysm.

Q-VD-OPh was administered every 48hours beginning 7 days after experimental aneurysm induction. Ultrasound was used to monitor expansion of aortic diameter. (A) Schematic of the experimental design. (B) Ultrasound image depicting method for measuring aortic diameter. Detailed description in methods. (C) Representative ultrasound images from heat inactivated

elastase (IE) or elastase (E) treated arteries. 14 day images are subdivided to DMSO and Q-VD-OPh treated groups. (D) Aortic measurements taken from ultrasound images. *$p<0.05$*.

Figure 3. Effective inhibition of cell death in established small aneurysm does not alter additional aneurysm features.

Heat inactivated elastase (IE) and elastase (E) treated tissues receiving either Q-VD-OPh or DMSO control were harvested 14 days after surgery for histological analysis. (A) Representative photos of 14 day aortic sections stained for elastin (Van-Gieson), scale bar=100µm. (B) Quantification of cell death in aortic tissue as identified by TUNEL stain, expressed as TUNEL positive (TUNEL+)/nuclei. *$p<0.05$.* (C) Co-stain TUNEL (red) overlay with DAPI (blue). Scale bar=100µm. (D) Quantification of macrophage content in aortic tissue as identified by CD68 stain, expressed as CD68(+)/nuclei. *$p<0.05$.* (E) Immunohistochemical (IHC) stain for macrophages (CD68+), scale bar=100µm.

Figure 4. Pan-caspase inhibition has differential effects on inflammatory cell populations.

Heat inactivated elastase (IE) and elastase (E) treated tissues receiving either Q-VD-OPh or DMSO control were harvested 14 days after surgery for histological analysis. (A,C,E) Quantification of leukocyte (A), neutrophil (C), and T lymphocyte (E) infiltration to aortic tissue as identified by CD45, Ly6G, and CD3 stains, respectively, and expressed as positive cell (+)/nuclei. *$p<0.05$.* (B,D,F) IHC stain for leukocyte (B), neutrophil (D), and T lymphocyte (F), scale bar=100µm.

Figure 1.

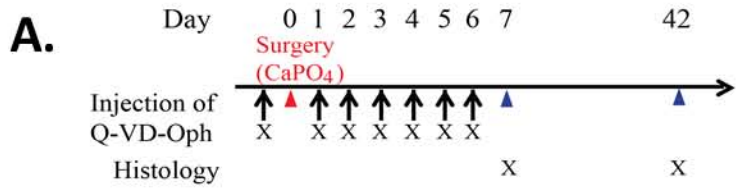
A.
Day
0 1 2 3 4 5 6 7
42
Surgery
(CaPO4)
Injection of
Q-VD-Oph
X X X X X X X
Histology
X
X

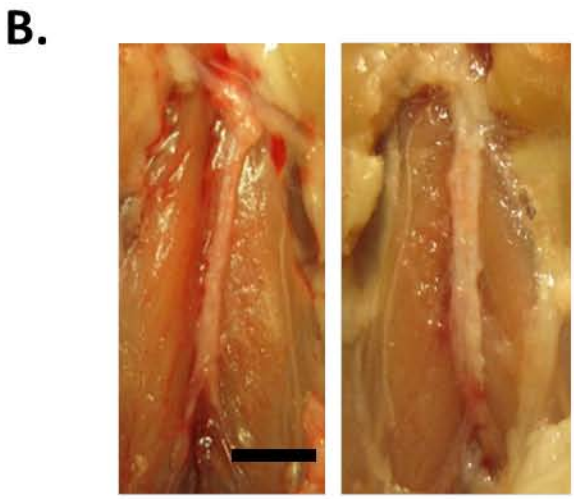
B.

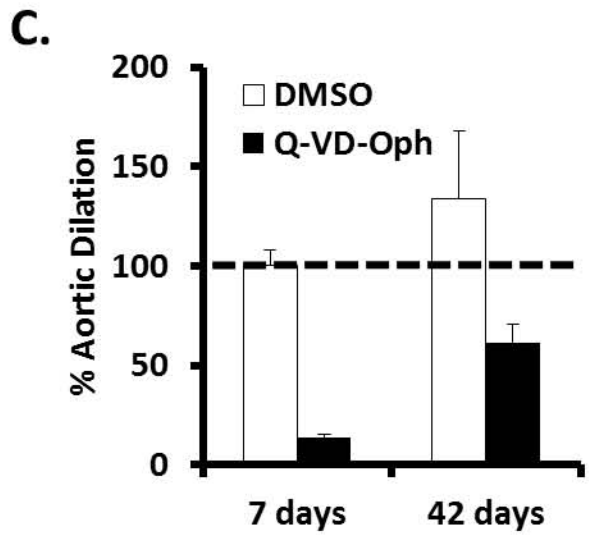
C.
200
150
100
50
0
% Aortic Dilation
DMSO
Q-VD-Oph
7 days
42 days

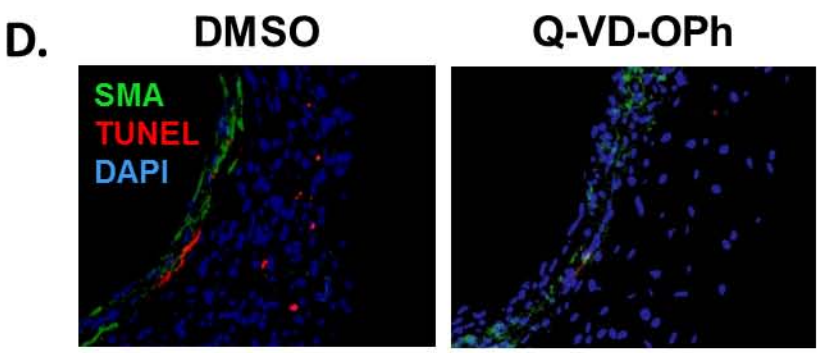
D.
DMSO
Q-VD-OPh
SMA
TUNEL
DAPI

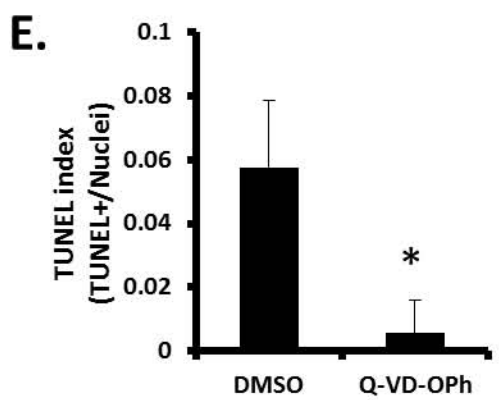
E.
0.1
0.08
0.06
0.04
0.02
0
TUNEL index
(TUNEL+/Nuclei)
*
DMSO
Q-VD-OPh

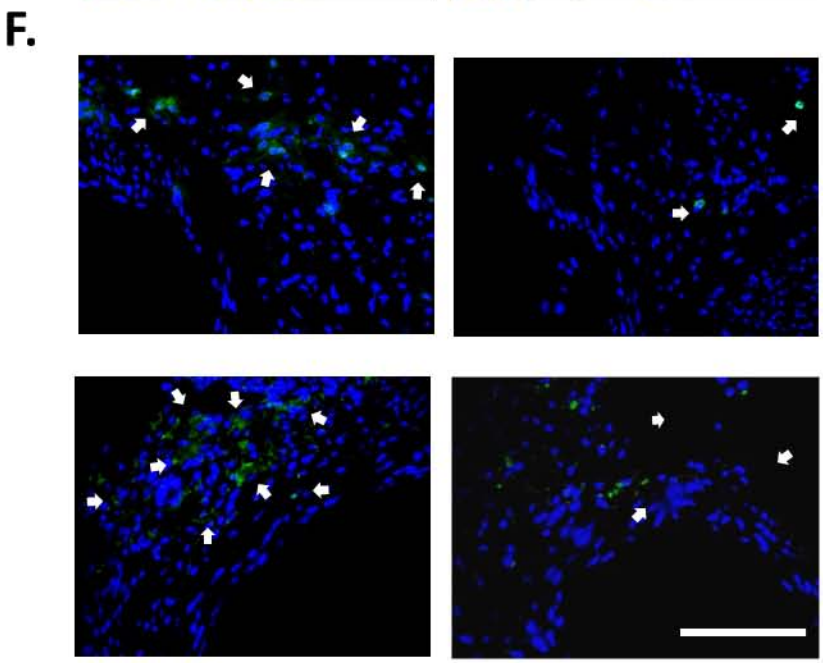
F.

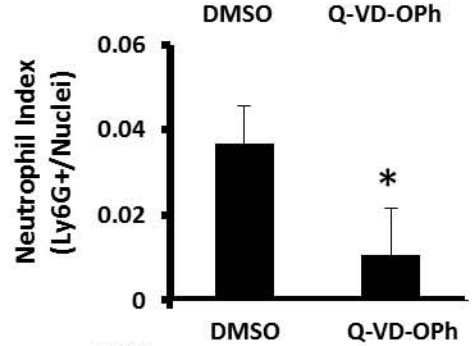
0.06
0.04
0.02
0
Neutrophil Index
(Ly6G+/Nuclei)
*
DMSO
Q-VD-OPh

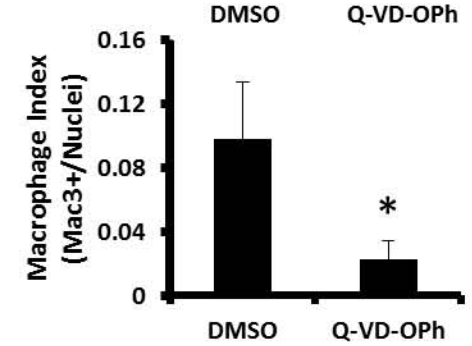
0.16
0.12
0.08
0.04
0
Macrophage Index
(Mac3+/Nuclei)
*
DMSO
Q-VD-OPh

Figure 2.

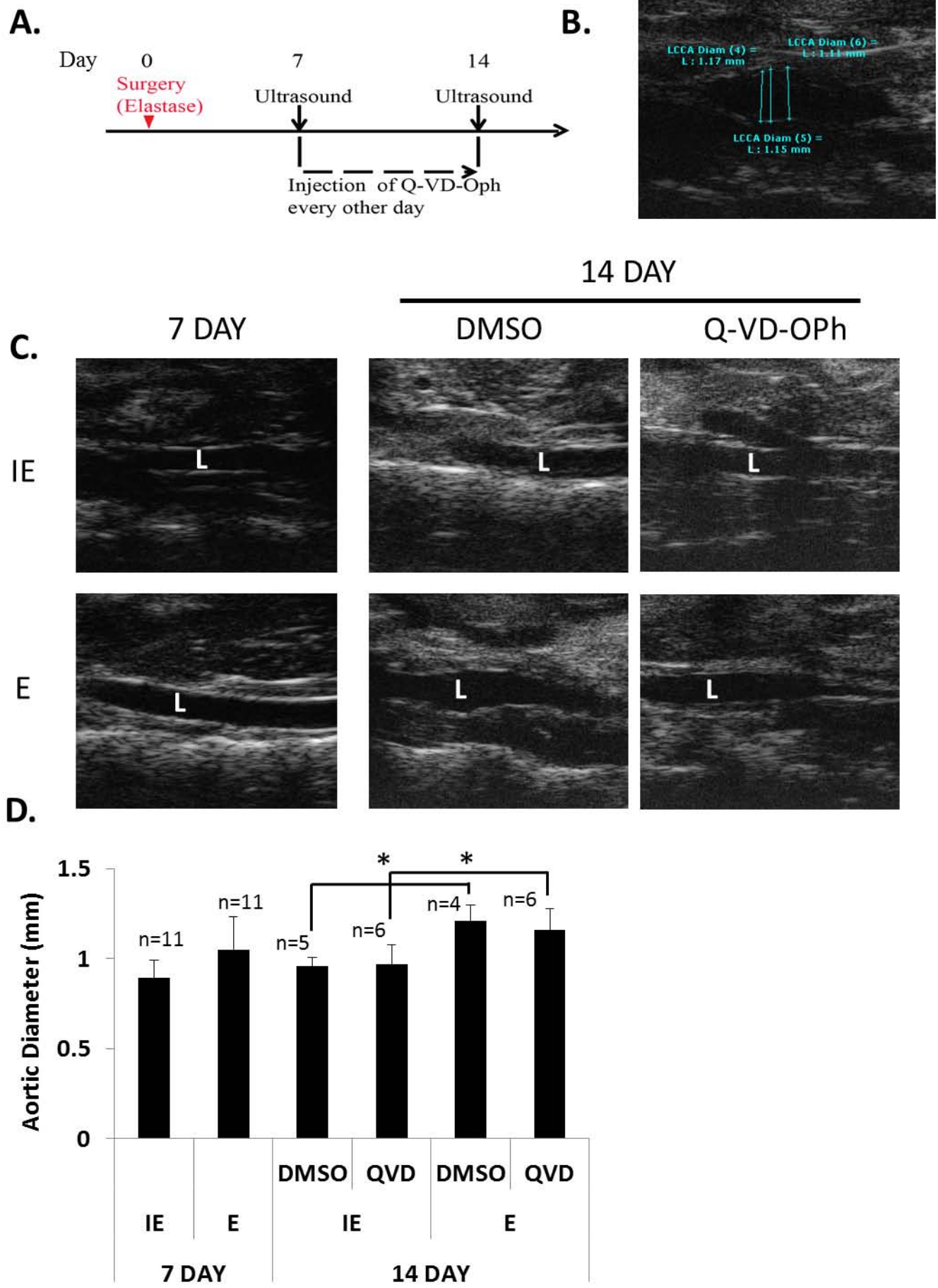
A.
Day
0
7
14
Surgery
(Elastase)
Ultrasound
Ultrasound
Injection of Q-VD-Oph
every other day
B.
LCCA Diam (4) =
L : 1.17 mm
LCCA Diam (6) =
L : 1.11 mm
LCCA Diam (5) =
L : 1.15 mm
C.
7 DAY
14 DAY
DMSO
Q-VD-OPh
IE
E
L
D.
Aortic Diameter (mm)
1.5
1
0.5
0
n=11
n=11
n=5
n=6
n=4
n=6
*
*
DMSO
QVD
DMSO
QVD
IE
E
IE
E
7 DAY
14 DAY

Figure 3.

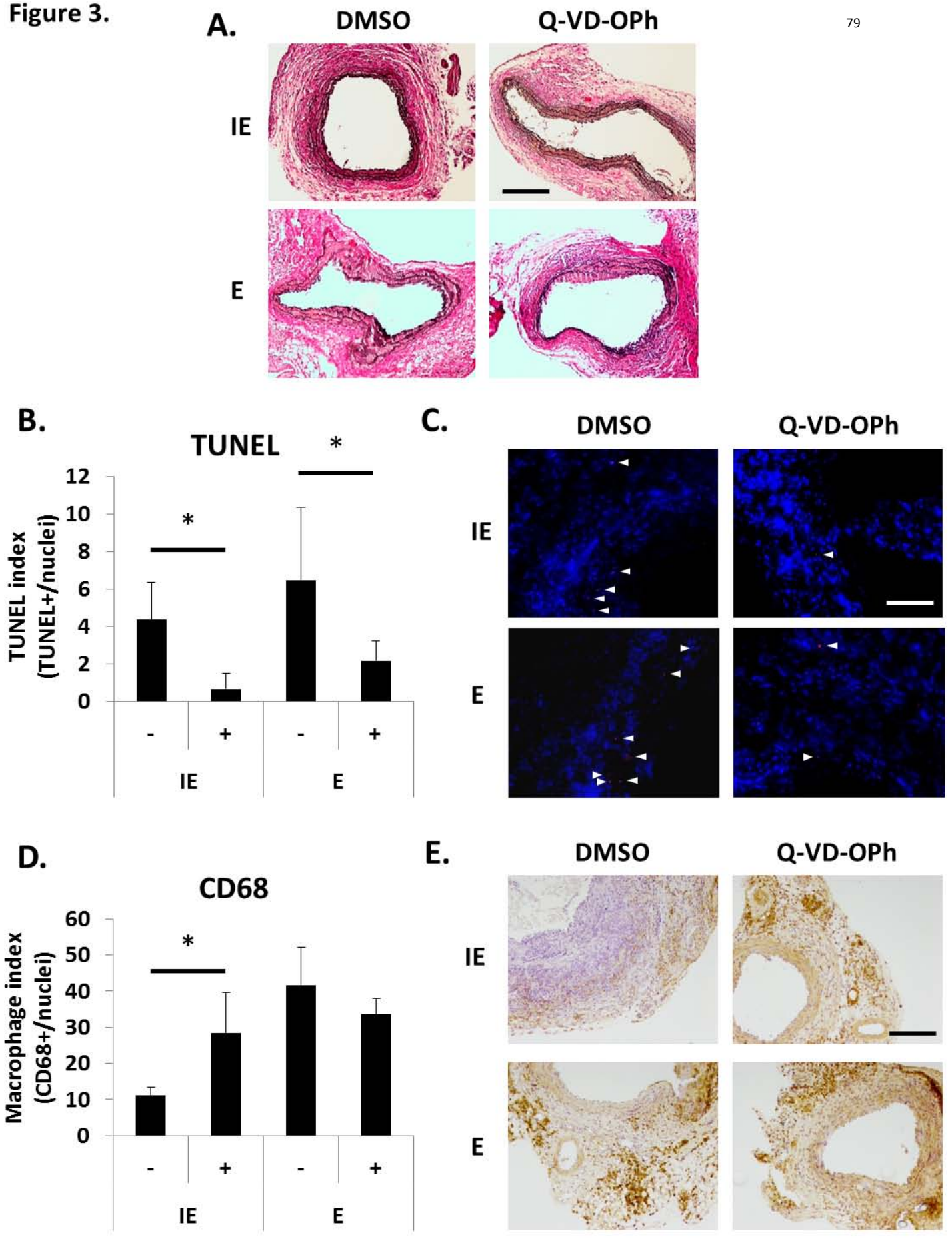
A.
DMSO
Q-VD-OPh
IE
E
B.
TUNEL
*
*
*
TUNEL index
(TUNEL+/nuclei)
12
10
8
6
4
2
0
-
+
-
+
IE
E
C.
DMSO
Q-VD-OPh
IE
E
D.
CD68
*
Macrophage index
(CD68+/nuclei)
60
50
40
30
20
10
0
-
+
-
+
IE
E
E.
DMSO
Q-VD-OPh
IE
E

Figure 4.

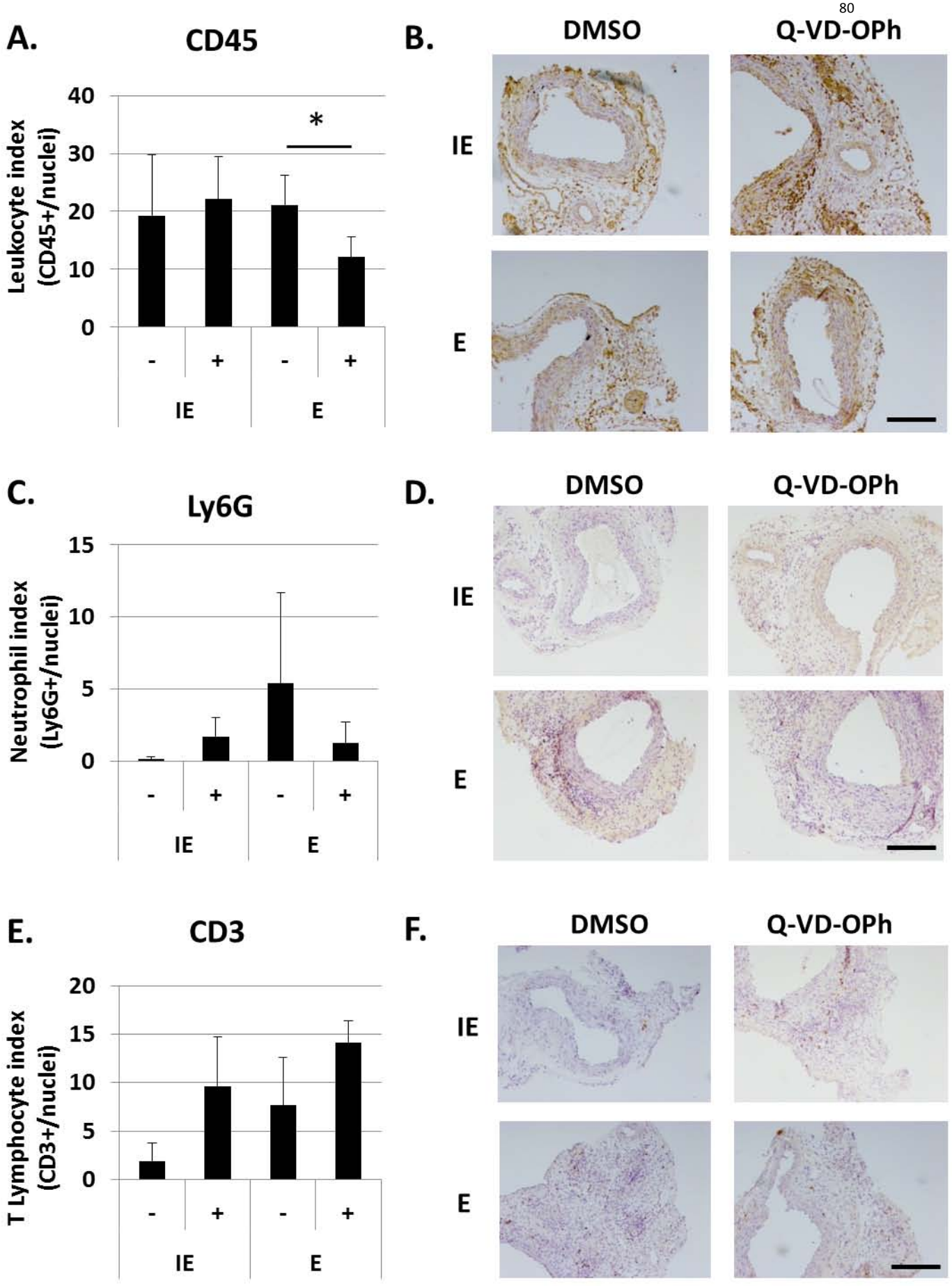
A.
CD45
Leukocyte index (CD45+/nuclei)
40
30
20
10
0
*
-
+
-
+
IE
E
B.
DMSO
Q-VD-OPh
IE
E
C.
Ly6G
Neutrophil index (Ly6G+/nuclei)
15
10
5
0
-
+
-
+
IE
E
D.
DMSO
Q-VD-OPh
IE
E
E.
CD3
T Lymphocyte index (CD3+/nuclei)
20
15
10
5
0
-
+
-
+
IE
E
F.
DMSO
Q-VD-OPh
IE
E

Supplemental Figure 1. Additional aneurysm features mediated by early administration of pan-caspase inhibitor in the CaPO4 model.

(A) Representative images of 42 day aortic section stained for elastin (Van-Gieson), scale bar=150µm. (B) Co-stain T lymphocyte (CD3) marker overlay with DAPI (blue), scale bar=150µm.

Supplemental Figure 2. Pan-caspase inhibition prevents aneurysm growth in the elastase model.

(A) Schematic of the experimental design. (B) Aortic dilation measured 7 days after elastase treatment in animals receiving either DMSO or Q-VD-OPh injections. % Aortic dilation is calculated as described in methods. Aneurysm is defined as a 100% increase (dashed line). (C) Co-stain TUNEL (red) overlay with DAPI (blue), scale bar=100µm. (D) Co-stain CD68 (green) overlay with DAPI (blue), scale bar=100µm.

Supplemental Figure 1

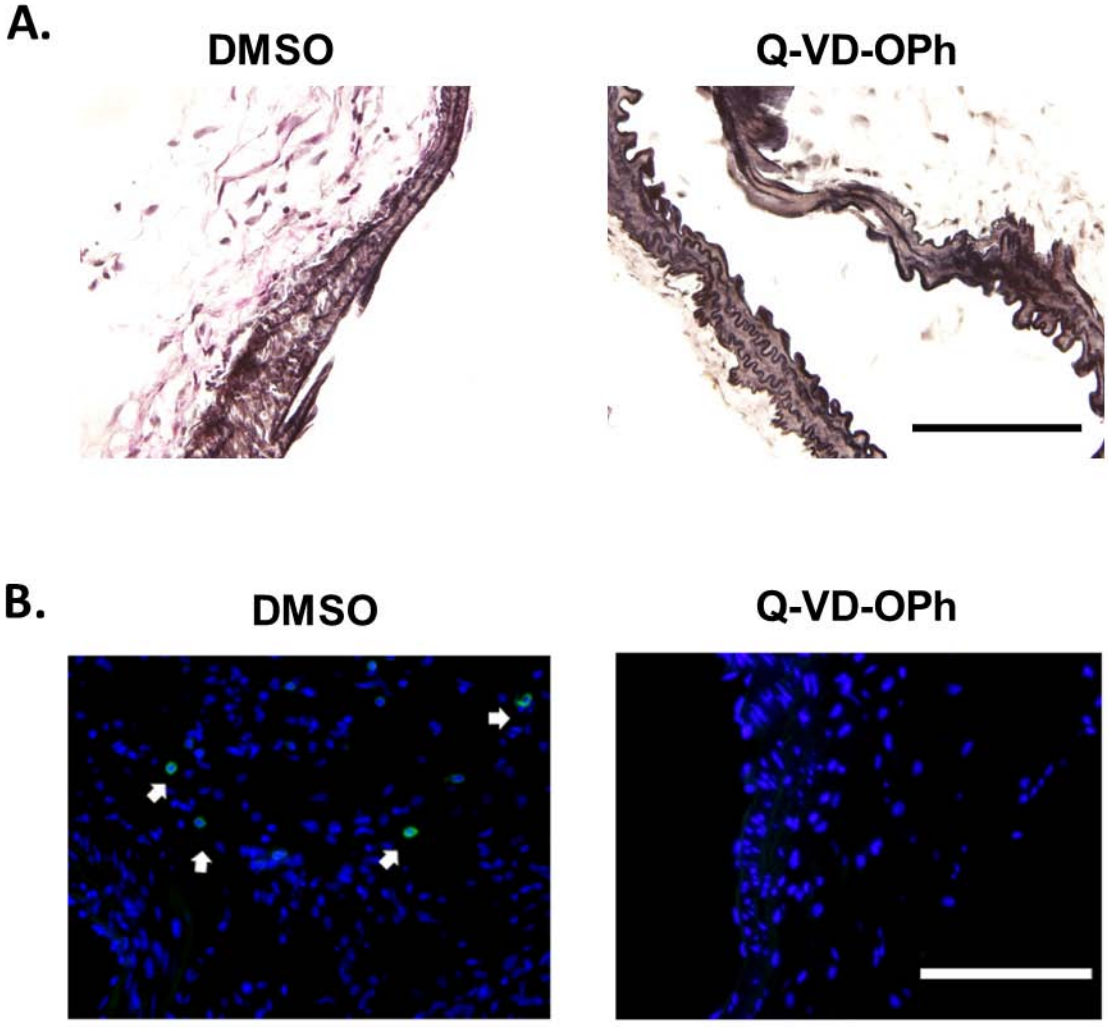

Supplemental Figure 2

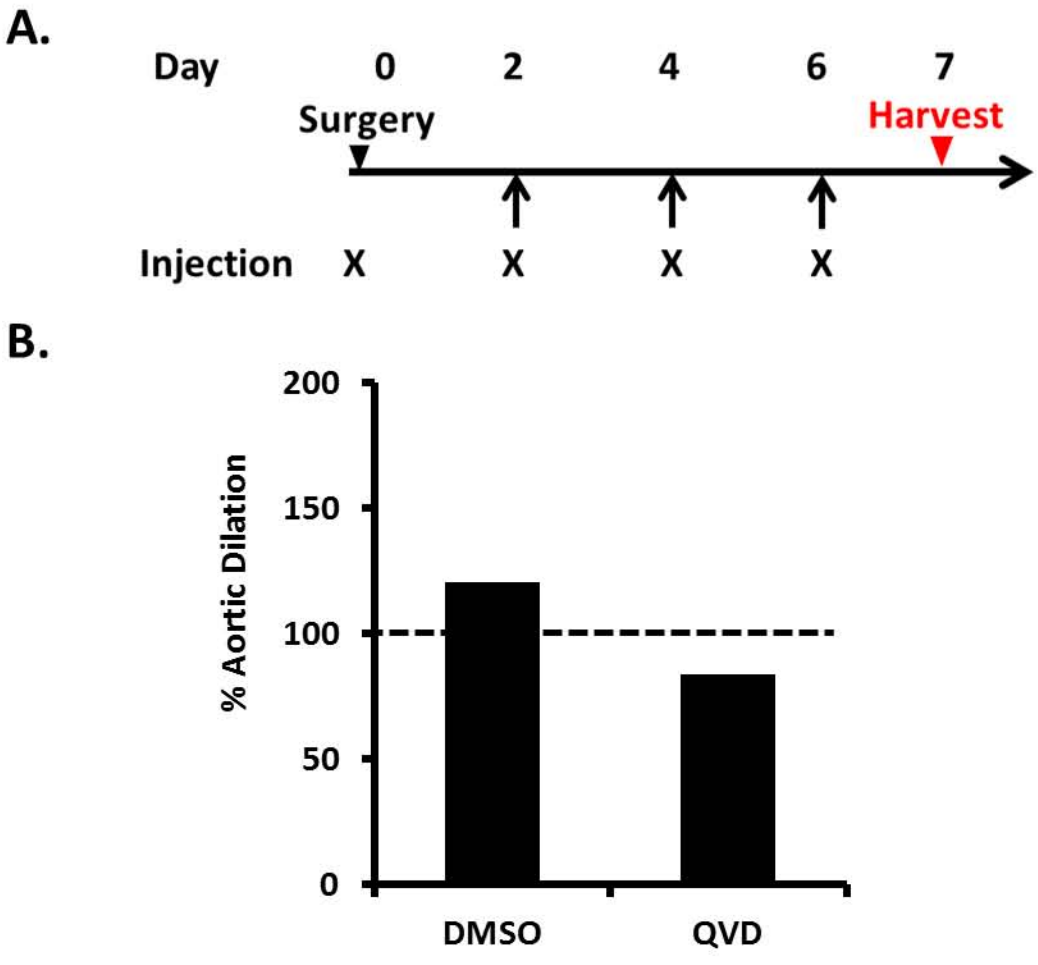

Transition II

Results from Chapter 2 provide two insights: (1) that caspase-mediated cell death is an important event that likely drives inflammation and tissue degradation in early aneurysm development, and (2) this role for caspase-mediated cell death does not exist in established aneurysm tissues.

Moving forward, we sought to further explore the role for cell death in early aneurysm by asking whether augmenting apoptosis in early aneurysm would create a larger aneurysm. We hypothesized that modification of an existing mouse model of aneurysm to promote greater levels of cell death would in turn promote a more dramatic inflammatory response and ultimately a larger aneurysm.

Chapter 3: "Accelerated Aneurysmal Dilation Associated with Apoptosis and Inflammation in a Newly Developed Calcium Phosphate Rodent Abdominal Aortic Aneurysm Model"

Published in Journal of Vascular Surgery 2012; 56(2): 455-461

Accelerated Aneurysmal Dilation Associated with Apoptosis and Inflammation in a Newly Developed Calcium Phosphate Rodent Abdominal Aortic Aneurysm Model

Dai Yamanouchi*, Stephanie Morgan*, Colin Stair, Stephen Seedial, Justin Lengfeld, K. Craig Kent, and Bo Liu

Division of Vascular Surgery, Department of Surgery, University of Wisconsin School of Medicine and Public Health, 600 Highland Avenue, Madison, WI 53792

Abstract

Objective

The Calcium Chloride ($CaCl_2$) model is a widely accepted rodent model for abdominal aortic aneurysm (AAA). Calcium deposition, mainly consisting of calcium phosphate ($CaPO_4$) crystals, has been reported to exist in both human and experimental aneurysms. $CaPO_4$ crystal has been utilized for in vitro DNA transfection by mixing $CaCl_2$ and Phosphate Buffered Saline (PBS). Here, we describe accelerated aneurysm formation resulting from a modification of the $CaCl_2$ model.

Methods

The modified $CaCl_2$, the $CaPO_4$ model, was created by applying PBS onto the mouse infrarenal aorta after $CaCl_2$ treatment. Morphological, histological and immunohistochemical analyses were performed on arteries treated with both the $CaPO_4$ model and the conventional $CaCl_2$ model as control. *In vitro* methods were carried out using a mixture of $CaCl_2$ and PBS to create $CaPO_4$ crystals. $CaPO_4$ induced apoptosis of primary cultured mouse vascular smooth muscle cells (VSMCs) was measured by DNA fragmentation ELISA.

Results

First, we showed that the $CaPO_4$ model produces AAA, defined as an increase of 50% or greater in the diameter of the aorta; faster than in the $CaCl_2$ model. $CaPO_4$ model showed significantly larger aneurysmal dilation at 7, 28, and 42 days as reflected by a maximum diameter fold change (measured in mm) of 1.69 ± 0.07, 1.99 ± 0.14 and 2.13 ± 0.09 as opposed to 1.22 ± 0.04, 1.48 ± 0.07 and 1.68±0.06 as seen in $CaCl_2$ model, respectively (n=6; $P<0.05$). A semi-quantitative grading analysis of elastin fiber integrity at 7 days revealed a significant increase in elastin degradation in the CaPO4 model as compared to $CaCl_2$ model (2.7±0.2 vs 1.5±0.2,

$p<0.05$, n=6). Significantly higher level of apoptosis occurred in the $CaPO_4$ model (apoptosis index at 1, 2, and 3 days post-surgery: 0.26 ± 0.14, 0.37± 0.14, and 0.33 ± 0.08 for $CaPO_4$ model and 0.012 ± 0.10, 0.15± 0.02, and 0.12 ± 0.05 for conventional $CaCl_2$ model) (n=3; $p<0.05$). An enhancement of macrophage infiltration and calcification was also observed at 3 and 7 days in $CaPO_4$. $CaPO_4$ induced approximately 3.7 times more apoptosis in VSMCs when compared to a mixture of $CaCl_2$ (n=4; $p<0.0001$) *in vitro*.

Conclusion

Our data shows that the $CaPO_4$ model accelerates aneurysm formation with the enhancement of apoptosis, macrophage infiltration and calcium deposition. This modified model, with its rapid and robust dilation, can be utilized as a new model for AAA.

Introduction

Abdominal aortic aneurysm (AAA) is a common vascular disease associated with high mortality. Aneurysm results from the culmination of a series of events that lead to disruption of structural integrity and segmental weakening of the abdominal aortic wall. AAA is the 10th leading cause of death in men over the age of fifty-five and claims as many as 30,000 deaths each year in the US[1]. It is estimated that the prevalence of AAA increases continuously in men over the age of 55 and reaches a peak of more than 10% in those 80 to 85 years old[2].

Several animal models have been created to aid investigation of pathophysiological events underlying human AAA, including models dependent upon genetic and/or chemical manipulation[3]. Genetic manipulations are often associated with defects in extracellular matrix maturation, disruption of lipid homeostasis, or alteration of angiotensin enzymes[4-7]. The chemically-induced aneurysm approaches include the intraluminal infusion of elastase and the periaortic application of calcium chloride ($CaCl_2$). A third chemical approach combines chemical and genetic approaches, using a systemic infusion of angiotensin II to mice genetically altered to compromise lipid homeostasis such as mice deficient in Apolipoprotein E (Apo E) or Low Density Lipoprotein (LDL) receptor[8-11].

Aneurysmal changes in the carotid artery of hyperlipidemic rabbits resulting from periaortic application of $CaCl_2$ was first described by Gertz, SD et al[12]. This method was later applied in the abdominal aortas of hyperlipidemic rabbits in combination with thioglycollate, as reported by Freestone et al[13] and subsequently adapted to mice [10, 14]. Typically, by applying $CaCl_2$ soaked gauze to the infrarenal aorta for 15- 20 minutes, one can reproducibly generate a aneurysmal dilation in the treated aortic segment within 4-6 weeks[14, 15]. This model does not

require the use of genetically modified mice. Similar to the elastase-induced mouse aneurysm, $CaCl_2$-induced aneurysmal dilation is accompanied by the depletion of medial layer smooth muscle cells, as well as elastin degradation, infiltration of lymphocytes and macrophages, elevation of pro-inflammatory cytokines and the increased activation of matrix metalloproteinases (MMPs) [10, 14, 15].

The mechanism by which adventitial application of $CaCl_2$ causes the above described molecular and cellular changes in the aortic wall is not entirely clear. Previous findings have identified calcium ion binding sites on both collagen and elastin, suggesting that $CaCl_2$ application may facilitate the degradation of these major arterial structure components[16]. Our own group has identified significant calcification also occurring in $CaCl_2$-treated arteries, mainly in the medial layer. We hypothesized that this calcification may also contribute to aneurysm formation, and explored the formation of these calcification deposits. Calcium phosphate ($CaPO_4$) crystals have been identified as the major component of calcification found in atherosclerosis[17-19], and have been suggested to have significant proinflammatory effects, induce apoptosis in various cell types, and stimulate production of pro-inflammatory cytokines from monocytes/macrophages and smooth muscle cells (SMCs)[20, 21].

In the current study, we tested whether calcium phosphate is a more potent stimulus than calcium chloride in stimulation of apoptosis and induction of inflammatory cytokines. Based on the $CaPO_4$ based cell transfection method, we adapted a method of calcium phosphate generation *in vivo* through a sequential application of $CaCl_2$ and phosphate buffered saline (PBS).[22-24] Compared to application of $CaCl_2$ alone, the sequential application of $CaCl_2$ and PBS produces a more severe, rapid dilation of the aneurysmal artery associated with

significantly enhanced smooth muscle apoptosis and inflammatory responses. While future studies are necessary to determine how this new method, termed the $CaPO_4$ model, may cause arterial injury, its rapid induction of aneurysmal dilation is advantageous and could be used as an additional rodent model in studies of AAA.

Materials and Methods

General Materials

Dulbecco's Modified Eagles Medium (DMEM) and cell culture reagents were from Gibco BRL Life Technologies. Chemicals, if not specified, were purchased from Sigma Chemical Co.

Mouse Models of AAA

Male C57BL/6 mice, 12 weeks of age, were purchased from Jackson Laboratory (Bar Harbor, ME). All mice had free access to a normal diet and water. $CaPO_4$ induced abdominal aortic aneurysm model were created through a method closely resembling the $CaCl_2$ induced model as described by Gertz et al.[25] Under the general anesthesia, midline incision was made and the infrarenal region of the abdominal aorta was isolated. A small piece of gauze soaked in 0.5M $CaCl_2$ was applied perivascularly for 10 minutes. This gauze is then replaced with another piece of phosphate buffered saline (PBS)-soaked gauze for 5 minutes. $CaCl_2$ induced aneurysm was created through a similar manner but with a single treatment of 0.5M $CaCl_2$ soaked gauze for 15 minutes. Histological analyses suggest that vascular injury appears to be more severe at the anterior surface where arterial tissue comes in contact with gauzes. Control mice received a single treatment of 0.5M Sodium Chloride (NaCl) soaked gauze for 15 minutes. The maximum external diameter of the infrarenal aorta was measured using a digital caliper (VWR Scientific, Radnor, PA) prior to treatment and at the time of tissue harvest. At selected time points, mice were sacrificed and tissues were perfusion-fixed with a mixture of 4% paraformaldehyde (PFA) in PBS at physiological perfusion pressure. Harvested tissue was further fixed in 4% PFA and imbedded in O.C.T. Compound (Sakura Tissue Tek, Netherlands). All sections were cut 6µm thick using a Leica CM3050S cryostat. All animal procedures were conducted in accordance with

experimental protocols that were approved by the Institutional Animal Care and Use Committee at the University of Wisconsin, Madison (Protocol M02284).

Histology and Immunohistochemistry

Van Geison stains were carried out using Chromaview Van Gieson kit (Richard Allan Scientific, Kalamazoo, MI) according to provided protocol. Elastin integrity was quantified using a grading system as described by Kitamonto et al: (1, no elastin degradation or mild elastin degradation; 2, moderate; 3, moderate to severe; and 4, severe elastin degradation).[26] Each section was numbered and photographed at 10x or 20x magnification, maintaining their respective numbers. Then, an objective participant graded the photographs according to the aforementioned scale and recorded the grade with the section number. Calcification was detected using Alizarin Red (Ricca Chemical Company; Arlington, TX). Quantification of calcium content was calculated using ImageJ Software as provided by the National Institutes of Health. Total area of calcified media (stained red) was calculated and divided by total medial area of the artery to yield the reported ratio(s).

For additional immunohistochemistry, arterial sections were permeabilized with 0.1% TritonX for 10 minutes at room temperature. Non-specific sites were blocked using 5% bovine serum albumin (BSA), 3% normal donkey serum in Tris-buffered Saline and Tween 20 (TBS-T) for 1 hour at room temperature. Primary antibodies to CD3, MCP-1, and Mac3 were purchased from Santa Cruz (Santa Cruz, CA), MOMA2 was purchased from Abcam (Cambridge, MA), Cleaved Caspase 3 (CC3) was purchased from Cell Signaling Technology (Boston, MA), and Smooth muscle alpha-actin (SMA) was purchased from Sigma-Aldrich (St. Louis, MO). Primary antibodies were diluted in previously described blocking solution and incubated overnight at

4°C. Apoptosis was identified through Terminal deoxynucleotidyl transferase dUTP nick end labeling (TUNEL) in an *In Situ* Cell Death Detection Kit (Roche, Indianapolis, IN), carried out according to kit directions. Fluorescent stains were completed using secondary antibodies purchased from Invitrogen Molecular Probes (Carlsbad, CA) and 4'6-diamidino-2-phenyl-indole, dihydrochloride (DAPI, Invitrogen, Carlsbad, CA) was used to detect nuclei. Staining was visualized with a Nikon Eclipse E600 upright microscope and digital images were acquired using a RetigaEXi CCD digital camera. Quantification of stains was performed in a manner to that previously described [27] using Image J Software. Data quantification was performed using at least 3 sections per artery.

Cell Culture

Primary mouse aortic SMCs from the aorta of C57BL/6 mice were isolated based on a protocol described by Clowes et al [28]. Briefly, aortas were perfused with PBS supplemented with 2% penicillin/streptavidin antibiotics. The aorta was isolated from the aortic arch to the iliac bifurcation and incubated 30 minutes in digestion buffer at 37°C. Adventitia was pulled away from the medial layer, tissues were minced, and further incubated for 4 hours at 37°C. Cells isolated from medial layer of individual mice were kept in separate dishes to allow a biological replicate from each animal. Tissue was spun to a pellet by centrifugation and washed with 10% FBS DMEM once, then suspended in a small volume of 10%FBS-DMEM and left undisturbed for 48 hours to allow cells to migrate from tissue. All cell types were maintained in DMEM supplemented with 10% fetal calf serum (FCS), 100 units/mL penicillin, and 100µg/mL streptomycin in a 5% CO_2/water-saturated incubator at 37°C.

In vitro $CaCl_2$ and $CaPO_4$ Treatments

10% FBS DMEM was replaced with 0.5% FBS DMEM 24 hours prior to all cell treatment. Cells designated for $CaCl_2$ treatment were washed with normal saline twice before being treated with $CaCl_2$ (final concentration 0.05M) diluted in normal saline. Treated cells were incubated at 37°C for 15 minutes, $CaCl_2$ solution was removed and cells were washed twice with 10%FBS DMEM and let rest 6 hours at 37°C. Cells designated for $CaPO_4$ treatment were washed twice with 1x PBS before being treated with $CaCl_2$ (final concentration 0.05M) diluted in 1x PBS for 15 minutes. The remainder of the treatment method was the same as the $CaCl_2$ group.

DNA Fragmentation ELISA

In vitro detection of apoptosis via fragmented DNA labeling was carried out using the Cell Death Detection ELISA kit (Roche, Indianapolis, Indiana) according to manufacturer's protocol.

Flow Cytometric Analysis

Apoptotic populations in treated cell groups were assessed by flow cytometry using a PE Annexin V Apoptosis Detection Kit (BD Pharmigen, San Diego, CA). Flow cytometric data was collected on a BD FACS Calibur Flow Cytometer equipped with a Cytek 633nm laser (Freemont, CA) and analysis was performed using Flow Jo software (TreeStar, Inc.).

Statistical analysis

Values were expressed as means ± standard error. Experiments were repeated at least three times unless stated otherwise. Differences between 2 groups were analyzed by Student's t test, and one-way analysis of variance (ANOVA) followed by Scheffe's test was used for multiple comparisons. Values of $P<0.05$ were considered significant.

Results

Calcium phosphate induces apoptosis in aortic SMCs

Primary cultured mouse aortic SMCs were treated with either $CaCl_2$ or $CaPO_4$; control SMCs were similarly treated with normal saline. At the end of treatment, cells were placed into normal growth media for 6 hours before being subjected to apoptotic evaluation. Analyses of DNA fragmentation indicated the presence of apoptotic cells in both $CaCl_2$- and $CaPO_4$-treated cells, however, $CaPO_4$ induced approximately 3.7 times more apoptosis of SMCs compared to $CaCl_2$ ($P<0.0001$) (Fig. 1A). Detailed cell profiling via FACS analysis showed that the majority of dead cells in the $CaCl_2$-treated group stained positive for both Annexin V and 7 AAD, indicating secondary necrosis. On the other hand, the majority of dead cells in the $CaPO_4$-treated group stained positive only for Annexin V, indicating apoptosis to dominate this treatment group (Fig. 1B and Table 1).

$CaPO_4$ exacerbates aneurysm formation in mice

To facilitate $CaPO_4$ crystal formation *in vivo*, we sequentially applied $CaCl_2$ and PBS, or $CaCl_2$ alone as a control, to the adventitial surface of mouse abdominal aorta. Mice were sacrificed at designated time points following the injury and the maximum diameter of the aortas was measured. Aneurysm development was assessed by determining the fold change in diameter, calculated as the post-surgical measurement divided by the diameter measured prior to injury. As shown in Fig. 2, the aortas treated by $CaPO_4$ showed significantly larger aneurysmal dilation at 7, 28 and 42 days as reflected by a maximum diameter fold change of 1.69 ± 0.07, 1.99 ± 0.14 and 2.13 ± 0.09 as opposed to 1.22 ± 0.04, 1.48 ± 0.07 and 1.68 ± 0.06 as seen in $CaCl_2$ model, respectively ($n=6$; $P<0.05$) (Fig 2A and B). The van Gieson staining of the aortic wall

at day 7 showed more fragmentation of the elastin layer in $CaPO_4$ treated aorta (Fig. 2C). A semi-quantitative grading analysis of elastin fiber integrity at 7 days revealed a significant increase in elastin degradation in the $CaPO_4$ model as compared to $CaCl_2$ model (Fig. 2D).

Calcium phosphate intensifies apoptosis in aneurysmal arteries

Next, we compared the magnitude of apoptosis following aneurysm induction with either $CaCl_2$ or $CaPO_4$ by harvesting arteries at 1, 2 and 3 days post-injury. Apoptosis in the aortic wall was evaluated by TUNEL staining at each time point. As demonstrated by representative image and graphical depiction, $CaPO_4$ injury induced significantly more apoptosis than $CaCl_2$ injury at 2 and 3 days post-injury (Fig. 3A and B, respectively). Most of the apoptotic cells were noted in the media and localized to cells that were positive for smooth muscle specific alpha actin (SMA) (Supp. Fig. 1).

Calcium phosphate-induced aneurysm is associated with inflammation and medial calcification

A prevalent feature of human and experimental aneurysms is significant inflammatory infiltrate. We have previously reported a relationship between apoptosis of SMCs and the inflammatory response(s) leading to the infiltration of macrophages and other inflammatory cells to the aortic wall[29]. At this notion, $CaPO_4$-treated arteries were stained for the presence of macrophages, as identified by the marker CD68. Representative images found in Figure 4A depict $CaPO_4$-treated arteries harvested 3 days after injury, showing significant macrophage infiltration. Figure 4B shows graphical representation of macrophage infiltration as determined by CD68 positive cells divided by total nuclei. Supplemental Figure 2 depicts additional inflammatory markers in day 3 $CaPO_4$-treated arteries. Macrophage marker Mac3, T

lymphocyte marker CD3, and the inflammatory cytokine monocyte chemoattractant protein-1 (MCP-1) evidenced a significant inflammatory response. Using cleaved (activated) caspase 3 as a marker for apoptosis, we evaluated the spatial relationship between apoptosis and inflammation. As shown in Supplemental Figure 3 A, monocytes and Macrophages, marked by MOMA, localized mostly in the adventitia. Using cleaved or activated caspase 3 as a marker for apoptosis, we found that the majority of monocytes and macrophages at this time point were not apoptotic, however, they tended to concentrate in areas proximal to apoptotic cells (Supp. Fig. 3).

Significant calcification in $CaPO_4$ treated arteries was easily noted visually and tactilely at the time of artery harvest. Cross sections of the aortas receiving treatment with either $CaCl_2$ or $CaPO_4$ injury were stained with Alizarin Red staining according to manufacturer's protocol. $CaPO_4$ injury caused pronounced medial calcification appearing around 48 hours post-injury, and maximizing around 7 days (Fig. 5A and B).

Discussion

Animal models of AAA have been utilized in a range of experiments to explore various aspects of AAA pathogenesis as well as potential methods of AAA treatment. Here, we reported the creation of mouse experimental AAA model with rapid and robust aneurysmal dilationdilation through sequential adventitial application of $CaCl_2$ and PBS. This modified $CaCl_2$ model, or the $CaPO_4$ model, displayed similar pathological and histological characteristics as the previously described $CaCl_2$ but at a higher magnitude.

We postulate that adventitial insult in the form of $CaCl_2$ application causes a series of tissue degenerative events, at least in part through formation of $CaPO_4$ crystals. This argument is supported by our finding that $CaCl_2$ did not cause significant degree of apoptosis or necrosis when applied to cultured mouse aortic SMCs. In contrast, cultured mouse aortic SMCs responded to $CaPO_4$ with massive apoptosis, findings consistent with reports from other groups[30-32].

Although the creation of aneurysm phenotype with either $CaCl_2$ or $CaPO_4$ is artificial, atherosclerotic calcification has been shown to consist mainly of $CaPO_4$ crystals, which is typically seen in the intimal and medial layer of the diseased human aorta[18 19, 33]. We did observe medial calcification in the arterial segments that sustained the $CaCl_2$ or $CaPO_4$ insult. Although substantial calcification is noted in these arteries by both tactile and immunohistochemical methods, the biological mechanisms underlying this ectopic calcification have yet to be identified. Thus, future studies may lend insight to these processes through identification of calcification regulating genes such as osteopontin.

Interestingly, robust apoptosis and calcification was observed in the medial layer of the aorta starting at around 2 days after surgery, a time point the elastin fibers appeared grossly intact.

A potential causal relationship between apoptosis and calcification has been conceptualized by Proudfoot and colleagues[34], who propose a model in which smooth muscle cell death may form apoptotic bodies in the arterial wall, which in turn may serve as a nucleus for vascular calcification[35]. In our time course studies, we noted the time line of apoptotic induction in the arterial wall, which was noted to begin around 24 hours, was closely followed by the detection of calcium deposition around 48 hours post injury. However, the link between SMC apoptosis and medial calcification has yet to be directly tested. Although aortic calcification has been reported in human AAA[36], the precise contribution calcification may make toward aneurysm progression is still controversial.

One important limitation within this study lies in the formation of $CaPO_4$ crystals. Although these crystals are known to be generated by mixing $CaCl_2$ with phosphate buffer, this methodology provides no means of controlling the formation of $CaPO_4$ crystals, nor of measuring the final concentration or composition of these crystals, especially *in vivo*. In preliminary studies, we tested the periaortic application of several forms of calcium phosphate including hydroxyapatite, nanocrystal and basic calcium phosphate. However, each of these calcium phosphate forms failed to induce aneurysm formation *in vivo* and produced little if any apoptosis *in vitro*. One possible explanation for this significant difference between calcium phosphate crystal types is size variations amongst these crystals, particularly in comparison to the naturally formed crystals, may not be appropriate for the endocytosis or autophagocytosis

of these crystals to induce apoptosis[37, 38]. In order to address a few questions surrounding the role of these $CaPO_4$ crystals, methods of interfering with crystal formation and/or the chemical reaction(s) that take place may provide mechanistic insights. Although the scope of this study does not allow such an experiment, future work must explore these methods in order to fully understand the role of $CaPO_4$ crystals in this newly described model. Furthermore, a better understanding of the role of calcification in aneurysm is necessary to fully understand the potential impact of this study.

Conclusion

In conclusion, we have shown that the creation of a $CaPO_4$ mouse AAA model through the modification of the conventional $CaCl_2$ model significantly accelerates aneurysm formation. $CaPO_4$ treatment also induced significant enhancement of apoptosis both *in vitro* and *in vivo*. Calcification and macrophage infiltration were also prominent features of the $CaPO_4$ aneurysm, sharing spatial and temporal similarities to the apoptosis within the medial layer. This model, with its rapid and robust dilation, can be utilized as a new model for mouse experimental AAA.

References

1. Kent KC, Zwolak RM, Jaff MR, Hollenbeck ST, Thompson RW, Schermerhorn ML, Sicard GA, Riles TS, Cronenwett JL. Screening for abdominal aortic aneurysm: A consensus statement. *J Vasc Surg*. 2004;39:267-269
2. Bengtsson H, Sonesson B, Bergqvist D. Incidence and prevalence of abdominal aortic aneurysms, estimated by necropsy studies and population screening by ultrasound. *Ann N Y Acad Sci*. 1996;800:1-24
3. Daugherty A, Cassis LA. Mouse models of abdominal aortic aneurysms. *Arterioscler Thromb Vasc Biol*. 2004;24:429-434
4. Brophy CM, Tilson JE, Braverman IM, Tilson MD. Age of onset, pattern of distribution, and histology of aneurysm development in a genetically predisposed mouse model. *J Vasc Surg*. 1988;8:45-48
5. Silence J, Collen D, Lijnen HR. Reduced atherosclerotic plaque but enhanced aneurysm formation in mice with inactivation of the tissue inhibitor of metalloproteinase-1 (timp-1) gene. *Circ Res*. 2002;90:897-903
6. Kuhlencordt PJ, Gyurko R, Han F, Scherrer-Crosbie M, Aretz TH, Hajjar R, Picard MH, Huang PL. Accelerated atherosclerosis, aortic aneurysm formation, and ischemic heart disease in apolipoprotein e/endothelial nitric oxide synthase double-knockout mice. *Circulation*. 2001;104:448-454
7. Nishijo N, Sugiyama F, Kimoto K, Taniguchi K, Murakami K, Suzuki S, Fukamizu A, Yagami K. Salt-sensitive aortic aneurysm and rupture in hypertensive transgenic mice that overproduce angiotensin ii. *Lab Invest*. 1998;78:1059-1066
8. Anidjar S, Salzmann JL, Gentric D, Lagneau P, Camilleri JP, Michel JB. Elastase-induced experimental aneurysms in rats. *Circulation*. 1990;82:973-981
9. Curci JA, Thompson RW. "Variable induction of experimental abdominal aortic aneurysms with different preparations of porcine pancreatic elastase". *J Vasc Surg*. 1999;29:385
10. Chiou AC, Chiu B, Pearce WH. Murine aortic aneurysm produced by periarterial application of calcium chloride. *J Surg Res*. 2001;99:371-376
11. Daugherty A, Manning MW, Cassis LA. Angiotensin ii promotes atherosclerotic lesions and aneurysms in apolipoprotein e-deficient mice. *J Clin Invest*. 2000;105:1605-1612
12. Gertz SD, Kurgan A, Eisenberg D. Aneurysm of the rabbit common carotid artery induced by periarterial application of calcium chloride in vivo. *J Clin Invest*. 1988;81:649-656
13. Freestone T, Turner RJ, Higman DJ, Lever MJ, Powell JT. Influence of hypercholesterolemia and adventitial inflammation on the development of aortic aneurysm in rabbits. *Arterioscler Thromb Vasc Biol*. 1997;17:10-17
14. Longo GM, Xiong W, Greiner TC, Zhao Y, Fiotti N, Baxter BT. Matrix metalloproteinases 2 and 9 work in concert to produce aortic aneurysms. *J Clin Invest*. 2002;110:625-632
15. Yoshimura K, Aoki H, Ikeda Y, Fujii K, Akiyama N, Furutani A, Hoshii Y, Tanaka N, Ricci R, Ishihara T, Esato K, Hamano K, Matsuzaki M. Regression of abdominal aortic aneurysm by inhibition of c-jun n-terminal kinase. *Nat Med*. 2005;11:1330-1338

16. Urry DW. Neutral sites for calcium ion binding to elastin and collagen: A charge neutralization theory for calcification and its relationship to atherosclerosis. *Proc. Nat. Acad. Sci. USA*. 1971;68:810-814
17. Bostrom K, Watson KE, Stanford WP, Demer LL. Atherosclerotic calcification: Relation to developmental osteogenesis. *Am J Cardiol*. 1995;75:88B-91B
18. Weissen-Plenz G, Nitschke Y, Rutsch F. Mechanisms of arterial calcification: Spotlight on the inhibitors. *Adv Clin Chem*. 2008;46:263-293
19. Villa-Bellosta R, Sorribas V. Calcium phosphate deposition with normal phosphate concentration. *Circ J*. 2011
20. Ewence AE, Bootman M, Roderick HL, Skepper JN, McCarthy G, Epple M, Neumann M, Shanahan CM, Proudfoot D. Calcium phosphate crystals induce cell death in human vascular smooth muscle cells: A potential mechanism in atherosclerotic plaque destabilization. *Circ Res*. 2008;103:e28-34
21. Pazar B, Ea HK, Narayan S, Kolly L, Bagnoud N, Chobaz V, Roger T, Liote F, So A, Busso N. Basic calcium phosphate crystals induce monocyte/macrophage il-1beta secretion through the nlrp3 inflammasome in vitro. *J Immunol*. 2011;186:2495-2502
22. Gertz SD, Kurgan A, Eisenberg D. Aneurysm of the rabbit common carotid artery induced by periarterial application of calcium chloride in vivo. *The Journal of Clinical Investigation*. 1988;81:649-656
23. Tang XN, Berman AE, Swanson RA, Yenari MA. Digitally quantifying cerebral hemorrhage using photoshop® and image j. *Journal of Neuroscience Methods*. 2010;190:240-243
24. Clowes A, Clowes M, Fringerle J, Reidy M. Kinetics of cellular poliferation after arterial injury: Role of acute distension in the induciton of smooth muscle proliferation. *Lab Invest*. 1989;60:360-364
25. Yamanouchi D, Morgan S, Kato K, Lengfeld J, Zhang F, Liu B. Effects of caspase inhibitor on angiotensin ii-induced abdominal aortic aneurysm in apolipoprotein e-deficient mice. *Arterioscler Thromb Vasc Biol*. 2010;30:702-707
26. Ewence AE, Bootman M, Roderick HL, Skepper JN, McCarthy G, Epple M, Neumann M, Shanahan CM, Proudfoot D. Calcium phosphate crystals induce cell death in human vascular smooth muscle cells. *Circulation Research*. 2008;103:e28-e34
27. Pazár B, Ea H-K, Narayan S, Kolly L, Bagnoud N, Chobaz V, Roger T, Lioté F, So A, Busso N. Basic calcium phosphate crystals induce monocyte/macrophage il-1β secretion through the nlrp3 inflammasome in vitro. *The Journal of Immunology*. 2011;186:2495-2502
28. Trion A, van der Laarse A. Vascular smooth muscle cells and calcification in atherosclerosis. *American Heart Journal*. 2004;147:808-814
29. Hunt JL, Fairman R, Mitchell ME, Carpenter JP, Golden M, Khalapyan T, Wolfe M, Neschis D, Milner R, Scoll B, Cusack A, Mohler ER, 3rd. Bone formation in carotid plaques: A clinicopathological study. *Stroke*. 2002;33:1214-1219
30. Proudfoot D, Skepper JN, Hegyi L, Bennett MR, Shanahan CM, Weissberg PL. Apoptosis regulates human vascular calcification in vitro : Evidence for initiation of vascular calcification by apoptotic bodies. *Circulation Research*. 2000;87:1055-1062
31. Reynolds JL, Joannides AJ, Skepper JN, McNair R, Schurgers LJ, Proudfoot D, Jahnen-Dechent W, Weissberg PL, Shanahan CM. Human vascular smooth muscle cells undergo vesicle-mediated calcification in response to changes in extracellular calcium and

phosphate concentrations: A potential mechanism for accelerated vascular calcification in esrd. *J Am Soc Nephrol*. 2004;15:2857-2867

32. Matsushita M, Nishikimi N, Sakurai T, Nimura Y. Relationship between aortic calcification and atherosclerotic disease in patients with abdominal aortic aneurysm. *Int Angiol*. 2000;19:276-279
33. Sarkar S, Korolchuk V, Renna M, Winslow A, Rubinsztein DC. Methodological considerations for assessing autophagy modulators: A study with calcium phosphate precipitates. *Autophagy*. 2009;5:307-313
34. Gao W, Ding WX, Stolz DB, Yin XM. Induction of macroautophagy by exogenously introduced calcium. *Autophagy*. 2008;4:754-761

Figure Legend

Figure 1. Apoptosis induced by Calcium phosphate treatment *in vitro*.

Cultured mouse aortic SMCs were treated with $CaCl_2$ or $CaPO_4$ as described in Materials and Methods. A) In vitro apoptosis determined by DNA fragmentation ELISA. Fold change determined with comparison to untreated cell group (Control). **p<0.0001, n=**4***. B) Representative results of flow cytometry analyses. Apoptotic and necrotic cells were identified by annexin V and 7AAD, respectively. *n=4.*

Figure 2. Aneurysm induction by $CaPO_4$ treatment in mouse model.

Mice were subjected to AAA induction with $CaCl_2$ or $CaPO_4$ and were sacrificed at indicated time points as described in Materials and Methods. A) Representative pictures of arterial dilation 7 days after surgery. B) Quantification of arterial expansion measured 3, 7, 28, and 42 days after surgery. Fold Change = Maximum Diameter/Pre-surgery diameter. **p < 0.05, n =6.* C) Van Gieson's stain depicting elastin layer degradation in representative treated arteries 7 days after surgery. Scale bar 100µm. D) Semi-quantification of elastin degradation in arteries harvested 7 days after surgery.

Figure 3. $CaPO_4$-induced aneurysm displays apoptosis

Mice were subjected to AAA induction with $CaCl_2$ or $CaPO_4$ and were sacrificed at indicated time points as described in Materials and Methods. A) Representative images of immunohistochemistry for apoptosis, as measured by TUNEL (red), nuclei shown by DAPI stain (blue) in treated arteries 3 days after injury. Scale bar = 100 µm. B) TUNEL index as determined by TUNEL positive cells/nuclei. Measurements taken from $CaCl_2$- (black bar, ■$CaCl_2$) and $CaPO_4$

–treated (white bars, □$CaPO_4$) arteries harvested 24, 48 or 72 hours after surgery. *$p < 0.05$, $n = 3$*.

Figure 4. Inflammation accompanies $CaPO_4$-induced aneurysm

Mice were subjected to AAA induction with $CaCl_2$ or $CaPO_4$ and were sacrificed at indicated time points as described in Materials and Methods. A) Representative images of immunohistochemistry for macrophage marker CD68 (green) in $CaCl_2$ - and $CaPO_4$ -treated aorta 3 days after injury. Nuclei stained with DAPI (blue). Scale bar = 100 µm. B) Graphical representation of macrophage infiltration as determined by CD68 positive cells/nuclei in treated arteries 24, 48, and 72h after treatment.. *$p < 0.05$, $n = 3$*.

Figure 5. $CaPO_4$-induced aneurysm samples contain medial calcification.

A) Arterial sections stained with Alizarin Red for calcium deposit detection, calcium appearing red on a pink and yellow background. 'Control' sections harvested from animals treated with NaCl only; '48 hour',' 72 hour', and '7 day' sections harvested at respective times after treatment by $CaPO_4$ surgery. Scale bar = 200 µm for all images. B) Quantification of calcium content in arterial sections harvested from arteries with the conventional $CaCl_2$ model (CaCl2) or the $CaPO_4$ model (CaPO4). Data was expressed as a ratio of the total calcified media divided by the total medial area of each arterial section. *n=4*.

Figure 1.

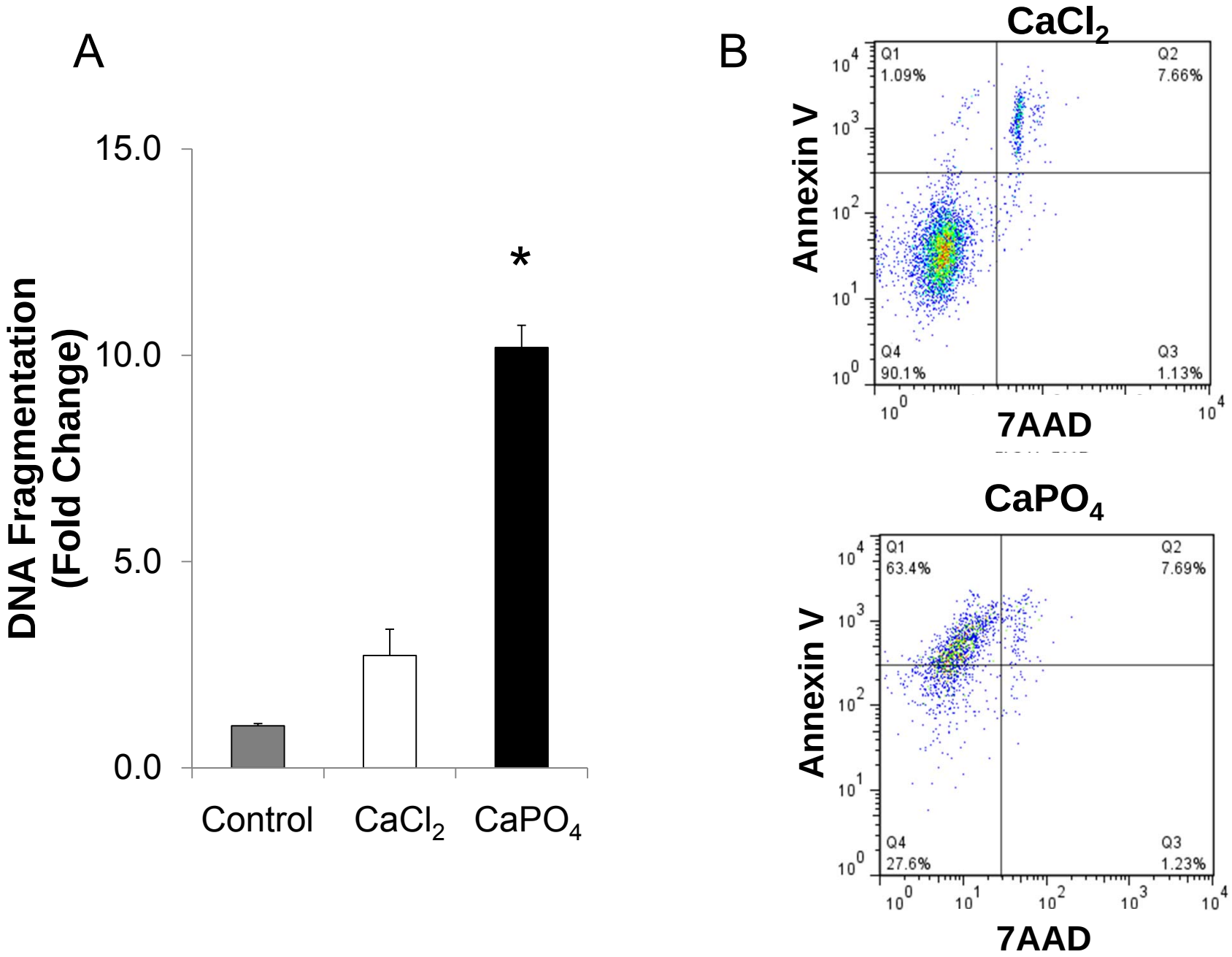
A
DNA Fragmentation (Fold Change)
15.0
10.0
5.0
0.0
*
Control
CaCl2
CaPO4
B
CaCl2
Annexin V
7AAD
Q1 1.09%
Q2 7.66%
Q4 90.1%
Q3 1.13%
CaPO4
Annexin V
7AAD
Q1 63.4%
Q2 7.69%
Q4 27.6%
Q3 1.23%

Figure 2.

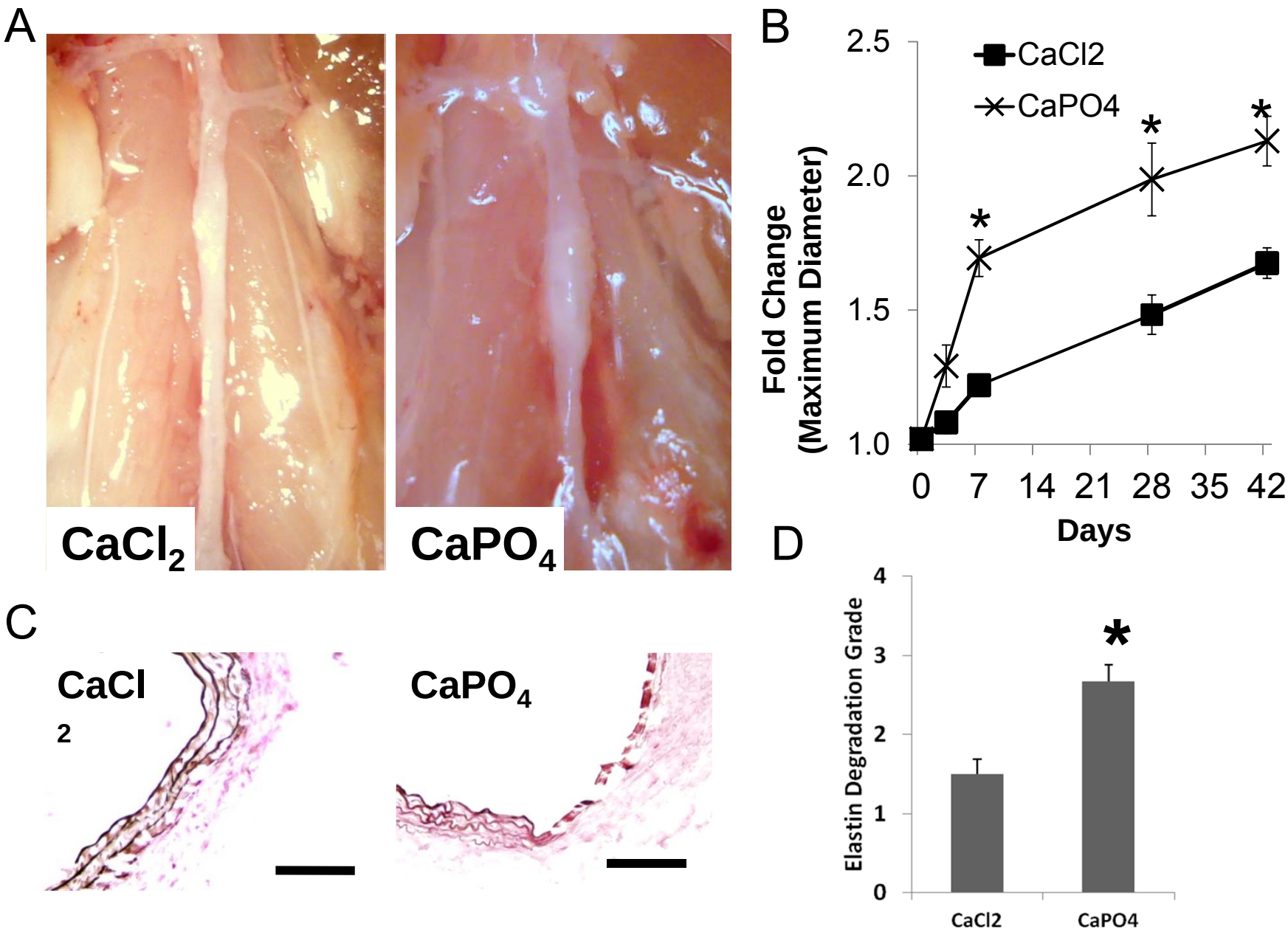
A
CaCl2
CaPO4
B
Fold Change (Maximum Diameter)
2.5
2.0
1.5
1.0
CaCl2
CaPO4
*
*
*
0
7
14
21
28
35
42
Days
C
CaCl2
CaPO4
D
Elastin Degradation Grade
4
3
2
1
0
*
CaCl2
CaPO4

Figure 3.

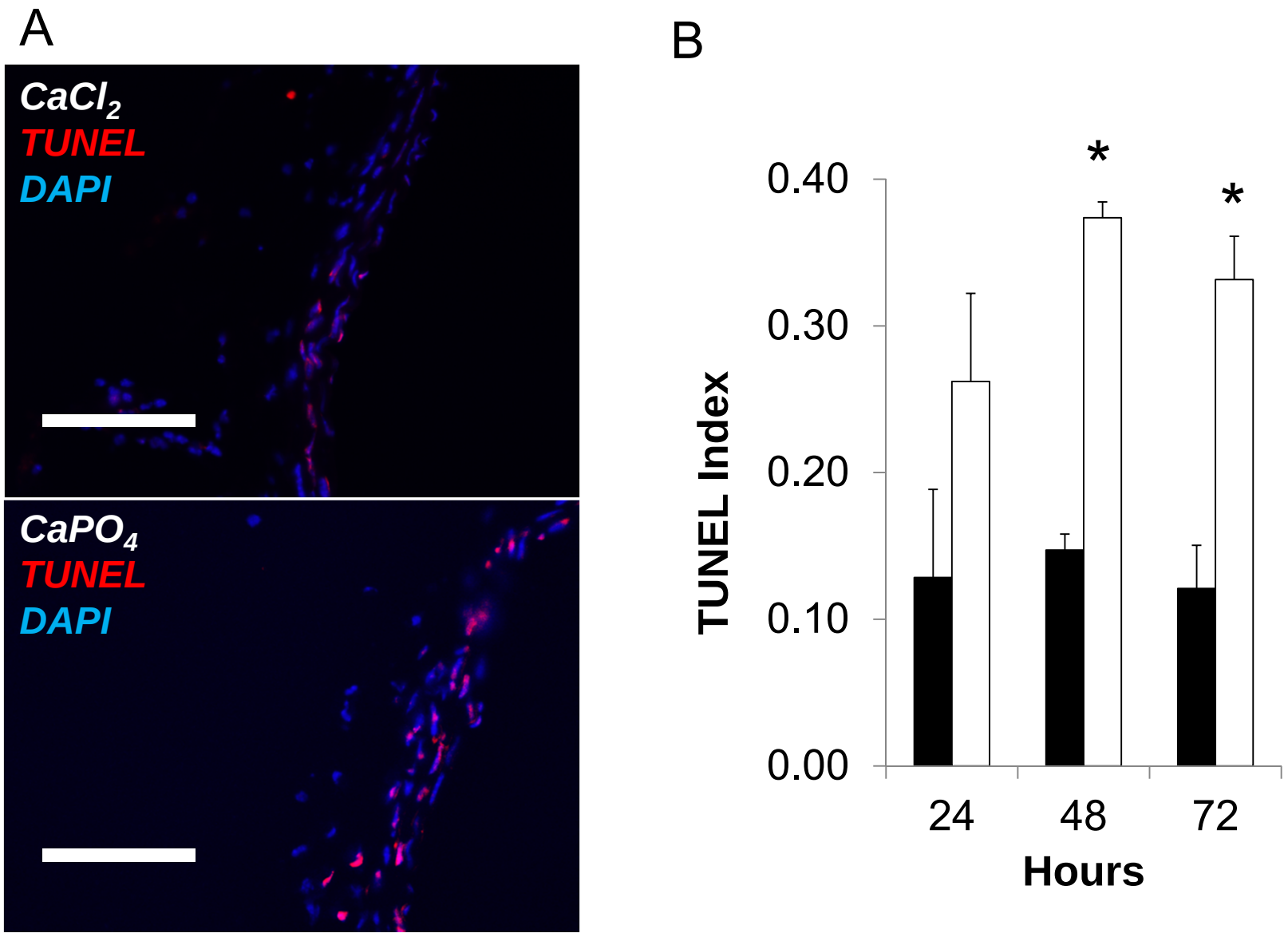
A
CaCl2
TUNEL
DAPI
CaPO4
TUNEL
DAPI
B
TUNEL Index
0.40
0.30
0.20
0.10
0.00
*
*
24
48
72
Hours

Figure 4.

A

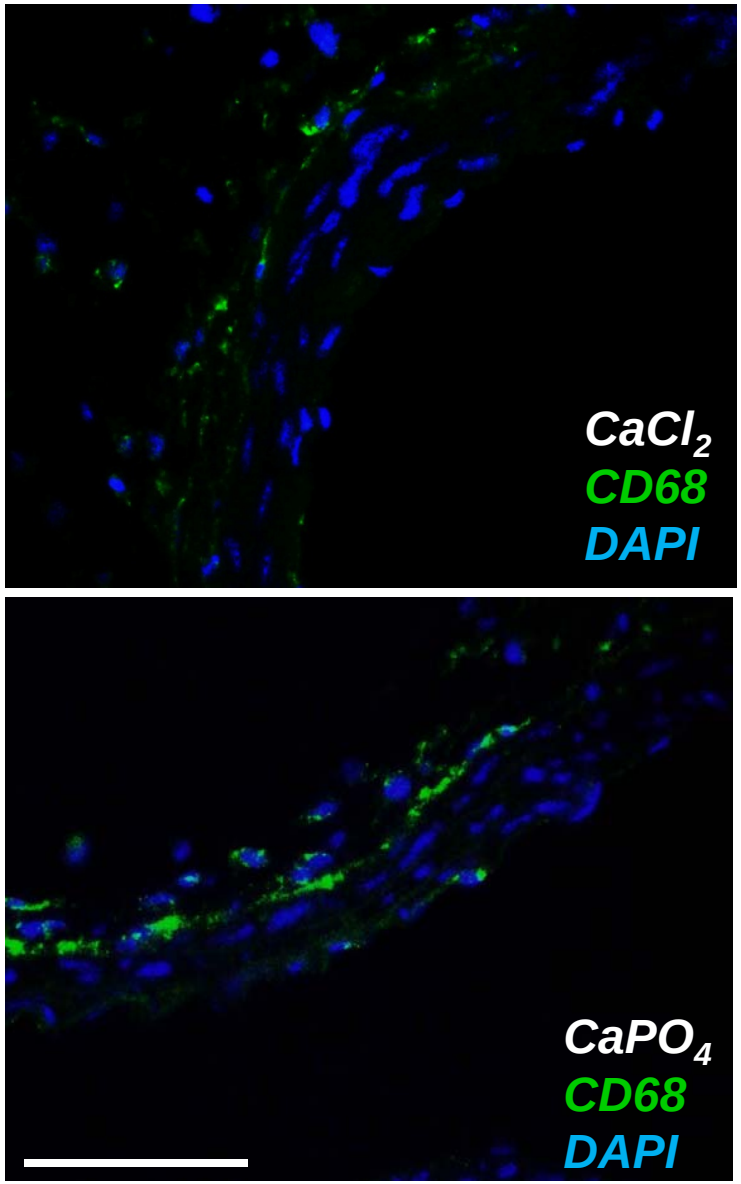
CaCl2
CD68
DAPI
CaPO4
CD68
DAPI

B

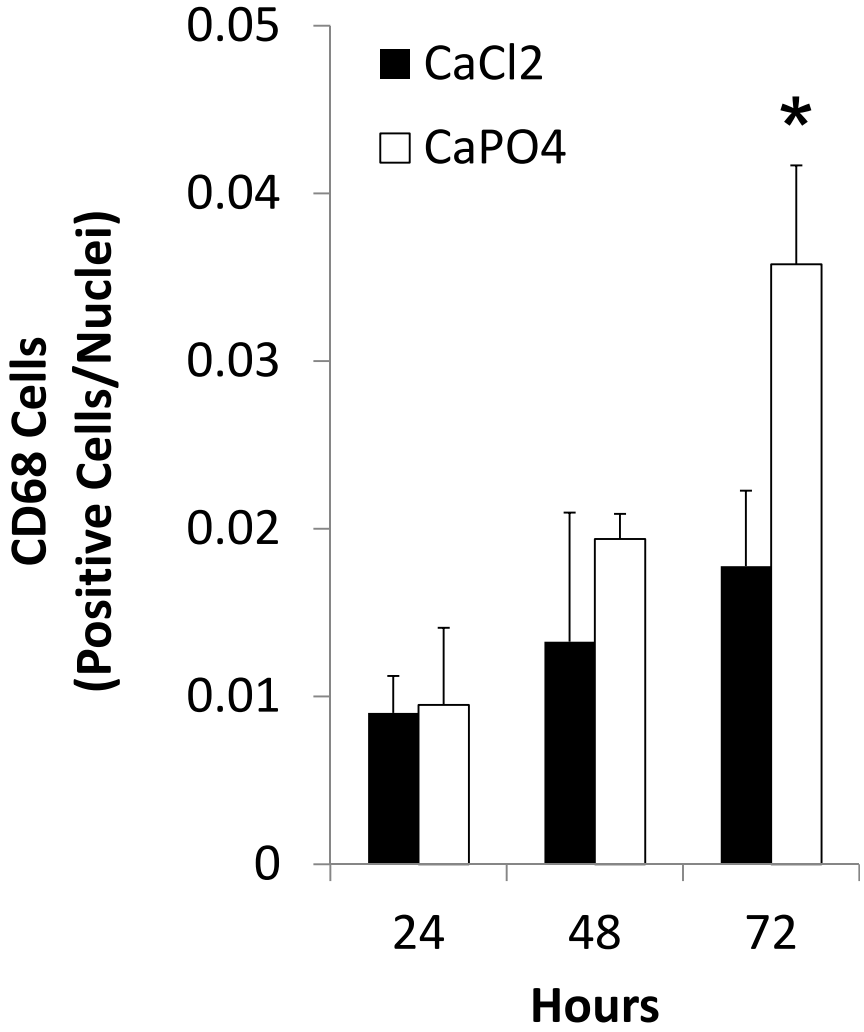
0.05
0.04
0.03
0.02
0.01
0
CaCl2
CaPO4
*
CD68 Cells
(Positive Cells/Nuclei)
24
48
72
Hours

A

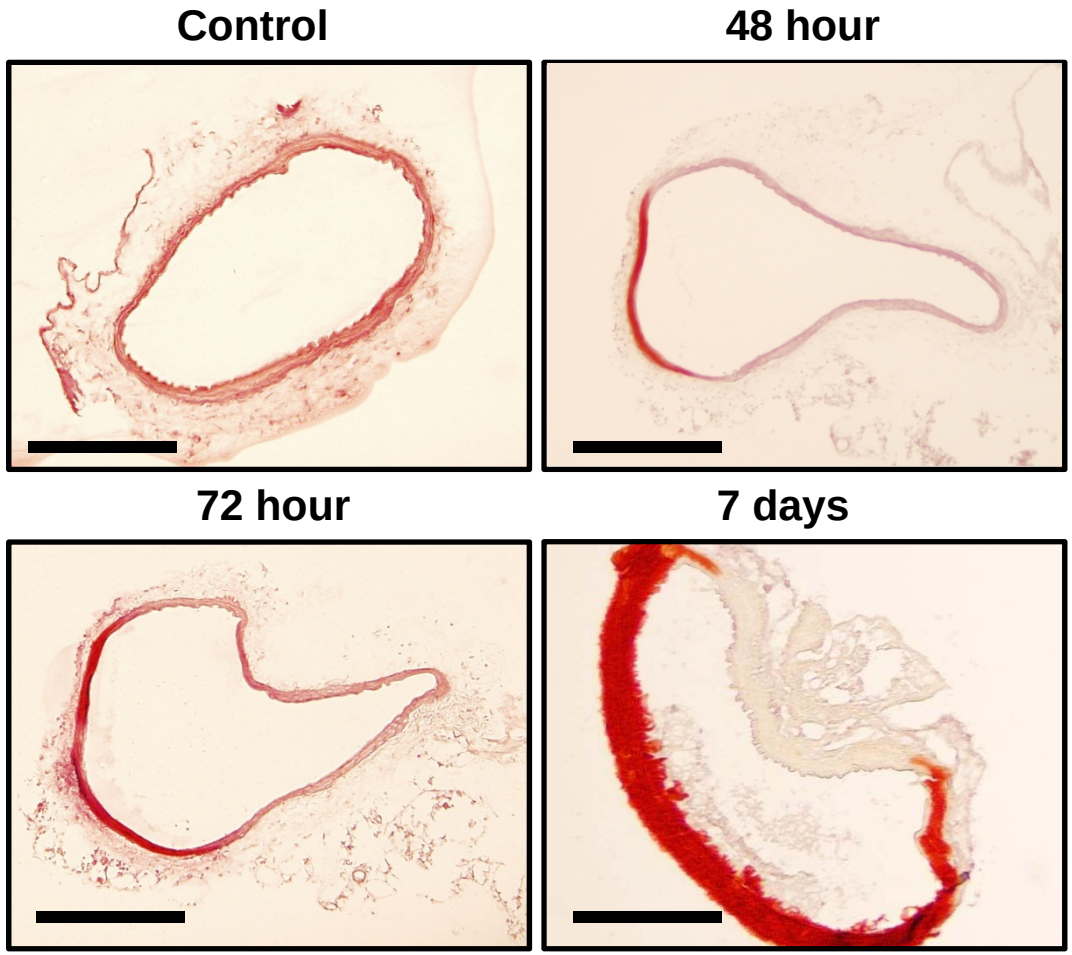
Control
48 hour
72 hour
7 days

B

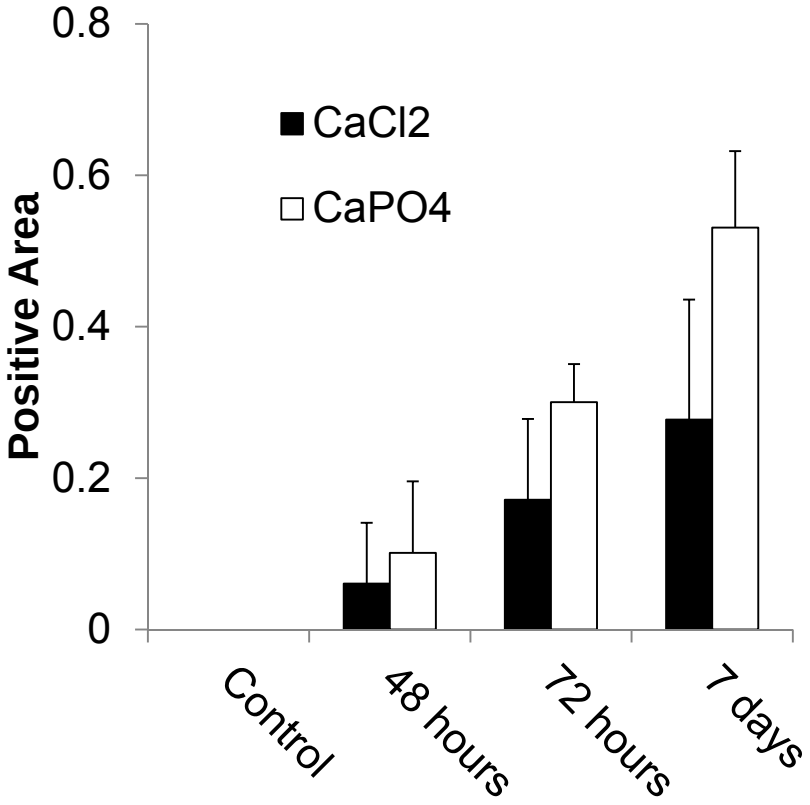
Positive Area
0.8
0.6
0.4
0.2
0
CaCl2
CaPO4
Control
48 hours
72 hours
7 days

Supplemental Figure 1.

Representative images of immunofluoresent stained $CaPO_4$-treated arteries harvested 3 days after injury. A) Apoptosis as identified by cleaved caspase 3 (red), overlay with nuclei (DAPI, blue). Scale bar 100 μm. B) Co-localization of the SMC marker smooth muscle alpha-actin (SMA, green) with TUNEL (red). Overlay with DAPI (blue). Scale bar 200 μm.

Supplemental Figure 2.

Representative images of $CaPO_4$-treated arteries harvested **7** days after injury stained for macrophages (Mac3), T lymphocytes (CD3), and the inflammatory cytokine Monocyte Chemoattractant Protein-1 (MCP-1).. Scale bar =100μm.

Supplemental Figure 3.

Mice were subjected to $CaPO_4$ treatment and sacrificed **7** days after. A) Representative photos showing inflammatory cells localized to adventitia, with monocytes and macrophages, marked by MOMA and the medial layer delineated by SMA (red), overlay with DAPI (blue). Left panel scale bar 200μm, right panel scale bar 100μm. B) A representative co-staining image depicting apoptosis (cleaved caspase-3 positive cells, Red) and inflammation (MOMA, green). Overlay with DAPI. Scale bar = 100 μm.

Table 1.

Analysis of cells after treatment with calcium chloride ($CaCl_2$) or calcium phosphate ($CaPO_4$) shown as % of total.

Supplemental Figure 1.

A.

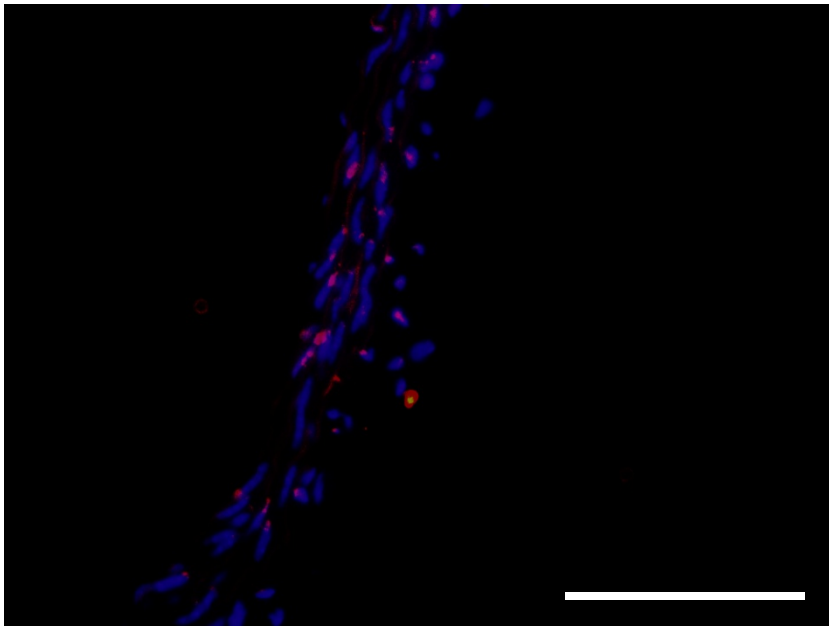

B.

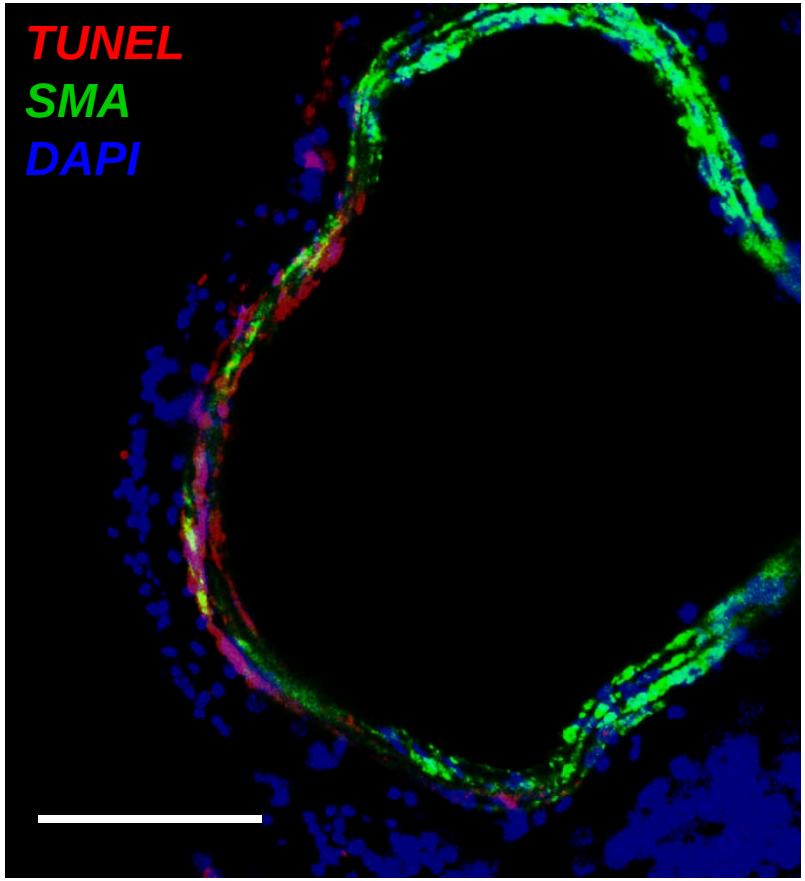

Supplemental Figure 2.

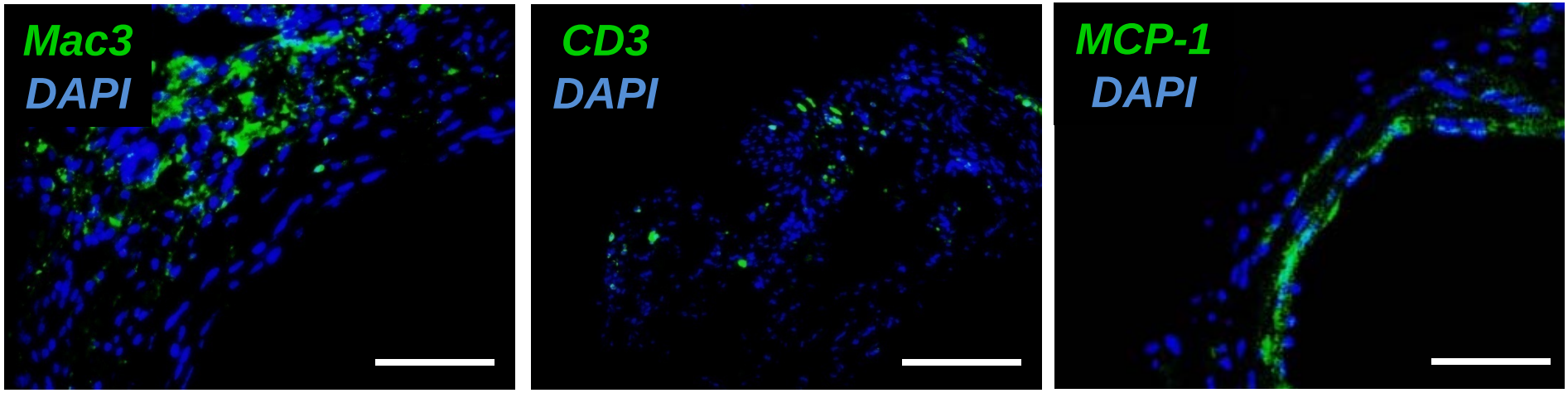

Supplemental Figure 3.

A.

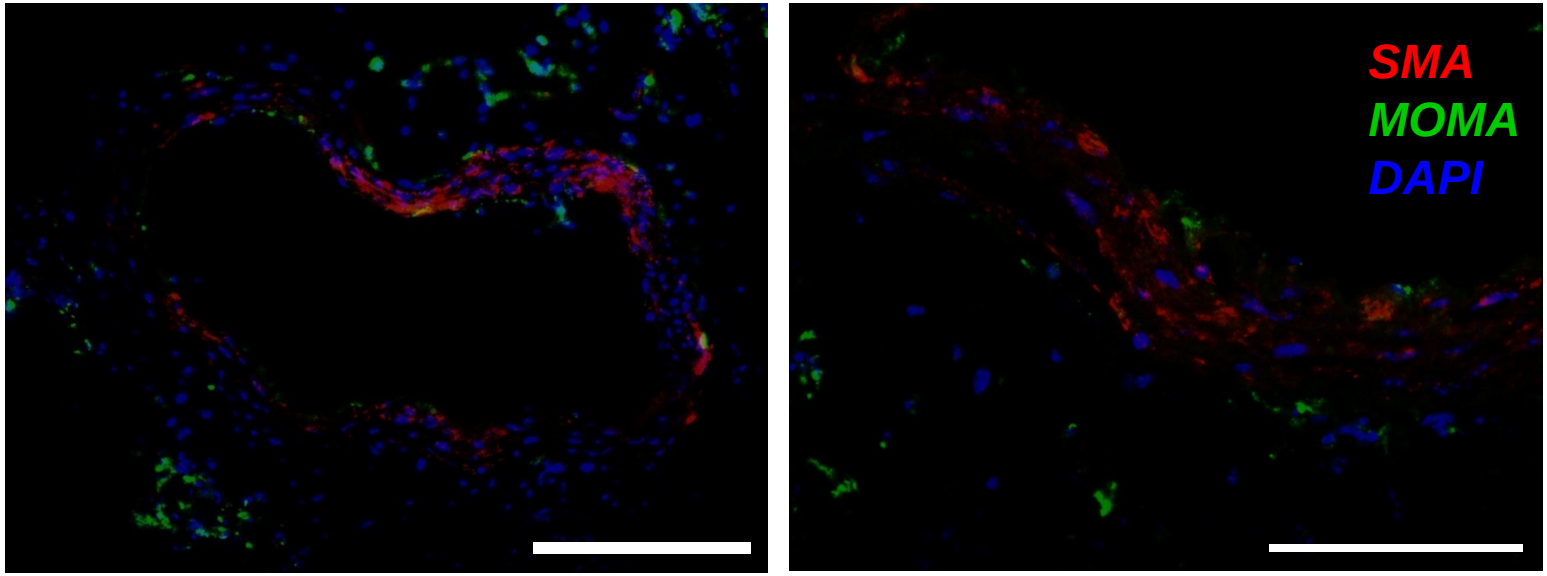

B.

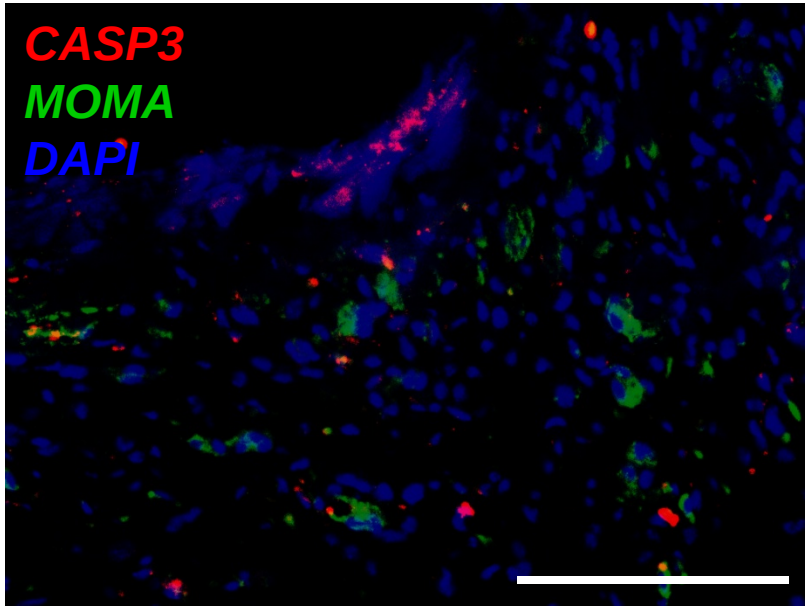

	Healthy (Negative)	*Apoptotic (Annexin V+)*	*Necrotic (7AAD+)*	*Secondary necrotic (Double +)*
$CaCl_2$	89.2 ± 1.27	1.08 ± 0.01	2.79 ± 2.35	6.94 ± 1.02
$CaPO_4$	22 ± 7.92[a]	68.8 ± 7.6[a]	1.4 ± 0.23	7.8 ± 0.14

7AAD, 7-aminoactinomycin D.

[a] $P < 0.05$ vs control.

Transition III

The CaPO4 model appears to work through the acceleration of apoptosis and inflammation to promote a fast-growing aneurysm. This finding confirms the role of apoptosis in aneurysm, as previously explored in Chapters 1 through 3. However, the method of apoptosis inhibition, that is, chemical inhibition of caspase activation, is a systemic administration that has untold consequences on the rest of the body. Clearly, to develop a therapeutic treatment, we must identify a more specific regulator of apoptosis.

Previously, research produced by Dr. Liu described a critical role for Protein Kinase C-delta (PKCδ) in smooth muscle cell (SMC) apoptosis[1]. Further, the expression of PKCδ was seen to be upregulated in human aneurysm tissue[2]. This information led us to believe that PKCδ may have a role in a murine aneurysm model. Using PKCδ knockout mice, previously developed by Miyamoto A et al.[3], we aimed to explore the role of PKCδ in murine aneurysm through the $CaCl_2$ model.

1. Kato K, Yamanouchi D, Esbona K, Kamiya K, Zhang F, Kent KC, Liu B. Caspase-mediated protein kinase c-{delta} cleavage is necessary for apoptosis of vascular smooth muscle cells. *Am J Physiol Heart Circ Physiol*. 2009;297:H2253-2261
2. Schubl S, Tsai S, Ryer EJ, Wang C, Hu J, Kent KC, Liu B. Upregulation of protein kinase c[delta] in vascular smooth muscle cells promotes inflammation in abdominal aortic aneurysm. *Journal of Surgical Research*. 2009;153:181-187
3. Miyamoto A, Nakayama K, Imaki H, Hirose S, Jiang Y, Abe M, Tsukiyama T, Nagahama H, Ohno S, Hatakeyama S, Nakayama KI. Increased proliferation of b cells and auto-immunity in mice lacking protein kinase c[delta]. *Nature*. 2002;416:865-869

Chapter 4: Elevated Protein Kinase C-delta Contributes to Aneurysm Pathogenesis through Stimulation of Apoptosis and Inflammatory Signaling

Published in Arteriosclerosis Thrombosis and Vascular Biology 2012; 32(10): 2493-2502

Elevated Protein Kinase C-delta Contributes to Aneurysm Pathogenesis through Stimulation of Apoptosis and Inflammatory Signaling

Morgan: PKCδ in abdominal aortic aneurysm

Stephanie Morgan, BS#, Dai Yamanouchi, MD&PhD#, Calvin Harberg, BS#, Qiwei Wang, MS#, Melissa Keller, BS+, Yi Si, MD&PhD#, William Burlingham, PhD+, Stephen Seedial, BS#, Justin Lengfeld, BS#, and Bo Liu, PhD#

#Division of Vascular Surgery

+Division of Transplant Surgery

Department of Surgery

University of Wisconsin Madison, Madison

School of Medicine and Public Health

Corresponding author: Bo Liu

1111 Highland Avenue, WIMR 5120, Madison, WI 53705

Tel: 608-263-5931, Fax: 608-262-3330

liub@surgery.wisc.edu

Word Count of Manuscript: 4,178

Word Count of Abstract: 200

ABSTRACT

Objective: Apoptosis of smooth muscle cells (SMCs) is a prominent pathological characteristic of Abdominal Aortic Aneurysm (AAA). We have previously shown that SMC apoptosis stimulates proinflammatory signaling in a mouse model of AAA. Here, we test whether Protein Kinase C-delta (PKCδ), an apoptotic mediator, participates in the pathogenesis of AAA by regulating apoptosis and proinflammatory signals.

Methods and Results: Mouse experimental AAA is induced by perivascular administration of $CaCl_2$. Mice deficient in PKCδ exhibit a profound reduction in aneurysmal expansion, SMC apoptosis, and transmural inflammation as compared to wildtype littermates. Delivery of PKCδ to the aortic wall of PKCδ$^{-/-}$ mice restores aneurysm, while overexpression of a dominant negative PKCδ mutant in the aorta of wildtype mice attenuates aneurysm. *In vitro*, PKCδ$^{-/-}$ aortic SMCs exhibit significantly impaired monocyte chemoattractant protein-1 (MCP-1) production. Ectopic administration of recombinant MCP-1 to the arterial wall of PKCδ$^{-/-}$ mice restores inflammatory response and aneurysm development.

Conclusions: PKCδ is an important signaling mediator for SMC apoptosis and inflammation in a mouse model of AAA. By stimulating MCP-1 expression in aortic SMCs, upregulated PKCδ exacerbates the inflammatory process, in turn perpetuating elastin degradation and aneurysmal dilatation. Inhibition of PKCδ may serve as a potential therapeutic strategy for AAA.

INTRODUCTION

Abdominal aortic aneurysm (AAA), a progressive aortic dilation, is a common vascular disease associated with high mortality. Aneurysm results from the culmination of a series of events that lead to disruption of structural integrity and segmental weakening of the abdominal aortic wall. An incomplete understanding of the biological mechanisms underlying the disease has limited the development of therapeutic treatment and diagnostic strategies, thus leaving surgical and endovascular procedures as the only treatment options for patients with abdominal aortic aneurysm.

Histologically, aneurysmal tissues are characterized by disruption of the elastic fibers in the aortic wall and extensive transmural infiltration of macrophages and lymphocytes [1-3]. These features have been consistently duplicated in animal models of AAA [4]. The prevailing view is that inflammatory cells, mainly macrophages, are the major source of matrix-degrading enzymes such as matrix metalloproteinases [5-9] and proinflammatory cytokines [10-12]. Anti-inflammatory strategies such as those that deplete neutrophils, lymphocytes, mast cells, or proinflammatory cytokines have been shown to prevent the upregulation of matrix metalloproteinases and attenuate aneurysm formation in mouse models of AAA [13-16].

Although the depletion of vascular smooth muscle cells (SMCs) is well documented in human aneurysmal tissues [17], potential interactions between SMCs and infiltrating inflammatory cells remain unclear. We have recently demonstrated that blocking apoptosis with a pan caspase inhibitor protected mice from angiotensin II-induced aneurysm expansion [18]. The caspase inhibitor not only prevented SMC depletion but also diminished

infiltration of macrophages and lymphocytes, suggesting a potential link between the apoptotic process and inflammatory signaling in the pathogenesis of aneurysm.

Protein kinase C-delta (PKCδ), a member of the PKC family of serine and threonine kinases, is a crucial mediator of SMC apoptosis [19-21]. Studies of PKCδ knockout (KO) mice reveal that mice lacking PKCδ develop normally but exhibit an apoptosis-resistant phenotype when subjected to models of vascular injury such as vein graft or carotid artery ligation [22, 23]. Conversely, gene transfer of PKCδ via an adenoviral vector led to excessive apoptosis of vascular SMCs in a rat carotid balloon injury model [23]. More recently, we showed that PKCδ may also be involved in the regulation of chemokine expression. Inhibition of PKCδ with rottlerin profoundly decreases the production of monocyte chemoattractant protein-1 (MCP-1) by aortic vascular SMCs and subsequently inhibits chemotaxis of inflammatory cells toward SMC-conditioned media [21].

We have previously shown that the expression of PKCδ is significantly higher in human aneurysmal aortic tissues as compared to normal arteries [21]. The collection of these tissues at the time of surgical repair precluded analysis of a potential causal relationship between PKCδ and aneurysm; specifically, whether PKCδ upregulation contributes to the pathophysiology of aneurysm or is merely a resultant phenomenon. To determine whether PKCδ is an integral mediator of SMC apoptosis and vascular inflammation during aneurysm pathogenesis, the current study tests the effects of PKCδ gene deficiency on aneurysm formation using the calcium chloride ($CaCl_2$) mouse model. In addition, we explored the potential molecular mechanisms by which PKCδ regulates the pro-inflammatory signals produced by apoptotic SMCs.

METHODS

The detailed methods are shown in online supplements.

Mouse Models of AAA

The generation of PKCδ target deletion in mice was described elsewhere[24]. PKCδ knockout mice and their wildtype littermates were generated by mating heterozygous pairs. C57BL/6 mice and ApoE$^{-/-}$ mice were purchased from Harlan Laboratories (Madison, WI) and Jackson Laboratory (Bar Harbor, ME), respectively. GFP transgenic mice were gifted from Dr. William Burlingham at the University of Wisconsin-Madison.

Male mice, 12 weeks of age, underwent a $CaCl_2$ –induced abdominal aortic aneurysm model as described previously [25-28]. Briefly, the infrarenal region of the aorta was isolated and treated with 0.5M $CaCl_2$ perivascularly via gauze for 20 minutes. Control mice were similarly treated with 0.5M of sodium chloride (NaCl). Tissues were fixed in 4% formaldehyde in phospho-buffered saline (PBS), embedded and cut to 6 or 8μm sections for OCT and paraffin-imbedded arteries, respectively.

Immunohistochemistry

Antibodies were purchased from Abcam (Cambridge, MA; IFN-γ, IL-6, MOMA2, MHC, and CD45), Santa Cruz (Santa Cruz, CA; CD3, MCP-1, Mac3, PKCδ, Ly6G, and CD68), Sigma-Aldrich (SMA), and Cell Signaling (Danvers, MA; Cleaved caspase-3). TUNEL staining kit was purchased from Roche (Madison, WI). Van Geison stains were carried out using Chromaview Van Gieson kit (Richard Allan Scientific, Kalamazoo, MI).

Cell Culture

The murine macrophage cell line RAW264.7 cells were obtained from American Type Culture Collection (ATCC, Manassas, VA). Primary mouse aortic SMCs from the aorta of both PKCδ KO and WT mice were isolated based on a protocol described by Clowes *et al.* [29].

Migration Assay

In vitro migration assay was carried out as previously described[30]. Briefly, RAW264.7 macrophages, or $CD11b^+$ cells isolated from bone marrow, were placed in a 5µm pore transwell insert. Conditioned and/or treated media were used as chemoattractants. Following 6 hours incubation, inserts were removed and stained with hematolxylin to facilitate nuclei visualization. The mean value of migrated cells was counted in eight high-power fields per membrane.

Bone Marrow Isolation and Sorting

Bone marrow was isolated from long bones, washed with PBS, and counted. Monocytes were collected from bone marrow by magnetic sorting using CD11b microbeads (Miltenyi Biotec, Boston, MA). Purity of the resulting $CD11b^+$ cells was assessed by flow cytometry using antibodies to CD3, CD11b, and CD45/B220 (Miltenyi Biotec).

Statistical Analysis

Values were expressed as mean ± standard error. Experiments were repeated at least three times unless stated otherwise. Differences between 2 groups were analyzed by Student's *t* test.

For time course comparison, one-way ANOVA analysis was followed by Bonferroni correction to adjust for multiple comparisons. Values of $p<0.05$ were considered significant.

More detailed methods are provided in Supplemental Methods.

RESULTS

PKCδ expression in experimental aneurysms

We subjected C57BL/6 male mice to perivascular treatment of 0.5M $CaCl_2$ (or equal concentration of NaCl) to the infrarenal region of the aorta and sacrificed the animals at selected time points. Administration of $CaCl_2$ led to gradual aortic dilatation associated with elastin fragmentation (Supplemental Figure 1). Immunohistochemical analysis showed a profound upregulation of PKCδ protein in the aortic media 3 and 7 days after $CaCl_2$ treatment (Figure 1A), a time frame at which aortic expansion was barely visible. The temporal and spatial pattern of PKCδ expression mirrored that of TUNEL positivity (Figure 1B). Confocal images confirmed the colocalization between PKCδ upregulation and apoptosis (TUNEL). Furthermore, PKCδ positive cells were primarily SMCs, as identified by Myosin Heavy Chain (MHC) (Figure 1C). A similar expression pattern of PKCδ and its association with apoptosis was also observed in angiotensin II-induced aneurysm in $apoE^{-/-}$ (Supplemental Figure 2). Western blot analysis confirmed the elevated level of PKCδ protein in $CaCl_2$-treated aortas as compared to the NaCl-treated controls (Figure 1D, E). Additionally, levels of the apoptosis-associated catalytic fragment of PKCδ became readily detectable in $CaCl_2$-treated group (Figure 1D).

Mice lacking PKCδ are resistant to AAA induction

To prove a potential role of PKCδ in AAA formation, we subjected PKCδ knockout (KO) mice and their wildtype (WT) littermates to aneurysm induction by $CaCl_2$. Forty-two days after the $CaCl_2$ treatment, abdominal aorta of WT mice were visibly inflamed and dilated while the arteries of KO mice appeared minimally affected (Figure 2A). The maximal external diameter of

the abdominal aorta was measured immediately prior to the $CaCl_2$ application and at the time of tissue harvest. As seen in Figure 2B, the baseline aortic diameters are comparable in PKCδ WT and KO mice. Six weeks after the $CaCl_2$ treatment, arteries of WT mice expanded to 1.04±0.08mm (96.6±31%), while arteries of KO mice expanded only to 0.74±0.06mm (39.7±9%) (Figure 2B). Similarly, PKCδ was shown to play a role in the elastase perfusion model of murine AAA. Inactive elastase produced minimal dilation of the artery in both WT and KO animals (0.77±0.06mm and 0.76±0.02mm, respectively; n=2), while active elastase treatment produced a more severe dilation in WT animals (1.47±0.16mm) compared to KO (0.97±0.29mm) (Supplemental Figure 3).

Histological analysis performed at 7 days after $CaCl_2$-treatment revealed similar elastin degradation in KO and WT arteries (Supplemental Figure 4). However, the same histological analysis 42 days after $CaCl_2$ treatment showed elastin fibers in arteries harvested from KO mice appeared continuous and organized, similar to NaCl-treated controls, whereas elastin fibers in $CaCl_2$-treated WT arteries appeared fragmented and disoriented (Figure 2C, D). Furthermore, PKCδ KO tissue harvested at 7 days displayed significantly reduced SMC apoptosis, as evidenced by confocal staining showing colocalization of MHC and apoptosis (TUNEL), as compared to WT samples (Figure 2E). Accordingly, cleaved Caspase-3 was nearly undetectable in PKCδ KO arteries, while it was abundant in the WT arteries (Supplemental Figure 5A, B). Furthermore, the percentage of nuclei staining positive for TUNEL was decreased from 24.1±3.4 in WT arteries to 12.5±2.9 in KO arteries (Data not shown). *In vitro* analysis of cultured SMCs confirmed the apoptosis-resistant phenotype. The lack of PKCδ diminished the ability of SMCs

to undergo apoptosis in response to TNFα, which was rescued by restoration of PKCδ expression with an adenoviral vector (Supplemental Figure 5C, D).

PKCδ is critical for the inflammatory response

Next, we analyzed macrophage infiltration, another important characteristic of aneurysm, in the aortas of both WT and KO animals. Immunohistochemical analysis revealed a profound reduction in the number of macrophages (Mac-3$^+$, CD68$^+$) detected in the aorta of PKCδ KO mice as compared to their WT littermates (Figure 3A, B). Additionally, neutrophils (Ly6G$^+$), leukocytes (CD45$^+$), and T cells (CD3$^+$) were shown to be present in the aortic samples of the PKCδ WT mice, mostly prevalent in the adventitia, and almost entirely absent in KO aortas (Supplemental Figure 6). Similarly, levels of AAA-associated inflammatory cytokines IL-6 and monocyte chemoattractant protein-1 (MCP-1) were markedly decreased by PKCδ gene deficiency (Figure 3C). To better quantify the altered cytokine expression, we analyzed aortic tissues using real-time (RT)-PCR analysis. As shown in Figure 3D, PKCδ gene deficiency caused a 50.7% and 48.1% reduction in mRNA levels of IL-6 and MCP-1 in TNFα-treated SMCs, respectively. Additionally, aneurysm-associated induction of IL-1β and INFγ was also significantly blunted in PKCδ KO mice (Supplemental Figure 7). There was also a small but statistically insignificant trend of reduction in TNF-α mRNA abundance.

PKCδ-deficient aortic SMCs are impaired in MCP-1 expression

The diminished inflammatory infiltrate in PKCδ KO mice could be caused by a lack of PKCδ-mediated chemokine production in the aortic wall or diminished migratory property of

monocytes. A complete blood count (CBC) performed on WT and KO animals showed no significant difference in white blood cell or red blood cell populations between the two genotypes (Supplemental Table 1). Furthermore, the percentage of monocytes ($CD11b^+$) in the bone marrow was comparable between the genotypes (Supplemental Figure 8A, B). In a chemotaxis assay, $CD11b^+$ monocytes isolated from KO and WT animals migrated with equal efficiency toward recombinant MCP-1 protein (Supplemental Figure 8C). Together, these data suggest that neither number nor migratory capability of bone marrow monocytes are affected by PKCδ gene deficiency.

RT-PCR analysis of aortic SMCs showed KO cells to have a nearly absolute impairment of MCP-1 production. Expression of IFNγ and IL-6 also appeared to be modulated by PKCδ, albeit to a lesser degree (Figure 4A). The dependence of MCP-1 expression on PKCδ was further demonstrated by ELISA measurement of MCP-1 production by cultured SMCs. Following treatment with TNFα, WT SMCs are shown to produce significantly more MCP-1 as compared to KO SMCs (Figure 4B). Furthermore, overexpression of PKCδ using adenoviral-mediated gene delivery (AdPKCδ) further enhanced the production of MCP-1 in WT SMCs (Figure 4C).

To further test the notion that PKCδ gene deficiency reduces the presence of proinflammatory aneurysm signals produced by the aortic wall, we examined the ability of aortic SMCs to attract RAW264.7 monocyte/macrophages. As shown in Figure 4D, the number of RAW264.7 cells that migrated toward media conditioned by KO SMCs was ~50% less than that toward media conditioned by WT SMCs. Furthermore, administration of an MCP-1

neutralizing antibody completely eliminated the ability of WT SMCs to stimulate migration, suggesting MCP-1 to be a critical proinflammatory signal released by aortic SMCs (Figure 4D).

Exogenous PKCδ reverses the aneurysm-resistant phenotype of KO mice

Data derived from the above *in vitro* analyses suggest that PKCδ gene deletion attenuates aneurysm development primarily through preventing aortic SMCs from undergoing apoptosis and/or producing proinflammatory chemokines, specifically MCP-1. To test this hypothesis, we developed an aortic tissue-specific gene transfer method to restore PKCδ expression in the arterial wall of KO mice. As described in Methods, adenovirus was administered to the aortic wall immediately following the removal of $CaCl_2$. This gene transfer method produced a localized transgene expression as illustrated by using an adenovirus encoding EGFP (AdGFP). While producing abundant GFP expression in the infrarenal region of the aortic wall, aortic administration of AdGFP did not produce transgene expression in circulating white blood cells (Supplemental Figure 9A, B).

To restore PKCδ expression in aortas of PKCδ KO mice, adenovirus expressing either PKCδ or β-galactosidase (AdPKCδ or AdLacZ) was administered to the infrarenal aorta of PKCδ KO mice. Mice were sacrificed after 7 or 42 days for histological and morphological analyses, respectively. Delivery of AdPKCδ successfully induced localized aortic expression of PKCδ in KO mice, mostly in the perivascular region and to a lesser degree in the SMA^+ media (Supplemental Figure 9C, D). Forty-two days after the $CaCl_2$ treatment, AdLacZ-treated PKCδ KO mice displayed minimum aortic expansion, with a final diameter measurement of 0.67±0.07mm (29.2±15.9%), indicating that viral infection alone did not alter the aneurysm-resistant

phenotype of KO mice. In comparison, delivery of AdPKCδ produced significant aortic expansion in KO mice (final diameter 1.11±0.21mm; 114.8±28.3%), an induction comparable to that seen in wildtype mice (Figure 5A, B). The apparent restoration of aneurysm formation shown to accompany aortic gene transfer of PKCδ is further evidenced by fragmented elastin fibers as well as TUNEL positive apoptotic cells and infiltrating monocytes/macrophages at 7 days after surgery (Figure 5C).

Aortic inhibition of PKCδ attenuates aneurysm formation in C57B/6 mice

To further demonstrate the importance of aortic PKCδ expression in aneurysm development, we tested the effect of aortic inhibition of PKCδ. Following the routine $CaCl_2$ treatment, C57BL/6 mice were subjected to local infection with either a dominant negative PKCδ mutant adenovirus (AdPKCδDN) or AdLacZ as control. Mice were sacrificed after 7 or 42 days for histological and morphological analyses, respectively. As shown in Figure 5D and E, treatment with AdPKCδDN produced a moderate but significant attenuation in aneurysm formation in C57B/6 mice as reflected by a reduction in aortic expansion as compared to the AdLacZ-treated mice (final aortic diameter measurement 0.74±0.11mm or 54.7±28.3%, and 1.05±0.06mm or 126.5±15.7%, respectively). Accordingly, local inhibition of PKCδ activity diminished elastin degradation, apoptotic activity, and infiltration of monocytes/macrophages in the arterial wall (Figure 5F).

Exogenous MCP-1 protein restores aneurysm to PKCδ KO animals

Various studies have implicated an important role for both MCP-1/CCR2 signaling in vascular diseases including atherosclerosis and AAA [31-34]. Both *in vivo* and *in vitro* analyses

within the current study indicate a reduction of MCP-1 expression caused by PKCδ gene deficiency; this prompted us to test whether delivery of exogenous MCP-1 to the arterial wall of PKCδ KO mice could restore aneurysm formation. Immediately following $CaCl_2$ treatment, recombinant MCP-1 protein suspended in pluronic gel was delivered to the infrarenal aortic region of KO mice. As vehicle controls, parallel groups of KO and WT mice were treated with pluronic gel + solvent. As shown in Figure 6A and B, solvent treated WT aortas developed aneurysmal expansion comparable to those previously observed in these mice at 42 days after $CaCl_2$ treatment (0.84±0.04mm, 73.7±8.2%). At this same time point, pluronic gel + solvent treated PKCδ KO aortas maintained their aneurysm-resistant phenotype despite the administration of pluronic gel, a stark contrast to the KO aortas treated with recombinant MCP-1 (Aortic diameter 0.62±0.06mm or 27.1±12.5%, and 0.91±0.04mm or 89.6±9.4%, respectively). Administration of recombinant MCP-1 in KO aorta created elastin degradation similar to that seen in solvent treated WT aorta, while solvent treated KO aortas remained largely unaffected. Further histological analysis of these samples revealed a marked increase of macrophage infiltration in the MCP-1 treated mice as compared to solvent-treated PKCδ KO mice. Of note, the level of aortic SMC apoptosis in PKCδ KO mice was not significantly altered by the MCP-1 administration (Figure 6C).

DISCUSSION

Our data for the first time provide direct evidence that PKCδ is an integral signaling molecule in the pathogenesis of abdominal aortic aneurysm. We showed that inhibition of PKCδ, either through targeted gene deletion or overexpression of a dominant negative mutant, protected mice from developing characteristic features of aneurysm including inflammation, disruption of elastin fibers, and loss of vascular SMCs. Additionally, the aneurysm-resistant phenotype was accompanied by diminished inflammatory infiltration, cytokine production, and medial apoptosis. These results not only confirm the importance of PKCδ in regulation of SMC apoptosis but also indicate a novel role for this kinase in the proinflammatory signaling cascade, at least in the aneurysm setting.

Although PKCδ is ubiquitously expressed in many tissues and cell types, results reported here suggest the role of this signaling protein in aneurysm pathophysiology may be primarily localized in vascular SMCs. Furthermore, our evidence suggests PKCδ may act largely through regulating expression of proinflammatory chemokines and cytokines, notably MCP-1. This notion is supported by several *in vivo* and *in vitro* findings: (1) PKCδ gene deficiency reduced the production of MCP-1 and other cytokines by aortic SMCs, but did not significantly alter the ability of monocytes to migrate; (2) an adenovirus-mediated delivery of PKCδ locally to the arterial wall was sufficient to rescue aneurysm development in PKCδ KO mice; (3) aorta-specific inhibition of PKCδ delivered a moderate but significant level of protection in C57B/6 mice; and (4) ectopic administration of MCP-1 to the aortic wall of PKCδ KO mice sufficiently rescued aneurysm development.

It has been postulated that vascular SMCs are the "soil" of AAA development [35]. Being a major source of ECM proteins, SMCs would be critical in counter balancing the upregulated proteolytic activities present in aneurysmal tissue. As such, the depletion of medial SMCs eliminates a cell population capable of directing connective tissue repair and may thus potentiate the degradation of the arterial wall and facilitate eventual rupture [36]. This study contains data supporting the idea that the dearth of connective tissue in AAA can be reversed in the presence of healthy SMCs, thus possibly either preventing or even reversing aneurysm growth. Specifically, we showed that arteries of $CaCl_2$-treated KO mice sustained a similar degree of initial damage to aortic elastin fibers as WT aorta, but by 42 days elastin integrity is restored in KO arteries.

Results from the current study further illustrate another important function of SMCs in vascular disease, i.e. as providing proinflammatory signals. The potential link between SMC apoptosis and the production of pro-inflammatory chemokines has been previously indicated in atherosclerosis. Using a mouse atherosclerosis model, Clarke and colleagues convincingly demonstrated that SMC apoptosis induces MCP-1 expression, inflammatory infiltrate, and other features of plaque rupture [37]. Recently, our own group demonstrated that blocking apoptosis with a pan-caspase inhibitor protected mice from angiotensin II-induced vascular inflammation and aneurysm expansion [18]. These data suggest that, while apoptosis and inflammation are most commonly considered unrelated events, apoptosis in an aneurysm setting may promote the inflammatory response. Such interaction between apoptosis and inflammation has been explored in atherosclerosis. Clarke and colleagues suggest that the pro-inflammatory property of apoptotic SMCs may be attributed to

inhibited phagocytosis generated in the hyperlipidemic environment in atherosclerotic arteries (31). Although abdominal aortic aneurysm is commonly associated with atherosclerosis, these two diseases are believe to be caused by distinct pathological processes. However, deficient phagocytosis is also being investigated as an underlying pathophysiological event in other types of inflammatory disorders, including autoimmue diseases (32), thus warranting the exploration of this process in the pathogenesis of AAA.

Another important finding described in this work is the apparent critical role of PKCδ in MCP-1 function during formation and progression of aneurysm. *In vitro* and *in vivo* evidence suggests that impaired production of MCP-1 expression by aortic SMCs was the primary mechanism underlying the aneurysm-resistant phenotype of PKCδ KO mice. Importantly, this notion is further supported by the evidence that localized aortic administration of recombinant MCP-1 to the aorta of PKCδ KO mice restored vascular inflammation, elastin degradation, and aneurysmal expansion. While several groups have explored the role of the CCR2/MCP-1 signaling axis in the aneurysm progression [31, 38-40], this work provides what we believe to be the first evidence suggesting MCP-1 to be a critical downstream effector of PKCδ signaling in the pathogenesis of aneurysm.

Although our study has implicated a critical role for MCP-1 in AAA, it is important to consider the large number of cytokines that likely play a role in AAA development and progression. Our RT-PCR analysis identified additional cytokines that may be regulated by PKCδ and require further investigation.

Interestingly, localized aortic delivery of exogenous MCP-1 failed to reverse the apoptosis-resistant phenotype of PKCδ KO mice. A similar number of $TUNEL^+$ cells were found in MCP-1 and solvent-treated PKCδ KO mice. In contrast, a similar rescue experiment delivering exogenous PKCδ to the arterial wall restored all aneurysm-related cellular events, i.e. inflammation, apoptosis, and elastin degradation, in $CaCl_2$ PKCδ KO arteries. These results not only underscore the critical role of PKCδ in the apoptotic response of SMCs, but also provide support for a novel relationship between PKCδ, MCP-1, and AAA. In the absence of this "master" mediator, apoptosis would be inhibited even when aortic SMCs are surrounded by infiltrating inflammatory cells, their inflammatory byproducts, and degraded elastin fibers. Based on rescue experiments presented here, as well as other data from the current and prior reports [19, 20], we propose a model in which PKCδ-mediated MCP-1 functions as a molecular link through which apoptotic SMCs stimulate the inflammatory process. Importantly, our model suggests that SMC apoptosis may contribute to aneurysm development primarily through the induction of inflammatory cytokines. That is, in the presence of abundant pro-inflammatory cytokines, such as the environment created by delivery of exogenous MCP-1 protein, the inflammatory and proteolytic events can proceed in full force without the participation of apoptosis.

Using a rat carotid balloon-injury model of intimal hyperplasia, our group recently showed that PKCδ mediated the expression of MCP-1, which was critical for the migration of adventitial fibroblasts to the media and neo-intima [41]. In the $CaCl_2$-treated aorta, we noted a marked expansion of the adventitia associated with abundant infiltration of macrophages and other inflammatory cells. While the presence of macrophages in the adventitia is a prominent

feature of AAA [31, 32, 35] and the role of adventitial fibroblasts in aneurysm has been explored to some extent by several groups [42-45], the precise relationship between adventitial fibroblasts, SMCs, and inflammatory cells in the context of AAA remains a highly interesting subject for future study. Evidence presented here shows the localization of IL-6 and macrophages predominantly in the adventitia, whereas MCP-1 production and apoptosis appears to occur primarily, though not exclusively, in the medial layer. It is also important to note that PKCδ, being a ubiquitously expressed protein, is also found in the adventitia. Whether PKCδ also contributes to aneurysm pathogenesis through adventitia cells should be explored in future studies given the prominent inflammatory response in the adventitia. However, several key questions remain to be addressed in models of AAA, for example, how adventitial fibroblasts may respond to medial SMC depletion, matrix degradation, and inflammatory cell infiltration.

Being a major signaling molecule, PKCδ can be activated by multiple extracellular and intracellular signals including growth factors, inflammatory cytokines, mechanical stimuli, and oxidative stress. Not all of these signals are able to induce apoptosis or the production of MCP-1. It remains to be determined whether the pro-apoptotic and proinflammatory functions of PKCδ are exerted through the same or partially overlapping pathways. We have previously shown that MAP kinase pathways are affected by PKCδ gene deficiency [20, 46]. Although the involvement of MAP kinases in the regulation of MCP-1 expression has been demonstrated [47] the precise molecular interaction between PKCδ and MAP kinases and how this interaction may influence MCP-1 expression remains to be determined. Additionally, Liu and colleagues recently demonstrated that PKCδ mediates the stability of MCP-1 mRNA in vascular SMCs using a chemical inhibitor of PKCδ [48]. Our group previously described the role of MAP kinases in

regulation of mRNA stability in vascular SMCs, leading us to speculate that PKCδ may control MCP-1 mRNA turnover through a MAP kinase-mediated mechanism [49].

Taken together, our data show that the stress response regulating apoptosis and inflammatory signaling in the arterial wall may be largely dependent upon PKCδ upregulation. Accordingly, inhibition of PKCδ attenuated vascular inflammation and preserved tissue integrity, resulting in the prevention of aneurysm development in a $CaCl_2$-induced model of AAA. Further, PKCδ gene deficiency appears to protect mice from developing aneurysm in the elastse model of AAA, as shown in Supplemental Figure 3. Unfortunately, the potential role of PKCδ in the Angiotensin II model is yet to be explored, as our attempts to breed $PKC\delta^{-/-}ApoE^{-/-}$ double knockout mice were unsuccessful. However, we did show that levels of PKCδ were significantly elevated in aortas of $ApoE^{-/-}$ mice treated with AngII. Taken together, we believe the elevated expression of this stress gene in human aneurysmal tissues, as well as the role we have shown it to play in mouse models, suggest it to be an attractive candidate for therapeutic target(s).

ACKNOWLEDGEMENTS

The authors would like to thank Drs. K. Craig Kent and Jon Mutsumura of the University of Wisconsin, Madison for intellectual inputs, Dr. Keiichi I Nakayama of Kyushu University in Japan for the generous gift of PKCδ knockout mice, Dr. T. Biden at the Garvan Institute of Australia for AdPKCδDN, and Drew Roenneburg of the University of Wisconsin, Madison for technical assistance in histology.

This work was supported by the National Institute of Health R01HL088447 (BL), American Heart Association 10GRNT3020052 (BL), Howard Hughes Medical Institute MSN135276 (SS), and the Ruth L. Kirschstein National Research Service Award T32 HL 07936 from the National Heart Lung and Blood Institute to the University of Wisconsin-Madison Cardiovascular Research Center (SM).

No disclosures to report.

REFERENCES

1. Ailawadi G, Eliason JL, Upchurch GR, Jr. Current concepts in the pathogenesis of abdominal aortic aneurysm. *J Vasc Surg*. 2003;38:584-588
2. Nordon I, Hinchliffe R, Holt P, Loftus I, Thompson M. Review of current theories for abdominal aortic aneurysm pathogenesis. *Vascular*. 2009;17:253-263
3. Wills A, Crowther MTM, Sayers R, Bell P. Pathogenesis of abdominal aortic aneurysms - cellular and biochemical mechanisms. *Eur J Vasc Endovasc Surg*. 1996;12:391-400
4. Daugherty A, Cassis LA. Mouse models of abdominal aortic aneurysms. *Arterioscler Thromb Vasc Biol*. 2004;24:429-434
5. Aziz F, Kuivaniemi H. Role of matrix metalloproteinase inhibitors in preventing abdominal aortic aneurysm. *Ann Vasc Surg*. 2007;21:392-401
6. Longo GM, Xiong W, Greiner TC, Zhao Y, Fiotti N, Baxter BT. Matrix metalloproteinases 2 and 9 work in concert to produce aortic aneurysms. *The Journal of Clinical Investigation*. 2002;110:625-632
7. Petrinec D, Liao S, Holmes DR, Reilly JM, Parks WC, Thompson RW. Doxycycline inhibition of aneurysmal degeneration in an elastase-induced rat model of abdominal aortic aneurysm: Preservation of aortic elastin associated with suppressed production of 92 kd gelatinase. *Journal of Vascular Surgery*. 1996;23:336-346
8. Pyo R, Lee JK, Shipley JM, Curci JA, Mao D, Ziporin SJ, Ennis TL, Shapiro SD, Senior RM, Thompson RW. Targeted gene disruption of matrix metalloproteinase-9 (gelatinase b) suppresses development of experimental abdominal aortic aneurysms. *The Journal of Clinical Investigation*. 2000;105:1641-1649
9. Thompson RW, Baxter BT. Mmp inhibition in abdominal aortic aneurysms. Rationale for a prospective randomized clinical trial. *Ann N Y Acad Sci*. 1999;878:159-178
10. Golledge ALV, Walker P, Norman PE, Golledge J. A systematic review of studies examining inflammation associated cytokines in human abdominal aortic aneurysm samples. *Disease Markers*. 2009;26:181-188
11. Golledge J, Tsao PS, Dalman RL, Norman PE. Circulating markers of abdominal aortic aneurysm presence and progression. *Circulation*. 2008;118:2382-2392
12. Shimizu K, Mitchell RN, Libby P. Inflammation and cellular immune responses in abdominal aortic aneurysms. *Arterioscler Thromb Vasc Biol*. 2006;26:987-994
13. Eliason JL, Hannawa KK, Ailawadi G, Sinha I, Ford JW, Deogracias MP, Roelofs KJ, Woodrum DT, Ennis TL, Henke PK, Stanley JC, Thompson RW, Upchurch GR, Jr. Neutrophil depletion inhibits experimental abdominal aortic aneurysm formation. *Circulation*. 2005;112:232-240
14. Xiong W, Zhao Y, Prall A, Greiner TC, Baxter BT. Key roles of cd4+ t cells and ifn-gamma in the development of abdominal aortic aneurysms in a murine model. *J Immunol*. 2004;172:2607-2612
15. Sun J, Sukhova GK, Yang M, Wolters PJ, MacFarlane LA, Libby P, Sun C, Zhang Y, Liu J, Ennis TL, Knispel R, Xiong W, Thompson RW, Baxter BT, Shi GP. Mast cells modulate the pathogenesis of elastase-induced abdominal aortic aneurysms in mice. *J Clin Invest*. 2007;117:3359-3368

16. Shimizu K, Shichiri M, Libby P, Lee RT, Mitchell RN. Th2-predominant inflammation and blockade of ifn-gamma signaling induce aneurysms in allografted aortas. *J Clin Invest*. 2004;114:300-308
17. Lopez-Candales A, Holmes D, Liao S, Scott M, Wickline S, Trompson R. Decreased vascular smooth muscle cell density in medial degeneration of human abdominal aortic aneurysms. *Am J Pathol*. 1997;150:993-1007
18. Yamanouchi D, Morgan S, Kato K, Lengfeld J, Zhang F, Liu B. Effects of caspase inhibitor on angiotensin ii-induced abdominal aortic aneurysm in apolipoprotein e-deficient mice. *Arterioscler Thromb Vasc Biol*. 2010;30:702-707
19. Kato K, Yamanouchi D, Esbona K, Kamiya K, Zhang F, Kent KC, Liu B. Caspase-mediated protein kinase c-{delta} cleavage is necessary for apoptosis of vascular smooth muscle cells. *Am J Physiol Heart Circ Physiol*. 2009;297:H2253-2261
20. Ryer EJ, Sakakibara K, Wang C, Sarkar D, Fisher PB, Faries PL, Kent KC, Liu B. Protein kinase c delta induces apoptosis of vascular smooth muscle cells through induction of the tumor suppressor p53 by both p38-dependent and p38-independent mechanisms. *Journal of Biological Chemistry*. 2005;280:35310-35317
21. Schubl S, Tsai S, Ryer EJ, Wang C, Hu J, Kent KC, Liu B. Upregulation of protein kinase c[delta] in vascular smooth muscle cells promotes inflammation in abdominal aortic aneurysm. *Journal of Surgical Research*. 2009;153:181-187
22. Leitges M, Mayr M, Braun U, Mayr U, Li C, Pfister G, Ghaffari-Tabrizi N, Baier G, Hu Y, Xu Q. Exacerbated vein graft arteriosclerosis in protein kinase cd null mice. *The Journal of Clinical Investigation*. 2001;108:1505-1512
23. Yamanouchi D, Kato K, Ryer EJ, Zhang F, Liu B. Protein kinase c delta mediates arterial injury responses through regulation of vascular smooth muscle cell apoptosis. *Cardiovasc Res*. 2010;85:434-443
24. Miyamoto A, Nakayama K, Imaki H, Hirose S, Jiang Y, Abe M, Tsukiyama T, Nagahama H, Ohno S, Hatakeyama S, Nakayama KI. Increased proliferation of b cells and auto-immunity in mice lacking protein kinase c[delta]. *Nature*. 2002;416:865-869
25. Gertz SD, Kurgan A, Eisenberg D. Aneurysm of the rabbit common carotid artery induced by periarterial application of calcium chloride in vivo. *The Journal of Clinical Investigation*. 1988;81:649-656
26. Ikonomidis JS, Gibson WC, Butler JE, McClister DM, Sweterlitsch SE, Thompson RP, Mukherjee R, Spinale FG. Effects of deletion of the tissue inhibitor of matrix metalloproteinases-1 gene on the progression of murine thoracic aortic aneurysms. *Circulation*. 2004;110:II-268-II-273
27. Kimura T, Yoshimura K, Aoki H, Imanaka-Yoshida K, Yoshida T, Ikeda Y, Morikage N, Endo H, Hamano K, Imaizumi T, Hiroe M, Aonuma K, Matsuzaki M. Tenascin-c is expressed in abdominal aortic aneurysm tissue with an active degradation process. *Pathology International*. 2011;61:559-564
28. Yoshimura K, Aoki H, Ikeda Y, Fujii K, Akiyama N, Furutani A, Hoshii Y, Tanaka N, Ricci R, Ishihara T, Esato K, Hamano K, Matsuzaki M. Regression of abdominal aortic aneurysm by inhibition of c-jun n-terminal kinase. *Nat Med*. 2005;11:1330-1338

29. Clowes A, Clowes M, Fringerle J, Reidy M. Kinetics of cellular poliferation after arterial injury: Role of acute distension in the induciton of smooth muscle proliferation. *Lab Invest*. 1989;60:360-364
30. Shimizu K, Shichiri M, Libby P, Lee RT, Mitchell RN. Th2-predominant inflammation and blockade of ifn-γ signaling induce aneurysms in allografted aortas. *The Journal of Clinical Investigation*. 2004;114:300-308
31. Daugherty A, Rateri DL, Charo IF, Owens AP, Howatt DA, Cassis LA. Angiotensin ii infusion promotes ascending aortic aneurysms: Attenuation by ccr2 deficiency in apoe-/- mice. *Clinical Science*. 2010;118:681-689
32. de Waard V, Bot I, de Jager SCA, Talib S, Egashira K, de Vries MR, Quax PHA, Biessen EAL, van Berkel TJC. Systemic mcp1/ccr2 blockade and leukocyte specific mcp1/ccr2 inhibition affect aortic aneurysm formation differently. *Atherosclerosis*. 2010;211:84-89
33. Libby P. Inflammation in atherosclerosis. *Nature*. 2002;420:868-874
34. Zhang L, Li HY, Li H, Zhao J, Su L, Zhang Y, Zhang SL, Miao JY. Lipopolysaccharide activated phosphatidylcholine-specific phospholipase c and induced il-8 and mcp-1 production in vascular endothelial cells. *Journal of Cellular Physiology*. 2011;226:1694-1701
35. Curci JA. Digging in the "soil" of the aorta to understand the growth of abdominal aortic aneurysms. *Vascular*. 2009;17:S21-29
36. Thompson RW, Liao S, Curci JA. Vascular smooth muscle cell apoptosis in abdominal aortic aneurysms. *Coron Artery Dis*. 1997;8:623-631
37. Clarke MC, Figg N, Maguire JJ, Davenport AP, Goddard M, Littlewood TD, Bennett MR. Apoptosis of vascular smooth muscle cells induces features of plaque vulnerability in atherosclerosis. *Nat Med*. 2006;12:1075-1080
38. Ishibashi M, Egashira K, Zhao Q, Hiasa K-i, Ohtani K, Ihara Y, Charo IF, Kura S, Tsuzuki T, Takeshita A, Sunagawa K. Bone marrow-derived monocyte chemoattractant protein-1 receptor ccr2 is critical in angiotensin ii-induced acceleration of atherosclerosis and aneurysm formation in hypercholesterolemic mice. *Arterioscler Thromb Vasc Biol*. 2004;24:e174-178
39. MacTaggart JN, Xiong W, Knispel R, Baxter BT. Deletion of ccr2 but not ccr5 or cxcr3 inhibits aortic aneurysm formation. *Surgery*. 2007;142:284-288
40. Moehle CW, Bhamidipati CM, Alexander MR, Mehta GS, Irvine JN, Salmon M, Upchurch Jr GR, Kron IL, Owens GK, Ailawadi G. Bone marrow–derived mcp1 required for experimental aortic aneurysm formation and smooth muscle phenotypic modulation. *The Journal of Thoracic and Cardiovascular Surgery*. 2011;142:1567-1574
41. Si Y, Ren J, Wang P, Rateri DL, Daugherty A, Shi X-D, Kent KC, Liu B. Protein kinase c-delta mediates adventitial cell migration through regulation of monocyte chemoattractant protein-1 expression in a rat angioplasty model. *Arteriosclerosis, Thrombosis, and Vascular Biology*. 2012;32:943-954
42. Maiellaro K, Taylor WR. The role of the adventitia in vascular inflammation. *Cardiovascular Research*. 2007;75:640-648
43. Sakata N, Nabeshima K, Iwasaki H, Tashiro T, Uesugi N, Nakashima O, Ito H, Kawanami T, Furuya K, Kojima M. Possible involvement of myofibroblast in the development of inflammatory aortic aneurysm. *Pathology - Research and Practice*. 2007;203:21-29

44. Tedesco MM, Terashima M, Blankenberg FG, Levashova Z, Spin JM, Backer MV, Backer JM, Sho M, Sho E, McConnell MV, Dalman RL. Analysis of in situ and ex vivo vascular endothelial growth factor receptor expression during experimental aortic aneurysm progression. *Arteriosclerosis, Thrombosis, and Vascular Biology*. 2009;29:1452-1457
45. Tieu BC, Lee C, Sun H, LeJeune W, Recinos A, Ju X, Spratt H, Guo D-C, Milewicz D, Tilton RG, Brasier AR. An adventitial il-6/mcp1 amplification loop accelerates macrophage-mediated vascular inflammation leading to aortic dissection in mice. *The Journal of Clinical Investigation*. 2009;119:3637-3651
46. Liu B, Ryer EJ, Kundi R, Kamiya K, Itoh H, Faries PL, Sakakibara K, Kent KC. Protein kinase c-[delta] regulates migration and proliferation of vascular smooth muscle cells through the extracellular signal-regulated kinase 1/2. *Journal of Vascular Surgery*. 2007;45:160-168
47. Fischer S, Weishaupt A, Troppmair J, Martini R. Increase of mcp-1 (ccl2) in myelin mutant schwann cells is mediated by mek-erk signaling pathway. *Glia*. 2008;56:836-843
48. Liu B, Dhawan L, Blaxall B, Taubman M. Protein kinase cδ mediates mcp-1 mrna stabilization in vascular smooth muscle cells. *Molecular and Cellular Biochemistry*. 2010;344:73-79
49. Sakakibara K, Kubota K, Worku B, Ryer EJ, Miller JP, Koff A, Kent KC, Liu B. Pdgf-bb regulates p27 expression through erk-dependent rna turn-over in vascular smooth muscle cells. *Journal of Biological Chemistry*. 2005;280:25470-25477

Figure 1. PKCδ expression correlates with apoptosis in an experimental aneurysm model. Aortas of C57B/6 mice were treated with $CaCl_2$ or NaCl and harvested 3, 7 and 14 days ($CaCl_2$ group) or 7 days (NaCl group) after surgery. (A) Cross sections stained for PKCδ (green) or apoptosis (TUNEL, red), and nuclei (DAPI, blue). Scale bar=200μm. (B) Positive cell ratio calculated as number of apoptotic (TUNEL+) or PKCδ positive cells divided by respective number of DAPI positive cells. *p<0.05 compared to NaCl control, n=6. (C) Representative confocal images for co-localization analysis in cross sections harvested 7 days after $CaCl_2$ treatment. Top panel: Co-stain TUNEL (red) and PKCδ (green). Bottom panel: Co-stain for SMCs (MHC, red) and PKCδ (green). Scale bar=50 μm, Overlay with DAPI (blue). (D) Representative Western blot analysis of PKCδ expression in tissues harvested from two different aortas of C57B/6 mice 7 days after NaCl or $CaCl_2$ treatment. (E) Quantification of PKCδ expression from Western blot, normalized to β-actin. PKCδ expression shown as a total of both cleaved and full-length portions. *p<0.05, n=4.

Figure 2. PKCδ knockout mice are resistant to aneurysm induction. (A) Representative photos of abdominal aortas of PKCδ wildtype (WT) and knockout (KO) mice, taken 42 days after the $CaCl_2$ treatment. Scale bar=5 mm. (B) Aortic diameter measured prior to (Pre, white bars), and 42 days after (Post, black bars), $CaCl_2$ treatment. *p<0.05 compared to the $CaCl_2$ treated KO arteries, n=6. (C) Representative photos of 42 day aortic sections stained for elastin (Van-Gieson), scale bar=100 μm. (D) Grading of elastin degradation in Van Gieson stained arteries harvested 42 days after surgery. *p<0.05 WT compared to KO, n=4. (E) Representative confocal images of arterial sections co-immunostained for TUNEL (red) and Myosin Heavy Chain

(MHC, green) overlay with DAPI (blue); arteries harvested 7 days after surgery, scale bar = 50μm.

Figure 3. PKCδ gene deficiency attenuates the inflammatory response in experimental aneurysm. (A) Macrophage infiltration as measured by immunofluorescent stain (IFC) for Mac3 (green), overlay with DAPI (blue) or by immunohistochemical stain (IHC) for CD68; scale bar = 200μm. (B) Quantification of macrophage infiltration in aneurysm tissue as identified by CD68 stain, expressed as CD68 positive cells/nuclei. *p<0.05 compared to $CaCl_2$ treated KO arteries, n=4. (C) IHC for inflammatory cytokine interleukin 6 (IL-6) and IFC for monocyte chemoattractant protein-1 (MCP-1). Scale bar=200 μm. (D) RT-PCR analysis of IL-6 and MCP-1 mRNA abundance in aorta of WT and KO animals 7 days after surgery. *p<0.05 compared to KO arteries, n=4.

Figure 4. PKCδ mediates production of MCP-1 by vascular SMCs. Cultured aortic SMCs isolated from PKCδ KO or WT mice were treated with TNFα (50ng/mL, for 6h) (A-C). (A) RT-PCR analysis of selected cytokines. (B) Levels of secreted MCP-1 protein, measured by ELISA. (C) Levels of MCP-1 protein secreted by WT cells infected with AdLacZ or AdPKC, followed by treatment with TNFα. (D) Migration of RAW264.7 macrophages in response to conditioned media harvested from TNFα treated WT or KO SMCs in the presence of an anti-MCP-1 antibody (a-MCP-1) or hamster IgG (IgG) as control. *p<0.05, n=3.

Figure 5. Acute manipulation of PKCδ by adenovirus alters aneurysm phenotype in mice. Adenoviruses encoding PKCδ (AdPKCδ) (A-C) or a dominant negative PKCδ mutant (AdPKCδ-DN) (D-F) were delivered to aortas of PKCδKO mice or C57B/6 mice, respectively, immediately following $CaCl_2$ treatment. AdLacZ was used as a control. (A&D) Representative photos of aortas taken 42 days after surgery. Scale bar=5mm. (B&E) Aortic diameter measured prior to (Pre, white bars), and 42 days after (Post, black bars), $CaCl_2$ treatment. *p<0.05, n=4 and n=5 in B and E, respectively. (C&F) Aortic sections stained for Van Gieson (elastin) at 42 days, TUNEL (red, 7 days), or monocytes and macrophages (MOMA, green, 7 days). Nuclei were stained by DAPI (blue). 'L' delineates arterial lumen. Scale bar=200μm.

Figure 6. Delivery of exogenous MCP-1 to PKCδ KO mice restores aneurysm formation. (A) Representative photos of abdominal aortas of WT or KO mice that received solvent or MCP-1 (80μM), taken 42 days after the $CaCl_2$ procedure; scale bar=5mm. (B) Aortic diameter measured prior to (Pre, white bars), and 42 days after (Post, black bars), $CaCl_2$ treatment. *p<0.05, n=4. (C) Aortic sections stained for Van Gieson (42 days), TUNEL (red, 7 days), or monocytes and macrophages (MOMA, green, 7 days). Nuclei were stained by DAPI (blue). 'L' delineates arterial lumen. Scale bar=200 μm.

FIGURE 1

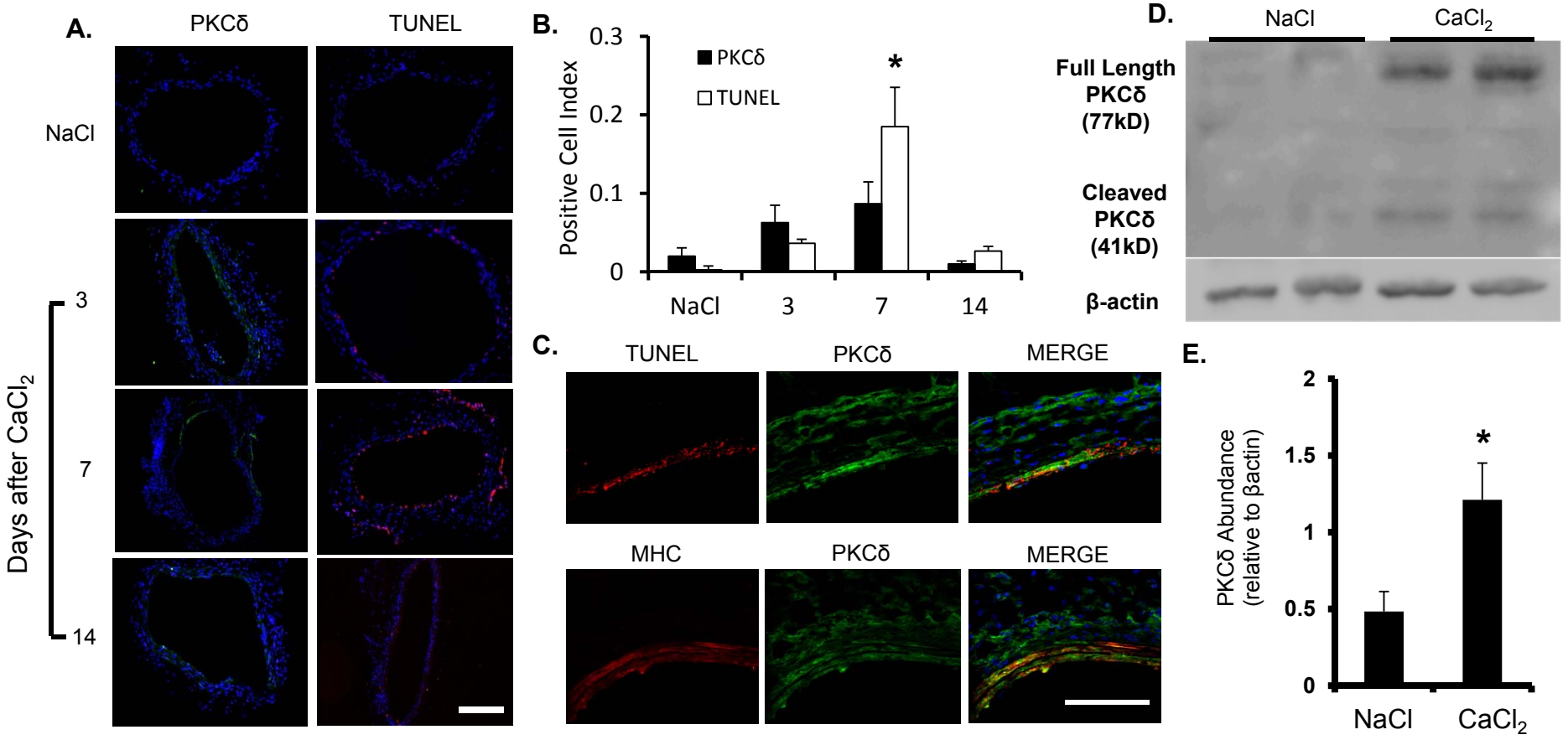
A.
PKCδ
TUNEL
NaCl
3
7
14
Days after CaCl2
B.
Positive Cell Index
0.3
0.2
0.1
0
PKCδ
TUNEL
*
NaCl
3
7
14
C.
TUNEL
PKCδ
MERGE
MHC
PKCδ
MERGE
D.
NaCl
CaCl2
Full Length PKCδ (77kD)
Cleaved PKCδ (41kD)
β-actin
E.
PKCδ Abundance (relative to βactin)
2
1.5
1
0.5
0
*
NaCl
CaCl2

FIGURE 2

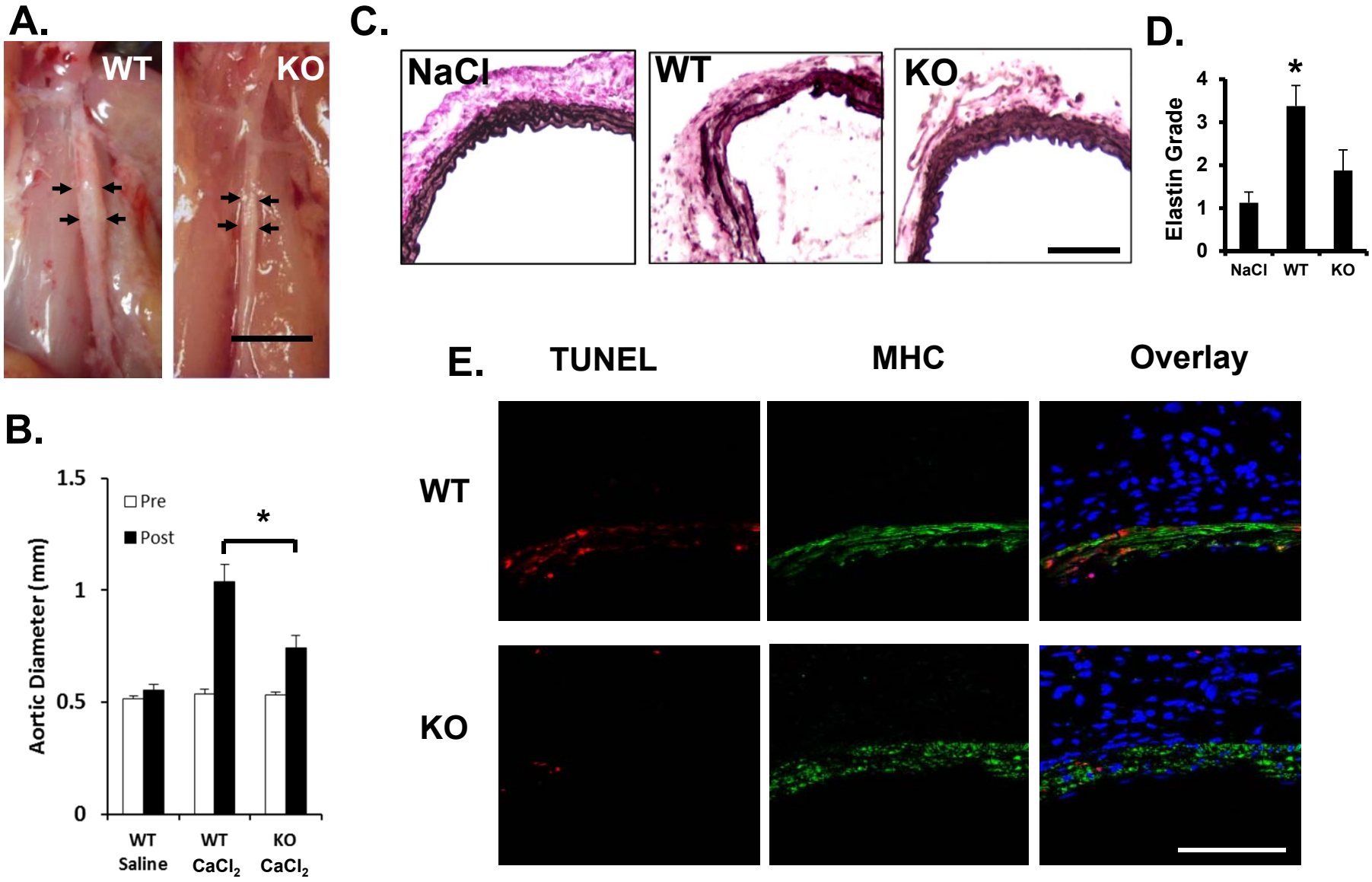
A.
WT
KO
B.
1.5
1
0.5
0
Pre
Post
*
Aortic Diameter (mm)
WT Saline
WT CaCl2
KO CaCl2
C.
NaCl
WT
KO
D.
Elastin Grade
4
3
2
1
0
*
NaCl
WT
KO
E.
TUNEL
MHC
Overlay
WT
KO

FIGURE 3

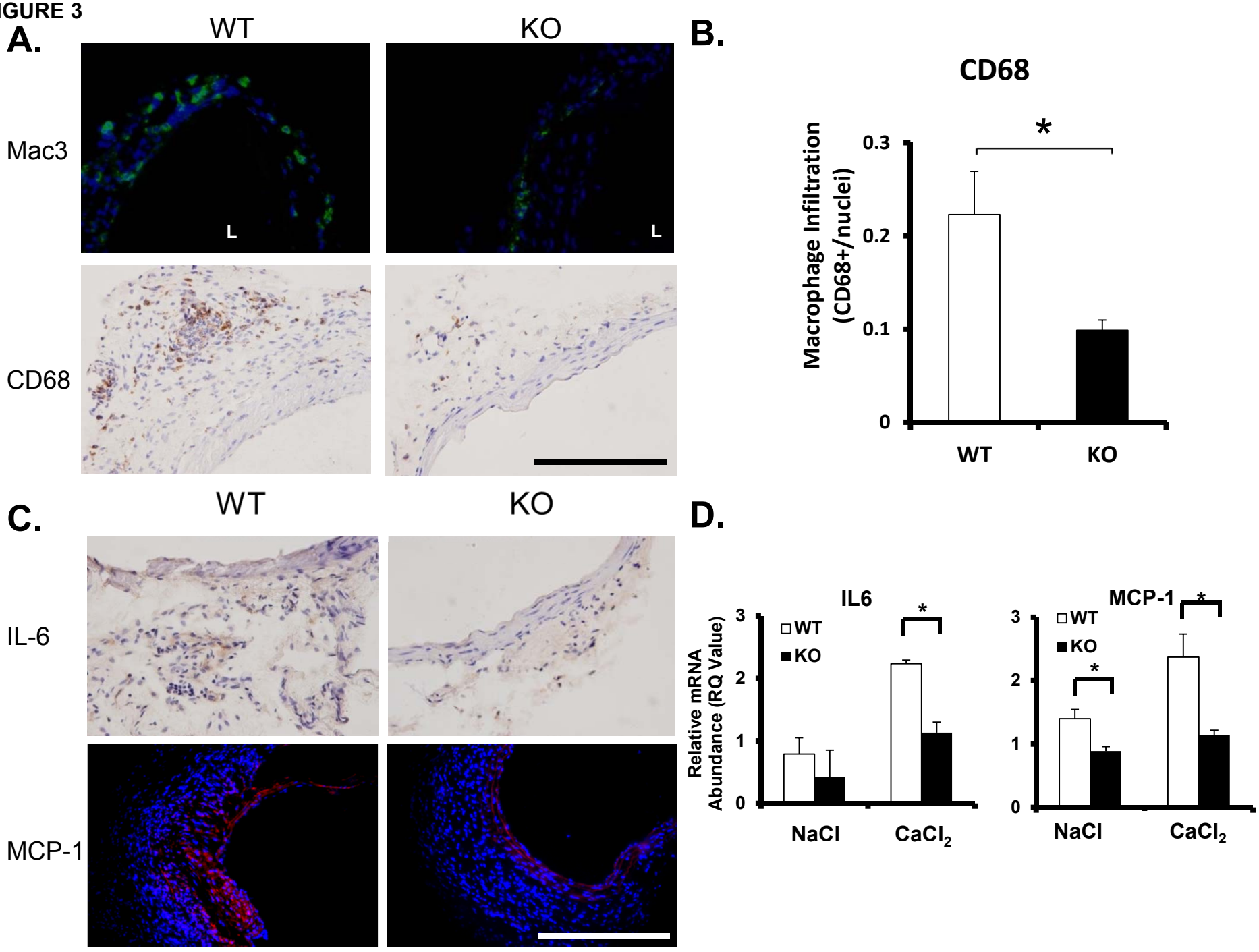
A.
WT
KO
Mac3
CD68
L
L
B.
CD68
Macrophage Infiltration
(CD68+/nuclei)
0.3
0.2
0.1
0
*
WT
KO
C.
WT
KO
IL-6
MCP-1
D.
IL6
MCP-1
Relative mRNA
Abundance (RQ Value)
WT
KO
3
2
1
0
*
NaCl
CaCl2

FIGURE 4

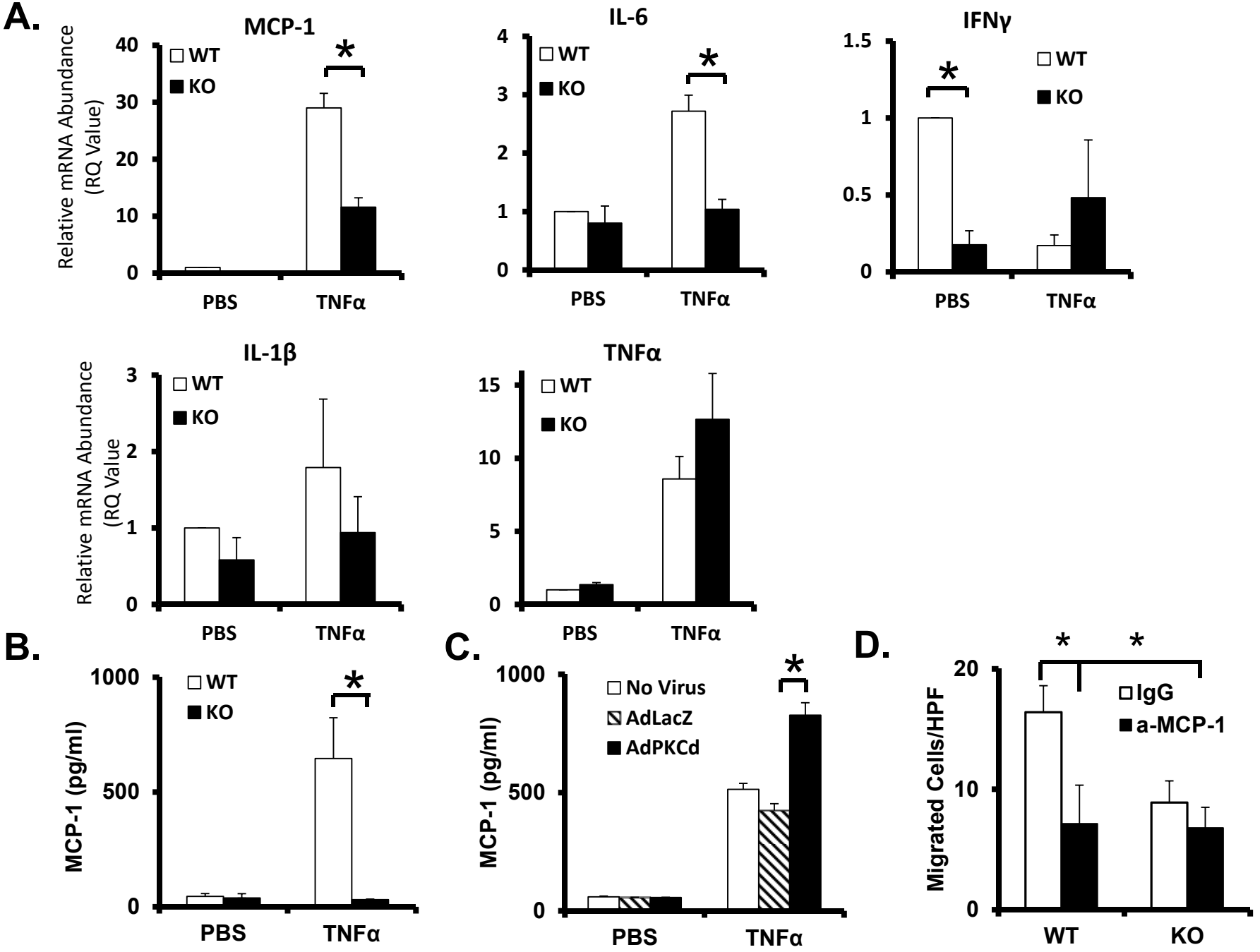
A.
MCP-1
IL-6
IFNγ
IL-1β
TNFα
Relative mRNA Abundance (RQ Value)
WT
KO
PBS
TNFα
*
B.
MCP-1 (pg/ml)
C.
No Virus
AdLacZ
AdPKCd
D.
Migrated Cells/HPF
IgG
a-MCP-1

Figure 5

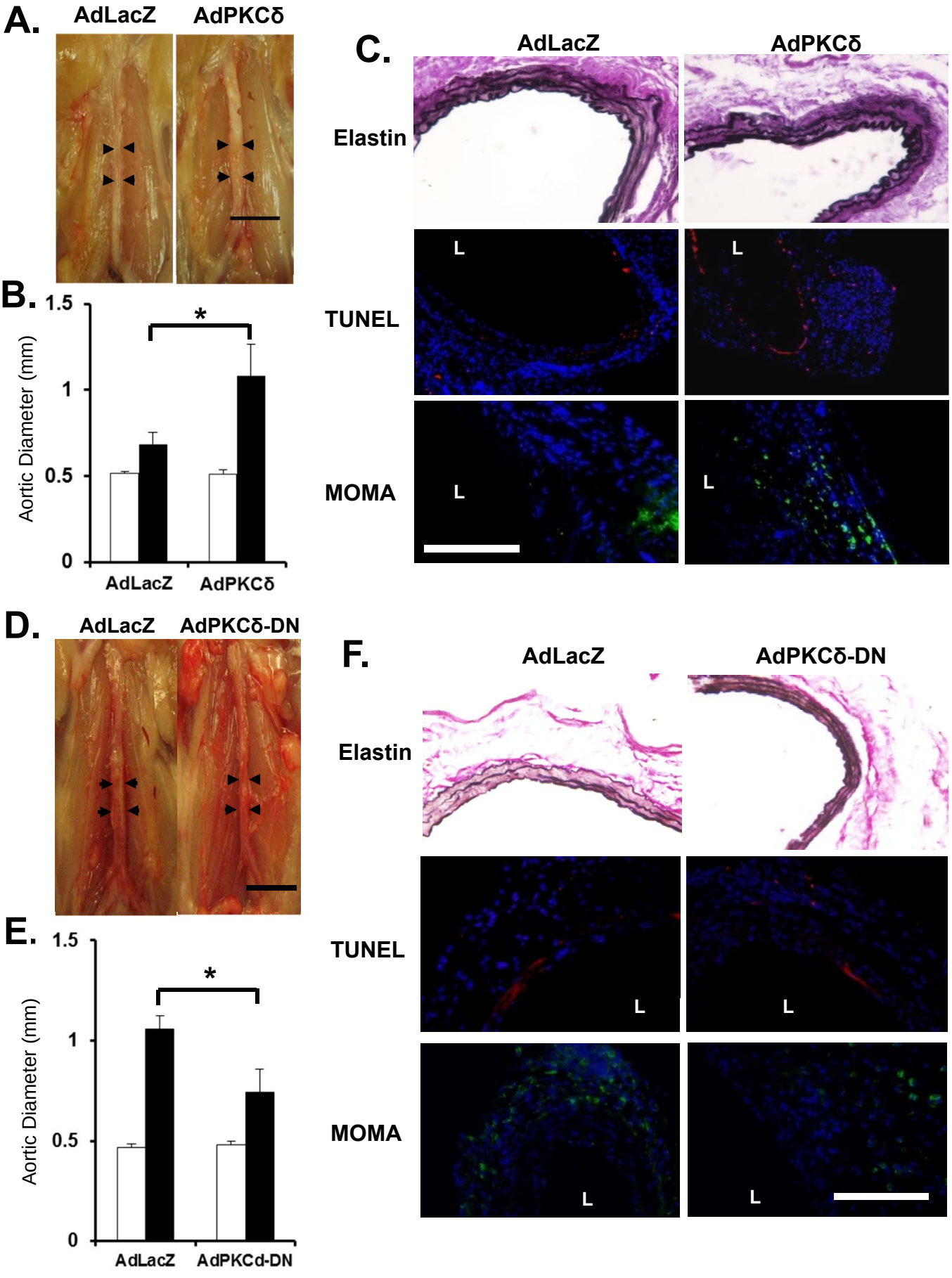
A.
AdLacZ
AdPKCδ
B.
Aortic Diameter (mm)
1.5
1
0.5
0
*
AdLacZ
AdPKCδ
C.
AdLacZ
AdPKCδ
Elastin
TUNEL
MOMA
L
D.
AdLacZ
AdPKCδ-DN
E.
Aortic Diameter (mm)
1.5
1
0.5
0
*
AdLacZ
AdPKCd-DN
F.
AdLacZ
AdPKCδ-DN
Elastin
TUNEL
MOMA
L

FIGURE 6

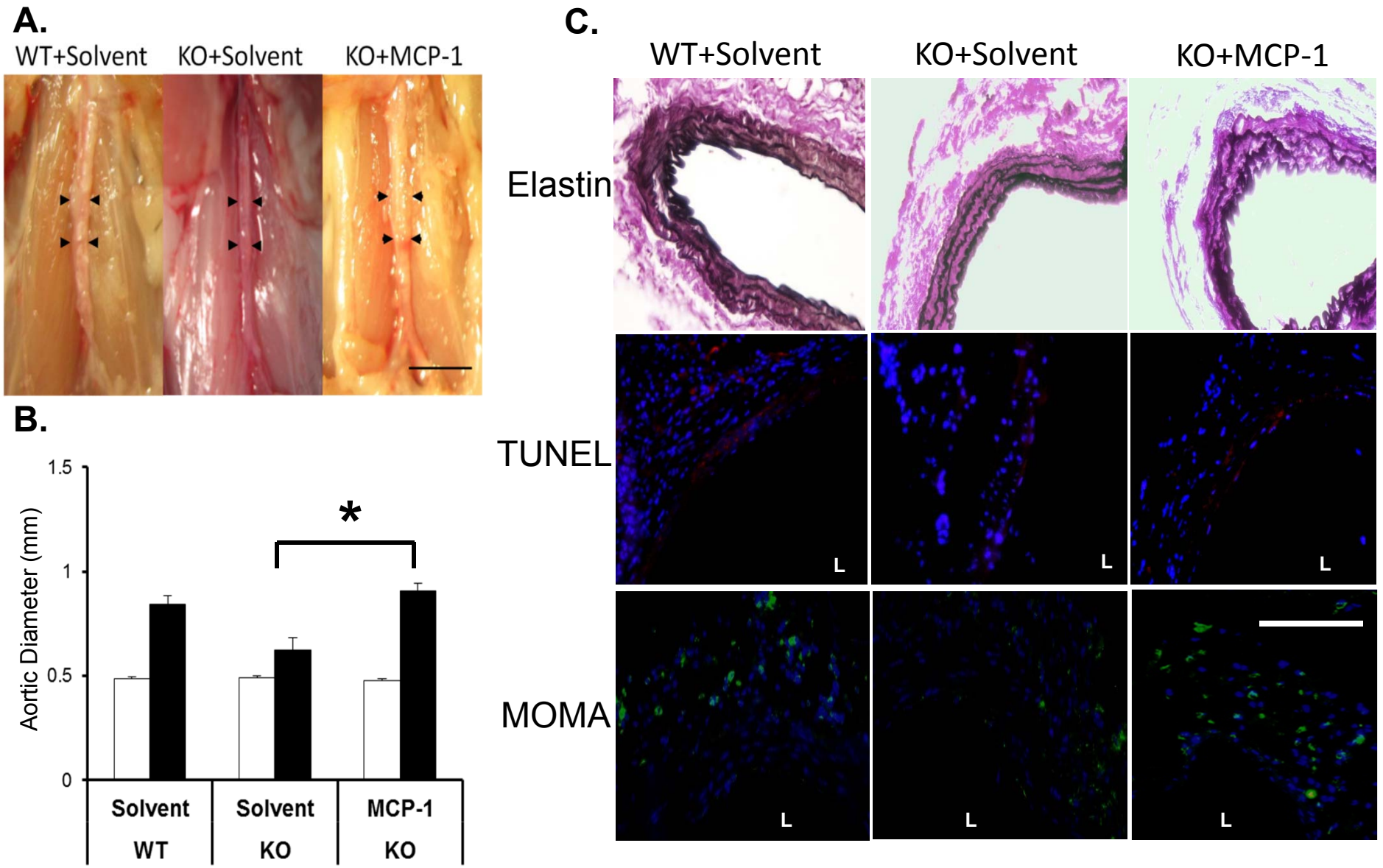
A.
WT+Solvent
KO+Solvent
KO+MCP-1
B.
Aortic Diameter (mm)
1.5
1
0.5
0
*
Solvent
WT
Solvent
KO
MCP-1
KO
C.
WT+Solvent
KO+Solvent
KO+MCP-1
Elastin
TUNEL
MOMA
L

Supplementary Table I. Complete Blood Count (CBC) results of PKCδ WT and KO mice. Red blood cells (RBC) and white blood cells (WBC) are shown; n=4.

Supplementary Figure I. Perivascular application of $CaCl_2$ induces progressive dilatation of abdominal aorta. (A) Representative photos of abdominal aortas of C57B/6 mice treated with 0.5M $CaCl_2$ or equal concentration of NaCl, taken 42 days after surgery. (B) Van Gieson stain to identify elastin continuity in aneurysmal ($CaCl_2$) and control (NaCl) aortas. Scale Bar=50μm. (C) Aortic expansion over the time course of 42 days measured by fold change of maximum diameters as calculated by dividing aortic diameter at time of sacrifice by aortic diameter prior to treatment.

Supplementary Figure II. PKCδ expression correlates with apoptosis in an experimental aneurysm model. (A) Infusion of AngII in $ApoE^{-/-}$ animals leads to induction of both PKCδ (green) and TUNEL (red) in the aortic wall, overlay with DAPI (blue).

Supplemental Figure III. PKCδ expression moderates aneurysmal expansion in an Elastase perfusion model of murine AAA. Aortic diameter measured prior to (Pre, white bars), and 14 days after (Post, black bars), Elastase perfusion treatment.

Supplemental Figure IV. $CaCl_2$ treatment causes similar early elastin damage in both PKCδ WT and KO aortas. Representative Van Gieson stains of arterial sections harvested 7 days after surgery.

Supplemental Figure V. The lack of PKCδ causes an apoptosis-resistant phenotype in vivo and in vitro. (A) Representative photos of immunohistochemistry for cleaved caspase-3 at 7 days,

scale bar=100μm. (B) Cleaved caspase 3 index. *p<0.05, n=6. (C) PKCδ KO SMCs were resistant to apoptosis induced by TNFα (50ng/mL, for 6h). (D) Adenovirus-mediated expression of exogenous PKCδ in PKCδ KO SMCs rescued the apoptotic phenotype. *p<0.05 compared to AdLacZ, n=3.

Supplemental Figure VI. PKCδ gene deficiency has a broad inhibitory effect on inflammatory infiltration. (A) IHC for neutrophils (Ly6G), T lymphocytes (CD3), and leukocytes (CD45) at 7 days; Scale Bar=200μm. Quantification of immunohistochemistry stains expressed as ratio of positive cells divided by nuclei. *p<0.05, n=6.

Supplementary Figure VII. PKCδ mediates expression of cytokines and chemokines in aortas. Total RNA was isolated from aortas of PKCδ WT or KO mice 7 days after surgery. mRNA levels of selected cytokines and chemokines were determined by RT-PCR. , *p<0.05, n=4.

Supplementary Figure VIII. PKCδ gene deficiency does not significantly affect the number or function of monocytes. (A) Bone marrow cells isolated from PKCδ WT or KO mice were stained with CD11b (monocytes), B220 APC-CY7 (B lymphocytes), and CD3 (T lymphocytes) for analysis by flow cytometry. (B) Purified monocyte population derived from whole bone marrow using $CD11b^+$ magnetic bead sorting technique compared to whole bone marrow and CD11b-depleted bone marrow. (C) $CD11b^+$ monocytes were isolated from bone marrow of PKCδ WT and KO mice. Migration of monocytes toward recombinant MCP-1 was analyzed by the trans-well assay, n=4.

Supplementary Figure IX. Perivascular application of adenovirus leads to aorta-specific gene transfer. (A&B) AdGFP or AdLacZ were administered perivascularly following $CaCl_2$ treatment. Green fluorescence was evaluated by fluorescent microscopy for GFP expression in the aortic wall, Scale bar=500μm, (A) or by flow cytometry for GFP expression in peripheral blood, $GFP^{+/+}$ and $GFP^{-/-}$ mice were used as positive and negative controls, respectively (B). (C&D) PKCδ KO mice were treated with Ad PKCδ or AdLacZ following the $CaCl_2$ procedure. Aortic sections were co-stained with antibodies specific to PKCδ (green) and smooth muscle cell-specific α-actin (SMA, red), overlay with DAPI (blue). Scale bar=200μm.

Supplemental Figure X. Elastin degradation scaling. Representative images depicting the grading scale used to evaluate elastin degradation in mouse aneurysmal tissue. Detailed description in Supplemental Methods.

Supplemental Figure XI. Representative control images for immunoflourescent staining. (A) Primary antibody alone for PKCδ and TUNEL (diluent only, no enzyme), overlay with DAPI. Scale bar = 200μm. (B) Secondary antibody only for green fluorescent anti-mouse (Anti-Mouse 488) and red fluorescent anti-rabbit (Anti-Rabbit 546), overlay with DAPI. Scale bar = 200μm.

Supplemental Figure I

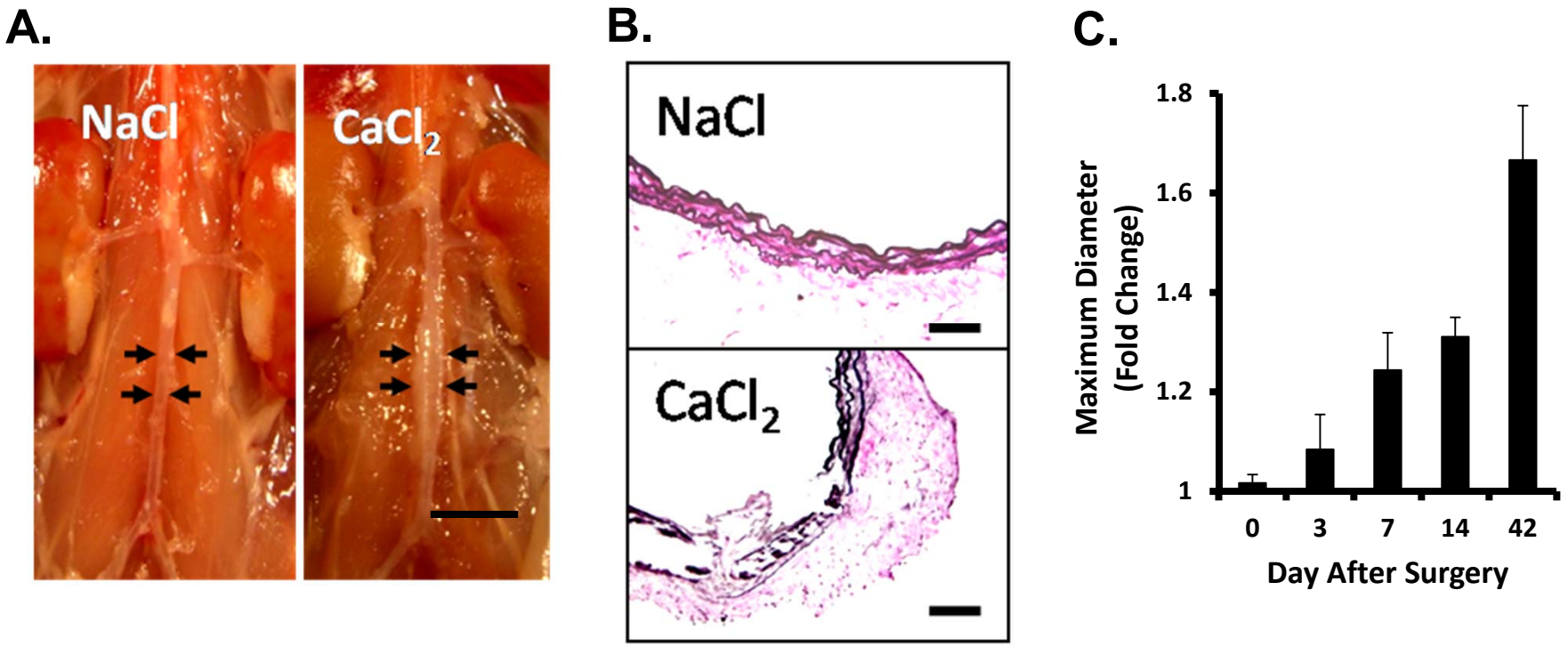

Supplemental Figure II

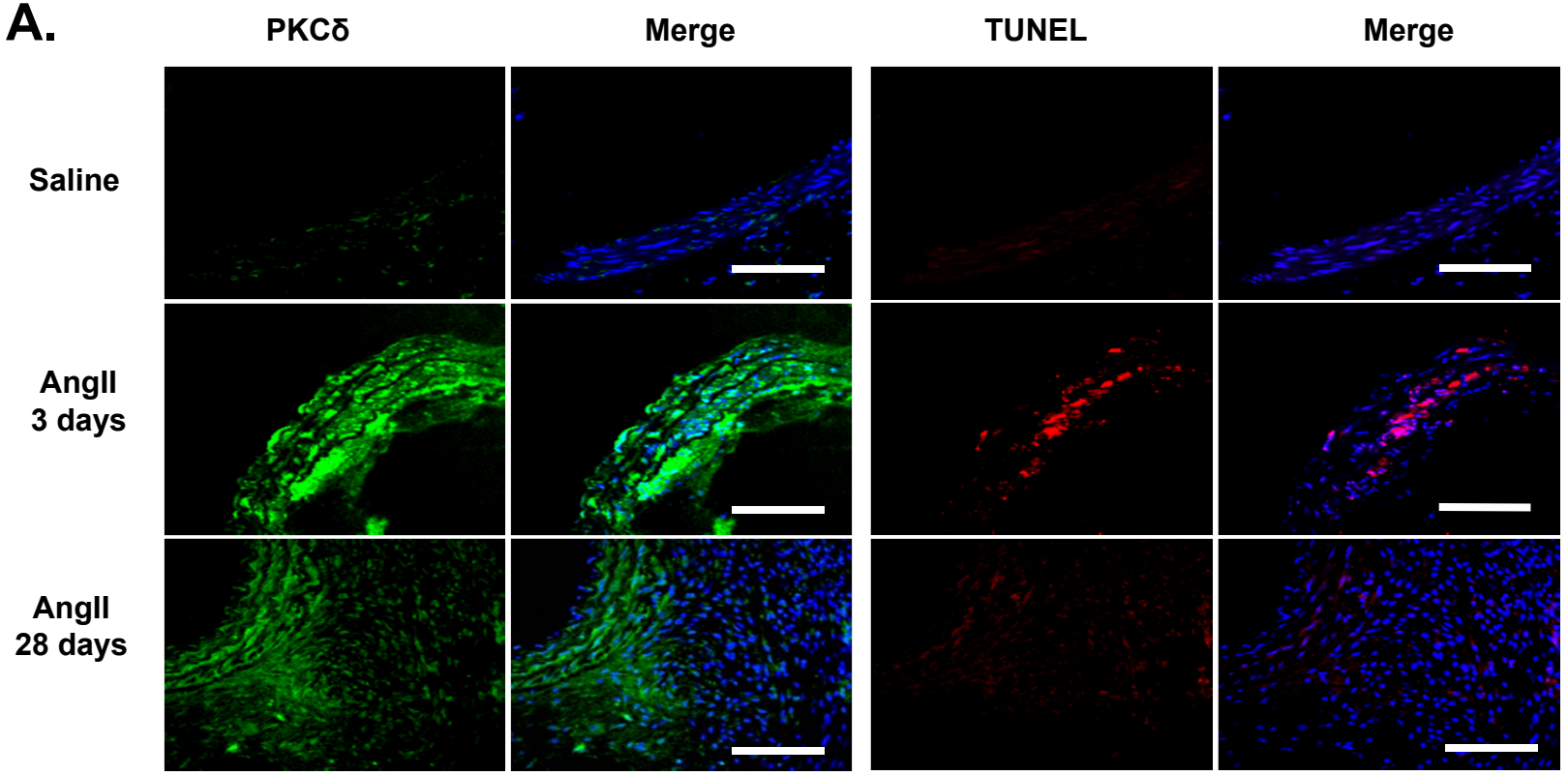

Supplemental Figure III

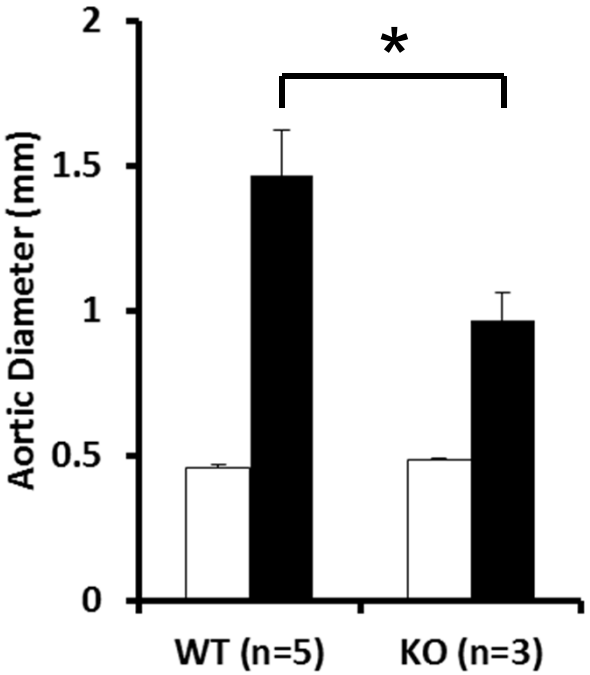

Supplemental Figure IV

WT

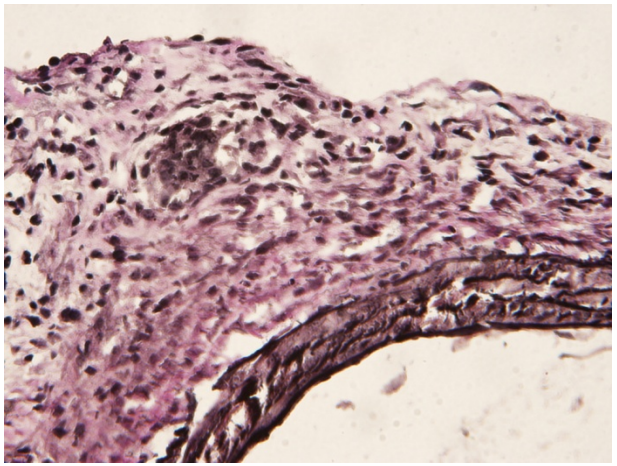

KO

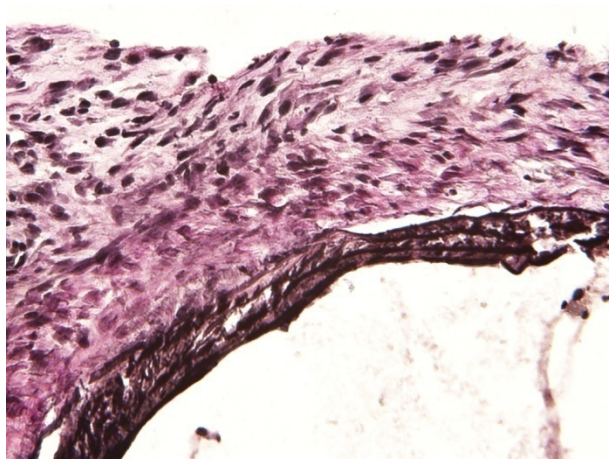

Supplemental Figure V

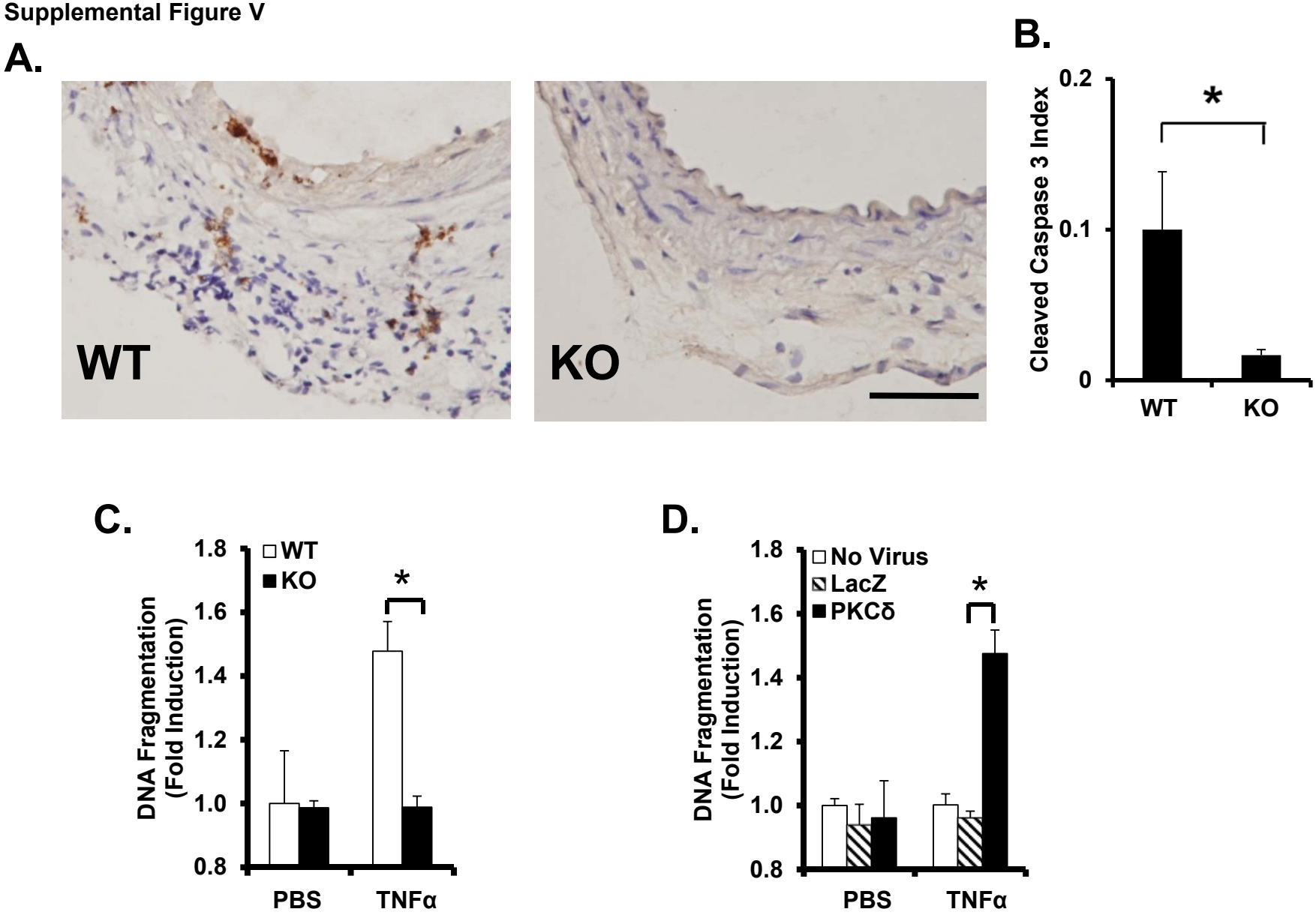

Supplemental Figure VI

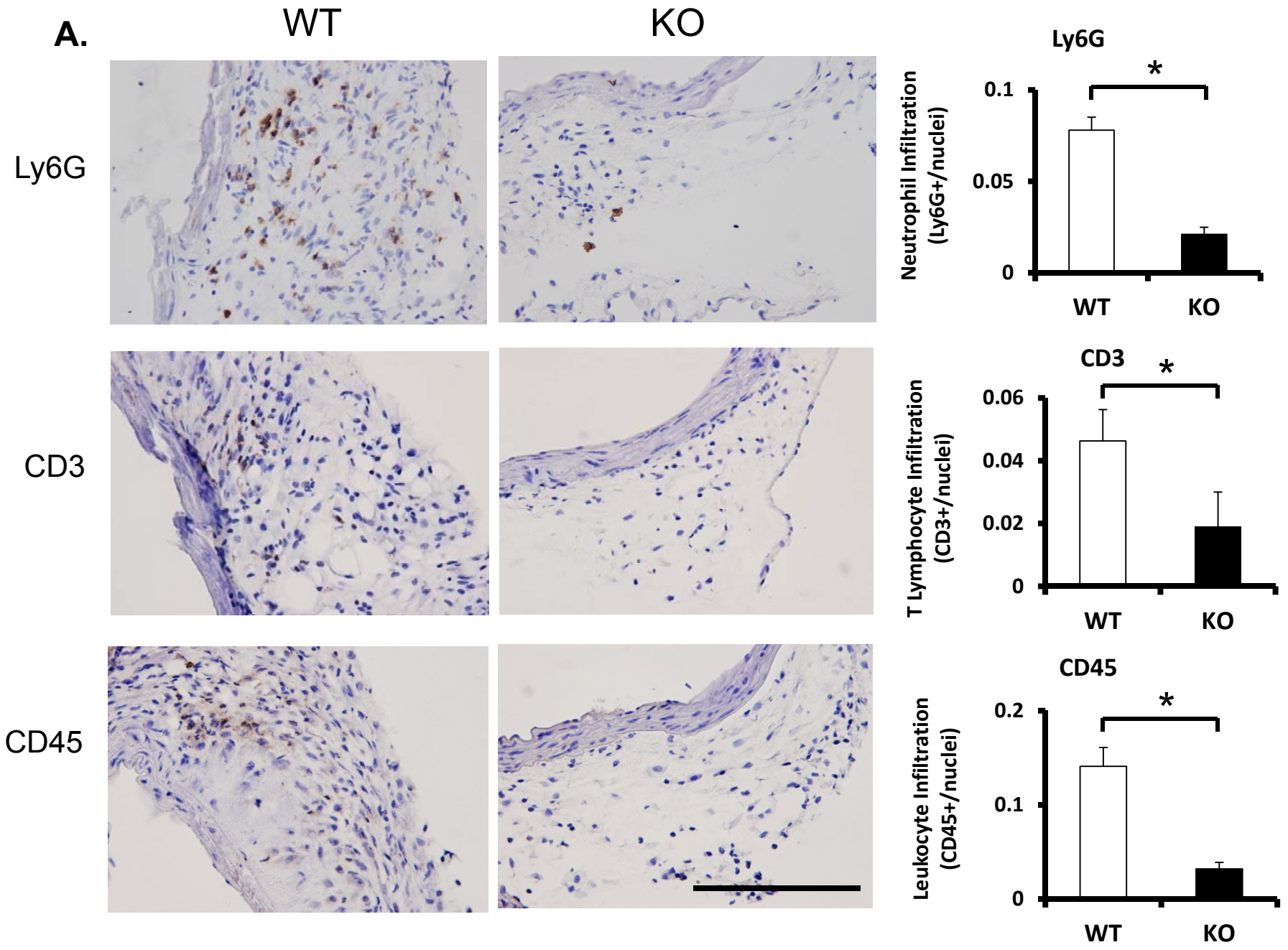

Supplemental Figure VII

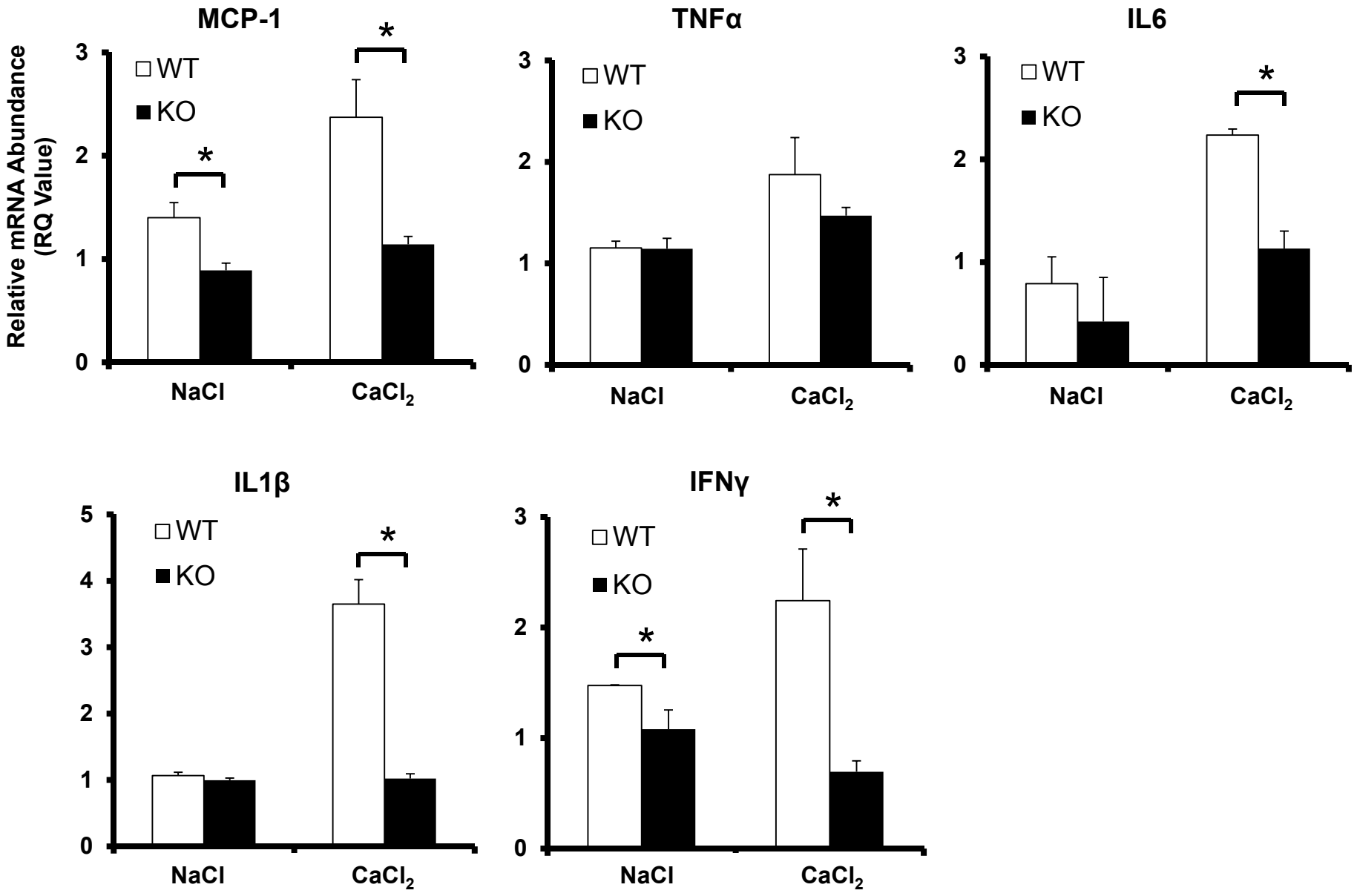

Supplemental Figure VIII

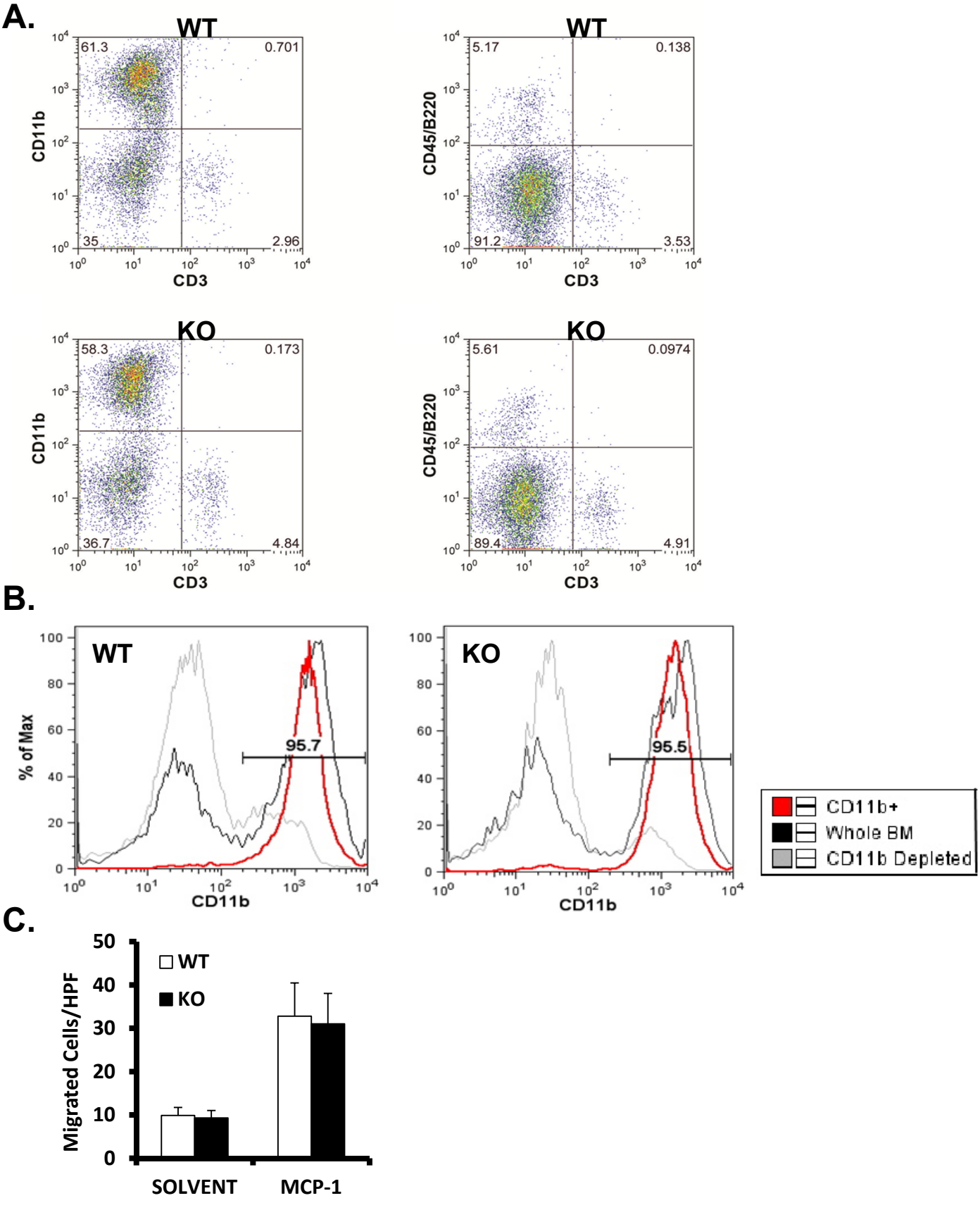

Supplemental Figure IX

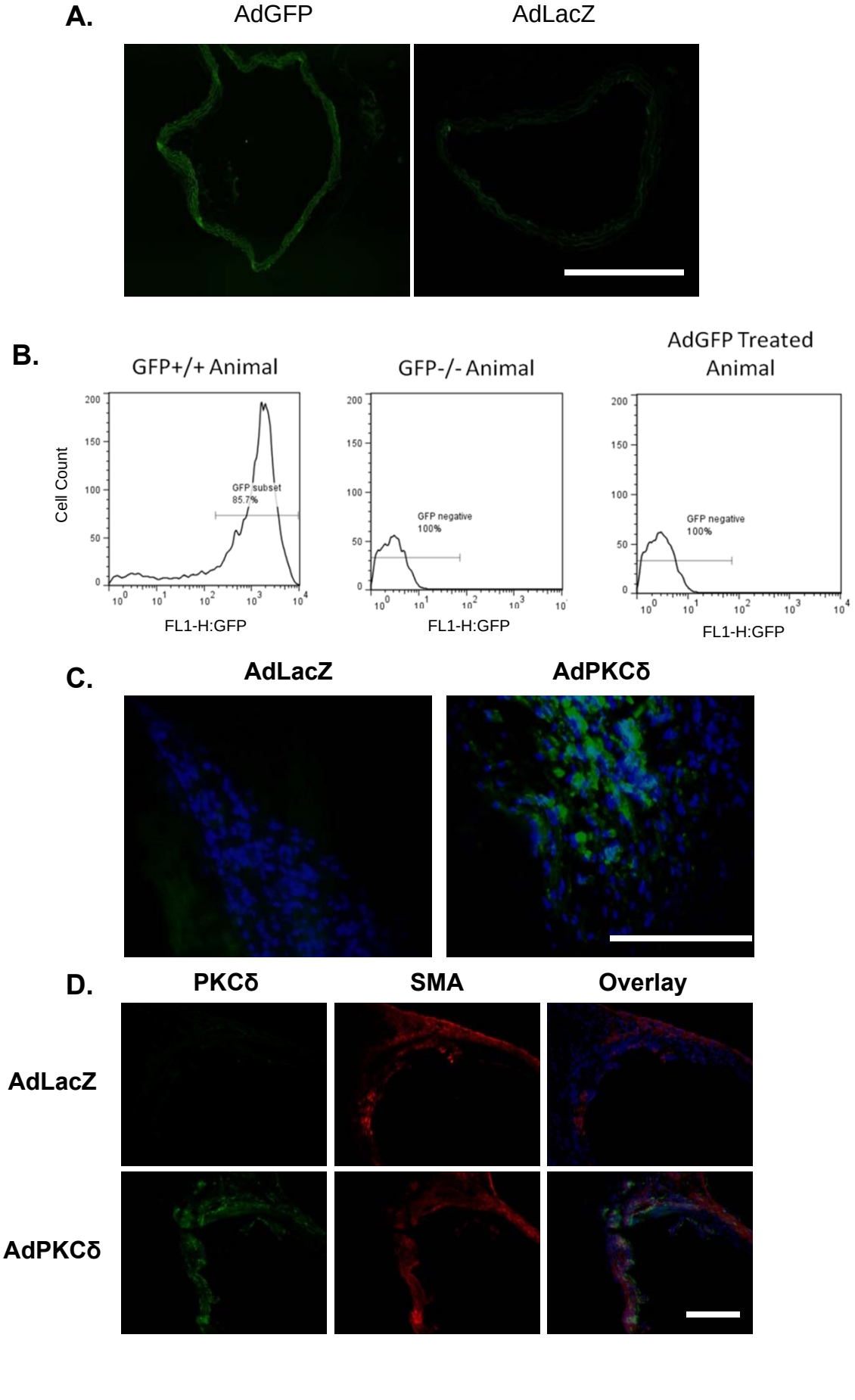

Supplemental Figure X

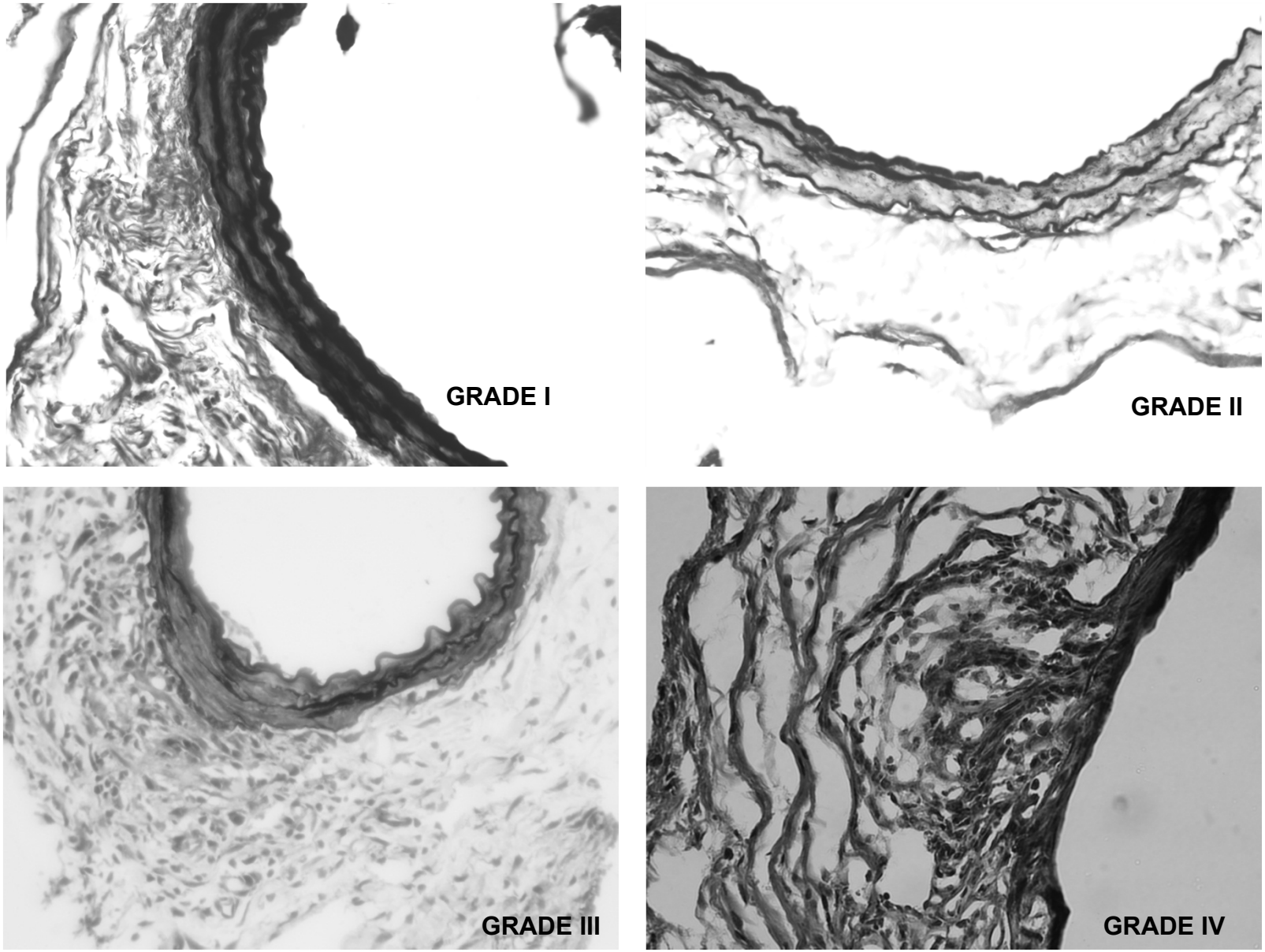

Supplemental Figure XI

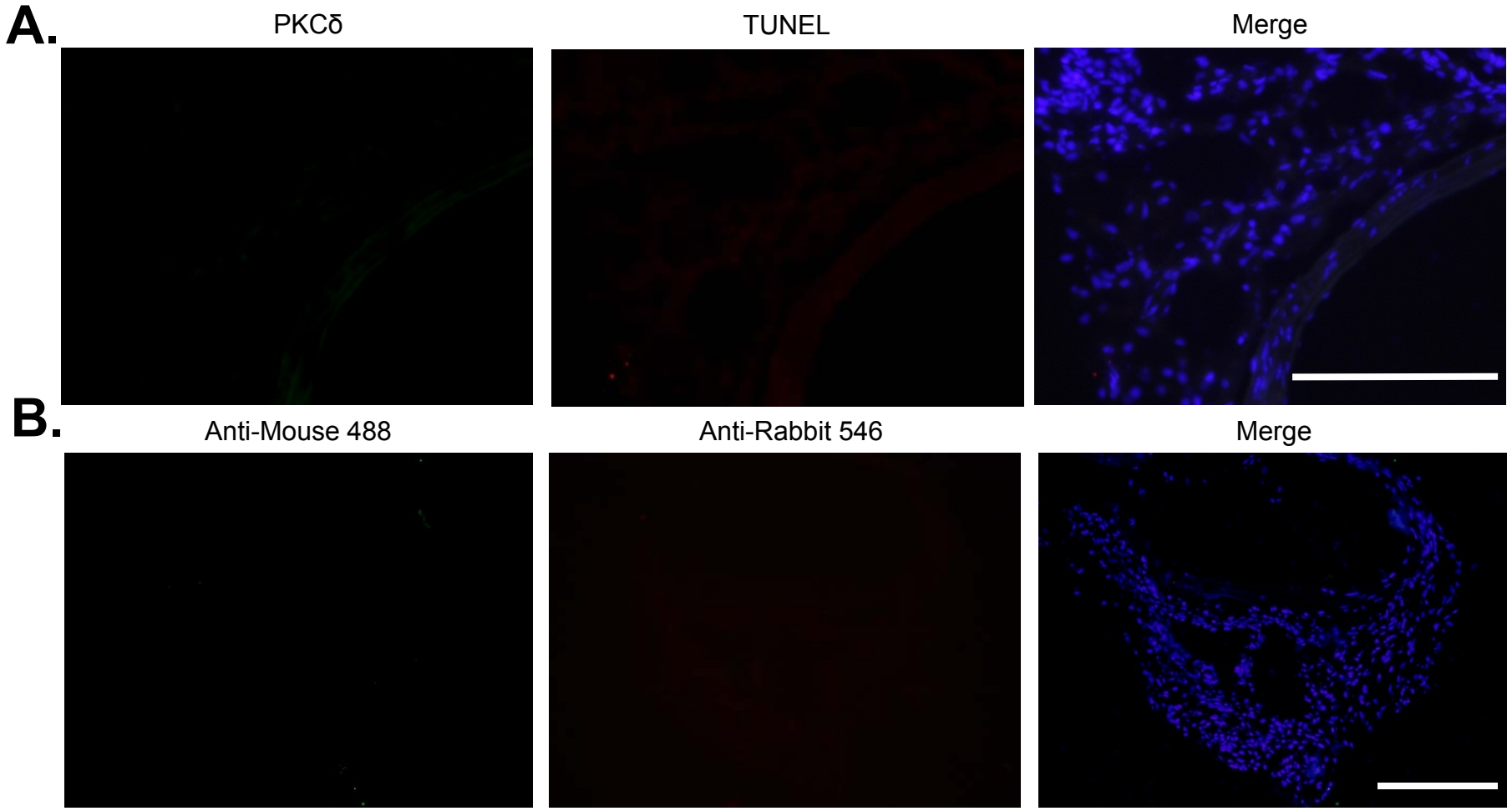

Supplemental Table I

	WT	KO
RBC (x10^6/µl)	7.78 ±0.56	8.49 ±0.34
WBC (x10^3/µl)	7.01 ±2.75	6.98 ±3.21

SUPPLEMENT MATERIAL

Supplemental Methods

Mouse Models of AAA

The generation of PKCδ target deletion in mice was described elsewhere[1]. PKCδ knockout mice and their wildtype littermates were generated by mating heterozygous pairs. C57BL/6 mice and apoE$^{-/-}$ mice were purchased from Harlan Laboratories (Madison, WI) and Jackson Laboratory (Bar Harbor, ME), respectively.

Male mice, 12 weeks of age, underwent a $CaCl_2$- or elastase- induced abdominal aortic aneurysm model as described previously[2-5]. Briefly, animals were anesthetized using continuous flow of 1-2% Isofluorane. For the $CaCl_2$, the infrarenal region of the aorta was isolated and treated with 0.5M $CaCl_2$ perivascularly via gauze for 20 minutes. Control mice were similarly treated with 0.5M of sodium chloride (NaCl). For the elastase model, the infrarenal region of the aorta was isolated temporary silk ligatures were placed around proximal and distal portions of the aorta. An aortotomy was created near the bifurcation using a 30-gauge needle and heat-tapered polyethylene tubing (Baxter Healthcare Corp., Illinois, USA) was introduced through the aortotomy and secured with a silk tie. The aorta was filled with saline containing 0.295 U/mL Type I porcine pancreatic elastase (Sigma, St. Louis, MO) at a constant pressure of 100mm Hg. For control, the elastase solution was heat-inactivated (100ºC) before use.

In $CaCl_2$ and Elastase model surgical procedures, Buprenorphine was administered subcutaneously at a dose of 0.05mg/kg immediately after surgery. Subsequently, a 2.5% Xylocaine topical ointment was applied to the suture site. Additional doses of Buprenorphine were given via intraperitoneal injection every 8-12

hours after surgery for the first 48 hours. The maximum external diameter of the infrarenal aorta was measured using a digital caliper (VWR Scientific, Radnor, PA) prior to treatment and at the time of tissue harvest.

For the Angiotensin II model, male, 24-week-old, apoE-deficient mice with a C57BL/6 background were implanted with a Alzet osmotic minipump (model 2004; Alzet, CA) delivering Angiotensin II (1000ng/kg/min) or saline subcutaneously for up to 4 weeks. The external aortic diameter was measured at the region showing maximum dilatation with a digital caliper (VWR, PA).

At selective time points, mice were killed by an overdose of isoflourane and tissues were perfusion-fixed with 4% formaldehyde in phospho-buffered saline (PBS). Tissues meant for immunohistochemical analyses were imbedded in O.C.T. Compound (Sakura Tissue Tek, Netherlands), and tissues meant for morphological analyses were processed for paraffin embedding. All frozen sections were cut to 6μm thick using a Leica CM3050S cryostat and paraffin sections were cut to 8μm thick using a Reichert-Jung 2050 SuperCut Microtome. All experiments were conducted in accordance with experimental protocols that were approved by the Institutional Animal Care and Use Committee at the University of Wisconsin-Madison (Protocol M02284).

	C57B6	PKCd WT	PKCd KO	PKCd HZ	GFP-/-	GFP+/+	ApoE-/-
PKCd and TUNEL timecourse and co-localization	12						
Fresh tissue western blot	8						
PKCd WT vs. KO Aneurysm		18	11				
Fresh tissue RNA extraction		6	6				
Adenovirus PKCd rescue in KO animals			14				
PKCd Dominant Negative	14						
Pluronic Gel MCP-1 Delivery		7	14				
Establish CaCl2 Model	18						
Elastase Model in WT/KO		8	4				
Angiotensin Upregulates PKCd in ApoE-/- mice							9
CBC table		3	3				
Bone Marrow Harvest and Monocyte Count		4	4				
Adenoviral-mediated Gene Delivery Test	4		4		2	2	
Breeding Pairs				40			
TOTALS	**56**	**46**	**60**	**80**	**2**	**2**	**9**

Immunohistochemistry

Van Geison stains were carried out using Chromaview Van Gieson kit (Richard Allan Scientific, Kalamazoo, MI) according to provided protocol. Elastin integrity was evaluated using a semi-quantitative methodology described previously: (1, no elastin degradation or mild elastin degradation; 2, moderate; 3, moderate to severe; and 4, severe elastin degradation)[6, 7]. Representative images for each grading score are provided in Supplemental Figure 10. Each section was numbered and photographed at 10x and 20x magnification, maintaining their respective numbers. Then, an objective participant graded the photographs according to the aforementioned scale and recorded the grade with the section number.

Arterial sections were permeabilized with 0.1% TritonX for 10 minutes at room temperature. Non-specific sites were blocked using 5% bovine serum albumin (BSA), 3% normal donkey serum in Tris-buffered Saline and Tween 20 (TBS-T) for 1 hour at room temperature. Primary antibodies to CD3, MCP-1, and CD68 were purchased from Santa Cruz (Santa Cruz, CA), IFN-γ, IL-6, MOMA2, CD45, and anti-smooth muscle specific Myosin heavy chain 11 (MHC) antibodies from Abcam (Cambridge, MA), and Cleaved Caspase 3 from Cell Signaling (Danvers, MA). All antibodies were diluted in previously described blocking solution and incubated overnight at 4°C. Fluorescent stains were completed using secondary antibodies purchased from Invitrogen Molecular Probes (Carlsbad, CA) and 4'6-diamidino-2-phenyl-indole, dihydrochloride (DAPI, Invitrogen, CA) was used to detect nuclei. Control images, included in Supplemental Figure 11A and B, show primary and secondary only antibody stains, respectively. Conventional stains were developed using secondary antibodies purchased from Bio Rad (Hercules, CA) with hematoxylin counter-stain. TUNEL staining kit was purchased from Roche (Madison, WI) and carried out according to the provided protocol. Staining was visualized with a Nikon Eclipse E800 upright microscope or Nikon A1RSi Confocal system, and digital images were acquired using a RetigaEXi CCD digital camera.

Microscope exposure settings were held constant for all images taken amongst experimental group sets. For example, the representative images shown in Figure 5C were all taken with ISO Sensitivity ISO400, with exposure time for MOMA (FITC-HYQ) at 1/7s, TUNEL (G-1A) at 1/3s, and DAPI (UV) at 1/180s. Similarly, representative values for confocal images shown in Figure 1C were Gain 5.95B and Offset 127 for green (PKCδ) and Gain 6.65B and Offset 127 for red (TUNEL).

Quantification of stains was performed in a manner to that previously described [8] using Image J Software as provided by the National Institutes of Health. Data quantification was performed using at least 3 sections per artery.

Fresh Tissue Western Blot

Aorta was harvested from NaCl or $CaCl_2$-treated WT and KO mice and the tissue was flash-frozen in liquid nitrogen to be processed at a later time. Aortic tissue was ground to a fine powder in a small amount of liquid nitrogen, and protein was extracted from the powder using radioimmunoprecipitation assay (RIPA) buffer consisting of 50mM TRIZMA HCl, 150mM NaCl, 1% Nonidet-P40, 0.5% sodium dioxycholate, 0.1% SDS (all reagents from Sigma-Aldrich, St. Louis, MO). Equal amounts of protein extracts were separated by sodium dodecyl sulfate polyacrylamide gel electrophoresis (SDS-PAGE) and transferred to PVDF membranes. The membranes were incubated with rabbit polyclonal antibodies to Protein Kinase Cδ, C-17 fragment from Santa Cruz (Santa Cruz, CA) and mouse monoclonal antibodies to β-actin (Sigma, MO) followed by horseradish peroxidase labeled goat anti-rabbit or anti-mouse IgG (Bio-Rad, Hercules, CA). Labeled proteins were visualized with an enhanced chemiluminescence system (Perkin-Elmer, Boston, MA).

Cell Culture

The murine macrophage cell line RAW264.7 cells were obtained from American Type Culture Collection (ATCC, Manassas, VA). Primary mouse aortic SMCs from the thoracic aorta of both PKCδ KO and WT mice were isolated based on a protocol

described by Clowes et al [9]. Briefly, aortas were perfused with phospho-buffered saline supplemented with 2% penicillin/streptavidin antibiotics. The aorta was isolated from the aortic arch to the iliac bifurcation and incubated 30 minutes in digestion buffer (DMEM, Bovine serum albumin, Collagenase, Soybean trypsin inhibitor, and Elastase Type III) at 37°C. Adventitia was pulled away from the medial layer, tissues were minced, and further digested for 4 hours at 37°C. Tissue was spun to a pellet by centrifugation and washed with 10%FBS DMEM once, before suspension in a small volume of 10%FBS-DMEM and left undisturbed for 48 hours to allow cells to migrate from tissue. All cell types were maintained in DMEM supplemented with 10% fetal calf serum (FCS), 100 units/mL penicillin, and 100μg/mL streptomycin in a 5% CO_2/water-saturated incubator at 37°C.

MCP-1 ELISA

The BD OptEIA ELISA kit was obtained from BD Biosciences (San Jose, CA), and carried out according to the manufacturer's protocol.

Real-Time PCR Analysis

Total RNA was isolated from cultured cells using Trizol reagent (Invitrogen, CA) according to manufacturer's protocol. For fresh tissue, aortic tissue was ground to a fine powder in a small amount of liquid nitrogen, and RNA was isolated from the powder using the RNeasy Plus Mini Kit (Qiagen, CA).

cDNA was synthesized using High Capacity cDNA Reverse Transcription Kit (Applied Biosystems, CA) on a Veriti 96-well Thermal Cycler (Applied Biosystems, CA). Primers

were purchased from Invitrogen and amplification was detected using SYBR Green PCR Master Mix (Applied Biosystems, CA). Real-time PCR was carried out using a 7500 Fast Real-time PCR System Machine (Applied Biosystems, CA). RQ value, where RQ= $(E_{target}^{\Delta CP_{target}(control-sample)})/ (E_{reference}^{\Delta CP_{ref}(control-sample)})$, the reference gene was GAPDH, and CP is defined as a 'crossing point', was used to compare expression of target cytokines.

Adenovirus Infection

The adenoviral vector that expresses wildtype PKCδ was created as described previously [10]. A recombinant adenoviral vector containing the dominant negative PKCδ (AdPKCδDN) [11] was obtained from Dr. T. Biden (Garvan Institute, Australia). *In vitro* adenovirus infection was carried out as described previously [12]. For perivascular adenovirus delivery, a small piece of latex was inserted underneath the aorta to create a 'cup' cradling the infrarenal aorta. After removal of the $CaCl_2$ –containing gauze from the artery, adenovirus suspended in saline ($2.5x10^9$ particle forming units (PFU)/mL) was added to the latex cup to bathe the artery for 20 minutes. Precautions were taken to avoid direct contact of viral solution with surrounding tissues.

Migration Assay

In vitro migration assay was carried out as previously described [13]. RAW 264.7 macrophages, or $CD11b^+$ cells isolated from bone marrow harvested from PKCδ KO or WT mice, were placed in a 5μm pore transwell insert (Corning Inc, Wilkes Barre, PA) to a density of 500,000cells/mL. Media conditioned by TNFα (R&D Systems, Minneapolis,

MN) stimulated aortic SMCs, or recombinant MCP-1 protein (R&D Systems, Minneapolis, MN) were used as chemoattractants. Following 6 hour incubation at 37°C, inserts were removed and washed with PBS, fixed with ice cold 70% Ethanol and stained with hematoxylin for nuclei visualization. The mean value of migrated cells counted in eight high-power fields per membrane was used as a measurement of migration.

Bone Marrow Isolation and Sorting

Bone marrow cells from both PKCδ KO and WT animals were isolated from long bones, washed with PBS, and counted. Monocytes were isolated from bone marrow by magnetic sorting using anti-CD11b microbeads (Miltenyi Biotec, Auburn CA). Purity of the resulting CD11b+ cells was assessed by flow cytometry using antibodies to CD3 (FITC), CD11b (APC), and CD45/B220 (APC-Cy7) (BD Pharmigen, San Diego, CA). Flow cytometric data was collected on a BD FACS Calibur Flow Cytometer equipped with a Cytek 633nm laser (Freemont, CA) and analysis was performed using Flow Jo software (TreeStar, Inc.).

Migration Assay

Chemotaxis assay was performed as described previously (cite). 2x10^5 macrophages (RAW264.7) were placed in the upper chamber of Costar 24-well transwell plates with 5um pore filters (Corning, Inc., Corning, NY). Cultured conditioned medium or control media was placed into the lower chambers or wells. Anti-MCP-1 antibody (Biolegend, CA) was used for neutralization of MCP-1. After incubating plates for 6h at 37C,

migrated cells were collected from the lower chambers and on the bottom of the filters were counted.

Statistical analysis

Values were expressed as mean ± standard error. Experiments were repeated at least three times unless stated otherwise. Differences between 2 groups were analyzed by Student's *t* test. For time course comparison, one-way ANOVA analysis was followed by Bonferroni correction to adjust for multiple comparisons. Values of $p<0.05$ were considered significant.

1. Miyamoto A, Nakayama K, Imaki H, Hirose S, Jiang Y, Abe M, Tsukiyama T, Nagahama H, Ohno S, Hatakeyama S, Nakayama KI. Increased proliferation of b cells and auto-immunity in mice lacking protein kinase c[delta]. *Nature*. 2002;416:865-869
2. Ikonomidis JS, Gibson WC, Butler JE, McClister DM, Sweterlitsch SE, Thompson RP, Mukherjee R, Spinale FG. Effects of deletion of the tissue inhibitor of matrix metalloproteinases-1 gene on the progression of murine thoracic aortic aneurysms. *Circulation*. 2004;110:II-268-II-273
3. Kimura T, Yoshimura K, Aoki H, Imanaka-Yoshida K, Yoshida T, Ikeda Y, Morikage N, Endo H, Hamano K, Imaizumi T, Hiroe M, Aonuma K, Matsuzaki M. Tenascin-c is expressed in abdominal aortic aneurysm tissue with an active degradation process. *Pathology International*. 2011;61:559-564
4. Yoshimura K, Aoki H, Ikeda Y, Fujii K, Akiyama N, Furutani A, Hoshii Y, Tanaka N, Ricci R, Ishihara T, Esato K, Hamano K, Matsuzaki M. Regression of abdominal aortic aneurysm by inhibition of c-jun n-terminal kinase. *Nat Med*. 2005;11:1330-1338
5. Pyo R, Lee JK, Shipley JM, Curci JA, Mao D, Ziporin SJ, Ennis TL, Shapiro SD, Senior RM, Thompson RW. Targeted gene disruption of matrix metalloproteinase-9 (gelatinase b) suppresses development of experimental abdominal aortic aneurysms. *The Journal of Clinical Investigation*. 2000;105:1641-1649

6. Kitamoto S, Sukhova GK, Sun J, Yang M, Libby P, Love V, Duramad P, Sun C, Zhang Y, Yang X, Peters C, Shi G-P. Cathepsin l deficiency reduces diet-induced atherosclerosis in low-density lipoprotein receptor–knockout mice. *Circulation*. 2007;115:2065-2075
7. Xiao J, Angsana J, Wen J, Smith SV, Park PW, Ford ML, Haller CA, Chaikof EL. Syndecan-1 displays a protective role in aortic aneurysm formation by modulating t cell–mediated responses. *Arteriosclerosis, Thrombosis, and Vascular Biology*. 2012;32:386-396
8. Tang XN, Berman AE, Swanson RA, Yenari MA. Digitally quantifying cerebral hemorrhage using photoshop® and image j. *Journal of Neuroscience Methods*. 2010;190:240-243
9. Clowes A, Clowes M, Fringerle J, Reidy M. Kinetics of cellular poliferation after arterial injury: Role of acute distension in the induciton of smooth muscle proliferation. *Lab Invest*. 1989;60:360-364
10. Ryer EJ, Hom RP, Sakakibara K, Nakayama KI, Nakayama K, Faries PL, Liu B, Kent KC. Pkc{delta} is necessary for smad3 expression and transforming growth factor {beta}-induced fibronectin synthesis in vascular smooth muscle cells. *Arterioscler Thromb Vasc Biol*. 2006;26:780-786
11. Carpenter L, Cordery D, Biden TJ. Protein kinase cδ activation by interleukin-β1 stabilizes inducible nitric-oxide synthase mrna in pancreatic β-cells. *Journal of Biological Chemistry*. 2001;276:5368-5374
12. Sakakibara K, Kubota K, Worku B, Ryer EJ, Miller JP, Koff A, Kent KC, Liu B. Pdgf-bb regulates p27 expression through erk-dependent rna turn-over in vascular smooth muscle cells. *Journal of Biological Chemistry*. 2005;280:25470-25477
13. Yamanouchi D, Kato K, Ryer EJ, Zhang F, Liu B. Protein kinase c delta mediates arterial injury responses through regulation of vascular smooth muscle cell apoptosis. *Cardiovasc Res*. 2010;85:434-443

Transition IV

Evidence gathered in Chapters 1-4 suggests a critical role for apoptosis in abdominal aortic aneurysm development. First, we showed early administration of a pan-caspase inhibitor could prevent aneurysm growth in three different murine models. The same caspase inhibitor was unable to block expansion of established aneurysm. However, evidence suggested that the inflammatory response appeared to be linked to cellular apoptosis and directly related to aneurysm formation. Interestingly, in Chapter 4, we showed that administration of recombinant monocyte chemoattractant protein-1 (MCP-1) to the aortic wall of protein kinase c-delta (PKCδ) knockout mice could restore inflammation as well as aneurysm formation without altering apoptosis in the tissue. Further, Clarke et al. demonstrated that SMC-specific induction of apoptosis was not sufficient to induce aneurysm[1]. This information indicates that inflammation, or a component of the inflammatory response, is likely the necessary event underlying aneurysm formation.

For many years, a critical role for macrophages has been described in the aneurysmal inflammatory environment. Macrophages are recruited to aneurysmal tissue where they are thought to secrete matrix- and elastin-degrading enzymes and inflammatory cytokines. Recently, macrophages have been described to fall in to at least two different subtypes as delineated by their phenotypes and functionality. Further, the different macrophage phenotypes have been shown to play distinct roles in various diseases such as atherosclerosis. In the next chapter, we explore the possibility that the inflammatory response driving aneurysm

may be dominated by inflammatory macrophages and/or lacking in anti-inflammatory macrophages.

1. Clarke MCH, Talib S, Figg NL, Bennett MR. Vascular smooth muscle cell apoptosis induces interleukin-1-directed inflammation. Effects of hyperlipidemia-mediated inhibition of phagocytosis. *Circ Res*. 2009:CIRCRESAHA.109.208389

Chapter 5: Macrophage Phenotypes in a Murine Model of AAA

Unpublished Work

Stephanie Morgan, Qiwei Wang, Calvin Harberg, and Bo Liu

ABSTRACT

OBJECTIVE

Histologic examination of human abdominal aortic aneurysm (AAA) tissue shows the presence of significant apoptosis, inflammation, and elastin degradation. The conventional view describes the contribution of inflammatory cells, particularly macrophages, to be the production of destructive enzymes such as matrix metalloproteinases and the secretion of proinflammatory cytokines. In the past decade, multiple studies have described several unique macrophage phenotypes. In this work, we aim to evaluate the role of two well-established macrophage phenotypes: inflammatory (M1) macrophages which produce proteases and proinflammatory cytokines, and alternatively activated (M2) macrophages which produce anti-inflammatory cytokines and extracellular matrix (ECM) components. Secondly, we will investigate whether the peroxisome proliferation activation receptor- gamma (PPARγ) agonist Rosiglitazone (RGZ) is capable of altering the M2 and/or M1 population profiles in experimental AAA.

METHODS

The elastase model of murine AAA was created using luminal perfusion of porcine elastase, or heat-inactivated elastase as control, in all experiments. Immunohistochemical, flow cyometric, and RT-PCR analysis were performed to identify macrophage phenotypes at 3, 7, and 14 days after surgery. RGZ (10mg/kg/day) was administered orally in order to manipulate macrophage phenotype. Macrophage phenotype content was evaluated using flow cytometry and immunohistochemistry. For in vitro experiments, a mouse bone marrow derived

monocyte/macrophage culture was created by harvesting bone marrow from long bones and culturing the mixture with 10% DMEM supplemented with L292-cell conditioned media. M1 type macrophages were driven from culture using LPS (100ng/mL), while M2 macrophages were driven using IL-4 (10ng/mL).

RESULTS

Elastase-perfused arteries were shown to contain a significantly higher number of total macrophages 7 and 14 days after surgery (803.9±331.5 vs. 449.5±177.9 at 7 days and 486.8±60.5 vs. 295.9±143.4 at 14 days, counts out of 10,000 events in IE vs. E-treated arteries, respectively; $p<0.05$). Further, the M2 macrophage population is significantly higher in IE-treated aortas as compared to E-treated tissues at 3 and 7 days after surgery (34.5±13.2% vs. 23.78±8% at 3 days and 26.59±2.92% vs. 15.8±6.77% at 7 days in IE vs. E treated tissues). Immunohistochemical analysis further confirmed presence of M1 and M2 macrophages in both IE and E treated tissues. RT-PCR analysis revealed elastase-treated arteries to contain significantly higher levels of both M1 and M2 markers at day 14.

Administration of RGZ to mice 5 days after treatment with either IE or E significantly reduced the size of elastase-induced aneurysm as compared to mice receiving DMSO injections (82.8±13.2% vs. 145.7±18.87%, respectively). Further, RGZ treatment was shown to increase the M2 macrophage population and significantly reduce the M1 macrophage population in E-treated tissues.

CONCLUSION

In the setting of aneurysm, an increased presence of M2 macrophages is associated with reduced aortic dilation. Aneurysmal tissues, on the other hand, contain a smaller percentage of M2 macrophages and an increased number of total macrophages. Free-standing apoptotic cells are more prevalent in aneurysmal tissue, suggesting that the M2:M1 balance may be associated with clearance of apoptotic debris.

INTRODUCTION

Abdominal Aortic Aneurysm (AAA) is a lethal vascular disease characterized by a weakening of the aortic wall and the subsequent expansion of aortic diameter. AAA is an age-related disease characterized by tissue-destructive features such as macrophage infiltration, smooth muscle cell (SMC) depletion, and elastin fragmentation[1-4]. The mechanisms that potentiate these features are poorly understood, a fact that has made therapeutic strategies elusive and leaving surgical intervention as the only treatment option.

The role of macrophages in aneurysm has long been understood to center main on the ability of these cells to produce elastin-degrading enzymes and pro-inflammatory cytokines[5-8]. These processes result in additional inflammation, augmenting the inflammatory processes occurring within the arterial wall. Multiple studies have evidenced the existence of a variety of macrophage subtypes (or phenotypes) existing within the larger macrophage population[9, 10]. The differentiation of these phenotypes results from the interaction of a macrophage with a tissue microenvironment. These phenotypes display unique characteristics and appear to possess differential functions within various diseases, including atherosclerosis[11, 12]. While various macrophage phenotypes have been suggested to exist, two phenotypes have been most thoroughly studied: classically activated (M1) and alternatively activated (M2) macrophages. The M1 macrophage is driven by inflammatory factors and is associated with tissue destruction. M2 macrophages, associated with IL-4 and IL-13 cytokines, promote angiogenesis and matrix remodeling and suppress tissue-destructive functions of immune responses[13, 14].

An additional distinguishing factor between M1 and M2 macrophages is their varied response to apoptotic cells. M2 polarization essentially forms a positive feedback loop in the setting of inflammation resolution, in which apoptotic cell uptake can 'switch on' M2 polarization signals, and macrophages of the M2 phenotype in turn promote apoptotic cell uptake. M1 macrophages, on the other hand, demonstrate reduced uptake of apoptotic cells[15]. Clarke et al. demonstrated that apoptotic cells that are not engulfed undergo a highly inflammatory process called 'secondary necrosis' which further drives inflammatory cell infiltration[16]. Thus, it follows that tissues with high levels of apoptosis and an insufficient M2 phenotype population would maintain an inflamed state with tissue degradation potential.

Promotion of M2 differentiation involves activation of nuclear receptors peroxisome proliferator activated receptor-gamma and –delta (PPARγ and PPARδ)[17, 18]. Agonists of these two receptors make up a class of drugs called thiazolidinediones (TZDs), including Thioglitazone and Rosiglitazone. Rosiglitazone has been used in various studies to drive M2 polarization, and has been shown to reduce development and rupture of aneurysm in the Angiotensin II-induced model of murine aneurysm [19, 20]. Rosiglitazone (RGZ) was shown to reduce c-Jun N-terminal kinase (JNK) phosphorylation and reduce toll-like receptor 4 (TLR4) expression. Further, RGZ was shown to reduce proinflammatory cytokines monocyte chemoattractant protein 1 (MCP1) and Macrophage inflammatory protein 1 α (MIP1α). However, mediation of macrophage phenotypes by RGZ has not been explored in aneurysm.

While a plethora of studies have shown M1 and M2 populations to play important roles in various diseases, very little work has been done to explore the role of these phenotypes in

human or experimental AAA. Understanding the role of these phenotypes in AAA could be an important component in understanding the mechanisms of the disease and may identify potential therapeutic targets. To explore whether M1 or M2 macrophages contribute to AAA progression, the current study utilizes the elastase-induced mouse model of AAA. We first tested the presence of macrophage phenotypes in aneurysmal tissues and evaluated their functions. Finally, we tested the efficacy of the PPARγ-agonist RGZ to drive M2 polarization and ameliorate AAA formation.

METHODS

Mouse Models of AAA

C57BL/6 mice were purchased from Jackson Laboratory (Bar Harbor, ME). All mice had free access to a normal diet and water. Male mice, 12 weeks of age, underwent elastase-induced experimental aneurysm was created as described previously[21]. Briefly, the aorta is isolated from the renal vein to the iliac bifurcation and occluded with silk suture proximally and distally of the isolation points. Then, an aortotomy is made with a 30-gauge needle and a catheter is used to perfuse the artery with 0.4144U/mL elastase or equal concentration heat inactivated elastase at constant pressure for 5 minutes. Once the catheter is removed, the aortotomy is closed with 11-0 suture. All animals were treated with elastase from the same lot, and heat-inactivated (5 minutes at 100ºC) elastase served as control. The maximum external diameter of the infrarenal aorta was measured using a digital caliper (VWR Scientific, Radnor, PA) prior to treatment (initial measurement) and at the time of tissue harvest (final measurement). Aortic expansion (% Aortic Dilation) was determined by first calculating the expansion (final measurement – initial measurement), and dividing that difference by the initial measurement: ((Final measurement – initial measurement)/Final measurement)*100. Aneurysm was defined as a 100% increase in aortic diameter.

For in vivo studies, Rosiglitazone (10mg/kg/day; Cayman Chemical, Ann Arbor, MI) was diluted in 1:3 DMSO:H_20 solution as described by manufacturer, and kept on ice. The drug was administered by oral gavage every 24 hours beginning 5 days after surgery and continuing until time of sacrifice at 14 days.

Flow Cytometry

For fresh tissue flow cytometry, arteries were harvested and processed for flow cytometry as previously described[22]. Briefly, arteries were incubated for 1hour at 37º in a digestion buffer containing 125U/mL Collagenase Type XI, 60U/mL Hyaluronidase Type I-S, 60U/mL DNAse1, 450U/mL Collagenase Type I. Arteries were then mashed through 70µm mesh screen and washed twice with phospho-buffered saline (PBS). For in vitro flow cytometry, cells were lifted using Accutase (Invitrogen, Grand Island, NY) and washed twice with PBS. All single-cell suspensions were blocked with TruStain fcX anti-mouse CD16/CD32 (BioLegend, San Diego, CA) for 5 minutes on ice before surface marker labeling. FITC conjugated CD86, CD206, LY6C and CD3; PE conjugated F4/80 and CD115; 7aad; PE-Cy5 B220; APC-CD11b and Ly6G; APC-Cy7CD45. κIsotype controls include FITC conjugated Rat IgG2a and IgM; PE Rat IgG2a; APC Rat IgG2b and IgG2a, and APC/Cy7 Rat IgG2b (Biolegend, San Diego, CA). Flow cytometric data was collected on a BD FACS Calibur Flow Cytometer equipped with a Cytek 633 laser (Freemont, CA) and analysis was performed using Flow Jo software (TreeStar, Inc.).

Engulfment Assays

RAW 264.7 cells were treated with either PBS (1:1000), LPS (100ng/mL), or IL-4 (10ng/mL) for 24 hours. 22 hours after RAW cells were treated, SMCs were placed under UV or normal white light for 5 minutes and then placed at 37ºc for recovery. 2 hours later, RAW264.7 cells were labeled with Vybrant DiD cell-labeling solution (13µL for 20 miuntes), and SMCs were labeled with Vybrant DiO cell-labeling solution (7µL for 13 minutes) (Invitrogen, Carlsbad, CA). Cell

suspensions were then washed and combined at a SMC:RAW ratio of 1:2. 6 hours after cells were combined, the suspensions were spun down and labeled with PE-conjugated CD68 (BioLegend, San Diego, CA) at room temperature for 20 minutes. Cells were washed and measured by flow cytometry.

Cell culture or arteries were prepared to single-cell suspension as described above. Single cell suspension was incubated with FluoSpheres Carboxylate-modified microspheres (Invitrogen, Grand Island, NY; 1µL/500,000 cells) for 20minutes at 37ºC. Mixtures were then washed twice with cold PBS and incubated with TruStain fcX anti-mouse CD16/CD32 for 5 minutes on ice before surface marker labeling.

Immunohistochemistry

Tissues were fixed in 4% formaldehyde in phospho-buffered saline (PBS), embedded and cut to 6µm sections for OCT and paraffin-imbedded arteries. Van Geison stains were carried out using Chromaview Van Gieson kit (Richard Allan Scientific, Kalamazoo, MI). Primary antibody for Ym1 was purchased from StemCell Technologies (Vancouver, BC, Canada), CD206 was purchased from BioLegend (San Diego, CA), iNOS was purchased from Abcam (Cambridge), and CD68 was purchased from AbD Serotec (Raleigh, NC). Primary antibodies were diluted in previously described blocking solution and incubated overnight at 4ºC. Apoptosis was identified through Terminal deoxynucleotidyl transferase dUTP nick end labeling (TUNEL) in an *In Situ* Cell Death Detection Kit (Roche, Indianapolis, IN), carried out according to kit directions. Fluorescent stains were completed using secondary antibodies purchased from Invitrogen Molecular Probes (Carlsbad, CA) and 4'6-diamidino-2-phenyl-indole, dihydrochloride (DAPI, Invitrogen, Carlsbad,

CA) was used to detect nuclei. Staining was visualized with a Nikon Eclipse Ti inverted microscope system and digital images were acquired using a Nikon DS-Ri1 digital camera. Quantification of stains was performed in a manner to that previously described[23] using Image J Software. Data quantification was performed using at least 3 sections per artery.

Cell Culture

The murine macrophage cell line RAW264.7 cells were obtained from American Type Culture Collection (ATCC, Manassas, VA). Primary monocyte cells were harvested and cultured as previously described[24]. Briefly, bone marrow was isolated from long bones and washed with PBS. Bone marrow was suspended in 10% DMEM supplemented with 10% L-cell conditioned media (LCCM). LCCM media was collected from L929 cells cultured in T-75 cm^2 filter cap flasks in DMEM for 7 days and filtered through 0.2µ. Media was changed after 3 days, and culture was ready for use at day 7 after harvest. Primary mouse aortic SMCs from the thoracic aorta of both PKCδ KO and WT mice were isolated based on a protocol described by Clowes et al [25]. Briefly, aortas were perfused with phospho-buffered saline supplemented with 2% penicillin/streptavidin antibiotics. The aorta was isolated from the aortic arch to the iliac bifurcation and incubated 30 minutes in digestion buffer (DMEM, Bovine serum albumin, Collagenase, Soybean trypsin inhibitor, and Elastase Type III) at 37°C. Adventitia was pulled away from the medial layer, tissues were minced, and further digested for 4 hours at 37°C. Tissue was spun to a pellet by centrifugation and washed with 10%FBS DMEM once, before suspension in a small volume of 10%FBS-DMEM and left undisturbed for 48 hours to allow cells to migrate from tissue. All cell types were maintained in DMEM supplemented with 10% fetal

calf serum (FCS), 100 units/mL penicillin, and 100µg/mL streptomycin in a 5% CO_2/water-saturated incubator at 37°C.

For macrophage polarization, cells were treated with LPS (100ng/mL; R&D Systems, Minneapolis, MN), IL-4 (10ng/mL; R&D Systems, Minneapolis, MN), or PBS control. 24 hours after administration, cell culture was collected for analysis. For in vitro studies, Rosiglitazone (10mg/kg/day; Cayman Chemical, Ann Arbor, MI) was diluted in 1:3 DMSO:H20 solution as described by manufacturer, and kept on ice. Rosiglitazone was then administered 30 minutes prior to treatment. The LXR agonists GW3965 (1µm) and TO-901317 (1µm) were purchased from Sigma Aldrich (St. Louis, MO) and prepared as directed by manufacturer. LXR agonists were administered 30 minutes prior to treatment with PBS or LPS.

Real-Time PCR Analysis

Total RNA was isolated from cultured cells using Trizol reagent (Invitrogen, CA) according to manufacturer's protocol. For fresh tissue, aortic tissue was ground to a fine powder in a small amount of liquid nitrogen, and RNA was isolated from the powder using the RNeasy Plus Mini Kit (Qiagen, CA).

cDNA was synthesized using High Capacity cDNA Reverse Transcription Kit (Applied Biosystems, CA) on a Veriti 96-well Thermal Cycler (Applied Biosystems, CA). Primers were purchased from Invitrogen and amplification was detected using SYBR Green PCR Master Mix (Applied Biosystems, CA). Real-time PCR was carried out using a 7500 Fast Real-time PCR System Machine (Applied Biosystems, CA). RQ value, where RQ= $(E_{target}{}^{\Delta CPtarget(control-sample)})/ (E_{reference}$

$^{\Delta CPref(control-sample)}$), the reference gene was GAPDH, and CP is defined as a 'crossing point', was used to compare expression of target cytokines.

Statistical Analysis

Values were expressed as mean ± standard error. Experiments were repeated at least three times unless stated otherwise. Differences between 2 groups were analyzed by Student's *t* test. Values of $p<0.05$ were considered significant.

RESULTS

Macrophage content in experimental aneurysm tissue

We subjected C57B/6 male mice to luminal perfusion of elastase or heat-inactivated elastase (IE) to the infrarenal region of the aorta and sacrificed animals at selected time points. Aortic expansion, elastin degradation, inflammatory infiltrate, and apoptosis evidenced successful aneurysm formation in elastase-treated mice at 7 and 14 days after surgery (Figure 1A, Supplemental Figure 1). Conversely, measurements of IE-treated aorta showed a small dilation by 7 days (47.9±8.02%), and no significant change at 14 days (46.39±6.92%). In comparison with IE-treated arteries, elastase-treated aortic tissue contained a significantly higher number of total macrophages (CD11b+F4/80+) as measured by flow cytometry 7 and 14 days after surgery (803.9±331.5 vs. 449.5±177.9 and 486.8±60.5 vs. 295.9±143.4 out of 10,000 events, respectively; $p<0.05$). The largest number of macrophages was seen 3 days after surgery, where IE –treated tissues contained 2476.7±375, and elastase-treated tissues contained 2261±885.6 macrophages, with no significant difference existing between the two treatment groups (Figure 1B). Immunochistochemical analysis of aortic tissue harvested 3 and 7 days after surgery supported flow cytometry results. Macrophage infiltration was significantly higher in elastase-treated tissues 7 days after surgery, but not at 3 days after surgery (Figure 1C). Immunohistochemical images showed that elastase-treated tissues consistently contain a greater number of free-standing apoptotic cells, despite the large number of macrophages present in the artery (Figure 1D). This evidence suggests that

macrophages present in the aneurysmal artery may have reduced engulfment capability, which could be attributed to macrophage phenotypes present in the arterial wall.

Macrophage phenotype characteristics in vitro

We adopted methods of macrophage polarization in vitro by using LPS (100ng/mL) and IL-4 (10ng/mL), known to drive M1 and M2 phenotypes respectively. First, flow cytometry was used to evaluate the M1 (CD86+) and M2 (CD206+) populations, shown as a percentage of CD68+ cells (Figure 2A). Secondly, fluorescent labeled smooth muscle cells (SMCs) were combined with RAWs in an engulfment assay that showed the percent of IL-4 treated RAWs engulfing SMCs was greater than the percent of LPS or control treated RAWS (Figure 2B). Finally, we used real-time (RT)-PCR to evaluate M1 (iNOS, TNFa) and M2 (Arginase 1, IL-10) markers in PBS, LPS, and IL-4 treated cells. Results showed that LPS treatment significantly upregulated all four markers as compared to PBS and IL-4 treatment groups (Figure 2C).

The broad relatively unspecific activation phenotype evidenced in the RAW cell line in Figure 2 prompted us to adopt a method of culturing primary monocyte/macrophages, bone marrow derived monocytes (BMDM) for treatment. Figure 3A shows that LPS induced M1-polarization, whereas IL-4 drove a larger percentage of M2 macrophages as compared to PBS and LPS –treated groups. Further, an engulfment assay using fluorophore-labeled latex beads reveals that M2-polarized macrophages display a greater engulfment capability as compared to M1 counterparts (Figure 3B, C). RT-PCR analysis revealed that M1 markers were upregulated in LPS-treated BMDM as compared to PBS and IL4 treated BMDM. Arg1 was upregulated in IL-4

treated cells as compared to PBS and LPS, but IL-10 did not appear to be significantly regulated by either LPS or IL4 treatment (Figure 3D).

Macrophage phenotype profiles in aneurysm

By immunostaining arterial tissue sections, we showed that both M1 (iNOS+CD68+) and M2 (CD206+CD68+) macrophages were present in human aneurysmal tissues (Figure 4A, B). Similarly, we showed that M1 (iNOS+CD68+) and M2 (Ym1+CD68+) macrophages were present in experimental aneurysm tissue (Figure 4C,D). To further explore M1 and M2 populations in experimental aneurysm tissue, we used flow cytometry to measure the M1 and M2 populations present in elastase and control-treated tissues harvested 3, 7, and 14 days after surgery. Total macrophage (CD11b+F4/80+) populations, as shown in Figure 1B, were further classified to either alternatively activated M2 macrophages (CD206+) or classically activated M1 macrophages (CD86+) (Supplemental Figure 2). M1 and M2 populations are expressed as a percentage of the total number of macrophages counted. The percentage of M2 macrophages is significantly lower in elastase-treated tissues at 3 and 7 days after surgery, while the percentage of M1 macrophages remains similar between elastase- and control- treated tissue at all timepoints (Figure 5A). A 'macrophage phenotype profile', or the 'M2:M1 ratio', was calculated by dividing the percentage of M2 macrophages by the percentage of M1 macrophages (Figure 5B).

Next, we aimed to evaluate markers of M1 and M2 macrophages using real-time (RT)-PCR analysis. As shown in Figure 6, no significant difference was seen in M1 or M2-associated markers between control and aneurysmal tissue at 3 and 7 days after surgery. 14 days after

surgery, however, the M2 markers FIZZ1 and Ym-1, as well as all M1 markers were significantly upregulated in elastase-induced aneurysm. Conversely, Arg-1 was moderately but insignificantly attenuated in elastase-perfused tissue 14 days after surgery.

Functionality of M1 and M2 macrophages

As previously described, we noted an apparent difference in engulfment capability between IE- and elastase-treated tissues when examined by histology. In order to explore this further, we set out to measure the engulfment capability of the macrophage phenotypes in our aneurysm model. To this end, we designed an experiment in which fluorophore-labeled beads were added to the cell isolates harvested from treated arteries. Using flow cytometry, we were then able to identify macrophages in the sample and evaluate their engulfment capacity using two parameters: percent of cells positive for fluorescent beads (% engulfing), and the mean fluorescence intensity (MFI) which indicates the number of beads/cell (capacity). As shown in Figure 7A and B, the percent of M2 cells engulfing beads appears generally higher at 3 and 7 days, but only measured as significant in elastase-treated tissue 3 days after surgery (Figure 7B). However, the MFI of M2 cells was significantly higher in elastase-treated tissues at 7 and 14 days after surgery, and in control-treated tissue 14 days after surgery (Figure 7C, D). Further, our results revealed the only difference seen in total macrophage populations harvested from elastase or control treated tissues to be a significant reduction in engulfment capacity of macrophages harvested from elastase-treated tissue 14 days after surgery (Figure 8 A, B).

PPARγ-agonist attenuates experimental aneurysm formation

Having shown M2 macrophages to be consistently downregulated in elastase treated tissues, we postulated that fewer M2 macrophages may in part be responsible for defective apoptotic cell clearance, and that these lingering apoptotic cells become necrotic and induce a substantial inflammatory response. Therefore, experimental manipulations that increase M2 differentiation may improve apoptotic cell clearance, thus attenuating inflammation and aneurysm progression. To test this hypothesis, we turned to chemical agonists of liver X receptor (LXR) and peroxisome proliferator-activated receptor gamma (PPARγ), which have been shown to favor M2 polarization. First, we used the in vitro macrophage polarization methodology described previously to perform preliminary tests using four different drugs suggested to have a role in macrophage phenotype differentiation. The LXR agonists GW3965 (1μm) and TO-901317 (1μm) had moderate success in driving M2 polarization in LPS treated BMDM (Figure 9A). PPARγ agonists Troglitazone (10μm) and Rosiglitazone (10μm) were shown to be more effective in driving M2 polarization (Figure 9B), and appeared to have a small role in increasing the percent of cells engulfing beads (Figure 9C). Data gathered in this study led us to carry Rosiglitazone (RGZ) toward in vivo application, administering RGZ, or DMSO control, to mice from both elastase and control-treated groups. As shown in Figure 10A and B, RGZ successfully inhibited elastase-induced aneurysmal expansion when administered 5 days after surgery (145.7±18.8 vs. 82.8±13.3% in DMSO and RGZ groups, respectively). Immunohistochemical analysis revealed a significant difference in elastin degradation (Figure 10C). As compared to DMSO, RGZ moderately reduced macrophage infiltration in elastase treated tissues, and significantly reduced macrophage infiltration to control-treated tissues (Figure 10D).

PPARγ-agonist drives M2 phenotype in elastase-induced aneurysm

M1 and M2 macrophage populations were measured using the flow cytometry-based method in DMSO and RGZ-treated mice. Results show that RGZ administration increased the percentage of M2 macrophages in both elastase and control treated tissue, though statistical significance was not reached (Figure 11A). The M1 population was also reduced in tissue harvested from RGZ treated mice, and the difference was significant in elastase-treated tissue. The M2:M1 ratio clearly shows that RGZ treatment creates a macrophage phenotype profile heavily favoring M2 macrophages (9.8 vs. 8.97 in elastase and control (IE) treated tissue, respectively), whereas an M2:M1 measuring 2.58 and 1.667 in elastase and control treated arteries (Figure 11B). Immunohistochemical analysis provides further evidence for the presence of both M1 and M2 macrophages in treated tissue. A qualitative assessment of tissue shows that RGZ reduces iNOS+ macrophages (CD68+), while increasing Ym1+ macrophages (Figure 12A, B).

DISCUSSION

While macrophages have long been known to play a crucial role in aneurysm, the conventional view has focused on these cells as one homogenous population capable of producing matrix degrading enzymes and pro-inflammatory factors[26, 27]. As our understanding of macrophages has improved, we have begun to describe the various subtypes of macrophages and describe their diverse characteristics[28]. The findings presented in this work detail what we believe to be the first exploration of macrophage phenotypes over time in a murine aneurysm model. More importantly, we have provided evidence that M2 macrophages are associated with cessation of aortic dilation, tissue repair, and elastin preservation in experimental aneurysm.

Using a quantitative flow cytometry based method, we provided a detailed description of the macrophage populations(s) found in aneurysmal tissue. Active and inactive elastase triggered a similar, dramatic initial inflammatory response, indicated by the large number of infiltrated macrophages 3 days after surgery. We believe this acute inflammatory response is a normal tissue response to the surgical procedure associated with the model and perhaps heat-stable contaminants in elastase. The fact that macrophage infiltration subsided in arteries treated with inactivated elastase indicates that what is observed in the control group is a typical acute inflammatory response that is successfully resolved. In contrast, immune resolution was markedly defected or delayed in elastase-treated arteries. This pattern accurately reflects the inflammatory environment that has been considered characteristic of aneurysm. Studying the macrophage population in more detail, we then showed that, when compared to elastase-

treated tissues, IE-treated tissues contained a greater percentage of M2 macrophages, indicating an environment that is anti-inflammatory and pro-tissue repair.

The prevalence of M2 phenotype macrophages in control-treated experimental aneurysm tissue is likely linked to the low number of free-standing apoptotic cells in this tissue. Conversely, elastase-treated tissues display a significantly higher number of apoptotic cells 7 days after surgery, a time point when total macrophage numbers remain significantly higher than IE-treated tissues. Histological analysis revealed that these apoptotic cells are not being effectively engulfed by the macrophages. Taken together, this evidence suggests that apoptotic cells in elastase-treated tissues may linger in the artery and undergo necrosis, a highly inflammatory process. The inflammatory environment reduces M2 macrophage polarization while recruiting additional macrophages, creating a persistent inflammatory state that degrades vascular tissue.

Results from this study further support a crucial role for M2 macrophages in attenuation of aneurysm formation by the use of the PPARγ agonist Rosiglitazone (RGZ) to drive M2 marophages in small aneurysm. Administering RGZ to animals that have undergone elastase-induced aneurysm surgery was shown to significantly reduce aneurysmal expansion as compared to DMSO administration. Examination of aortic tissue harvested from these animals revealed a higher number of M2 macrophages present in the tissue and accordingly increased M2:M1 ratio values. As compared to DMSO control, RGZ administration did not significantly reduce total macrophage number in elastase treated tissues. This result suggests that the macrophage phenotype present in tissue is likely much more important than the total number

of macrophages found in the tissue. It is important to note that RGZ administration was begun 5 days after surgery and was capable of interfering with the ongoing inflammatory processes in the treated tissue, suggesting that RGZ may in fact be a candidate for therapeutic intervention strategies.

When examining results of our study, we found that expressing the macrophage population profile as a ratio, the M2:M1 ratio, was a simple and effective way of describing the balance of the two phenotypes. When the ratio is near 1, arteries show aneurysm hallmarks such as elastin degradation and apoptosis. Conversely, larger ratios indicated arteries in which tissue integrity was preserved and a healing process was likely underway. While the M1:M2 ratio is a good indicator for overall tissue environment, it does mask the individual macrophage populations. In our model, a larger ratio almost always indicated an increase in M2 macrophages, but conceivably this ratio could go up if M1 numbers fell. Thus, it is important to supplement the M2:M1 ratio with numbers from each population.

When considering results from this study, it should be noted that we have chosen to focus on only two macrophage phenotypes. As our understanding of macrophages expands, so too does the number of macrophage phenotypes identified. Appropriately, then, our data shows that M1 and M2 phenotypes identified in our tissue samples only make up around 50% of the total macrophages measured in the same sample. This suggests that there are various other macrophage phenotypes present in the tissue and their potential contributions to the disease and its development should not be ignored.

Macrophages are very plastic cells, and the idea of 'polarization' is an oversimplification of the process. It is likely that, at any one point, macrophages possess characteristics of one or more identified subsets. It is for this reason, we chose to do three different measurements for the identification of M1 and M2 subsets in our tissue (i.e. flow cytometry, RT-PCR, engulfment assays), but it is also for this reason that our study is significantly limited. In the future, it will be important to expand upon these findings to include additional macrophage subtypes as well as additional methods of identification such as laser capture microdissection and/or cell sorting.

In addition, it will be beneficial to explore additional methods of manipulating M2 macrophage population in aneurysm. In addition to PPARγ agonists, LXR agonists are another class of nuclear receptors that are capable of modulating macrophage differentiation[15]. The potential use of LXR agonists to modulate macrophage phenotypes thus curb aneurysm progression is further supported by our in vitro demonstration of the pro-M2 effect of these agents. Another important consideration for translating PPARγ or LXR agonists to aneurysm therapy is toxicity of these drugs. In collaboration with material scientists, our lab is exploring tissue-specific drug delivery using nanotechnology.

In summary, data presented in this chapter implicate that the selective reduction in M2 macrophage polarization is at least in part responsible for the defected inflammation resolution and tissue repair. Furthermore, we provided proof-of-concept evidence that promoting M2 phenotype with PPARγ agonists may be an effective drug therapy for aneurysm treatment.

1. Choke E, Cockerill G, Wilson WR, Sayed S, Dawson J, Loftus I, Thompson MM. A review of biological factors implicated in abdominal aortic aneurysm rupture. *Eur J Vasc Endovasc Surg*. 2005;30:227-244
2. Golledge ALV, Walker P, Norman PE, Golledge J. A systematic review of studies examining inflammation associated cytokines in human abdominal aortic aneurysm samples. *Disease Markers*. 2009;26:181-188
3. Golledge J, Tsao PS, Dalman RL, Norman PE. Circulating markers of abdominal aortic aneurysm presence and progression. *Circulation*. 2008;118:2382-2392
4. Nordon IM HR, Loftus IM, Thompson MM. Pathophysiology and epidemiology of abdominal aortic aneurysms. *Nature Reviews Cardiology*. 2011;8:92-102
5. Middleton RK, Lloyd GM, Bown MJ, Cooper NJ, London NJ, Sayers RD. The pro-inflammatory and chemotactic cytokine microenvironment of the abdominal aortic aneurysm wall: A protein array study. *Journal of Vascular Surgery*. 2007;45:574-580
6. Aziz F, Kuivaniemi H. Role of matrix metalloproteinase inhibitors in preventing abdominal aortic aneurysm. *Ann Vasc Surg*. 2007;21:392-401
7. Longo GM, Xiong W, Greiner TC, Zhao Y, Fiotti N, Baxter BT. Matrix metalloproteinases 2 and 9 work in concert to produce aortic aneurysms. *The Journal of Clinical Investigation*. 2002;110:625-632
8. Rizas KD IN, Tilson MD 3rd. . Immune cells and molecular mediators in the pathogenesis of the abdominal aortic aneurysm. *Cardio Rev*. 2009;17:201-210
9. Murray PJ, Wynn TA. Obstacles and opportunities for understanding macrophage polarization. *Journal of Leukocyte Biology*.
10. Mantovani A, Biswas SK, Galdiero MR, Sica A, Locati M. Macrophage plasticity and polarization in tissue repair and remodelling. *The Journal of Pathology*. 2013;229:176-185
11. Leitinger SAaN. Phenotypic modulation of macrophages in response to plaque lipids. *Current Opinion in Lipidology*. 2011;22:335-342
12. I.M.J. Wolfs MD, MPJ de Winther. Differentiation factors and cytokines in the atherosclerotic plaque micro-environment as a trigger for macrophage polarisation. *Thrombosis and Haemostasis*. 2011;106:763-771
13. Kigerl KA GJ, Ankeny DP, Alexander JK, Donnelly DJ, Popvich PG. Identification of two distinct macrophage subsets with divergent effects causing either neurotoxicity or regeneration in the injured mouse spinal cord. *Neurobiology of Disease*. 2009;29:13435-13444
14. Mantovani A, Sica A, Locati M. Macrophage polarization comes of age. *Immunity*. 2005;23:344-346
15. Korns D FS, Fernandez-Boyanapalli R, Henson PM, Bratton DL. . Modulation of macrophage efferocytosis in inflammation. *Frontiers in Immunology*. 2011;2
16. Clarke MCH, Talib S, Figg NL, Bennett MR. Vascular smooth muscle cell apoptosis induces interleukin-1-directed inflammation. Effects of hyperlipidemia-mediated inhibition of phagocytosis. *Circ Res*. 2009:CIRCRESAHA.109.208389
17. Bouhlel MA, Derudas B, Rigamonti E, Dievart R, Brozek J, Haulon S, Zawadzki C, Jude B, Torpier G, Marx N, Staels B, Chinetti-Gbaguidi G. Ppargamma activation primes human monocytes into alternative m2 macrophages with anti-inflammatory properties. *Cell Metab*. 2007;6:137-143
18. Odegaard JI, Ricardo-Gonzalez RR, Goforth MH, Morel CR, Subramanian V, Mukundan L, Red Eagle A, Vats D, Brombacher F, Ferrante AW, Chawla A. Macrophage-specific ppargamma controls alternative activation and improves insulin resistance. *Nature*. 2007;447:1116-1120
19. Jones A, Deb R, Torsney E, Howe F, Dunkley M, Gnaneswaran Y, Gaze D, Nasr H, Loftus IM, Thompson MM, Cockerill GW. Rosiglitazone reduces the development and rupture of experimental aortic aneurysms. *Circulation*. 2009;119:3125-3132

20. Pirianov G, Torsney E, Howe F, Cockerill GW. Rosiglitazone negatively regulates c-jun n-terminal kinase and toll-like receptor 4 proinflammatory signalling during initiation of experimental aortic aneurysms. *Atherosclerosis*. 2012;225:69-75
21. Pyo R, Lee JK, Shipley JM, Curci JA, Mao D, Ziporin SJ, Ennis TL, Shapiro SD, Senior RM, Thompson RW. Targeted gene disruption of matrix metalloproteinase-9 (gelatinase b) suppresses development of experimental abdominal aortic aneurysms. *The Journal of Clinical Investigation*. 2000;105:1641-1649
22. Galkina E, Kadl A, Sanders J, Varughese D, Sarembock IJ, Ley K. Lymphocyte recruitment into the aortic wall before and during development of atherosclerosis is partially l-selectin dependent. *J Exp Med*. 2006;203:1273-1282
23. Tang XN, Berman AE, Swanson RA, Yenari MA. Digitally quantifying cerebral hemorrhage using photoshop® and image j. *Journal of Neuroscience Methods*. 2010;190:240-243
24. Weischenfeldt J, Porse B. Bone marrow-derived macrophages (bmm): Isolation and applications. *CSH Protoc*. 2008;2008:pdb prot5080
25. Clowes A, Clowes M, Fringerle J, Reidy M. Kinetics of cellular poliferation after arterial injury: Role of acute distension in the induciton of smooth muscle proliferation. *Lab Invest*. 1989;60:360-364
26. Tieu BC, Lee C, Sun H, LeJeune W, Recinos A, Ju X, Spratt H, Guo D-C, Milewicz D, Tilton RG, Brasier AR. An adventitial il-6/mcp1 amplification loop accelerates macrophage-mediated vascular inflammation leading to aortic dissection in mice. *The Journal of Clinical Investigation*. 2009;119:3637-3651
27. Daugherty A, Rateri DL, Charo IF, Owens AP, Howatt DA, Cassis LA. Angiotensin ii infusion promotes ascending aortic aneurysms: Attenuation by ccr2 deficiency in apoe-/- mice. *Clinical Science*. 2010;118:681-689
28. Lawrence T, Natoli G. Transcriptional regulation of macrophage polarization: Enabling diversity with identity. *Nat Rev Immunol*. 2011;11:750-761

Figure 1. Differential macrophage content relates to aneurysm expansion in the elastase-induced mouse model of AAA.

(A) Aortic Dilation measured in elastase (E) and heat-inactivated elastase (IE) tissues 3, 7, and 14 days after surgery. % Aortic dilation is calculated as described in methods. *$p<0.05$*, as compared to IE-treated tissues measured at same timepoint. (B) Total number of macrophages measured in IE and E-treated tissues 3, 7, and 14 days after surgery. *$p<0.05$*. (C) Quantification of IHC stain for macrophage (CD68+) content in IE and E-treated tissues harvested 3 and 7 days after surgery. *$p<0.05$.* (D) Representative co-stain for macrophages (CD68, green) and apoptosis (TUNEL, red) overlay with DAPI. Scale bar=50μm.

Figure 2. A mouse macrophage cell line may not be an accurate model for macrophage polarization.

(A) M1 (CD86+, white bar) and M2 (CD206+, black bar) populations identified by flow cytometry in RAW264.7 monocyte/macrophages treated with PBS, LPS, or IL-4. Populations are shown as a percent of the total number of macrophages identified. n=1. (B) Percent of RAW264.7 cells from PBS, LPS, or IL-4 treatment groups engulfing healthy (untreated, CTL) or apoptotic (UV light-treated, UV) smooth muscle cells (SMCs). (C) RT-PCR of selected M1 (iNOS, TNFα) and M2 (Arginase-1, IL-10) associated genes. *$p<0.05$*, n=3.

Figure 3. Bone marrow derived monocytes can be stimulated to differentiate to M1 or M2 phenotypes.

(A) M1 (CD86+, white bar) and M2 (CD206+, black bar) populations measured by flow cytometry in bone marrow derived monocyte/macrophages (BMDM) treated with PBS, LPS, or IL-4. Populations are shown as a percent of the total number of macrophages identified. n=2. (B) Percent of M1 (white bar) and M2 (black bar) engulfing fluorescent beads 20 minutes (m), 30m, 1 hour (h), and 2 hours after adding beads to cell suspension. n=1. (C) Mean fluorescent intensity (MFI) of M1 (white bar) and M2 (black) cells from experiment in (B). (D) RT-PCR of selected M1 (iNOS, TNFα) and M2 (Arginase-1, IL-10) associated genes. n=1.

Figure 4. M1 and M2 phenotype markers are present in human and experimental aneurysm tissue.

(A) Co-stain for macrophages (CD68, green) and M1 marker (iNOS, red) overlay with nuclei (DAPI, blue) in human AAA tissue. 20x scale bar=100μm, 40x scale bar=50μm. (B) Co-stain for M2 macrophages (CD206, green) and apoptotic cells (TUNEL, red) overlay with nuclei (DAPI, blue) in human AAA tissue. (C) Co-stain for M2 macrophages (Ym1, red) and macrophages (CD68, green) overlay with nuclei (DAPI, blue) in mouse tissue treated with heat-inactivated elastase or elastase. Scale bar=50μm. (D) Co-stain for M1 macrophages (iNOS, red) and macrophages (CD68, green) overlay with nuclei (DAPI, blue) in mouse tissue treated with heat-inactivated elastase or elastase. Scale bar=100μm.

Figure 5. M2 macrophage phenotypes are more prevalent in inactive elastase-treated tissues.

(A) M1 (Δ) and M2 (□) populations in heat inactivated elastase (IE, dashed line) and elastase (E, solid line) treated arteries harvested from mice 3, 7, and 14 days after surgery. Expressed as a percentage of total macrophages counted. *$p<0.05$* as compared to M1 IE; *$p<0.05$* as

compared to M2 E; *##p<0.05* as compared to M1 E. (B) M2:M1 ratio (%M2 macrophages/%M1 macrophages) in IE (white bar) and E (black bar) treated aortic tissues 3, 7, and 14 days after surgery calculated from (A).

Figure 6. M1 and M2 related genes are upregulated in developed experimental aneurysm.

(A) RT-PCR analysis of selected M1 (iNOS, IFNγ, MCP-1, TNFα) and M2 (IL-10, Arginase-1 (Arg1), FIZZ1, and YM-1) related genes measured in heat-inactivated elastase (IE) and elastase (E) treated tissues 3, 7, and 14 days after surgery. **p<0.05*; n=5 for 3 day IE and E, n=4 for 7 day IE and n=6 for 7 day E, n=3 for 14 day IE and E.

Figure 7. M1 and M2 macrophage phenotypes possess differential engulfment capabilities in control and aneurysmal tissues.

(A,B) Percent of M1 (white bar) and M2 (black bar) engulfing fluorescent beads in inactive elastase (A) or elastase (B) treated tissues. **p<0.05*. (C) Mean fluorescent intensity (MFI) of M1 (white bar) and M2 (black bar) cells from experiment in (A). (D) MFI of M1 (white bar) and M2 (black bar) cells from experiment (B). (A-D) **p<0.05*; n=3 for 3, 7, and 14 day samples.

Figure 8. Engulfment capability of total macrophage population reduced in developed experimental aneurysm.

(A) Percent of total macrophages engulfing fluorescent beads in inactive elastase (IE) or elastase (E) treated tissues 3, 7, and 14 days after surgery. n=3. (B) Mean fluorescent intensity (MFI) of total macrophage cells from experiment (A). **p<0.05*, n=3.

Figure 9. A PPARγ agonist promotes M2 dominated population in bone marrow derived monocytes.

(A) Bone marrow derived monocyte/macrophages (BMDM) were pre-treated with LXR agonists TO-901317 (TO) or GW3965 (GW) followed by stimulation with LPS or PBS control. M1 (CD86+, white bar) and M2 (CD206+, black bar) populations were measure by flow cytometry. Populations are shown as a percent of the total number of macrophage identified. n=1. (B-C) BMDM were stimulated with PBS, LPS, or IL-4 with (+) or without (-) Rosiglitazone pre-treatment. (B) M1 (white bar) and M2 (black bar) populations measured by flow cytometry. Populations are shown as a percent of the total number of macrophages identified. n=2. (C) Percent of M1 (white bar) and M2 (black bar) engulfing fluorescent beads. n=1.

Figure 10. A PPARγ agonist reduces aneurysm formation in a mouse model of AAA.

(A) Aortic Dilation measured in heat-inactivated elastase (IE) and elastase (E) treated tissues from mice receiving Rosiglitazone (RGZ) or DMSO control injections. Final measurements taken 14 days after surgery, Aortic dilation is calculated as described in methods. *$*p<0.05$*. (B) Representative photos of abdominal aortas of mice treated with Inactive Elastase or Elastase and receiving injections of either DMSO or RGZ. Images taken at day 14, scale bar=5mm. (C) Representative images of 14 day aortic sections stained for elastin (Van Gieson), scale bar=200µm. (D) Total number of macrophages measured in IE and E-treated tissues harvested 14 days after surgery from mice receiving RGZ and DMSO injections. *$*p<0.05.$* n=3 for both treatment groups receiving DMSO, n=4 for both groups receiving RGZ.

Figure 11. Administration of a PPARγ drives M2 differentiation in treated aortic tissue.

(A) M1 (white bar) and M2 (black bar) populations in heat inactivated elastase (IE) and elastase (E) treated arteries harvested 14 days after surgery from mice receiving Rosiglitazone (RGZ) or control (DMSO) injections. Expressed as a percentage of total macrophages counted. ***p<0.05* as compared to CD206 cells within treatment group. (B) M2:M1 ratio (%M2 macrophages/%M1 macrophages) in IE and E treated tissues harvested from mice receiving DMSO and RGZ injections, calculated from (A).

Figure 12. Immunohistochemistry reveals presence of M1 and M2 macrophages in aortic tissue.

(A) Co-stain for M1 macrophages (iNOS, red) and macrophages (CD68, green) overlay with nuclei (DAPI, blue) in aortic tissue treated with heat-inactivated elastase or elastase and receiving Rosiglitazone (RGZ) or control (DMSO) injections. Scale bar=100µm. (B) Co-stain for M2 macrophages (Ym1, red) and macrophages (CD68, green) overlay with nuclei (DAPI, blue) in aortic tissue treated with heat-inactivated elastase or elastase and receiving RGZ or DMSO injections. Scale bar=50µm.

Figure 1.

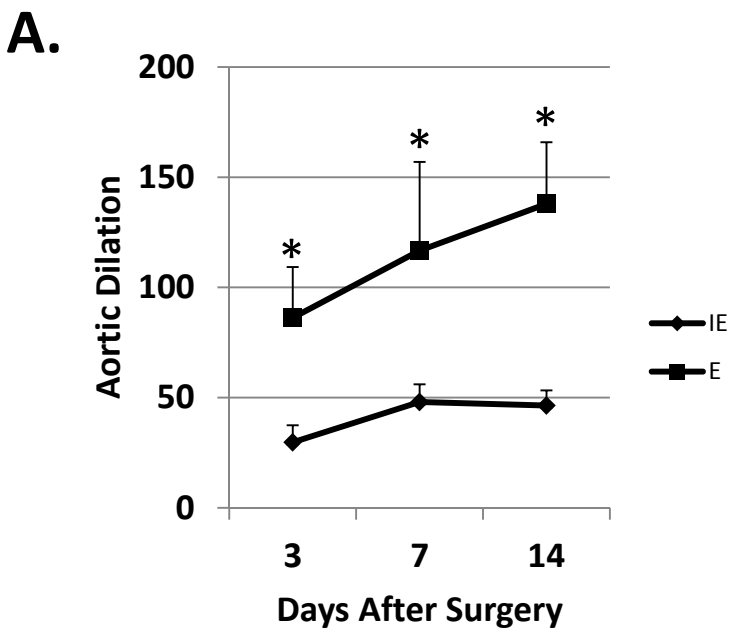
A.
200
150
100
50
0
Aortic Dilation
*
*
*
IE
E
3
7
14
Days After Surgery

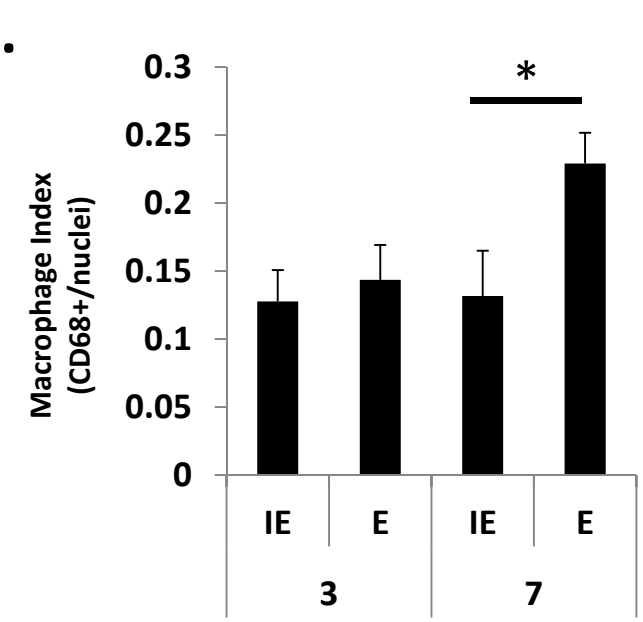
C.
0.3
0.25
0.2
0.15
0.1
0.05
0
Macrophage Index
(CD68+/nuclei)
*
IE
E
IE
E
3
7

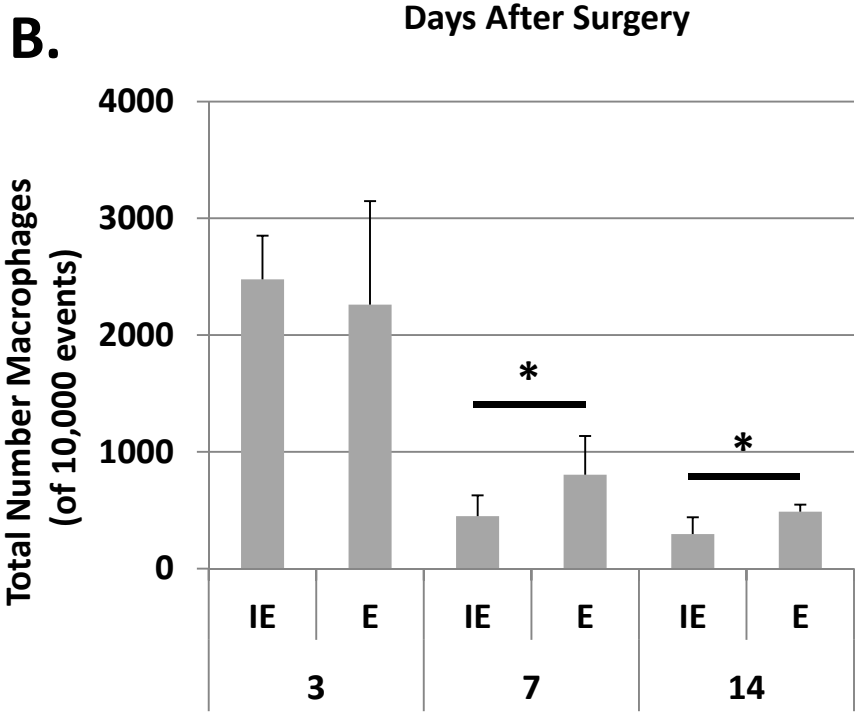
B.
4000
3000
2000
1000
0
Total Number Macrophages
(of 10,000 events)
*
*
IE
E
IE
E
IE
E
3
7
14

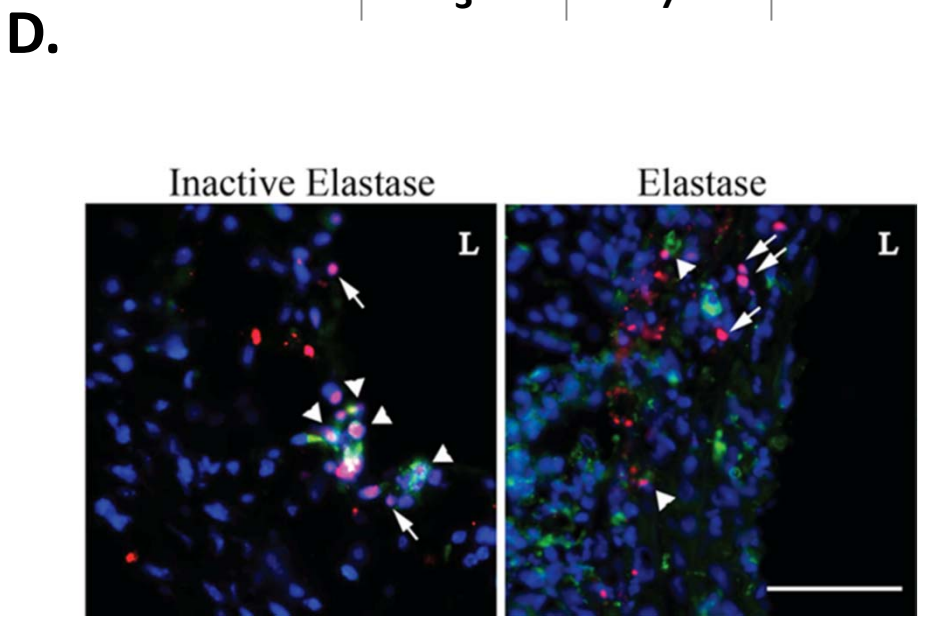
D.
Inactive Elastase
Elastase
L
L

Figure 2.

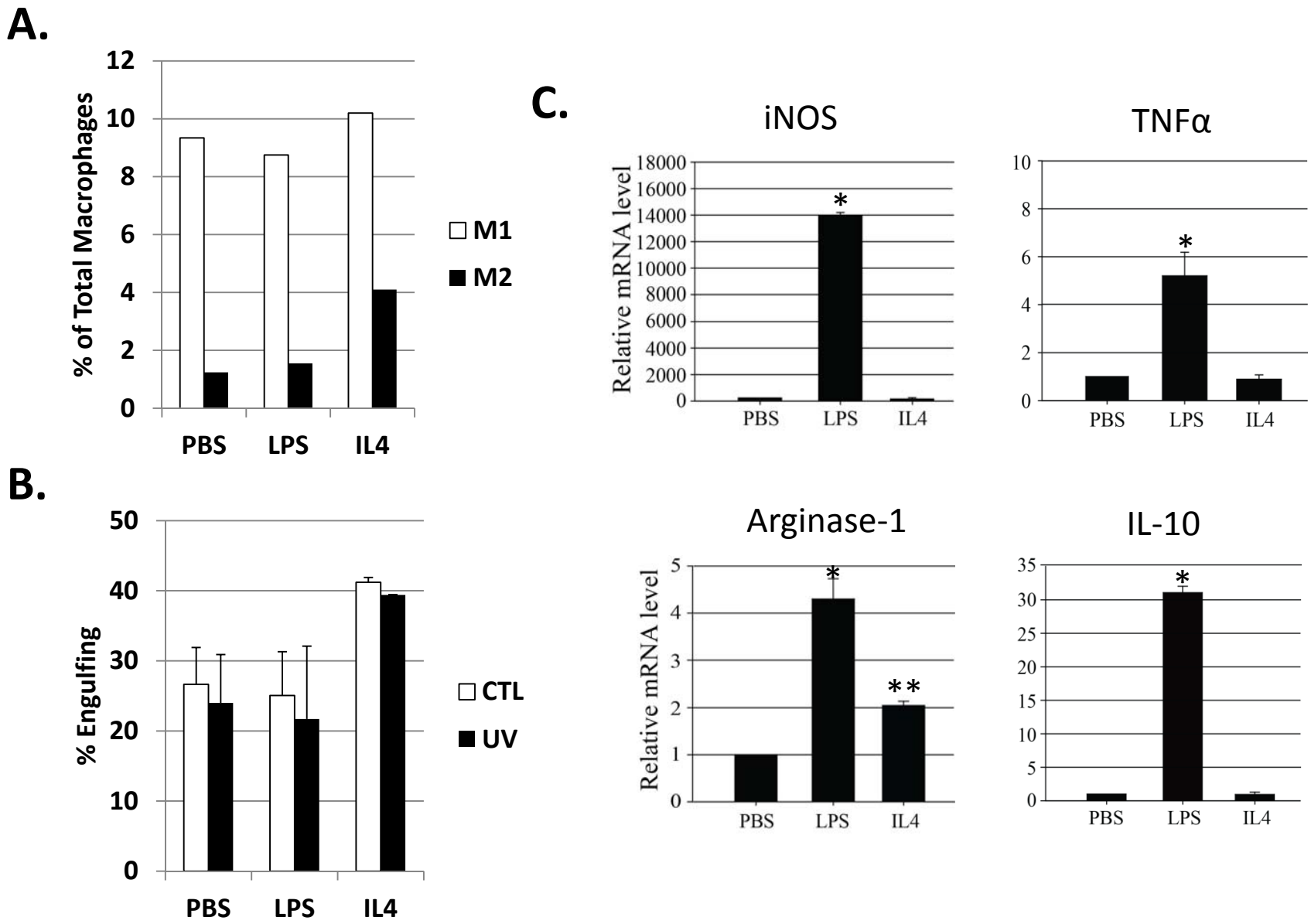
A.
% of Total Macrophages
12
10
8
6
4
2
0
PBS
LPS
IL4
M1
M2
B.
% Engulfing
50
40
30
20
10
0
PBS
LPS
IL4
CTL
UV
C.
iNOS
Relative mRNA level
18000
16000
14000
12000
10000
8000
6000
4000
2000
0
PBS
LPS
IL4
*
TNFα
10
8
6
4
2
0
PBS
LPS
IL4
*
Arginase-1
Relative mRNA level
5
4
3
2
1
0
PBS
LPS
IL4
*
**
IL-10
35
30
25
20
15
10
5
0
PBS
LPS
IL4
*

Figure 3.

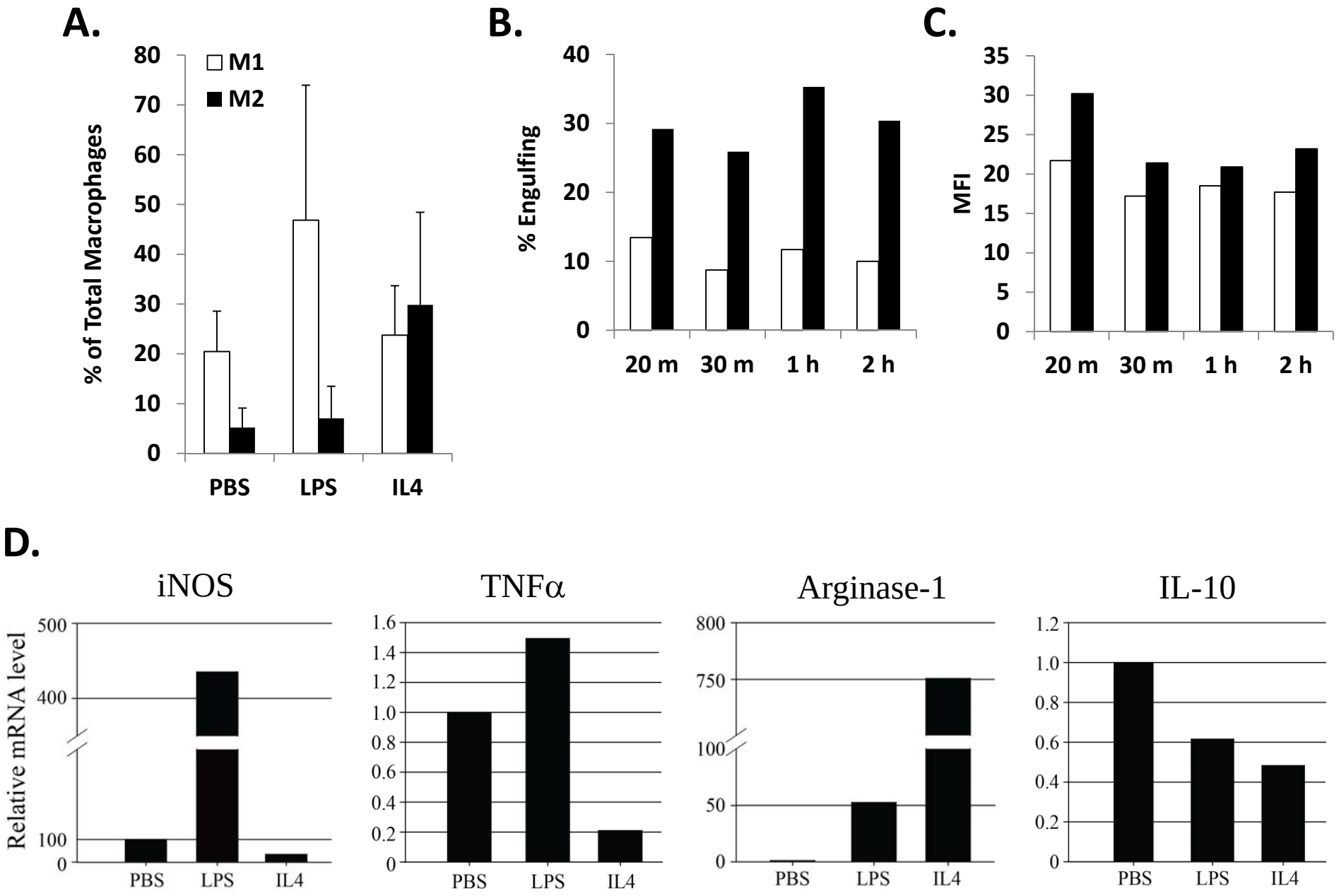
A.
% of Total Macrophages
M1
M2
PBS
LPS
IL4
B.
% Engulfing
20 m
30 m
1 h
2 h
C.
MFI
20 m
30 m
1 h
2 h
D.
iNOS
TNFα
Arginase-1
IL-10
Relative mRNA level
PBS
LPS
IL4

Figure 4.

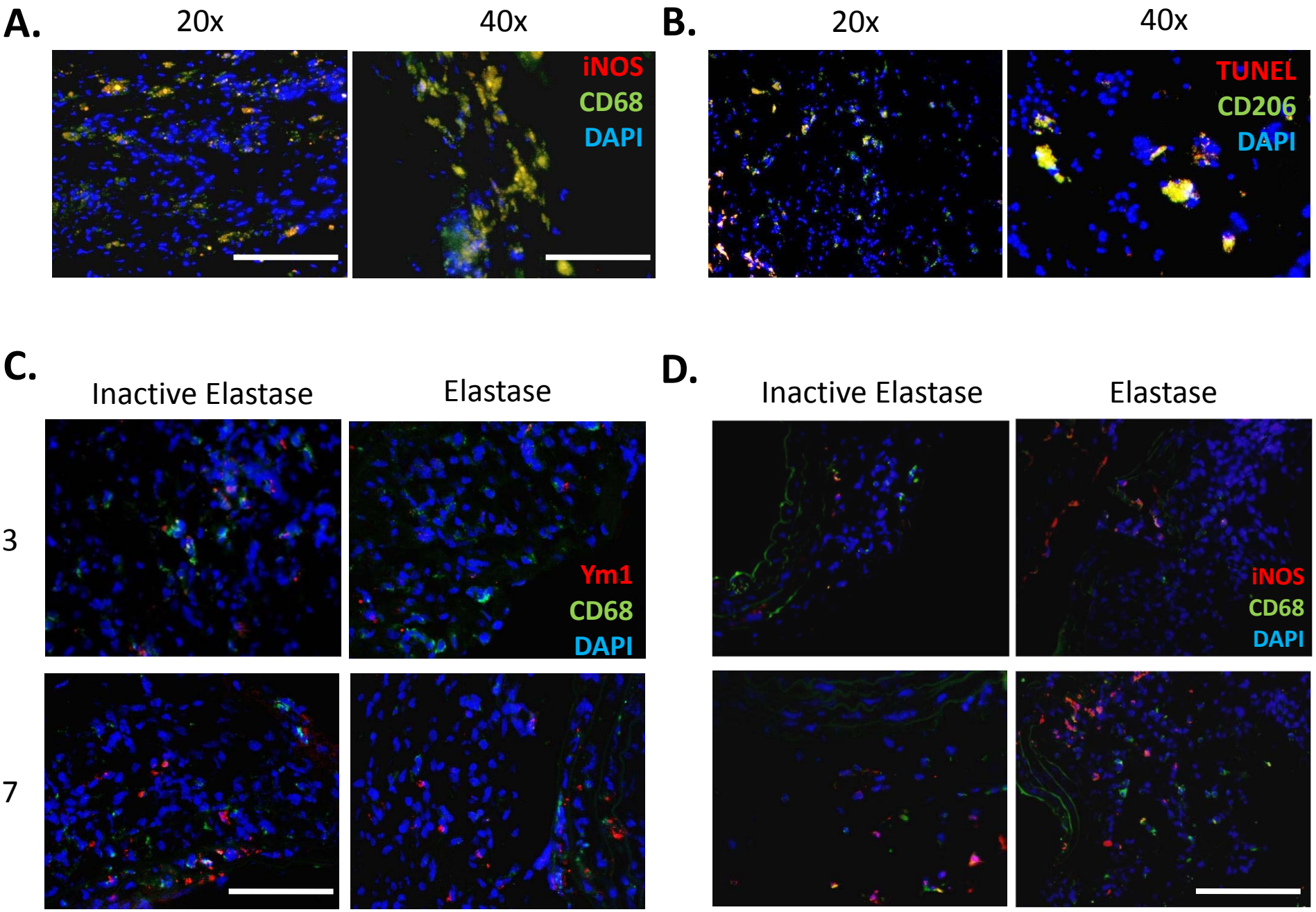
A.
20x
40x
iNOS
CD68
DAPI
B.
20x
40x
TUNEL
CD206
DAPI
C.
Inactive Elastase
Elastase
3
Ym1
CD68
DAPI
7
D.
Inactive Elastase
Elastase
iNOS
CD68
DAPI

Figure 5.

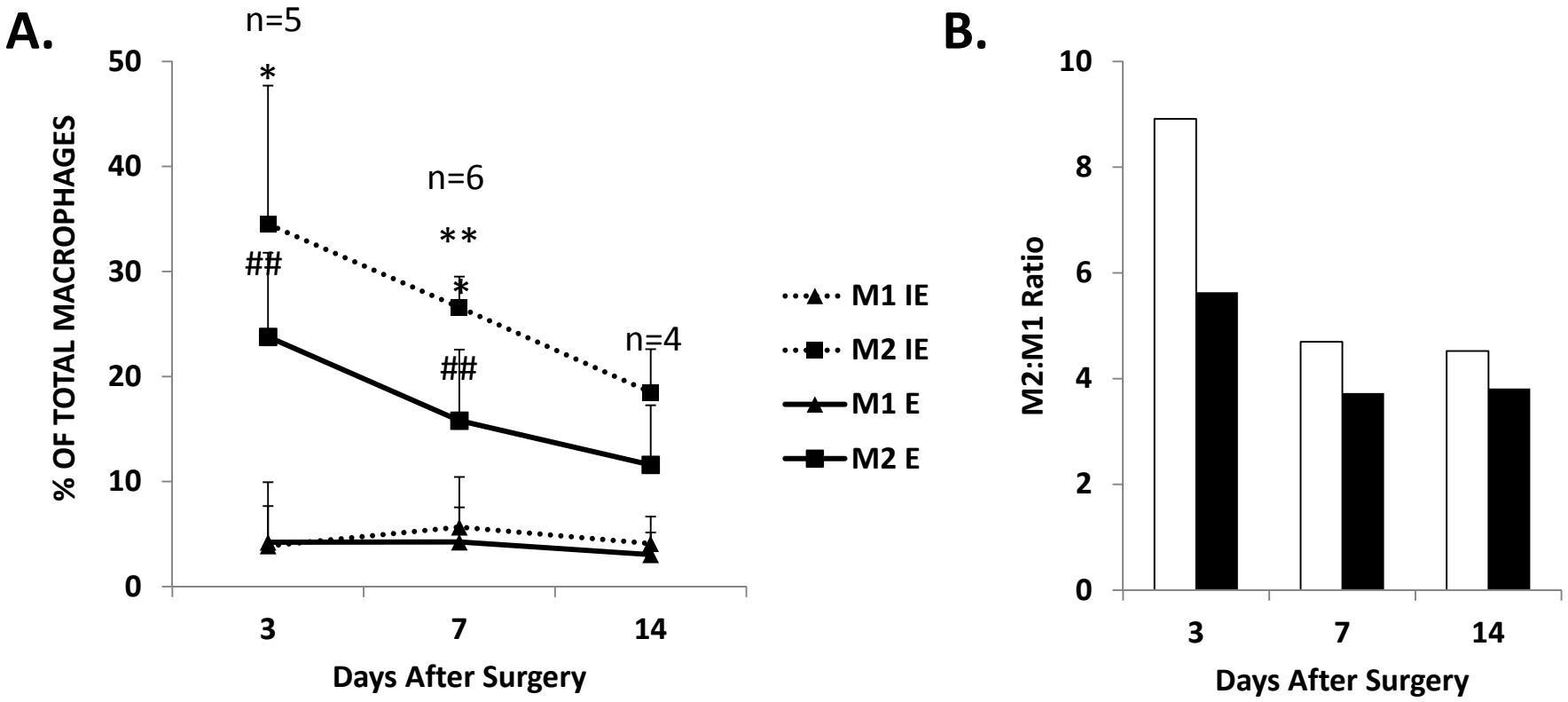
A.
n=5
n=6
n=4
*
**
*
##
##
50
40
30
20
10
0
% OF TOTAL MACROPHAGES
3
7
14
Days After Surgery
M1 IE
M2 IE
M1 E
M2 E
B.
10
8
6
4
2
0
M2:M1 Ratio
3
7
14
Days After Surgery

Figure 6.

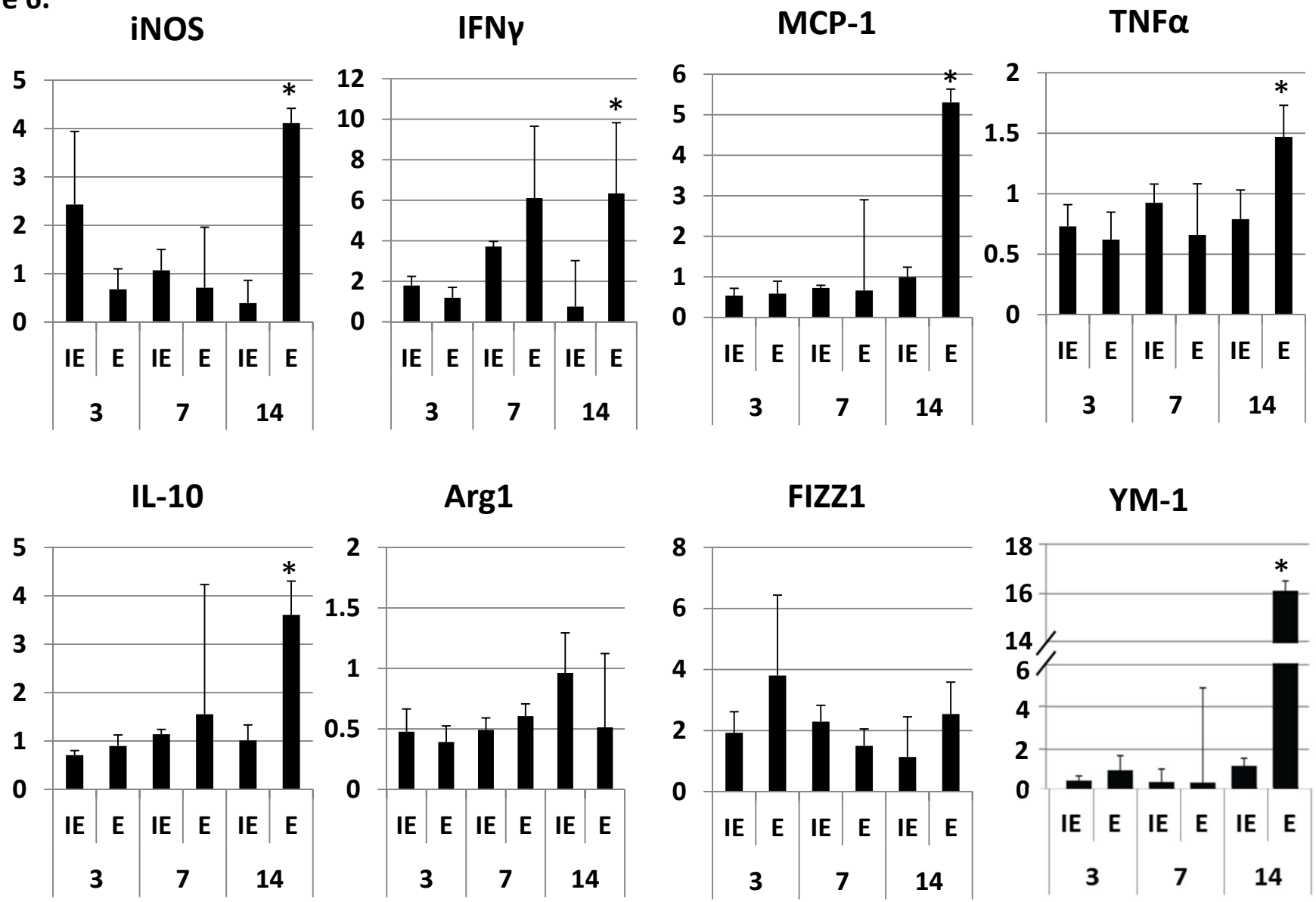

Figure 7.

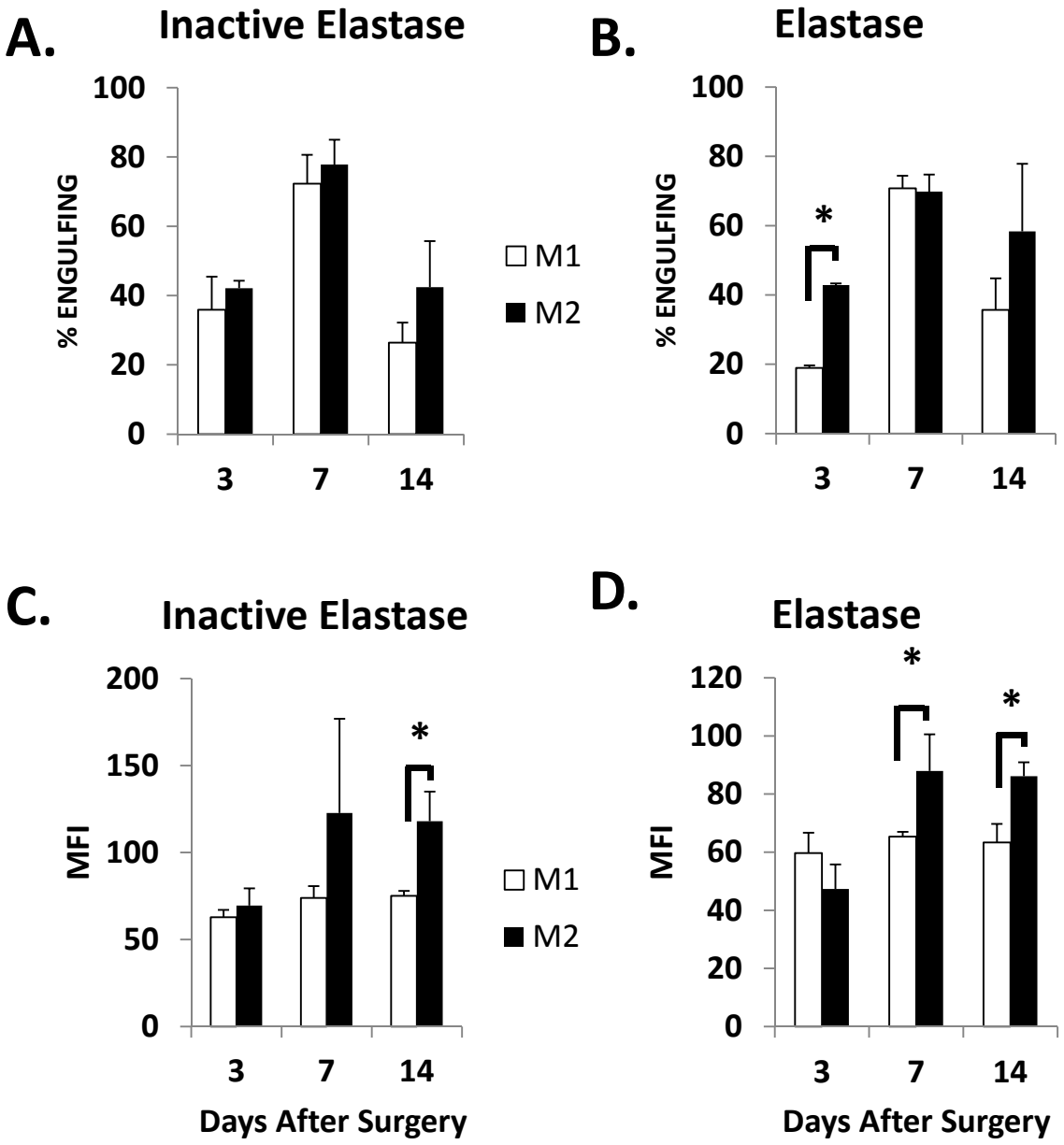
A.
Inactive Elastase
% ENGULFING
100
80
60
40
20
0
3
7
14
M1
M2
B.
Elastase
% ENGULFING
*
C.
Inactive Elastase
MFI
200
150
100
50
0
*
Days After Surgery
D.
Elastase
MFI
120
100
80
60
40
20
0
*
*
Days After Surgery

Figure 8.

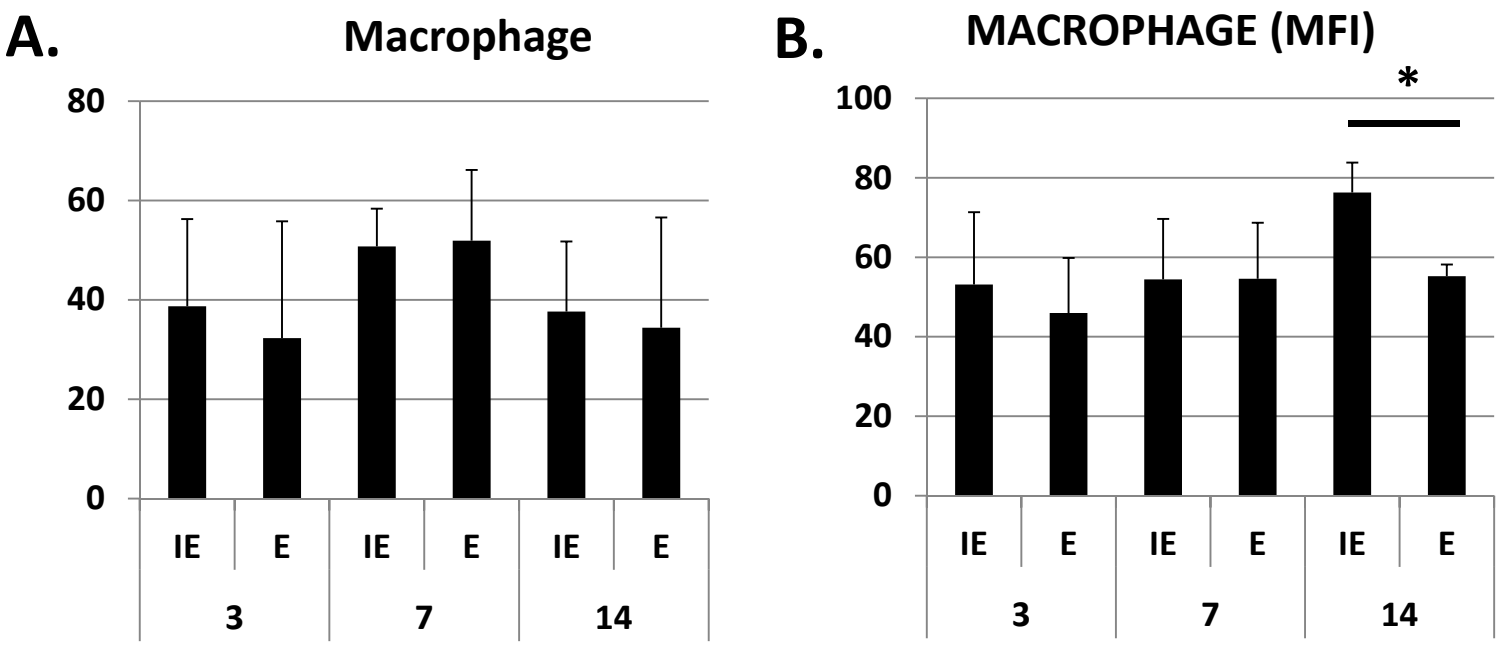
A.
Macrophage
80
60
40
20
0
IE
E
IE
E
IE
E
3
7
14
B.
MACROPHAGE (MFI)
*
100
80
60
40
20
0
IE
E
IE
E
IE
E
3
7
14

Figure 9.

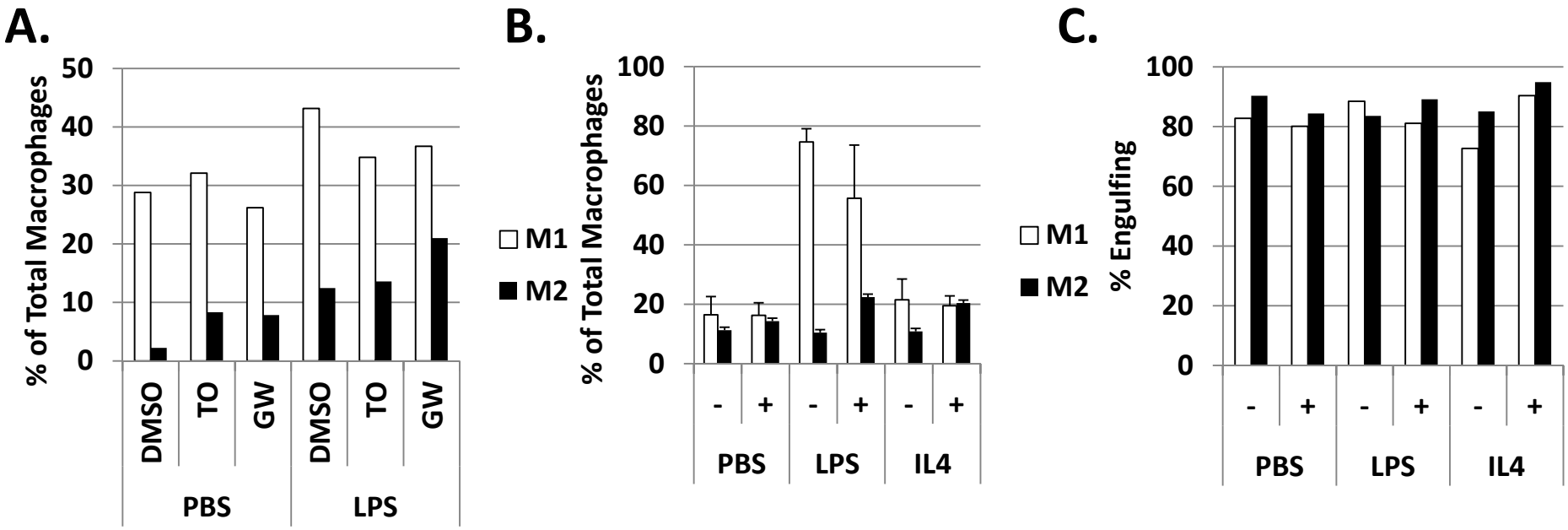
A.
% of Total Macrophages
50
40
30
20
10
0
DMSO
TO
GW
DMSO
TO
GW
PBS
LPS
B.
% of Total Macrophages
100
80
60
40
20
0
M1
M2
-
+
-
+
-
+
PBS
LPS
IL4
C.
% Engulfing
100
80
60
40
20
0
M1
M2
-
+
-
+
-
+
PBS
LPS
IL4

Figure 10.

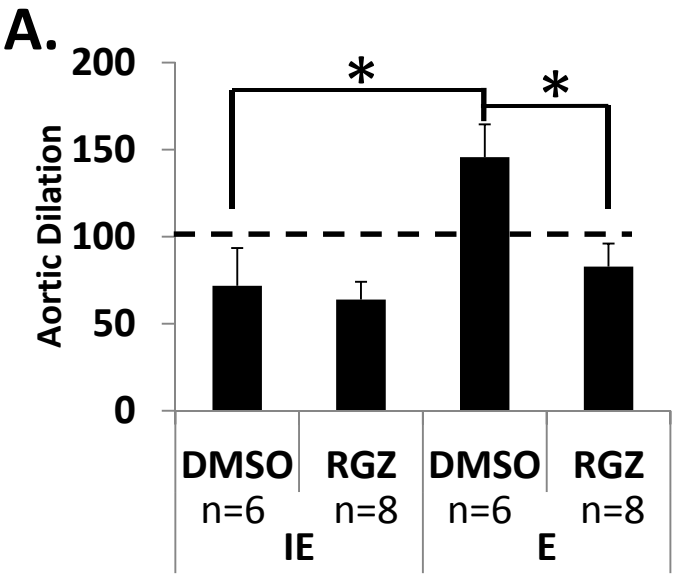
A.
200
150
100
50
0
Aortic Dilation
*
*
DMSO
RGZ
DMSO
RGZ
n=6
n=8
n=6
n=8
IE
E

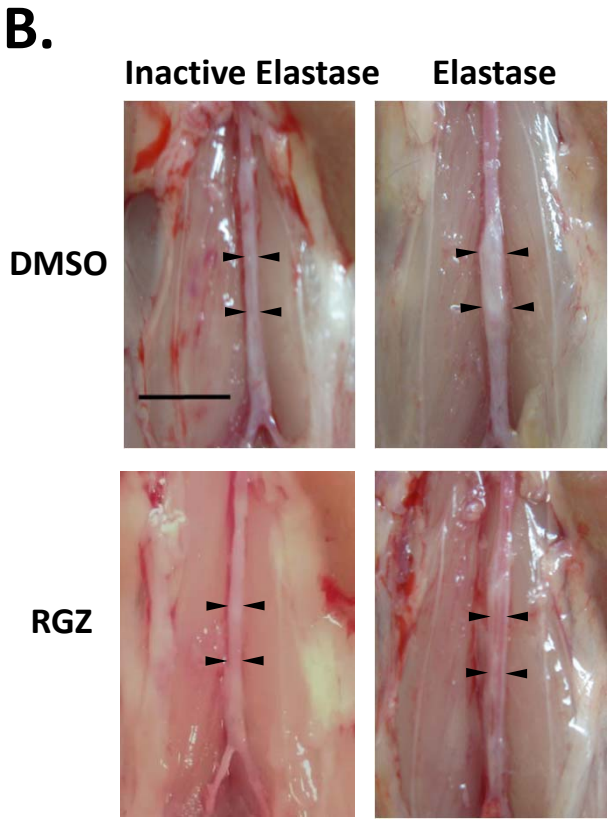
B.
Inactive Elastase
Elastase
DMSO
RGZ

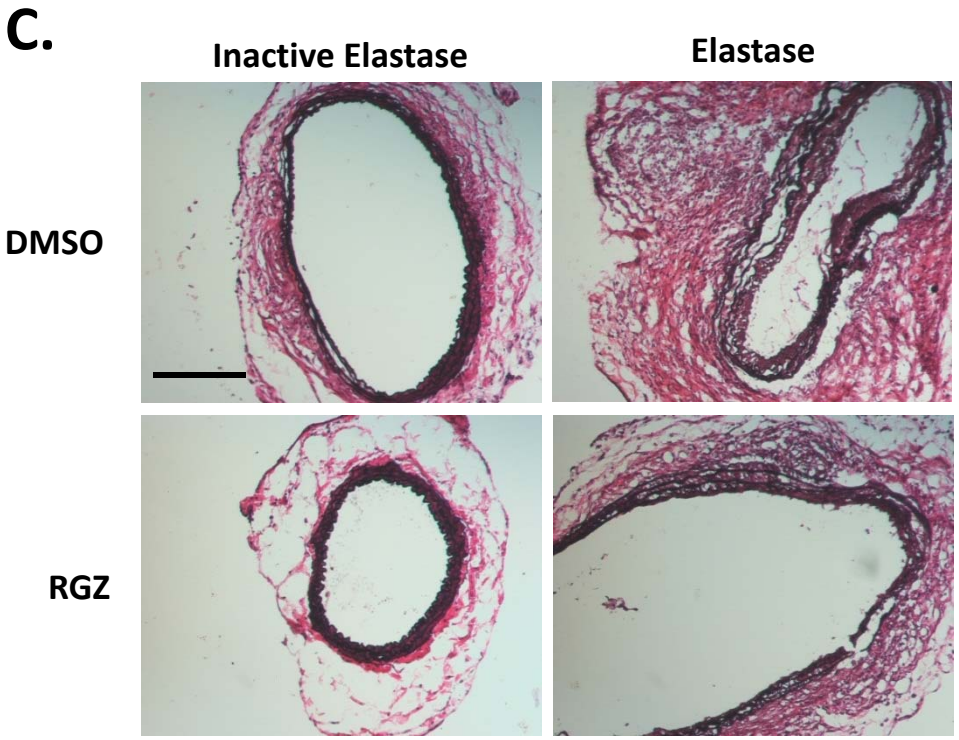
C.
Inactive Elastase
Elastase
DMSO
RGZ

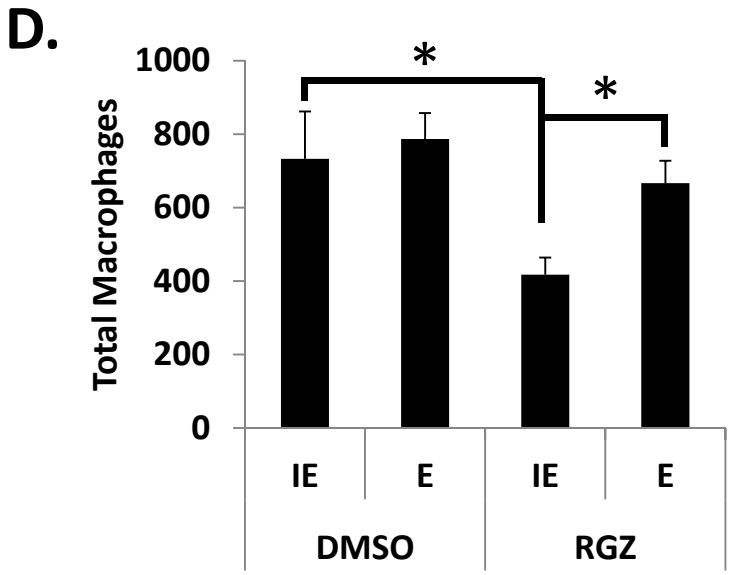
D.
1000
800
600
400
200
0
Total Macrophages
*
*
IE
E
IE
E
DMSO
RGZ

Figure 11.

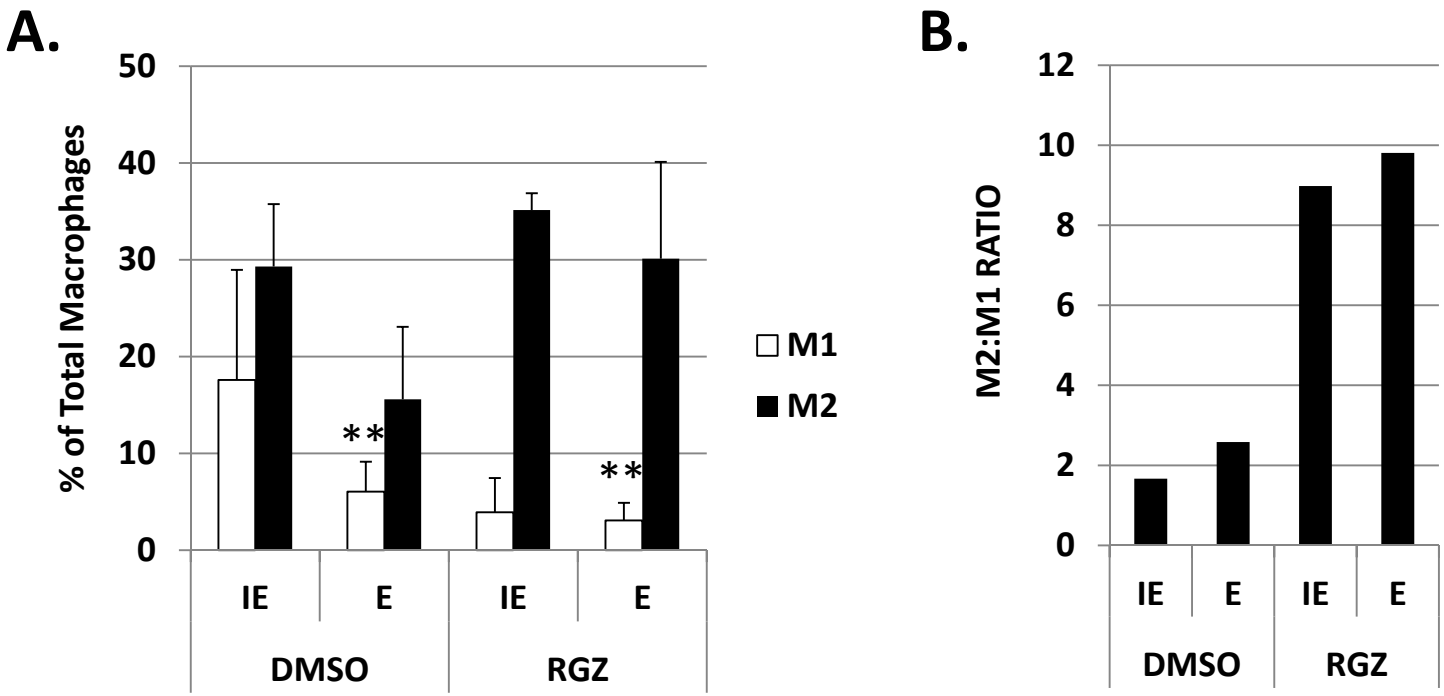
A.
% of Total Macrophages
50
40
30
20
10
0
**
**
IE
E
IE
E
DMSO
RGZ
M1
M2
B.
M2:M1 RATIO
12
10
8
6
4
2
0
IE
E
IE
E
DMSO
RGZ

Figure 12.

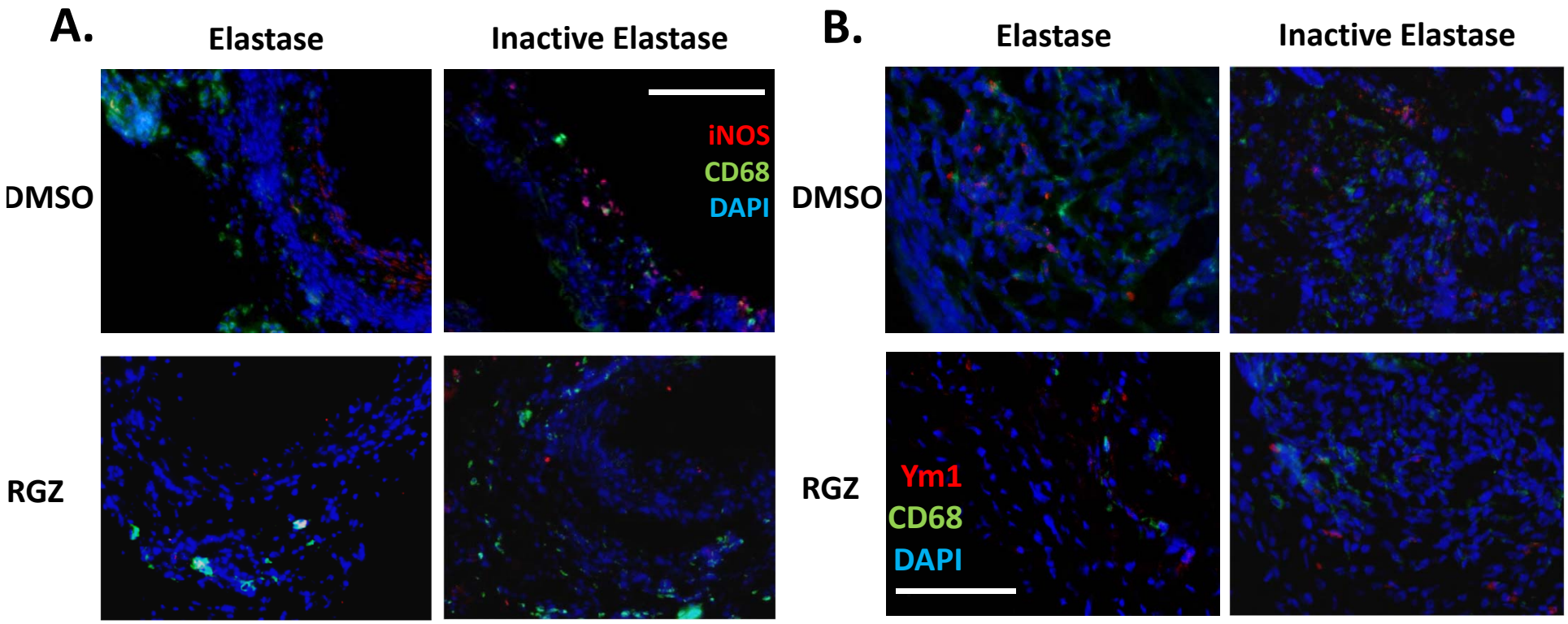
A.
Elastase
Inactive Elastase
DMSO
RGZ
iNOS
CD68
DAPI
B.
Elastase
Inactive Elastase
DMSO
RGZ
Ym1
CD68
DAPI

Supplemental Figure 1. Elastase-induced model of murine aneurysm.

(A) Representative photos of IE-treated aorta (left) and elastase-treated aorta (right) 14 days after surgery. Scale bar=5mm. (B) Representative images of 14 day aortic section stained for elastin (Van-Gieson), scale bar=100µm. (C) Co-stain macrophages (CD68, green, top panel) and apoptosis (TUNEL, red, bottom panel) overlay with nuclei (DAPI, blue). Scale bar=100µm.

Supplemental Figure 2. Gating Process for Identification of M1 and M2 phenotypes in fresh tissue.

Cells are first gated according to size to isolate leukocyte and macrophage-sized events. Dead cells are eliminated using 7AAD. Leukocytes are evaluated as CD45+, and macrophages are identified as being CD11b+F4/80+. Finally, macrophages are tested for positivity for CD86 (M1, not shown) or CD206 (M2).

Supplemental Figure 1.

A.

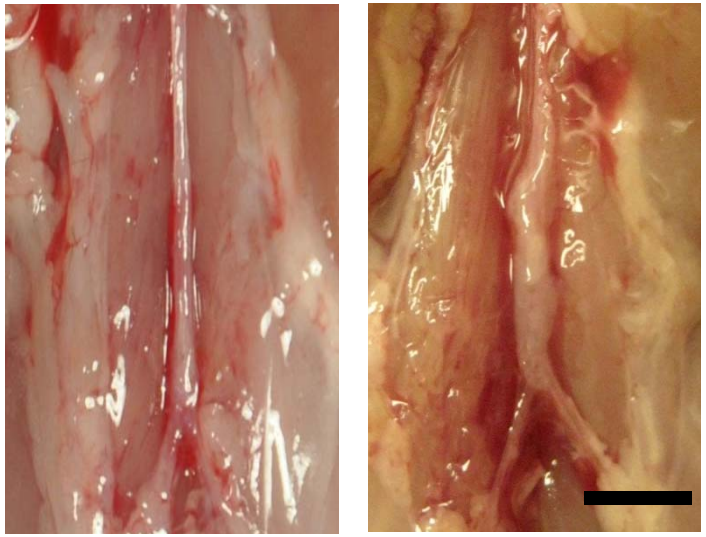

B.

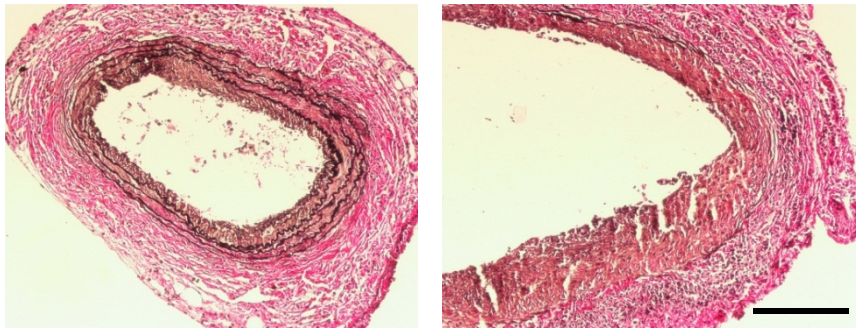

C.

CD68

TUNEL

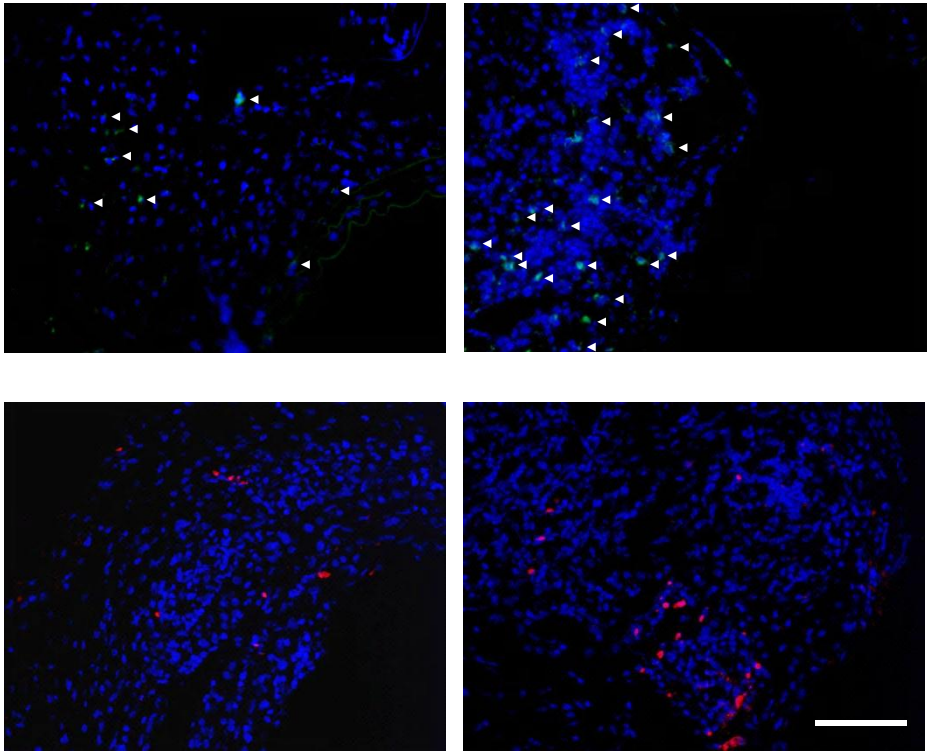

Supplemental Figure 2

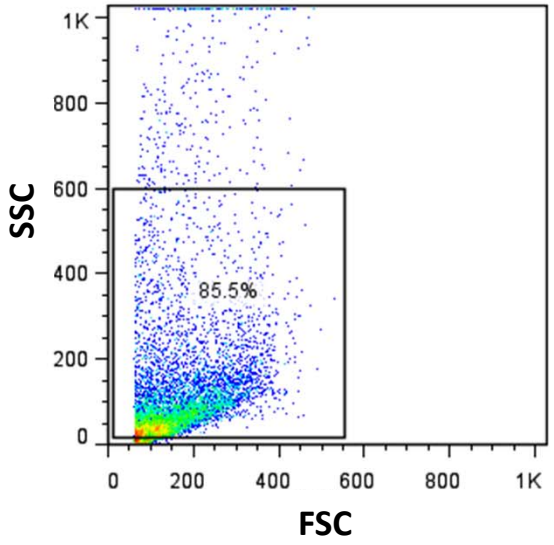

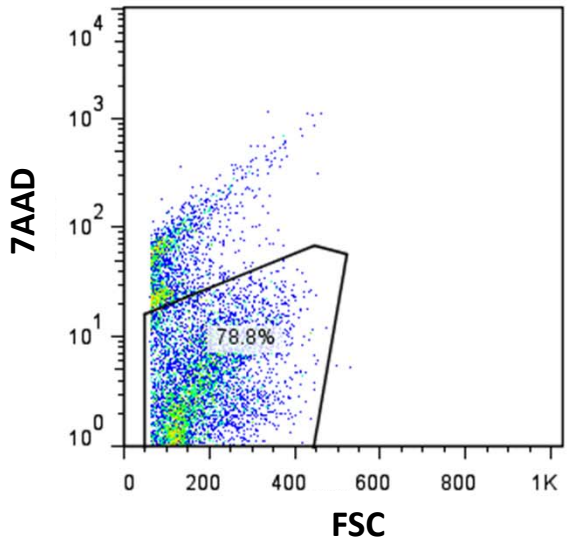

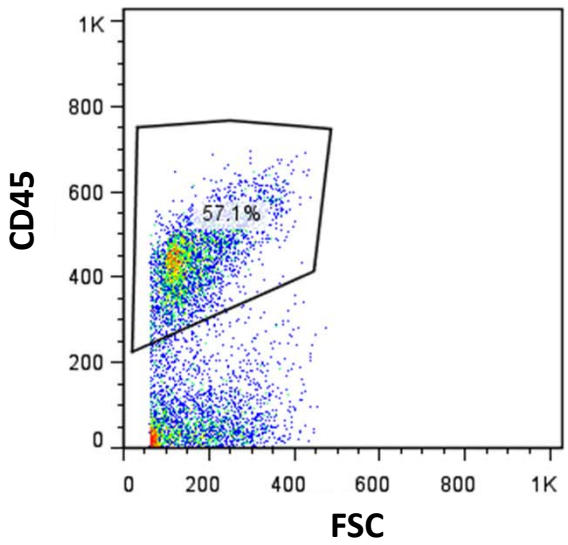

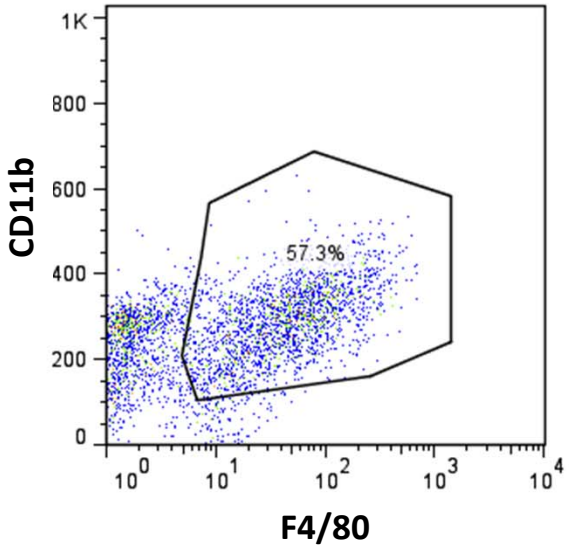

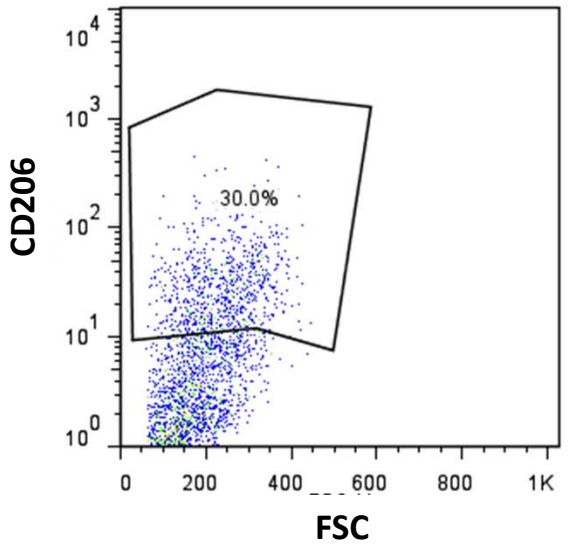

DISCUSSION

In the preceding work, I have provided evidence indicating that smooth muscle cell (SMC) apoptosis and inflammation are critical and intertwined events that drive aneurysm formation in several experimental models. Additionally, I have shown that the inflammatory environment that characterizes an experimental AAA model may be attributable to a shift in the inflammatory macrophage population. Further, I have shown that a drug capable of driving anti-inflammatory macrophage polarization can ameliorate aneurysm progression in an animal model. Taken together, my thesis provides a novel insight in regard to pathophysiology of a major human disease: SMC death, inflammation, and macrophage phenotypes interact to drive an inflammatory environment that potentiates aneurysm disease.

The relationship between caspase-mediated cell death and the subsequent inflammatory response in aneurysm is a novel idea. Apoptosis is generally a non-inflammatory or even anti-inflammatory event. The general a belief is that the apoptotic event in aneurysm is pathological because it reduces the number of smooth muscle cells which are a major cource of extracellular matrix proteins. However, recent studies of other disease processes suggest that the unsuccessful clearance of apoptotic cells from tissue can lead to a highly inflammatory state in the tissues[1-3]. In Chapters 1 and 2, we showed that the pan-caspase inhibitor Q-VD-OPh can prevent the formation of experimental aneurysm, likely through the reduction of apoptosis and inflammation. Conversely, beginning administration of the same caspase inhibitor 7 days after aneurysm induction showed no significant change in aneurysm progression. These results

suggest that caspase-mediated events are critical for inflammation and aneurysm formation, at least in mice. The altered effect of caspase inhibition in aneurysm progression may result from the promoted survival of inflammatory cells or a diminished importance of SMC death in later stages of the disease.

In Chapter 3, I described a modified aneurysm model capable of driving a more dramatic apoptotic response in vitro and in vivo. We showed this apoptosis phenotype to result in a similarly upregulated inflammatory response. Further, aneurysms induced by this new model were shown to expand to a larger size and at a faster pace than the model from which it was modified. Collectively, data presented in Chapter 3 further support our idea that a generalized manipulation of apoptosis causes a correlated inflammatory response in three aneurysm models.

Protein Kinase C-delta (PKCδ) is a signaling molecule that has been shown by our group and others to be an important apoptotic mediator. Using two different models of aneurysm in mice, I showed that PKCδ knockout (KO) mice are resistant to aneurysm formation and display a significantly lower level of smooth muscle cell apoptosis and vascular inflammation. Furthermore, I showed that the aortic expression of PKCδ is necessary for aneurysm formation, and that ectopic delivery of recombinant MCP-1 protein to the arterial wall is sufficient to restore aneurysm in PKCδ KO mice. This evidence, provided in Chapter 4, indicates that SMC apoptosis and the inflammatory response are crucial for aneurysm formation in mice, and that an inflammatory cascade driven by MCP-1 can override a lack of apoptosis in PKCδ KO mice.

Ultimately, my thesis provides evidence that aneurysm induction promotes a macrophage population skewed toward an inflammatory state, that is, a larger number of M1 inflammatory macrophages than control-treated tissues. Further, M2 anti-inflammatory macrophage numbers are significantly reduced in elastase-treated tissues as compared to control treated tissues 3 days after treatment. We believe this reduced M2 content could 'set the stage' for an inflammatory state in these tissues. Evidence from Chapter 5 also showed that driving M2 polarization using the PPARγ agonist Rosiglitazone could successfully prevent the expansion of elastase-induced aneurysm when administered 5 days after surgery. Collectively, data from Chapter 5 demonstrate that aneurysmal tissues contain a macrophage profile that may not be conducive to healing processes and instead drive a chronic inflammatory state, and that shifting this macrophage population toward healing phenotype may be an effective therapeutic strategy.

The work provided in my thesis provides evidence for a novel paradigm by which aneurysm may develop and progress. Specifically, we show that apoptotic events are inextricably linked to an inflammatory response, which ultimately generates a pathological state overrun with cell death and inflammatory cell products. Cumulatively, the pathological state feeds back upon itself to potentiate aneurysm formation and progression.

Conventionally, apoptosis has been considered a contributor to aneurysm simply by eliminating vascular smooth muscle cells from the arterial wall, a population of cells capable of producing extracellular matrix proteins. Here, we present a novel paradigm in which apoptosis and cell death plays a critical role in aneurysm by promoting production of inflammatory

cytokines. Importantly, it is likely that apoptosis itself is not the direct cause, but rather an unsuccessful clearance of the apoptotic population which can drive the highly inflammatory events of secondary necrosis. This stipulation suggests that the inflammatory response that follows these cell death events may be the critical factor in aneurysm development and progression. Indeed, evidence I provided shows that driving an inflammatory response by delivering recombinant MCP-1 locally to the aorta can also restore aneurysm formation in PKCδ KO mice. This evidence suggests that the inflammatory response is pivotal to aneurysm formation and needs to be taken into consideration in designing drug therapies for aneurysm.

In addition to serving as a therapeutic target, inflammation - particularly the type of inflammatory cells present in the aneurysm - may be useful in assessment of aneurysm progression. Specifically, my work provides the first evidence we are aware of that describes the macrophage phenotypes in aneurysm and ties the presence of M1 macrophages to aneurysm growth. Further, we were able to show for the first time that driving M2 macrophage polarization with the administration of Rosiglitazone (RZD) could prevent expansion of established aneurysm. Together, our evidence suggests that detecting and manipulating a more specific component of the inflammatory response could be used to monitor and treat aneurysm.

Interestingly, the existing literature concerning the role of PPARγ in murine aneurysm is controversial. Subramanian et al reported that SMC-specific deletion of PPARγ has no effect on aneurysm formation[4] while Hamblin et al showed an aneurysm promoting effect[5]. The fact that two different models of aneurysm induction were used may contribute to the discrepancy.

Using the PPARγ agonist RZD, several groups successfully showed a prevention of aneurysm formation and rupture in the AngII-induced model of murine aneurysm[6, 7]. Our data support the notion that chemical activation of PPARγ is beneficial. While the precise cell type(s) that may be benefit most from PPARγ activation remains to be elucidated, our data clear showed the therapeutic potential of PPARγ agonist in amelioration of exiting aneurysm. The RZD class of drugs has approved by FDA in treatment of diabetes, however, was found to be accompanied by significant cardiovascular risks. Thus, modification of the drug itself or the use of targeting mechanism(s) may be necessary for use in humans.

While several of our studies indicated a role for MCP-1 specifically in aneurysm, the role for various other inflammatory cytokines cannot be ignored. MCP-1 is a potent chemotactic factor capable of attracting various types and large numbers of inflammatory cells, but recruited inflammatory cells then likely produce a slew of inflammatory cytokines. Thus, while MCP-1 may be one chemokine capable of instigating a substantial inflammatory response, it is likely not the only chemokine capable of such an action. Further, MCP-1 is almost certainly not solely responsible for the inflammatory state found in aneurysmal tissues. In order to appropriately target this inflammation, a more thorough understanding of the components of this inflammation must be achieved.

Insights provided in this work have led us to several exciting new directions. We aim to explore another potential method of manipulating macrophage phenotypes, namely, microRNAs (miRNAs). miRNAs have been shown to have various roles in multiples diseases, including vascular disease such as atherosclerosis and aneurysm[8-10]. Targeting of these dynamic

molecules could provide a more feasible approach for interfering with inflammation and/or macrophage phenotypes in aneurysm and will certainly provide an interesting future direction for our study.

One of the main predictors for aneurysm development is age, with about 8% of men over the age of 65 displaying aneurysm development, and the prevalence amongst women growing rapidly[11-13]. In order to address this factor, we plan to explore the role of the changing extracellular matrix in aneurysm development. As people age, arteries have been shown to become more stiff, reflecting a change in the extracellular matrix composition and/or protein crosslinking. Further, particular extracellular matrix proteins or environments have been shown to be involved in mediating macrophage phenotype polarization[14, 15]. Using this information, we aim to explore the role of aging-related arterial stiffness in aneurysm models and the subsequent regulation of macrophage polarization. Ultimately, evidence from these proposed studies may provide a way of altering macrophage phenotypes and the inflammatory state of aneurysm to counteract the pathogenic activities taking place within the aging arterial wall.

1. Bennett M, Yu H, Clarke M. Signalling from dead cells drives inflammation and vessel remodelling. *Vascular Pharmacology*. 2012;56:187-192
2. Clarke MC, Littlewood TD, Figg N, Maguire JJ, Davenport AP, Goddard M, Bennett MR. Chronic apoptosis of vascular smooth muscle cells accelerates atherosclerosis and promotes calcification and medial degeneration. *Circ Res*. 2008;102:1529-1538
3. Zheng Y, Gardner SE, Clarke MCH. Cell death, damage-associated molecular patterns, and sterile inflammation in cardiovascular disease. *Arteriosclerosis, Thrombosis, and Vascular Biology*. 2011;31:2781-2786
4. Subramanian V, Golledge J, Ijaz T, Bruemmer D, Daugherty A. Pioglitazone-induced reductions in atherosclerosis occur via smooth muscle cell–specific interaction with pparγ. *Circulation Research*. 2010;107:953-958
5. Hamblin M, Chang L, Zhang H, Yang K, Zhang J, Chen YE. Vascular smooth muscle cell peroxisome proliferator-activated receptor-γ deletion promotes abdominal aortic aneurysms. *Journal of Vascular Surgery*. 2010;52:984-993
6. Pirianov G, Torsney E, Howe F, Cockerill GW. Rosiglitazone negatively regulates c-jun n-terminal kinase and toll-like receptor 4 proinflammatory signalling during initiation of experimental aortic aneurysms. *Atherosclerosis*. 2012;225:69-75
7. Jones A DR, Torsney E, Howe F, Dunkley M, Gnaneswaran Y, Gaze D, Nasr H, Loftus IM, Thompson MM, Cockerill GW. Rosiglitazone reduces the development and rupture of experimental aortic aneurysms. *Circulation*. 2009;119:3125-3132
8. Wei Y, Schober A, Weber C. Pathogenic arterial remodeling: The good and bad of microrna. *American Journal of Physiology - Heart and Circulatory Physiology*. 2013;304:H1050-H1059
9. Mayr M, Zampetaki A, Willeit P, Willeit J, Kiechl S. Microrna within the continuum of postgenomics biomarker discovery. *Arteriosclerosis, Thrombosis, and Vascular Biology*. 2013;33:206-214
10. Pahl MC DK, Gabel G, Hinterseher I, Elmore JR, Schworer CM, Peeler TC, Franklin DP, Gray JL, Carey DJ, Tromp G, Kuivaniemi H. Microrna expression signature in human abdominal aortic aneurysms. *BMC Medical Genomics*. 2012;5
11. Moxon JV, Parr A, Emeto TI, Walker P, Norman PE, Golledge J. Diagnosis and monitoring of abdominal aortic aneurysm: Current status and future prospects. *Current Problems in Cardiology*. 2010;35:512-548
12. Norman PE, Powell JT. Abdominal aortic aneurysm: The prognosis in women is worse than in men. *Circulation*. 2007;115:2865-2869
13. Study CASGVASSWAAAAPMAS. A comparative study of the prevalence of abdominal aortic aneurysms in the united kingdom, denmark, and australia. *Journal of Medical Screening*. 2001;8:46-50
14. Kajahn J FS, Rueckert E, Forstreuter I, Hintze V, Moeller S, Simon JC. Artificial extracellular matrices composed of collagen i and high sulfated hyaluronan modulate monocyte to macrophage differentation under conditions of sterile inflammation. *Biomatter*. 2012;2:226-273
15. Weidenbusch M AH. Tissue microenvironments define and get reinforced by macrophage phenotypes in homeostasis or during inflammation, repair, and fibrosis. *Journal of Innate Immunity*. 2012;4:463-477

CHAPTER CONTRIBUTION SUMMARIES

Chapter 1 Contribution Summary

Dr. Dai Yamanouchi produces Figures 1-3. I produced the data and statistical analysis for Figure 4A-F, but did not contribute to Figure 4G. I provided the data and statistical analysis for Supplemental Figure 2B and Supplemental Figure 6.

Chapter 2 Contribution Summary

I provided all data and statistical analysis for Figure 1. Dr. Timothy Hacker obtained ultrasound images for Figure 2 and Dr. Guoqing Song performed the surgeries for Figure 2, though I compiled measurement data for Figure 2. I provided Figure 3A-D, and Drew Roennenberg performed the immunohistochemical stain in Figure 3E as well as Figure 4B, D, and F. For each of these stains, I provided images and quantification (Figure 3D, 4A, C, E). I provided all data and analysis of Supplemental Figures.

Chapter 3 Contribution Summary

I provided data and analysis for Figure 1. Dai Yamanouchi provided Figure 2A and C, while I provided Figures 2B and D. I provided Figures 3-5. Dai Yamanouchi is also credited with production of the CaPO4 model itself. I provided all Supplemental Figures.

Chapter 4 Contribution Summary

The original surgical evidence suggesting that Protein Kinase C-delta knockout mice were resistant to aneurysm formation was provided by Dai Yamanouchi. I provided Figure 1 A,

B, D, and E. I stained the tissue used for confocal imaging in Figure 1C, but Qiwei Wang provided the images. Dai Yamanouchi provided Figure 2A and B, and I provided Figure 2C-E. Conventional IHC in Figure 3 was performed by Drew Roennenberg, and I provided all imaging and quantitation in the rest of the figure. I also performed the RNA harvest and RT-PCR analysis depicted in Figure 3D. Figure 4A, B, and D was provided by myself, and Dai Yamanouchi provided Figure 4C. I provided the entirety of Figure 5 and 6. I produced Supplemental Table 1. Dai Yamanouchi provided Supplemental Figures I, and II. All additional Supplemental Figures were provided by me, with aid from Melissa Keller for Supplemental Figure 8 and 9B.

Chapter 5 Contribution Summary

I provided Figure 1A, B, and C, and Qiwei Wang contributed the images for Figure 1B. I provided Figure 2A and B, and Qiwei Wang performed RT-PCR for Figure 2C. I provided Figure 3A, B, C, while Qiwei Wang again produced RT-PCR data for Figure 3D. I provided all additional Figures, including Supplemental Figures. Calvin Harberg and Qiwei Wang assisted in culturing BMDM and in the administration of RZD in this chapter.

Arteriosclerosis, Thrombosis, and Vascular Biology

JOURNAL OF THE AMERICAN HEART ASSOCIATION

Elevated Protein Kinase C-δ Contributes to Aneurysm Pathogenesis Through Stimulation of Apoptosis and Inflammatory Signaling

Stephanie Morgan, Dai Yamanouchi, Calvin Harberg, Qiwei Wang, Melissa Keller, Yi Si, William Burlingham, Stephen Seedial, Justin Lengfeld and Bo Liu

Arterioscler Thromb Vasc Biol. 2012;32:2493-2502; originally published online August 9, 2012;
doi: 10.1161/ATVBAHA.112.255661
Arteriosclerosis, Thrombosis, and Vascular Biology is published by the American Heart Association, 7272 Greenville Avenue, Dallas, TX 75231

Print ISSN: 1079-5642. Online ISSN: 1524-4636

Elevated Protein Kinase C-δ Contributes to Aneurysm Pathogenesis Through Stimulation of Apoptosis and Inflammatory Signaling

Stephanie Morgan, Dai Yamanouchi, Calvin Harberg, Qiwei Wang, Melissa Keller, Yi Si, William Burlingham, Stephen Seedial, Justin Lengfeld, Bo Liu

Objective—Apoptosis of smooth muscle cells (SMCs) is a prominent pathological characteristic of abdominal aortic aneurysm (AAA). We have previously shown that SMC apoptosis stimulates proinflammatory signaling in a mouse model of AAA. Here, we test whether protein kinase C-δ (PKCδ), an apoptotic mediator, participates in the pathogenesis of AAA by regulating apoptosis and proinflammatory signals.

Methods and Results—Mouse experimental AAA is induced by perivascular administration of $CaCl_2$. Mice deficient in PKCδ exhibit a profound reduction in aneurysmal expansion, SMC apoptosis, and transmural inflammation as compared with wild-type littermates. Delivery of PKCδ to the aortic wall of PKCδ$^{-/-}$ mice restores aneurysm, whereas overexpression of a dominant negative PKCδ mutant in the aorta of wild-type mice attenuates aneurysm. In vitro, PKCδ$^{-/-}$ aortic SMCs exhibit significantly impaired monocyte chemoattractant protein-1 production. Ectopic administration of recombinant monocyte chemoattractant protein-1 to the arterial wall of PKCδ$^{-/-}$ mice restores inflammatory response and aneurysm development.

Conclusion—PKCδ is an important signaling mediator for SMC apoptosis and inflammation in a mouse model of AAA. By stimulating monocyte chemoattractant protein-1 expression in aortic SMCs, upregulated PKCδ exacerbates the inflammatory process, in turn perpetuating elastin degradation and aneurysmal dilatation. Inhibition of PKCδ may serve as a potential therapeutic strategy for AAA. **(*Arterioscler Thromb Vasc Biol*. 2012;32:2493-2502.)**

Key Words: aneurysms ■ apoptosis ■ vascular biology ■ inflammation ■ protein kinase C-δ

Abdominal aortic aneurysm (AAA), a progressive aortic dilation, is a common vascular disease associated with high mortality. Aneurysm results from the culmination of a series of events that lead to disruption of structural integrity and segmental weakening of the abdominal aortic wall. An incomplete understanding of the biological mechanisms underlying the disease has limited the development of therapeutic treatment and diagnostic strategies, thus leaving surgical and endovascular procedures as the only treatment options for patients with AAA.

Histologically, aneurysmal tissues are characterized by disruption of the elastic fibers in the aortic wall and extensive transmural infiltration of macrophages and lymphocytes.[1–3] These features have been consistently duplicated in animal models of AAA.[4] The prevailing view is that inflammatory cells, mainly macrophages, are the major source of matrix-degrading enzymes, such as matrix metalloproteinases[5–9] and proinflammatory cytokines.[10–12] Anti-inflammatory strategies, such as those that deplete neutrophils, lymphocytes, mast cells, or proinflammatory cytokines, have been shown to prevent the upregulation of matrix metalloproteinases and attenuate aneurysm formation in mouse models of AAA.[13–16]

Although the depletion of vascular smooth muscle cells (SMCs) is well documented in human aneurysmal tissues,[17] potential interactions between SMCs and infiltrating inflammatory cells remain unclear. We have recently demonstrated that blocking apoptosis with a pan caspase inhibitor protected mice from angiotensin II–induced aneurysm expansion.[18] The caspase inhibitor not only prevented SMC depletion but also diminished infiltration of macrophages and lymphocytes, suggesting a potential link between the apoptotic process and inflammatory signaling in the pathogenesis of aneurysm.

Protein kinase C-δ (PKCδ), a member of the PKC family of serine and threonine kinases, is a crucial mediator of SMC apoptosis.[19–21] Studies of PKCδ knockout (KO) mice reveal that mice lacking PKCδ develop normally but exhibit an apoptosis-resistant phenotype when subjected to models of vascular injury, such as vein graft or carotid artery ligation.[22,23] Conversely, gene transfer of PKCδ via an adenoviral vector led to excessive apoptosis of vascular SMCs in a rat carotid balloon injury model.[23] More recently, we showed that PKCδ may

Received on: February 4, 2012; final version accepted on: July 30, 2012.

From the Division of Vascular Surgery (S.S., D.Y., C.H., Q.W., Y.S., S.S., J.L., B.L.), and Division of Transplant Surgery (M.K., W.B.), Department of Surgery, School of Medicine and Public Health, University of Wisconsin–Madison, Madison, WI.

The online-only Data Supplement is available with this article at http://atvb.ahajournals.org/lookup/suppl/doi:10.1161/ATVBAHA.112.255661/-/DC1.

Correspondence to Bo Liu, 1111 Highland Avenue, WIMR 5120, Madison, WI 53705. E-mail liub@surgery.wisc.edu

Arterioscler Thromb Vasc Biol **is available at http://atvb.ahajournals.org** **DOI: 10.1161/ATVBAHA.112.255661**

also be involved in the regulation of chemokine expression. Inhibition of PKCδ with rottlerin profoundly decreases the production of monocyte chemoattractant protein-1 (MCP-1) by aortic vascular SMCs and, subsequently, inhibits chemotaxis of inflammatory cells toward SMC-conditioned media.[21]

We have previously shown that the expression of PKCδ is significantly higher in human aneurysmal aortic tissues as compared with normal arteries.[21] The collection of these tissues at the time of surgical repair precluded analysis of a potential causal relationship between PKCδ and aneurysm, specifically, whether PKCδ upregulation contributes to the pathophysiology of aneurysm or is merely a resultant phenomenon. To determine whether PKCδ is an integral mediator of SMC apoptosis and vascular inflammation during aneurysm pathogenesis, the current study tests the effects of PKCδ gene deficiency on aneurysm formation using the $CaCl_2$ mouse model. In addition, we explored the potential molecular mechanisms by which PKCδ regulates the proinflammatory signals produced by apoptotic SMCs.

Materials and Methods

A detailed description of the Materials and Methods are shown in online-only Data Supplement.

Mouse Models of AAA

The generation of PKCδ target deletion in mice was described elsewhere.[24] PKCδ KO mice and their wild-type (WT) littermates were generated by mating heterozygous pairs. C57BL/6 mice and apolipoprotein E–deficient mice were purchased from Harlan Laboratories (Madison, WI) and Jackson Laboratory (Bar Harbor, ME), respectively. Green fluorescent protein transgenic mice were gifted by Dr William Burlingham of the University of Wisconsin–Madison.

Male mice, aged 12 weeks, underwent a $CaCl_2$–induced AAA model as described previously.[25–28] Briefly, the infrarenal region of the aorta was isolated and treated with 0.5 mol/L $CaCl_2$ perivascularly via gauze for 20 minutes. Control mice were similarly treated with 0.5 mol/L of NaCl. Tissues were fixed in 4% formaldehyde in PBS, embedded and cut to 6- or 8-μm sections for optimal cutting temperature and paraffin-imbedded arteries, respectively.

Immunohistochemistry

Antibodies were purchased from Abcam (Cambridge, MA; interferon-γ, interleukin [IL]-6, monocyte+macrophage antibody, myosin heavy chain, and CD45), Santa Cruz (Santa Cruz, CA; CD3, MCP-1, Mac3, PKCδ, Ly6G, and CD68), Sigma-Aldrich (smooth muscle actin), and Cell Signaling (Danvers, MA; Cleaved caspase-3). Terminal deoxynucleotidyl transferase dUTP nick end labeling (TUNEL) staining kit was purchased from Roche (Madison, WI). Van Geison stains were carried out using Chromaview Van Gieson kit (Richard Allan Scientific, Kalamazoo, MI).

Cell Culture

The murine macrophage cell line RAW264.7 cells were obtained from American Type Culture Collection (ATCC, Manassas, VA). Primary mouse aortic SMCs from the aorta of both PKCδ KO and WT mice were isolated based on a protocol described by Clowes et al**.** [29]

Migration Assay

In vitro migration assay was carried out, as previously described.[16] Briefly, RAW264.7 macrophages, or $CD11b^+$ cells isolated from bone marrow, were placed in a 5-μm pore Transwell insert. Conditioned and treated media were used as chemoattractants. After 6 hours of incubation, inserts were removed and stained with hematolxylin to facilitate nuclei visualization. The mean value of migrated cells was counted in 8 high-power fields per membrane.

Bone Marrow Isolation and Sorting

Bone marrow was isolated from long bones, washed with PBS, and counted. Monocytes were collected from bone marrow by magnetic sorting using CD11b microbeads (Miltenyi Biotec, Boston, MA). Purity of the resulting $CD11b^+$ cells was assessed by flow cytometry using antibodies to CD3, CD11b, and CD45/B220 (Miltenyi Biotec).

Statistical Analysis

Values were expressed as mean±SE. Experiments were repeated at least 3 times unless stated otherwise. Differences between the 2 groups were analyzed by Student *t* test. For time course comparison, 1-way ANOVA analysis was followed by Bonferroni correction to adjust for multiple comparisons. Values of $P<0.05$ were considered significant.

Results

PKCδ Expression in Experimental Aneurysms

We subjected C57BL/6 male mice to perivascular treatment of 0.5 mol/L $CaCl_2$ (or equal concentration of NaCl) to the infrarenal region of the aorta and euthanized the animals at selected time points. Administration of $CaCl_2$ led to gradual aortic dilatation associated with elastin fragmentation (Figure I in the online-only Data Supplement). Immunohistochemical analysis showed a profound upregulation of PKCδ protein in the aortic media 3 and 7 days after the $CaCl_2$ treatment (Figure 1A), a time frame at which aortic expansion was barely visible. The temporal and spatial pattern of PKCδ expression mirrored that of the TUNEL positivity (Figure 1B). Confocal images confirmed the colocalization between PKCδ upregulation and apoptosis (TUNEL). Furthermore, PKCδ-positive cells were primarily SMCs, as identified by myosin heavy chain (Figure 1C). A similar expression pattern of PKCδ and its association with apoptosis was also observed in angiotensin II–induced aneurysm in apolipoprotein E–deficient mice. (Figure II in the online-only Data Supplement). Western blot analysis confirmed the elevated level of PKCδ protein in $CaCl_2$-treated aortas as compared with the NaCl-treated controls (Figure 1D and 1E). Additionally, levels of the apoptosis-associated catalytic fragment of PKCδ became readily detectable in $CaCl_2$-treated group (Figure 1D).

Mice Lacking PKCδ Are Resistant to AAA Induction

To prove a potential role of PKCδ in AAA formation, we subjected PKCδ KO mice and their WT littermates to aneurysm induction by $CaCl_2$. Forty-two days after the $CaCl_2$ treatment, abdominal aorta of WT mice were visibly inflamed and dilated whereas the arteries of KO mice appeared minimally affected (Figure 2A). The maximal external diameter of the abdominal aorta was measured immediately before the $CaCl_2$ application and at the time of tissue harvest. As seen in Figure 2B, the baseline aortic diameters are comparable in PKCδ WT and KO mice. Six weeks after the $CaCl_2$ treatment, arteries of WT mice expanded to 1.04±0.08 mm (96.6±31%), whereas arteries of KO mice expanded only to 0.74±0.06 mm (39.7±9%) (Figure 2B). Similarly, PKCδ was shown to play a role in the elastase perfusion model of murine AAA. Inactive

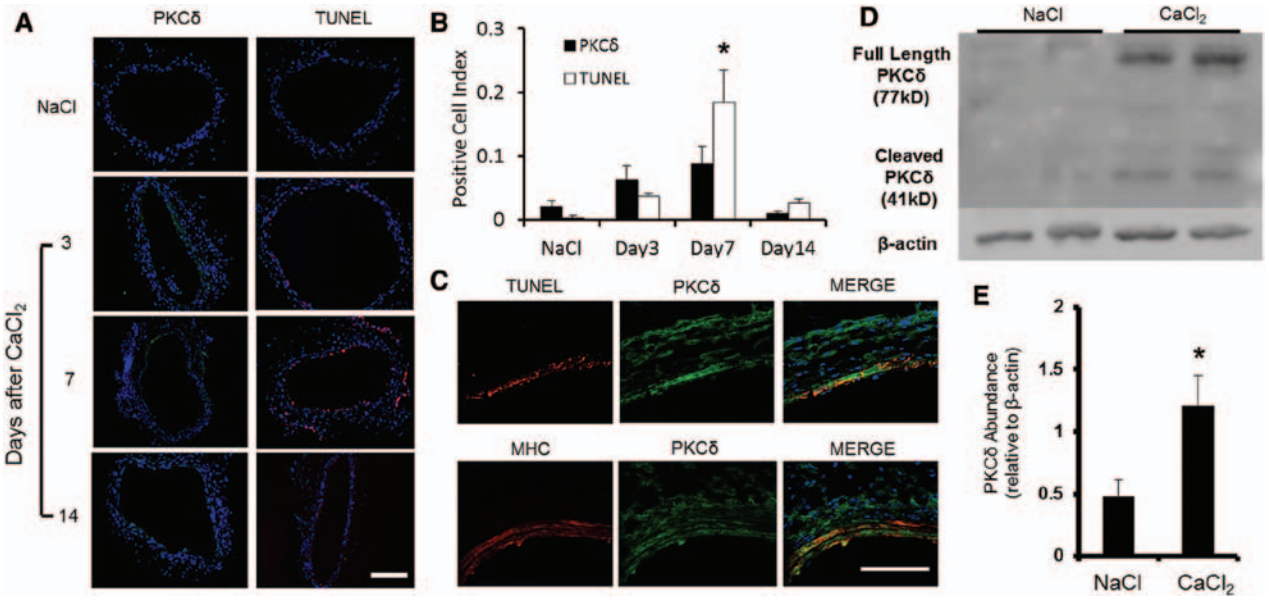

Figure 1. Protein kinase C-δ (PKCδ) expression correlates with apoptosis in an experimental aneurysm model. Aortas of C57B/6 mice were treated with $CaCl_2$ or NaCl and harvested 3, 7, and 14 days ($CaCl_2$ group) or 7 days (NaCl group) after surgery. **A**, Cross sections stained for PKCδ (green) or apoptosis (terminal deoxynucleotidyl transferase dUTP nick end labeling [TUNEL], red), and nuclei (DAPI, blue). Scale bar, 200 μm; magnification, 10×. **B**, Positive cell ratio calculated as number of apoptotic (TUNEL+) or PKCδ-positive cells divided by respective number of DAPI-positive cells. *P<0.05 compared with NaCl control; n=6. **C**, Representative confocal images for colocalization analysis in cross sections harvested 7 days after $CaCl_2$ treatment. Top panel: Costain TUNEL (red) and PKCδ (green). Bottom panel: Costain for smooth muscle cells (myosin heavy chain [MHC], red) and PKCδ (green). Scale bar, 50 μm; magnification, 40× Overlay with DAPI (blue). **D**, Representative Western blot analysis of PKCδ expression in tissues harvested from 2 different aortas of C57B/6 mice 7 days after NaCl or $CaCl_2$ treatment. **E**, Quantification of PKCδ expression from Western blot, normalized to β-actin. PKCδ expression shown as a total of both cleaved and full-length portions. *P<0.05; n=4.

elastase produced minimal dilation of the artery in both WT and KO animals (0.77±0.06 mm and 0.76±0.02 mm, respectively; n=2), whereas active elastase treatment produced a more severe dilation in WT animals (1.47±0.16 mm) compared with KO (0.97±0.29 mm) (Figure III in the online-only Data Supplement).

Histological analysis performed at 7 days after $CaCl_2$ treatment revealed similar elastin degradation in KO and WT arteries (Figure IV in the online-only Data Supplement). However, the same histological analysis 42 days after the $CaCl_2$ treatment showed elastin fibers in arteries harvested from KO mice appeared continuous and organized, similar to NaCl-treated controls, whereas elastin fibers in $CaCl_2$–treated WT arteries appeared fragmented and disoriented (Figure 2C and 2D). Furthermore, PKCδ KO tissue harvested at 7 days displayed significantly reduced SMC apoptosis, as evidenced by confocal staining showing colocalization of myosin heavy chain and apoptosis (TUNEL), as compared with WT samples (Figure 2E). Accordingly, cleaved Caspase-3 was nearly undetectable in PKCδ KO arteries, whereas it was abundant

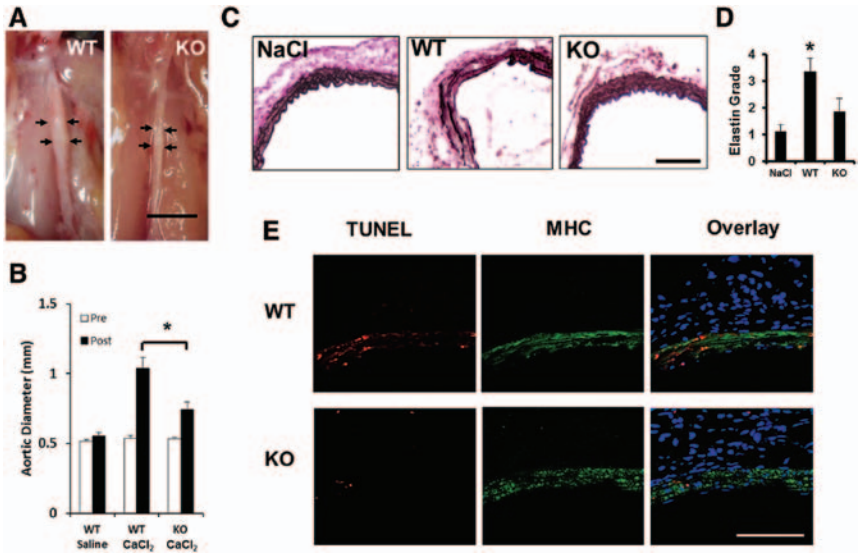

Figure 2. Protein kinase C-δ (PKCδ) knockout (KO) mice are resistant to aneurysm induction. **A**, Representative photos of abdominal aortas of PKCδ wild-type (WT) and knockout (KO) mice, taken 42 days after the $CaCl_2$ treatment. Scale bar, 5 mm. **B**, Aortic diameter measured before (white bars) and 42 days after (black bars) $CaCl_2$ treatment. *P<0.05 compared with the $CaCl_2$–treated KO arteries; n=6. **C**, Representative photos of 42-day aortic sections stained for elastin (Van Gieson); scale bar, 100 μm; magnification, 40×. **D**, Grading of elastin degradation in Van Gieson–stained arteries harvested 42 days after surgery. *P<0.05 WT compared with KO; n=4. **E**, Representative confocal images of arterial sections coimmunostained for terminal deoxynucleotidyl transferase dUTP nick end labeling (TUNEL; red) and myosin heavy chain (MHC; green) overlaid with DAPI (blue); arteries harvested 7 days after surgery; scale bar, 50 μm; magnification 40×.

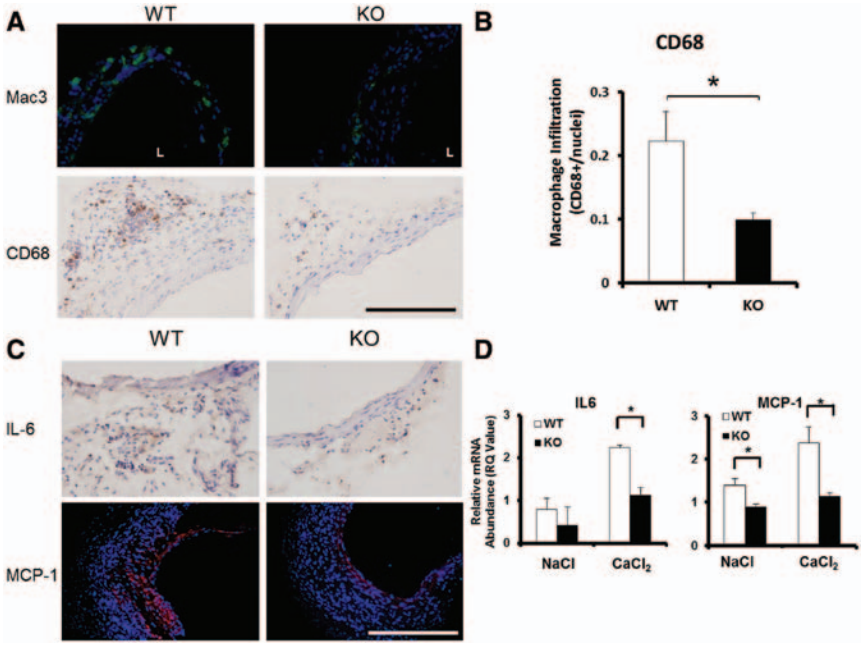

Figure 3. Protein kinase C-δ (PKCδ) gene deficiency attenuates the inflammatory response in experimental aneurysm. **A**, Macrophage infiltration as measured by immunofluorescent stain (IFC) for Mac3 (green), overlaid with DAPI (blue), or by immunohistochemical stain (IHC) for CD68; scale bar, 200 μm; magnification 40×. **B**, Quantification of macrophage infiltration in aneurysm tissue as identified by CD68 stain, expressed as CD68-positive cells/nuclei. *P<0.05 compared with $CaCl_2$-treated knockout (KO) arteries; n=4. **C**, IHC for inflammatory cytokine interleukin 6 (IL-6) and IFC for monocyte chemoattractant protein-1 (MCP-1). Scale bar, 200 μm; magnification 40×. **D**, Real-time polymerase chain reaction analysis of IL-6 and MCP-1 mRNA abundance in aorta of wild-type (WT) and KO animals 7 days after surgery. *P<0.05 compared with KO arteries; n=4.

in the WT arteries (Figure VA and VB in the online-only Data Supplement). Furthermore, the percentage of nuclei staining positive for TUNEL was decreased from 24.1±3.4 in WT arteries to 12.5±2.9 in KO arteries (data not shown). In vitro analysis of cultured SMCs confirmed the apoptosis-resistant phenotype. The lack of PKCδ diminished the ability of SMCs to undergo apoptosis in response to tumor necrosis factor-δ, which was rescued by restoration of PKCδ expression with an adenoviral vector (Figure VC and VD in the online-only Data Supplement).

PKCδ Is Critical for the Inflammatory Response

Next, we analyzed macrophage infiltration, another important characteristic of aneurysm, in the aortas of both WT and KO animals. Immunohistochemical analysis revealed a profound reduction in the number of macrophages (Mac-3$^+$, CD68$^+$) detected in the aorta of PKCδ KO mice as compared with their WT littermates (Figure 3A and 3B). Additionally, neutrophils (Ly6G$^+$), leukocytes (CD45$^+$), and T cells (CD3$^+$) were shown to be present in the aortic samples of the PKCδ WT mice, mostly prevalent in the adventitia, and almost entirely absent in KO aortas (Figure VI in the online-only Data Supplement). Similarly, levels of AAA-associated inflammatory cytokines IL-6 and MCP-1 were markedly decreased by PKCδ gene deficiency (Figure 3C). To better quantify the altered cytokine expression, we analyzed aortic tissues using real-time polymerase chain reaction analysis. As shown in Figure 3D, PKCδ gene deficiency caused a 50.7% and 48.1% reduction in mRNA levels of IL-6 and MCP-1 in tumor necrosis factor-δ–treated SMCs, respectively. Additionally, aneurysm-associated induction of IL-1δ and IFN-δ was also significantly blunted in PKCδ KO mice (Figure VII in the online-only Data Supplement). There was also a small but statistically insignificant trend of reduction in the tumor necrosis factor-δ mRNA abundance.

PKCδ-Deficient Aortic SMCs Are Impaired in MCP-1 Expression

The diminished inflammatory infiltrate in PKCδ KO mice could be caused by a lack of PKCδ-mediated chemokine production in the aortic wall or diminished migratory property of monocytes. A complete blood count performed on WT and KO animals showed no significant difference in white blood cell or red blood cell populations between the 2 genotypes (Table I in the online-only Data Supplement). Furthermore, the percentage of monocytes (CD11b$^+$) in the bone marrow was comparable between the genotypes (Figure VIIIA and VIIIB in the online-only Data Supplement). In a chemotaxis assay, CD11b$^+$ monocytes isolated from KO and WT animals migrated with equal efficiency toward recombinant MCP-1 protein (Figure VIIIC in the online-only Data Supplement). Together, these data suggest that neither number nor migratory capability of bone marrow monocytes are affected by PKCδ gene deficiency.

Real-time polymerase chain reaction analysis of aortic SMCs showed KO cells to have a nearly absolute impairment of MCP-1 production. Expression of interferon-γ and IL-6 also appeared to be modulated by PKCδ, albeit to a lesser degree (Figure 4A). The dependence of MCP-1 expression on PKCδ was further demonstrated by ELISA measurement of MCP-1 production by cultured SMCs. After treatment with tumor necrosis factor-α, WT SMCs are shown to produce significantly more MCP-1 as compared with KO SMCs (Figure 4B). Furthermore, overexpression of PKCδ using adenoviral-mediated gene delivery (AdPKCδ) further enhanced the production of MCP-1 in WT SMCs (Figure 4C).

To further test the notion that PKCδ gene deficiency reduces the presence of proinflammatory aneurysm signals produced by the aortic wall, we examined the ability of aortic SMCs to attract RAW264.7 monocyte/macrophages. As shown in Figure 4D, the number of RAW264.7 cells that migrated toward media conditioned by KO SMCs was ≈50% less than

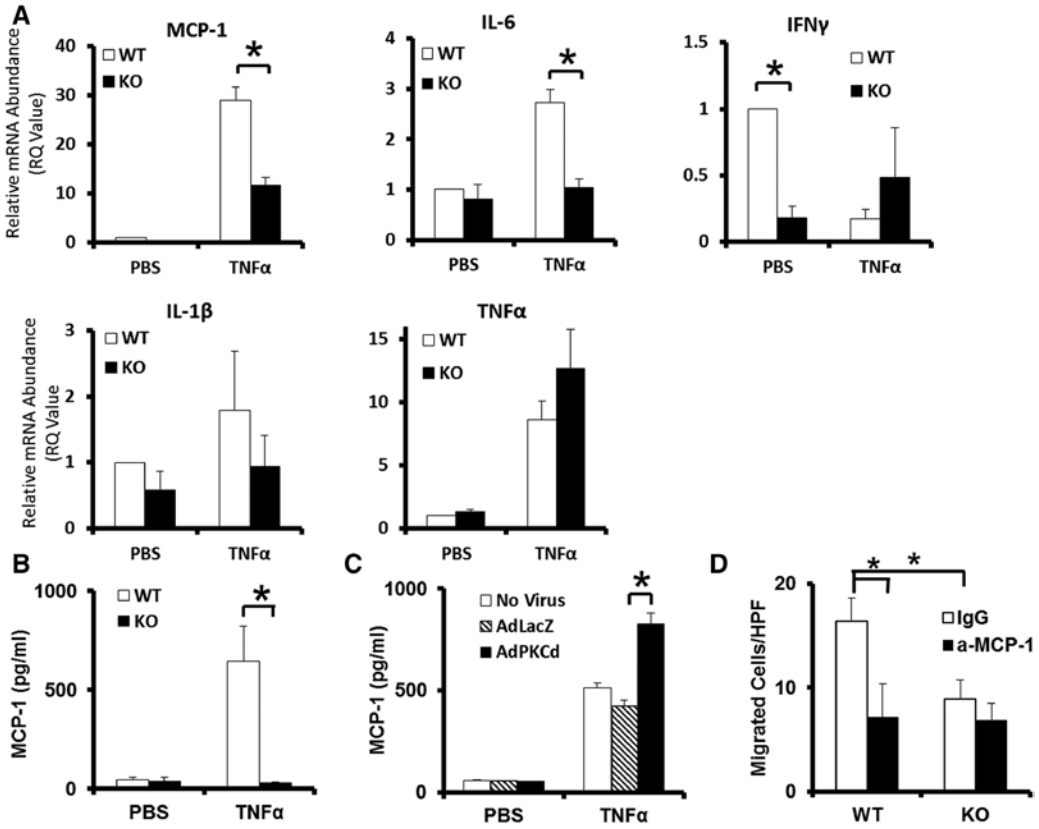

Figure 4. Protein kinase C-δ (PKCδ) mediates production of monocyte chemoattractant protein-1 (MCP-1) by vascular smooth muscle cells (SMCs). Cultured aortic SMCs isolated from PKCδ knockout (KO) or wild-type (WT) mice were treated with tumor necrosis factor-α (TNF-α; 50 ng/mL, for 6 hours; **A–C**). **A**, Real-time polymerase chain reaction analysis of selected cytokines measured by relative quantitation (RQ) value. **B**, Levels of secreted MCP-1 protein, measured by ELISA. **C**, Levels of MCP-1 protein secreted by WT cells infected with adenovirus expressing beta-galactosidase (AdLacZ) or adenoviruses encoding PKCδ (AdPKCδ), followed by treatment with TNFα. **D**, Migration of RAW264.7 macrophages in response to conditioned media harvested from TNFα treated WT or KO SMCs in the presence of an anti–MCP-1 antibody (a-MCP-1) or hamster IgG (IgG) as control. HPF indicates high power field. *P<0.05; n=3. IL indicates interleukin.

that toward media conditioned by WT SMCs. Furthermore, administration of an MCP-1–neutralizing antibody completely eliminated the ability of WT SMCs to stimulate migration, suggesting MCP-1 to be a critical proinflammatory signal released by aortic SMCs (Figure 4D).

Exogenous PKCδ Reverses the Aneurysm-Resistant Phenotype of KO Mice

Data derived from the above in vitro analyses suggest that PKCδ gene deletion attenuates aneurysm development primarily through preventing aortic SMCs from undergoing apoptosis and producing proinflammatory chemokines, specifically MCP-1. To test this hypothesis, we developed an aortic tissue–specific gene transfer method to restore PKCδ expression in the arterial wall of KO mice. As described in the Materials and Methods section, adenovirus was administered to the aortic wall immediately after the removal of $CaCl_2$. This gene transfer method produced a localized transgene expression as illustrated by using an adenovirus encoding enhanced green fluorescent protein (AdGFP). While producing abundant green fluorescent protein expression in the infrarenal region of the aortic wall, aortic administration of adenovirus encoding green fluorescent protein did not produce transgene expression in circulating white blood cells (Figure IXA and IXB in the online-only Data Supplement).

To restore PKCδ expression in the aortas of PKCδ KO mice, adenovirus expressing either PKCδ or β-galactosidase (AdPKCδ or AdLacZ, respectively) was administered to the infrarenal aorta of PKCδ KO mice. Mice were euthanized after 7 or 42 days for histological and morphological analyses, respectively. Delivery of AdPKCδ successfully induced localized aortic expression of PKCδ in KO mice, mostly in the perivascular region and to a lesser degree in the smooth muscle actin positive media (Figure IXC and IXD in the online-only Data Supplement). Forty-two days after the $CaCl_2$ treatment, AdLacZ-treated PKCδ KO mice displayed minimum aortic expansion, with a final diameter measurement of 0.67±0.07 mm (29.2±15.9%), indicating that viral infection alone did not alter the aneurysm-resistant phenotype of KO mice. In comparison, delivery of AdPKCδ produced significant aortic expansion in KO mice (final diameter 1.11±0.21 mm; 114.8±28.3%), an induction comparable with that seen in WT mice (Figure 5A and 5B). The apparent restoration of aneurysm formation shown to accompany aortic gene transfer of PKCδ is further evidenced by fragmented elastin fibers, as well as TUNEL-positive apoptotic cells and infiltrating monocytes/macrophages, at 7 days after surgery (Figure 5C).

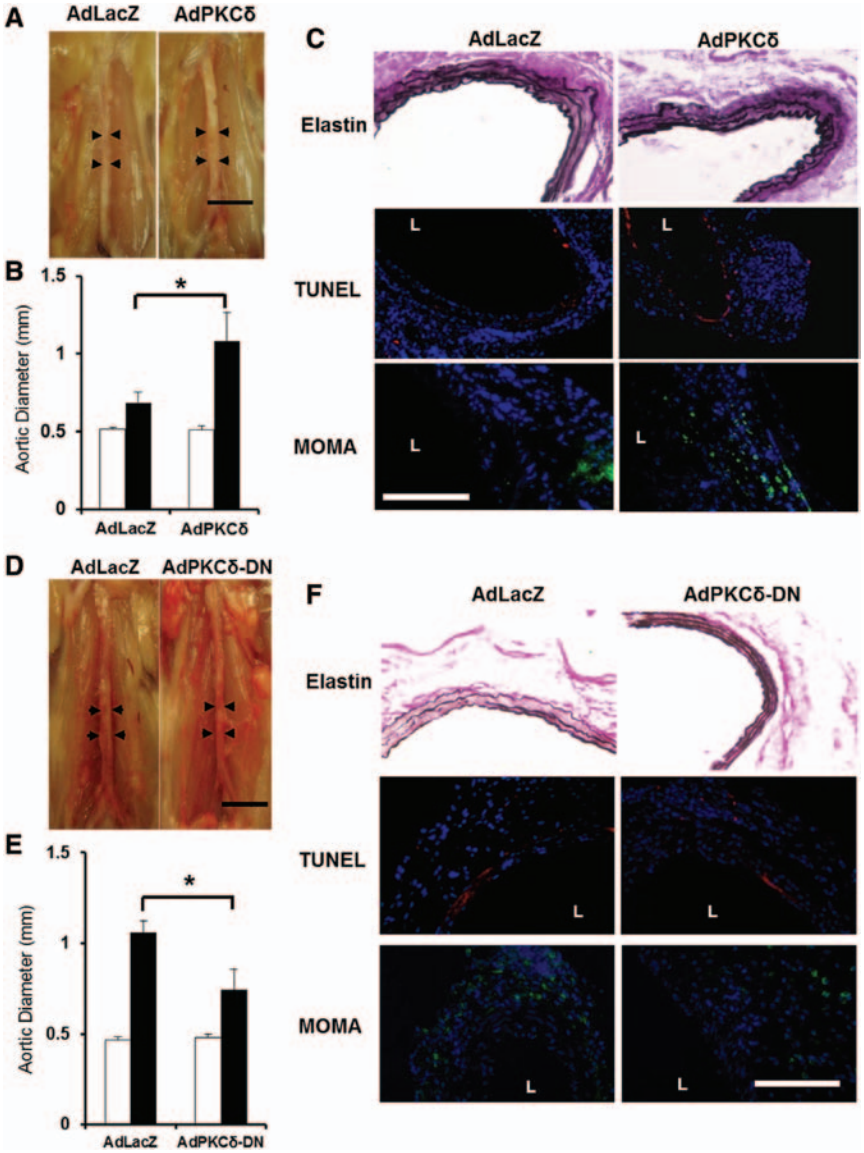

Figure 5. Acute manipulation of protein kinase C-δ (PKCδ) by adenovirus alters aneurysm phenotype in mice. Adenoviruses encoding PKCδ (AdPKCδ) (**A–C**) or a dominant negative PKCδ mutant (AdPKCδ-DN) (**D–F**) were delivered to aortas of PKCδ knockout (KO) mice or C57B/6 mice, respectively, immediately after $CaCl_2$ treatment. AdLacZ was used as a control. **A** and **D**, Representative photos of aortas taken 42 days after surgery. Scale bar, 5 mm. **B** and **E**, Aortic diameter measured before (white bars) and 42 days after (black bars) $CaCl_2$ treatment. *P<0.05; n=4 and n=5 in **B** and **E**, respectively. **C** and **F**, Aortic sections stained for Van Gieson (elastin) at 42 days, terminal deoxynucleotidyl transferase dUTP nick end labeling (TUNEL; red, 7 days), or monocytes and macrophages (monocyte+macrophage antibody [MOMA], green; 7 days). Nuclei were stained by DAPI (blue). L delineates arterial lumen. Scale bar, 200 μm; magnification, 40×.

Aortic Inhibition of PKCδ Attenuates Aneurysm Formation in C57B/6 Mice

To further demonstrate the importance of aortic PKCδ expression in aneurysm development, we tested the effect of aortic inhibition of PKCδ. After the routine $CaCl_2$ treatment, C57BL/6 mice were subjected to local infection with either a dominant negative PKCδ mutant adenovirus or AdLacZ as control. Mice were euthanized after 7 or 42 days for histological and morphological analyses, respectively. As shown in Figure 5D and 5E, treatment with dominant negative PKCδ mutant produced a moderate but significant attenuation in aneurysm formation in C57B/6 mice as reflected by a reduction in aortic expansion as compared with the AdLacZ-treated mice (final aortic diameter measurement 0.74±0.11 mm or 54.7±28.3%, and 1.05±0.06 mm or 126.5±15.7%, respectively). Accordingly, local inhibition of PKCδ activity diminished elastin degradation, apoptotic activity, and infiltration of monocytes/macrophages in the arterial wall (Figure 5F).

Exogenous MCP-1 Protein Restores Aneurysm to PKCδ KO Animals

Various studies have implicated an important role for both MCP-1/C-C chemokine receptor 2 signaling in vascular diseases, including atherosclerosis and AAA.[30–33] Both in vivo and in vitro analyses within the current study indicate a reduction of MCP-1 expression caused by PKCδ gene deficiency; this prompted us to test whether delivery of exogenous MCP-1 to the arterial wall of PKCδ KO mice could restore aneurysm formation. Immediately after the $CaCl_2$ treatment, recombinant MCP-1 protein suspended in pluronic gel was delivered to the infrarenal aortic region of KO mice. As vehicle controls, parallel groups of KO and WT mice were treated with pluronic gel + solvent. As shown in Figure 6A and 6B, solvent-treated WT aortas developed aneurysmal expansion comparable with those previously observed in these mice at 42 days after the $CaCl_2$ treatment (0.84±0.04 mm; 73.7±8.2%). At this same time point, pluronic gel + solvent-treated PKCδ KO aortas maintained their aneurysm-resistant phenotype despite the

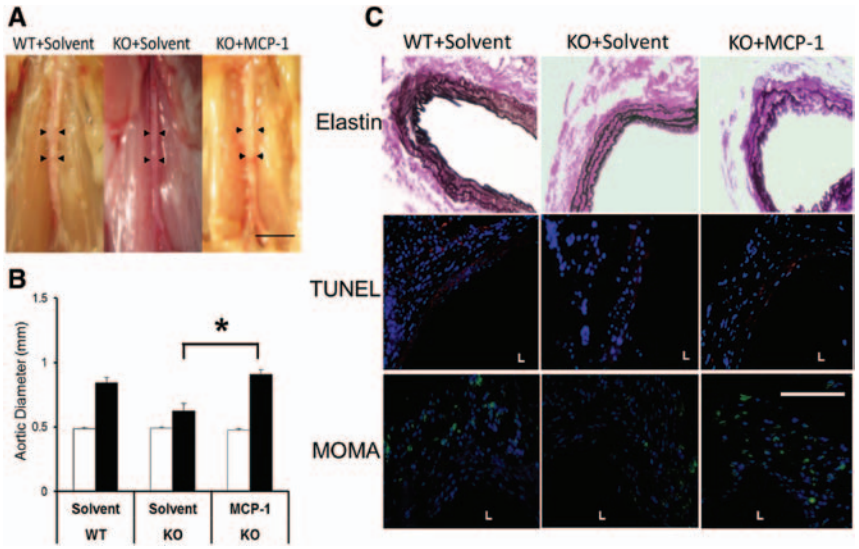

Figure 6. Delivery of exogenous MCP-1 to PKCδ KO mice restores aneurysm formation. **A**, Representative photos of abdominal aortas of wild-type (WT) or knockout (KO) mice that received solvent or monocyte chemoattractant protein-1 (MCP-1) (80 μmol/L), taken 42 days after the $CaCl_2$ procedure; scale bar, 5 mm. **B**, Aortic diameter measured before (white bars) and 42 days after (black bars) $CaCl_2$ treatment. *P<0.05; n=4. **C**, Aortic sections stained for Van Gieson (42 days), terminal deoxynucleotidyl transferase dUTP nick end labeling (TUNEL; red; 7 days), or monocytes and macrophages (MOMA; green; 7 days). Nuclei were stained by DAPI (blue). L delineates arterial lumen. Scale bar, 200 μm; magnification, 40×.

administration of pluronic gel, a stark contrast to the KO aortas treated with recombinant MCP-1 (aortic diameter 0.62±0.06 mm or 27.1±12.5%, and 0.91±0.04 mm or 89.6±9.4%, respectively). Administration of recombinant MCP-1 in KO aorta created elastin degradation similar to that seen in the solvent-treated WT aorta, whereas solvent-treated KO aortas remained largely unaffected. Further histological analysis of these samples revealed a marked increase of macrophage infiltration in the MCP-1–treated mice as compared with solvent-treated PKCδ KO mice. Of note, the level of aortic SMC apoptosis in PKCδ KO mice was not significantly altered by the MCP-1 administration (Figure 6C).

Discussion

Our data for the first time provide direct evidence that PKCδ is an integral signaling molecule in the pathogenesis of AAA. We showed that inhibition of PKCδ, either through targeted gene deletion or overexpression of a dominant negative mutant, protected mice from developing characteristic features of aneurysm, including inflammation, disruption of elastin fibers, and loss of vascular SMCs. Additionally, the aneurysm-resistant phenotype was accompanied by diminished inflammatory infiltration, cytokine production, and medial apoptosis. These results not only confirm the importance of PKCδ in the regulation of SMC apoptosis but also indicate a novel role for this kinase in the proinflammatory signaling cascade, at least in the aneurysm setting.

Although PKCδ is ubiquitously expressed in many tissues and cell types, results reported here suggest that the role of this signaling protein in aneurysm pathophysiology may be primarily localized in vascular SMCs. Furthermore, our evidence suggests PKCδ may act largely through regulating expression of proinflammatory chemokines and cytokines, notably MCP-1. This notion is supported by several in vivo and in vitro findings: (1) PKCδ gene deficiency reduced the production of MCP-1 and other cytokines by aortic SMCs, but did not significantly alter the ability of monocytes to migrate; (2) an adenovirus-mediated delivery of PKCδ locally to the arterial wall was sufficient to rescue aneurysm development in PKCδ KO mice; (3) aorta-specific inhibition of PKCδ delivered a moderate but significant level of protection in C57B/6 mice; and (4) ectopic administration of MCP-1 to the aortic wall of PKCδ KO mice sufficiently rescued aneurysm development.

It has been postulated that vascular SMCs are the soil of AAA development.[34] Being a major source of extracellular matrix proteins, SMCs would be critical in counter balancing the upregulated proteolytic activities present in aneurysmal tissue. As such, the depletion of medial SMCs eliminates a cell population capable of directing connective tissue repair and may, thus, potentiate the degradation of the arterial wall and facilitate eventual rupture.[35] This study contains data supporting the idea that the dearth of connective tissue in AAA can be reversed in the presence of healthy SMCs, thus either preventing or even reversing aneurysm growth. Specifically, we showed that the arteries of $CaCl_2$-treated KO mice sustained a similar degree of initial damage to aortic elastin fibers as WT aorta but by 42 days elastin integrity is restored in KO arteries.

Results from the current study further illustrate another important function of SMCs in vascular disease, (ie, as providing proinflammatory signals). The potential link between SMC apoptosis and the production of proinflammatory chemokines has been previously indicated in atherosclerosis. Using a mouse atherosclerosis model, Clarke et al[36] convincingly demonstrated that SMC apoptosis induces MCP-1 expression, inflammatory infiltrate, and other features of plaque rupture. Recently, our own group demonstrated that blocking apoptosis with a pan-caspase inhibitor protected mice from angiotensin II–induced vascular inflammation and aneurysm expansion.[18] These data suggest that, although apoptosis and inflammation are most commonly considered unrelated events, apoptosis in an aneurysm setting may promote the inflammatory response. Such interaction between apoptosis and inflammation has been explored in atherosclerosis. Clarke et al[30] suggest that the proinflammatory property of apoptotic SMCs may be attributed to inhibited phagocytosis generated in the hyperlipidemic environment in atherosclerotic arteries. Although AAA is commonly associated with atherosclerosis, these 2 diseases

are believed to be caused by distinct pathological processes. However, deficient phagocytosis is also being investigated as an underlying pathophysiological event in other types of inflammatory disorders, including autoimmue diseases,[31] thus warranting the exploration of this process in the pathogenesis of AAA.

Another important finding described in this work is the apparent critical role of PKCδ in MCP-1 function during formation and progression of aneurysm. In vitro and in vivo evidence suggests that impaired production of MCP-1 expression by aortic SMCs was the primary mechanism underlying the aneurysm-resistant phenotype of PKCδ KO mice. Importantly, this notion is further supported by the evidence that localized aortic administration of recombinant MCP-1 to the aorta of PKCδ KO mice restored vascular inflammation, elastin degradation, and aneurysmal expansion. Although several groups have explored the role of the CCR2/MCP-1 signaling axis in the aneurysm progression,[30,37–39] this work provides what we believe to be the first evidence suggesting MCP-1 to be a critical downstream effector of PKCδ signaling in the pathogenesis of aneurysm.

Although our study has implicated a critical role for MCP-1 in AAA, it is important to consider the large number of cytokines that likely play a role in AAA development and progression. Our real-time polymerase chain reaction analysis identified additional cytokines that may be regulated by PKCδ and require further investigation.

Interestingly, localized aortic delivery of exogenous MCP-1 failed to reverse the apoptosis-resistant phenotype of PKCδ KO mice. A similar number of TUNEL$^+$ cells were found in MCP-1 and solvent–treated PKCδ KO mice. In contrast, a similar rescue experiment delivering exogenous PKCδ to the arterial wall restored all aneurysm-related cellular events (ie, inflammation, apoptosis, and elastin degradation in $CaCl_2$ PKCδ KO arteries). These results not only underscore the critical role of PKCδ in the apoptotic response of SMCs but also provide support for a novel relationship between PKCδ, MCP-1, and AAA. In the absence of this master mediator, apoptosis would be inhibited even when aortic SMCs are surrounded by infiltrating inflammatory cells, their inflammatory byproducts, and degraded elastin fibers. Based on rescue experiments presented here, as well as other data from the current and earlier reports,[19,20] we propose a model in which PKCδ-mediated MCP-1 functions as a molecular link through which apoptotic SMCs stimulate the inflammatory process. Importantly, our model suggests that SMC apoptosis may contribute to aneurysm development primarily through the induction of inflammatory cytokines. That is, in the presence of abundant proinflammatory cytokines, such as the environment created by delivery of exogenous MCP-1 protein, the inflammatory and proteolytic events can proceed in full force without the participation of apoptosis.

Using a rat carotid balloon injury model of intimal hyperplasia, our group recently showed that PKCδ mediated the expression of MCP-1, which was critical for the migration of adventitial fibroblasts to the media and neointima.[40] In the $CaCl_2$-treated aorta, we noted a marked expansion of the adventitia associated with abundant infiltration of macrophages and other inflammatory cells. Although the presence of macrophages in the adventitia is a prominent feature of AAA[30,31,34] and the role of adventitial fibroblasts in aneurysm has been explored to some extent by several groups,[41–44] the precise relationship between adventitial fibroblasts, SMCs, and inflammatory cells in the context of AAA remains a highly interesting subject for future study. Evidence presented here shows the localization of IL-6 and macrophages predominantly in the adventitia, whereas MCP-1 production and apoptosis appears to occur primarily, though not exclusively, in the medial layer. It is also important to note that PKCδ, being a ubiquitously expressed protein, is also found in the adventitia. Whether PKCδ also contributes to aneurysm pathogenesis through adventitia cells should be explored in future studies given the prominent inflammatory response in the adventitia. However, several key questions remain to be addressed in models of AAA, for example, how adventitial fibroblasts may respond to medial SMC depletion, matrix degradation, and inflammatory cell infiltration.

Being a major signaling molecule, PKCδ can be activated by multiple extracellular and intracellular signals, including growth factors, inflammatory cytokines, mechanical stimuli, and oxidative stress. Not all of these signals are able to induce apoptosis or the production of MCP-1. It remains to be determined whether the proapoptotic and proinflammatory functions of PKCδ are exerted through the same or partially overlapping pathways. We have previously shown that mitogen-activated protein (MAP) kinase pathways are affected by PKCδ gene deficiency.[20,45] Although the involvement of MAP kinases in the regulation of MCP-1 expression has been demonstrated,[46] the precise molecular interaction between PKCδ and MAP kinases and how this interaction may influence MCP-1 expression remains to be determined. Additionally, Liu et al[47] recently demonstrated that PKCδ mediates the stability of MCP-1 mRNA in vascular SMCs using a chemical inhibitor of PKCδ. Our group previously described the role of MAP kinases in regulation of mRNA stability in vascular SMCs, leading us to speculate that PKCδ may control MCP-1 mRNA turnover through a MAP kinase–mediated mechanism.[48]

Taken together, our data show that the stress response regulating apoptosis and inflammatory signaling in the arterial wall may be largely dependent upon PKCδ upregulation. Accordingly, inhibition of PKCδ attenuated vascular inflammation and preserved tissue integrity, resulting in the prevention of aneurysm development in a $CaCl_2$-induced model of AAA. Further, PKCδ gene deficiency appears to protect mice from developing aneurysm in the elastse model of AAA, as shown in Figure III in the online-only Data Supplement. Unfortunately, the potential role of PKCδ in the Angiotensin II model is yet to be explored, as our attempts to breed PKCδ$^{-/-}$ apolipoprotein E–deficient, double KO mice were unsuccessful. However, we did show that levels of PKCδ were significantly elevated in aortas of apolipoprotein E–deficient mice treated with Angiotensin II. Taken together, we believe the elevated expression of this stress gene in human aneurysmal tissues, as well as the role we have shown it to play in mouse models, suggest it to be an attractive candidate for therapeutic target(s).

Acknowledgments

We thank Drs K. Craig Kent and Jon Mutsumura of the University of Wisconsin, Madison for intellectual inputs, Dr Keiichi I. Nakayama of Kyushu University in Japan for the generous gift of PKCδ KO mice, Dr T. Biden at the Garvan Institute of Australia for dominant negative PKCδ mutant, and Drew Roenneburg of the University of Wisconsin, Madison for technical assistance in histology.

Sources of Funding

This work was supported by National Institutes of Health grant R01HL088447 (Dr Lou), American Heart Association grant 10GRNT3020052 (Dr Lou), Howard Hughes Medical Institute grant MSN135276 (S. Seedial), and Ruth L. Kirschstein National Research Service Award T32 HL 07936 from the National Heart, Lung, and Blood Institute to the University of Wisconsin–Madison Cardiovascular Research Center (S. Morgan).

Disclosures

None.

References

1. Ailawadi G, Eliason JL, Upchurch GR Jr. Current concepts in the pathogenesis of abdominal aortic aneurysm. *J Vasc Surg*. 2003;38:584–588.
2. Nordon IM, Hinchliffe RJ, Holt PJ, Loftus IM, Thompson MM. Review of current theories for abdominal aortic aneurysm pathogenesis. *Vascular*. 2009;17:253–263.
3. Wills A, Thompson MM, Crowther M, Sayers RD, Bell PR. Pathogenesis of abdominal aortic aneurysms–cellular and biochemical mechanisms. *Eur J Vasc Endovasc Surg*. 1996;12:391–400.
4. Daugherty A, Cassis LA. Mouse models of abdominal aortic aneurysms. *Arterioscler Thromb Vasc Biol*. 2004;24:429–434.
5. Aziz F, Kuivaniemi H. Role of matrix metalloproteinase inhibitors in preventing abdominal aortic aneurysm. *Ann Vasc Surg*. 2007;21:392–401.
6. Longo GM, Xiong W, Greiner TC, Zhao Y, Fiotti N, Baxter BT. Matrix metalloproteinases 2 and 9 work in concert to produce aortic aneurysms. *J Clin Invest*. 2002;110:625–632.
7. Petrinec D, Liao S, Holmes DR, Reilly JM, Parks WC, Thompson RW. Doxycycline inhibition of aneurysmal degeneration in an elastase-induced rat model of abdominal aortic aneurysm: preservation of aortic elastin associated with suppressed production of 92 kD gelatinase. *J Vasc Surg*. 1996;23:336–346.
8. Pyo R, Lee JK, Shipley JM, Curci JA, Mao D, Ziporin SJ, Ennis TL, Shapiro SD, Senior RM, Thompson RW. Targeted gene disruption of matrix metalloproteinase-9 (gelatinase B) suppresses development of experimental abdominal aortic aneurysms. *J Clin Invest*. 2000;105:1641–1649.
9. Thompson RW, Baxter BT. MMP inhibition in abdominal aortic aneurysms. Rationale for a prospective randomized clinical trial. *Ann N Y Acad Sci*. 1999;878:159–178.
10. Golledge AL, Walker P, Norman PE, Golledge J. A systematic review of studies examining inflammation associated cytokines in human abdominal aortic aneurysm samples. *Dis Markers*. 2009;26:181–188.
11. Golledge J, Tsao PS, Dalman RL, Norman PE. Circulating markers of abdominal aortic aneurysm presence and progression. *Circulation*. 2008;118:2382–2392.
12. Shimizu K, Mitchell RN, Libby P. Inflammation and cellular immune responses in abdominal aortic aneurysms. *Arterioscler Thromb Vasc Biol*. 2006;26:987–994.
13. Eliason JL, Hannawa KK, Ailawadi G, Sinha I, Ford JW, Deogracias MP, Roelofs KJ, Woodrum DT, Ennis TL, Henke PK, Stanley JC, Thompson RW, Upchurch GR Jr. Neutrophil depletion inhibits experimental abdominal aortic aneurysm formation. *Circulation*. 2005;112:232–240.
14. Xiong W, Zhao Y, Prall A, Greiner TC, Baxter BT. Key roles of CD4+ T cells and IFN-gamma in the development of abdominal aortic aneurysms in a murine model. *J Immunol*. 2004;172:2607–2612.
15. Sun J, Sukhova GK, Yang M, Wolters PJ, MacFarlane LA, Libby P, Sun C, Zhang Y, Liu J, Ennis TL, Knispel R, Xiong W, Thompson RW, Baxter BT, Shi GP. Mast cells modulate the pathogenesis of elastase-induced abdominal aortic aneurysms in mice. *J Clin Invest*. 2007;117:3359–3368.
16. Shimizu K, Shichiri M, Libby P, Lee RT, Mitchell RN. Th2-predominant inflammation and blockade of IFN-gamma signaling induce aneurysms in allografted aortas. *J Clin Invest*. 2004;114:300–308.
17. López-Candales A, Holmes DR, Liao S, Scott MJ, Wickline SA, Thompson RW. Decreased vascular smooth muscle cell density in medial degeneration of human abdominal aortic aneurysms. *Am J Pathol*. 1997;150:993–1007.
18. Yamanouchi D, Morgan S, Kato K, Lengfeld J, Zhang F, Liu B. Effects of caspase inhibitor on angiotensin II-induced abdominal aortic aneurysm in apolipoprotein E-deficient mice. *Arterioscler Thromb Vasc Biol*. 2010;30:702–707.
19. Kato K, Yamanouchi D, Esbona K, Kamiya K, Zhang F, Kent KC, Liu B. Caspase-mediated protein kinase C-delta cleavage is necessary for apoptosis of vascular smooth muscle cells. *Am J Physiol Heart Circ Physiol*. 2009;297:H2253–H2261.
20. Ryer EJ, Sakakibara K, Wang C, Sarkar D, Fisher PB, Faries PL, Kent KC, Liu B. Protein kinase C delta induces apoptosis of vascular smooth muscle cells through induction of the tumor suppressor p53 by both p38-dependent and p38-independent mechanisms. *J Biol Chem*. 2005;280:35310–35317.
21. Schubl S, Tsai S, Ryer EJ, Wang C, Hu J, Kent KC, Liu B. Upregulation of protein kinase cdelta in vascular smooth muscle cells promotes inflammation in abdominal aortic aneurysm. *J Surg Res*. 2009;153:181–187.
22. Leitges M, Mayr M, Braun U, Mayr U, Li C, Pfister G, Ghaffari-Tabrizi N, Baier G, Hu Y, Xu Q. Exacerbated vein graft arteriosclerosis in protein kinase Cdelta-null mice. *J Clin Invest*. 2001;108:1505–1512.
23. Yamanouchi D, Kato K, Ryer EJ, Zhang F, Liu B. Protein kinase C delta mediates arterial injury responses through regulation of vascular smooth muscle cell apoptosis. *Cardiovasc Res*. 2010;85:434–443.
24. Miyamoto A, Nakayama K, Imaki H, Hirose S, Jiang Y, Abe M, Tsukiyama T, Nagahama H, Ohno S, Hatakeyama S, Nakayama KI. Increased proliferation of B cells and auto-immunity in mice lacking protein kinase Cdelta. *Nature*. 2002;416:865–869.
25. Gertz SD, Kurgan A, Eisenberg D. Aneurysm of the rabbit common carotid artery induced by periarterial application of calcium chloride in vivo. *J Clin Invest*. 1988;81:649–656
26. Ikonomidis JS, Gibson WC, Butler JE, McClister DM, Sweterlitsch SE, Thompson RP, Mukherjee R, Spinale FG. Effects of deletion of the tissue inhibitor of matrix metalloproteinases-1 gene on the progression of murine thoracic aortic aneurysms. *Circulation*. 2004;110(11 Suppl 1): II268–II273.
27. Kimura T, Yoshimura K, Aoki H, Imanaka-Yoshida K, Yoshida T, Ikeda Y, Morikage N, Endo H, Hamano K, Imaizumi T, Hiroe M, Aonuma K, Matsuzaki M. Tenascin-C is expressed in abdominal aortic aneurysm tissue with an active degradation process. *Pathol Int*. 2011;61:559–564.
28. Yoshimura K, Aoki H, Ikeda Y, Fujii K, Akiyama N, Furutani A, Hoshii Y, Tanaka N, Ricci R, Ishihara T, Esato K, Hamano K, Matsuzaki M. Regression of abdominal aortic aneurysm by inhibition of c-Jun N-terminal kinase. *Nat Med*. 2005;11:1330–1338.
29. Clowes AW, Clowes MM, Fingerle J, Reidy MA. Kinetics of cellular proliferation after arterial injury. V. Role of acute distension in the induction of smooth muscle proliferation. *Lab Invest*. 1989;60:360–364.
30. Daugherty A, Rateri DL, Charo IF, Owens AP, Howatt DA, Cassis LA. Angiotensin II infusion promotes ascending aortic aneurysms: attenuation by CCR2 deficiency in apoE-/- mice. *Clin Sci*. 2010;118:681–689.
31. de Waard V, Bot I, de Jager SC, Talib S, Egashira K, de Vries MR, Quax PH, Biessen EA, van Berkel TJ. Systemic MCP1/CCR2 blockade and leukocyte specific MCP1/CCR2 inhibition affect aortic aneurysm formation differently. *Atherosclerosis*. 2010;211:84–89.
32. Libby P. Inflammation in atherosclerosis. *Nature*. 2002;420:868–874.
33. Zhang L, Li HY, Li H, Zhao J, Su L, Zhang Y, Zhang SL, Miao JY. Lipopolysaccharide activated phosphatidylcholine-specific phospholipase C and induced IL-8 and MCP-1 production in vascular endothelial cells. *J Cell Physiol*. 2011;226:1694–1701.
34. Curci JA. Digging in the "soil" of the aorta to understand the growth of abdominal aortic aneurysms. *Vascular*. 2009;17(Suppl 1):S21–S29.
35. Thompson RW, Liao S, Curci JA. Vascular smooth muscle cell apoptosis in abdominal aortic aneurysms. *Coron Artery Dis*. 1997;8:623–631.
36. Clarke MC, Figg N, Maguire JJ, Davenport AP, Goddard M, Littlewood TD, Bennett MR. Apoptosis of vascular smooth muscle cells induces features of plaque vulnerability in atherosclerosis. *Nat Med*. 2006;12: 1075–1080.
37. Ishibashi M, Egashira K, Zhao Q, Hiasa K, Ohtani K, Ihara Y, Charo IF, Kura S, Tsuzuki T, Takeshita A, Sunagawa K. Bone marrow-derived monocyte chemoattractant protein-1 receptor CCR2 is critical in angiotensin II-induced acceleration of atherosclerosis and aneurysm formation in hypercholesterolemic mice. *Arterioscler Thromb Vasc Biol*. 2004;24:e174–e178.

38. MacTaggart JN, Xiong W, Knispel R, Baxter BT. Deletion of CCR2 but not CCR5 or CXCR3 inhibits aortic aneurysm formation. *Surgery*. 2007;142:284–288.
39. Moehle CW, Bhamidipati CM, Alexander MR, Mehta GS, Irvine JN, Salmon M, Upchurch GR Jr, Kron IL, Owens GK, Ailawadi G. Bone marrow-derived MCP1 required for experimental aortic aneurysm formation and smooth muscle phenotypic modulation. *J Thorac Cardiovasc Surg*. 2011;142:1567–1574.
40. Si Y, Ren J, Wang P, Rateri DL, Daugherty A, Shi XD, Kent KC, Liu B. Protein kinase C-δ mediates adventitial cell migration through regulation of monocyte chemoattractant protein-1 expression in a rat angioplasty model. *Arterioscler Thromb Vasc Biol*. 2012;32:943–954.
41. Maiellaro K, Taylor WR. The role of the adventitia in vascular inflammation. *Cardiovasc Res*. 2007;75:640–648.
42. Sakata N, Nabeshima K, Iwasaki H, Tashiro T, Uesugi N, Nakashima O, Ito H, Kawanami T, Furuya K, Kojima M. Possible involvement of myofibroblast in the development of inflammatory aortic aneurysm. *Pathol Res Pract*. 2007;203:21–29.
43. Tedesco MM, Terashima M, Blankenberg FG, Levashova Z, Spin JM, Backer MV, Backer JM, Sho M, Sho E, McConnell MV, Dalman RL. Analysis of in situ and ex vivo vascular endothelial growth factor receptor expression during experimental aortic aneurysm progression. *Arterioscler Thromb Vasc Biol*. 2009;29:1452–1457.
44. Tieu BC, Lee C, Sun H, Lejeune W, Recinos A 3rd, Ju X, Spratt H, Guo DC, Milewicz D, Tilton RG, Brasier AR. An adventitial IL-6/MCP1 amplification loop accelerates macrophage-mediated vascular inflammation leading to aortic dissection in mice. *J Clin Invest*. 2009;119:3637–3651.
45. Liu B, Ryer EJ, Kundi R, Kamiya K, Itoh H, Faries PL, Sakakibara K, Kent KC. Protein kinase C-delta regulates migration and proliferation of vascular smooth muscle cells through the extracellular signal-regulated kinase ½. *J Vasc Surg*. 2007;45:160–168.
46. Fischer S, Weishaupt A, Troppmair J, Martini R. Increase of MCP-1 (CCL2) in myelin mutant Schwann cells is mediated by MEK-ERK signaling pathway. *Glia*. 2008;56:836–843.
47. Liu B, Dhawan L, Blaxall BC, Taubman MB. Protein kinase Cδ mediates MCP-1 mRNA stabilization in vascular smooth muscle cells. *Mol Cell Biochem*. 2010;344:73–79.
48. Sakakibara K, Kubota K, Worku B, Ryer EJ, Miller JP, Koff A, Kent KC, Liu B. PDGF-BB regulates p27 expression through ERK-dependent RNA turn-over in vascular smooth muscle cells. *J Biol Chem*. 2005;280:25470–25477.

From the Midwestern Vascular Surgical Society

Accelerated aneurysmal dilation associated with apoptosis and inflammation in a newly developed calcium phosphate rodent abdominal aortic aneurysm model

Dai Yamanouchi, MD, PhD, Stephanie Morgan, BS, Colin Stair, BS, Stephen Seedial, BS, Justin Lengfeld, BS, K. Craig Kent, MD, and **Bo Liu, PhD,** *Madison, Wisc*

Objective: **The calcium chloride ($CaCl_2$) model is a widely accepted rodent model for abdominal aortic aneurysms (AAAs). Calcium deposition, mainly consisting of calcium phosphate ($CaPO_4$) crystals, has been reported to exist in human and experimental aneurysms. $CaPO_4$ crystals have been used for in vitro DNA transfection by mixing $CaCl_2$ and phosphate-buffered saline (PBS). Here, we describe accelerated aneurysm formation resulting from a modification of the $CaCl_2$ model.**
Methods: **A modified $CaCl_2$ model, the $CaPO_4$ model, was created by applying PBS onto the mouse infrarenal aorta after $CaCl_2$ treatment. Morphologic, histologic, and immunohistochemical analyses were performed on arteries treated with the $CaPO_4$ model and the conventional $CaCl_2$ model as the control. In vitro methods were performed using a mixture of $CaCl_2$ and PBS to create $CaPO_4$ crystals. $CaPO_4$- induced apoptosis of primary cultured mouse vascular smooth muscle cells (VSMCs) was measured by DNA fragmentation enzyme-linked immunosorbent assay.**
Results: **The $CaPO_4$ model produces AAA, defined as an increase of ≥50% in the diameter of the aorta, faster than in the $CaCl_2$ model. The $CaPO_4$ model showed significantly larger aneurysmal dilation at 7, 28, and 42 days, as reflected by a maximum diameter (measured in mm) fold-change of 1.69 ± 0.07, 1.99 ± 0.14, and 2.13 ± 0.09 vs 1.22 ± 0.04, 1.48 ± 0.07, and 1.68 ± 0.06 in a $CaCl_2$ model, respectively (n = 6; $P < .05$). A semiquantitative grading analysis of elastin fiber integrity at 7 days revealed a significant increase in elastin degradation in the $CaPO_4$ model compared with the $CaCl_2$ model (2.7 ± 0.2 vs 1.5 ± 0.2; n = 6, $P < .05$). A significantly higher level of apoptosis occurred in the $CaPO_4$ model (apoptosis index at 1, 2, and 3 days postsurgery: 0.26 ± 0.14, 0.37 ± 0.14, and 0.33 ± 0.08 vs 0.012 ± 0.10, 0.15 ± 0.02, and 0.12 ± 0.05 in the conventional $CaCl_2$ model; n = 3; $P < .05$). An enhancement of macrophage infiltration and calcification was also observed at 3 and 7 days in the $CaPO_4$ model. $CaPO_4$ induced approximately 3.7 times more apoptosis in VSMCs than a mixture of $CaCl_2$ (n = 4; $P < .0001$) in vitro.**
Conclusions: **The $CaPO_4$ model accelerates aneurysm formation with the enhancement of apoptosis, macrophage infiltration, and calcium deposition. This modified model, with its rapid and robust dilation, can be used as a new model for AAAs. (J Vasc Surg 2012;■■:■■■.)**

Clinical Relevance: **Animal models of abdominal aortic aneurysms (AAAs) have been used in a range of experiments to explore various aspects of pathogenesis and potential methods of treatment. The conventional calcium chloride ($CaCl_2$) model has been widely accepted as an experimental animal model with many pathologic similarities with human AAAs. This conventional model typically shows aneurysmal dilation at 4 to 6 weeks after injury. We have created a mouse experimental AAA model with rapid and robust aneurysmal dilation through the modification of the conventional $CaCl_2$ model that uses calcium phosphate. This modified model, with its rapid and robust dilation, can be used as a new model for AAAs.**

Abdominal aortic aneurysm (AAA) is a common vascular disease associated with high mortality. Aneurysm results from the culmination of a series of events that lead to disruption of structural integrity and segmental weakening of the abdominal aortic wall. AAA is the 10th leading cause of death in men aged >55 years and causes as many as 30,000 deaths each year in the United States.[1] The prevalence of AAAs increases continuously in men aged >55 years and reaches an estimated peak of >10% in those aged 80 to 85 years.[2]

Several animal models have been created to aid investigation of pathophysiologic events underlying human

From the Division of Vascular Surgery, Department of Surgery, University of Wisconsin School of Medicine and Public Health.
This work was supported by the National Institute of Health R01HL088447 (B.L. and K.K.), American Heart Association 10GRNT3020052 (B.L. and S.M.), and Howard Hughes Medical Institute MSN135276 (S.S.).
Author conflict of interest: none.
Presented at the Thirty-fifth Annual Meeting of the Midwestern Vascular Surgical Society, Chicago, Ill, September 15-17, 2011.

Additional material for this article may be found online at www.jvascsurg.org.
Reprint requests: Bo Liu, PhD, 1111 Highland Ave, Madison, WI 53792 (e-mail: liub@surgery.wisc.edu).
The editors and reviewers of this article have no relevant financial relationships to disclose per the JVS policy that requires reviewers to decline review of any manuscript for which they may have a conflict of interest.
0741-5214/$36.00

doi:10.1016/j.jvs.2012.01.038

AAAs, including models that depend on genetic or chemical manipulation, or both.[3] Genetic manipulations are often associated with defects in extracellular matrix maturation, disruption of lipid homeostasis, or alteration of angiotensin enzymes.[4-7] The chemically induced aneurysm approaches include the intraluminal infusion of elastase and the periaortic application of calcium chloride ($CaCl_2$). A third chemical approach combines chemical and genetic approaches, using a systemic infusion of angiotensin II to mice genetically altered to compromise lipid homeostasis such as mice deficient in apolipoprotein E or low-density lipoprotein receptor.[8-11]

Aneurysmal changes in the carotid artery of hyperlipidemic rabbits resulting from periaortic application of $CaCl_2$ was first described by Gertz et al.[12] This method was later applied in the abdominal aortas of hyperlipidemic rabbits in combination with thioglycollate, as reported by Freestone et al[13] and subsequently adapted to mice.[10,14] By applying $CaCl_2$-soaked gauze to the infrarenal aorta for 15 to 20 minutes, one can typically generate aneurysmal dilation in the treated aortic segment within 4 to 6 weeks.[14,15] This model does not require the use of genetically modified mice. Similar to the elastase-induced mouse aneurysm, $CaCl_2$-induced aneurysmal dilation is accompanied by the depletion of medial layer smooth muscle cells (SMCs), as well as elastin degradation, infiltration of lymphocytes and macrophages, elevation of proinflammatory cytokines, and the increased activation of matrix metalloproteinases (MMPs).[10,14,15]

The mechanism by which the adventitial application of $CaCl_2$ causes these molecular and cellular changes in the aortic wall is not entirely clear. Previous findings have identified calcium ion binding sites on both collagen and elastin, suggesting that $CaCl_2$ application may facilitate the degradation of these major arterial structural components.[16] Our group has identified significant calcification also occurring in $CaCl_2$-treated arteries, mainly in the medial layer. We hypothesized that this calcification might also contribute to aneurysm formation and explored the formation of these calcification deposits. Calcium phosphate ($CaPO_4$) crystals have been identified as the major component of calcification found in atherosclerosis[17-19] and have been suggested to have significant proinflammatory effects, induce apoptosis in various cell types, and stimulate production of proinflammatory cytokines from monocytes, macrophages, and SMCs.[20,21]

In the current study, we tested whether $CaPO_4$ is a more potent stimulus than $CaCl_2$ in stimulation of apoptosis and induction of inflammatory cytokines. Based on the $CaPO_4$-based cell transfection method, we adapted a method of $CaPO_4$ generation in vivo through a sequential application of $CaCl_2$ and phosphate-buffered saline (PBS).[22-24] Compared with the application of $CaCl_2$ alone, the sequential application of $CaCl_2$ and PBS produces a more severe, rapid dilation of the aneurysmal artery associated with significantly enhanced smooth muscle apoptosis and inflammatory responses. Although future studies are necessary to determine how this new method, termed the $CaPO_4$ model, may cause arterial injury, its rapid induction of aneurysmal dilation is advantageous and could be used as an additional rodent model in studies of AAA.

METHODS

All animal procedures in this study were conducted in accordance with experimental protocols that were approved by the Institutional Animal Care and Use Committee at the University of Wisconsin, Madison (Protocol M02284).

General materials. Dulbecco's modified Eagle's medium (DMEM) and cell culture reagents were from Gibco BRL Life Technologies, Grand Island, NY. Chemicals, if not specified, were purchased from Sigma Chemical Co. St Louis, MO.

Mouse models of AAAs. Male 12-week-old C57BL/6 mice were purchased from Jackson Laboratory (Bar Harbor, Me). All mice had free access to a normal diet and water. The $CaPO_4$-induced AAA model was created through a method closely resembling the $CaCl_2$-induced model as described by Gertz et al.[12] Under general anesthesia, the infrarenal region of the abdominal aorta was isolated through a midline incision. A small piece of gauze soaked in 0.5 mol/L $CaCl_2$ was applied perivascularly for 10 minutes. This gauze was replaced with another piece of PBS-soaked gauze for 5 minutes. The $CaCl_2$-induced aneurysm was created through a similar manner but with one 15-minute treatment of gauze soaked with 0.5 mol/L $CaCl_2$. Control mice received one treatment of 0.5 mol/L sodium chloride (NaCl) soaked gauze for 15 minutes.

Histologic analyses suggest that vascular injury appears to be more severe at the anterior surface where arterial tissue comes in contact with gauzes. The maximum external diameter of the infrarenal aorta was measured using a digital caliper (VWR Scientific, Radnor, Pa) before treatment and at the time of tissue harvest.

At selected intervals, mice were euthanized and tissues were perfusion-fixed with a mixture of 4% paraformaldehyde in PBS at physiologic perfusion pressure. Harvested tissue was further fixed in 4% paraformaldehyde and imbedded in optimal cutting temperature compound (Sakura Tissue Tek, Alphen aan den Rijn, The Netherlands). All sections were cut 6-μm thick using a Leica CM3050S cryostat.

Histology and immunohistochemistry. Samples were stained with van Gieson using the Chromaview Van Gieson kit (Richard-Allan Scientific, Kalamazoo, Mich) according to the provided protocol. Elastin integrity was quantified using a grading system as described by Kitamonto et al[25]: no elastin degradation or mild elastin degradation, 1; moderate, 2; moderate to severe, 3; and severe elastin degradation, 4. Each section was numbered and photographed at original magnification ×10 or ×20, maintaining their respective numbers. Then, an objective participant used the scale to grade the photographs and recorded the grade with the section number.

Calcification was detected using Alizarin Red (Ricca Chemical Co, Arlington, Tex). Quantification of calcium

content was calculated using ImageJ Software (National Institutes of Health, Bethesda, Md). Total area of calcified media (stained red) was calculated and divided by total medial area of the artery to yield the reported ratio(s).

For additional immunohistochemistry, arterial sections were permeabilized with 0.1% TritonX for 10 minutes at room temperature. Nonspecific sites were blocked using 5% bovine serum albumin and 3% normal donkey serum in Tris-buffered saline and Tween 20 for 1 hour at room temperature. Primary antibodies to CD3, monocyte chemoattractant protein-1 (MCP-1), and Mac3 were purchased from Santa Cruz Biotechnology (Santa Cruz, Calif), anti-monocyte/macrophage-specific antibody (MOMA2) was purchased from Abcam (Cambridge, Mass), cleaved caspase 3 was purchased from Cell Signaling Technology (Boston, Mass), and smooth muscle-α actin (SMA) was purchased from Sigma-Aldrich (St. Louis, Mo).

Primary antibodies were diluted in previously described blocking solution and incubated overnight at 4°C. Apoptosis was identified through terminal deoxynucleotide transferase-mediated deoxy uridine triphosphate nick-end labeling (TUNEL) in an In Situ Cell Death Detection Kit (Roche, Indianapolis, Ind) according to kit directions. Fluorescent stains were completed using secondary antibodies purchased from Invitrogen Molecular Probes (Carlsbad, Calif), and 4′,6-diamidino-2-phenylindole (DAPI; Invitrogen, Carlsbad, Calif) was used to detect nuclei. Staining was visualized with a Nikon Eclipse E600 upright microscope, and digital images were acquired using a RetigaEXi CCD digital camera. Quantification of stains was performed in a manner to that previously described[26] using ImageJ Software. Data quantification was performed using at least three sections per artery.

Cell culture. Primary mouse aortic SMCs from the aorta of C57BL/6 mice were isolated by using a protocol described by Clowes et al.[27] Briefly, aortas were perfused with PBS supplemented with 2% penicillin/streptavidin antibiotics. The aorta was isolated from the aortic arch to the iliac bifurcation and incubated 30 minutes in digestion buffer at 37°C. Adventitia was pulled away from the medial layer, and tissues were minced and further incubated for 4 hours at 37°C. Cells isolated from the medial layer of individual mice were kept in separate dishes to allow a biologic replicate from each animal. Tissue was spun to a pellet by centrifugation and washed with 10% fetal bovine serum (FBS) DMEM once, then suspended in a small volume of 10% FBS-DMEM and left undisturbed for 48 hours to allow cells to migrate from the tissue. All cell types were maintained in DMEM supplemented with 10% fetal calf serum, 100 U/mL penicillin, and 100 μg/mL streptomycin in a 5% CO_2/water-saturated incubator at 37°C.

In vitro $CaCl_2$ and $CaPO_4$ treatments. The 10% FBS DMEM was replaced with 0.5% FBS DMEM 24 hours before all cell treatment. Cells designated for $CaCl_2$ treatment were washed with normal saline twice before being treated with $CaCl_2$ (final concentration 0.05 mol/L) diluted in normal saline. Treated cells were incubated at 37°C for 15 minutes, the $CaCl_2$ solution was removed, and cells were washed twice with 10% FBS DMEM and let rest 6 hours at 37°C. Cells designated for $CaPO_4$ treatment were washed twice with 1× PBS before being treated with $CaCl_2$ (final concentration 0.05 mol/L) diluted in 1× PBS for 15 minutes. The remainder of the treatment method was the same as the $CaCl_2$ group.

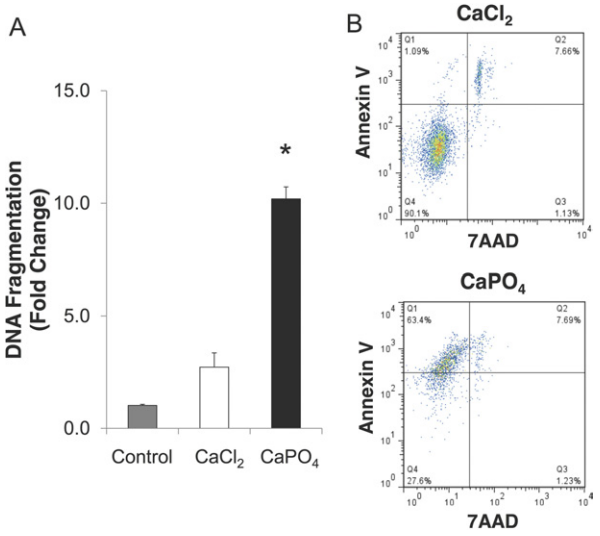

Fig 1. Apoptosis induced by calcium phosphate (*$CaPO_4$*) treatment in vitro. Cultured mouse aortic smooth muscle cells were treated with calcium chloride (*$CaCl_2$*) or $CaPO_4$ as described in the Methods section. **A,** In vitro apoptosis determined by DNA fragmentation enzyme-linked immunosorbent assay. Fold-change was determined with comparison to untreated cell group (control; n = 4). *$P < .0001$. **B**, Representative results of flow cytometry analyses. Apoptotic and necrotic cells were identified by annexin V and 7-aminoactinomycin D (*7AAD*), respectively (n = 4). The *error bars* show the standard error.

Table. Analysis of cells after treatment with calcium chloride (*$CaCl_2$*) or calcium phosphate (*$CaPO_4$*), shown as % of total

	Healthy (Negative)	*Apoptotic (Annexin V+)*	*Necrotic (7AAD+)*	*Secondary necrotic (Double+)*
$CaCl_2$	89.2 ± 1.27	1.08 ± 0.01	2.79 ± 2.35	6.94 ± 1.02
$CaPO_4$	22.0 ± 7.92[a]	68.8 ± 7.6[a]	1.4 ± 0.23	7.8 ± 0.14

7ADD, 7-aminoactinomycin D.
[a]$P < .05$ vs control.

DNA fragmentation enzyme-linked immunosorbent assay. In vitro detection of apoptosis via fragmented DNA labeling was done using the Cell Death Detection enzyme-linked immunosorbent kit (Roche, Indianapolis, Ind) according to the manufacturer's protocol.

Flow cytometric analysis. Apoptotic populations in treated cell groups were assessed by flow cytometry using a PE Annexin V Apoptosis Detection Kit (BD Pharmigen, San Diego, Calif). Flow cytometric data were collected on a

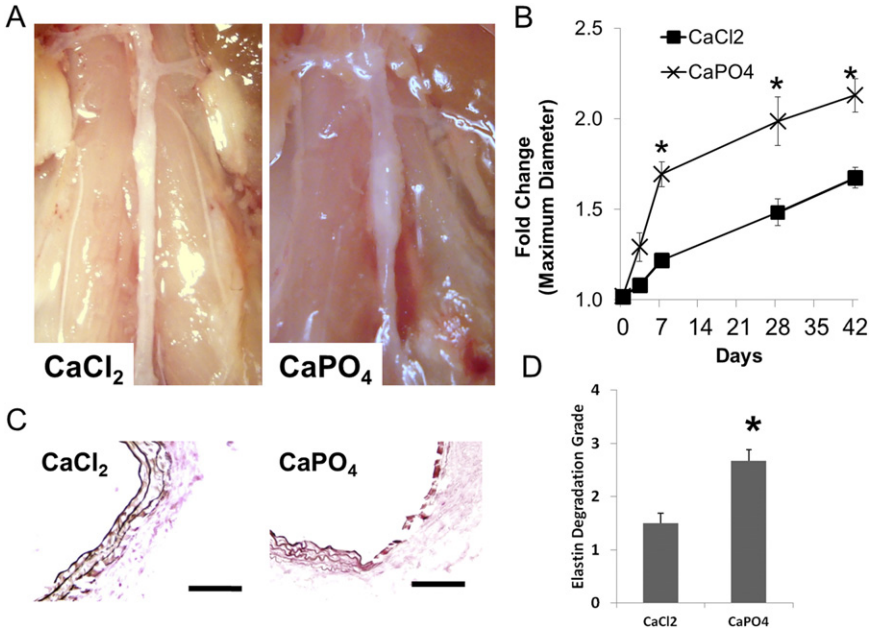

Fig 2. Mice were subjected to abdominal aortic aneurysm (AAA) induction with calcium chloride ($CaCl_2$) or calcium phosphate ($CaPO_4$) and were euthanized at indicated times as described in the Methods section. **A**, Representative pictures of arterial dilation 7 days after surgery. **B,** Quantification of arterial expansion measured 3, 7, 28, and 42 days after surgery (n = 6). Fold change calculated as maximum diameter/presurgery diameter. *$P < .05$. **C,** Van Gieson stain shows elastin layer degradation in representative treated arteries 7 days after surgery. *Scale bar* = 100 μm. **D,** Semiquantification of elastin degradation in arteries harvested 7 days after surgery. The *error bars* show the standard error.

BD fluorescence-activated cell sorting (FACS) Calibur Flow Cytometer equipped with a Cytek 633-nm laser (Freemont, Calif) and analysis was performed using FlowJo software (TreeStar Inc, Ashland, Ore).

Statistical analysis. Values are expressed as means ± standard error. Experiments were repeated at least three times, unless stated otherwise. Differences between two groups were analyzed by the Student *t*-test. One-way analysis of variance (ANOVA), followed by the Scheffe test, was used for multiple comparisons. Values of $P < .05$ were considered significant.

RESULTS

$CaPO_4$ induces apoptosis in aortic SMCs. Primary cultured mouse aortic SMCs were treated with $CaCl_2$ or $CaPO_4$; control SMCs were similarly treated with normal saline. At the end of treatment, cells were placed into normal growth media for 6 hours before undergoing apoptotic evaluation. Analyses of DNA fragmentation indicated the presence of apoptotic cells in $CaCl_2$-and $CaPO_4$-treated cells, however, $CaPO_4$ induced approximately 3.7 times more apoptosis of SMCs than $CaCl_2$ ($P < .0001$; Fig 1, *A*). Detailed cell profiling by FACS analysis showed that most of the dead cells in the $CaCl_2$-treated group stained positive for annexin V and 7-aminoactinomycin D, indicating secondary necrosis. However, most of the dead cells in the $CaPO_4$-treated group stained positive only for annexin V, indicating apoptosis to dominate this treatment group (Fig 1, *B*; Table).

$CaPO_4$ exacerbates aneurysm formation in mice. To facilitate $CaPO_4$ crystal formation in vivo, we sequentially applied $CaCl_2$ and PBS, or $CaCl_2$ alone as a control, to the adventitial surface of mouse abdominal aorta. Mice were euthanized at designated intervals after the injury, and the maximum diameter of the aortas was measured. Aneurysm development was assessed by determining the fold-change in diameter, calculated as the postsurgical measurement divided by the diameter measured before injury. As shown in Fig 2, the aortas treated by $CaPO_4$ showed significantly larger aneurysmal dilation at 7, 28, and 42 days, as reflected by a maximum diameter fold-change of, respectively, 1.69 ± 0.07, 1.99 ± 0.14, and 2.13 ± 0.09 in the $CaPO_4$ model vs 1.22 ± 0.04, 1.48 ± 0.07, and 1.68 ±0.06 in the $CaCl_2$ model (n = 6; $P < .05$; Fig 2, *A* and *B*). The van Gieson staining of the aortic wall at day 7 showed more fragmentation of the elastin layer in $CaPO_4$-treated aortas (Fig 2, *C*). A semiquantitative grading analysis of elastin fiber integrity at 7 days revealed a significant increase in elastin degradation in the $CaPO_4$ model compared with the $CaCl_2$ model (Fig 2, *D*).

$CaPO_4$ intensifies apoptosis in aneurysmal arteries. Next, we compared the magnitude of apoptosis after aneurysm induction with $CaCl_2$ or $CaPO_4$ by harvesting arteries at 1, 2, and 3 days after injury. Apoptosis in the aortic wall

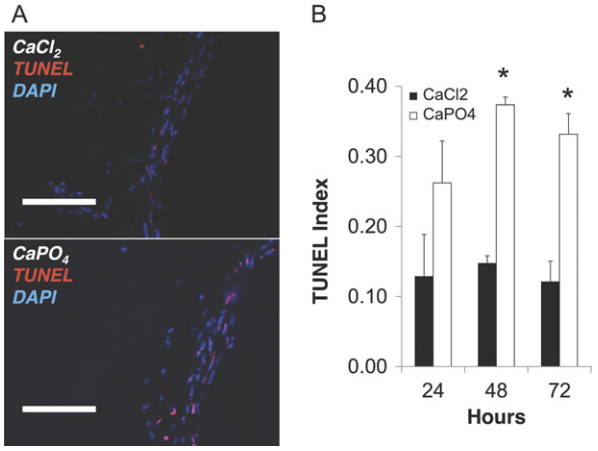

Fig 3. Calcium phosphate (*$CaPO_4$*)-induced aneurysm displays apoptosis. Mice underwent abdominal aortic aneurysm induction with calcium chloride (*$CaCl_2$*) or $CaPO_4$ and were euthanized at indicated times as described in the Methods section. **A,** Representative images of immunohistochemistry for apoptosis, as measured by terminal deoxynucleotide transferase-mediated deoxy uridine triphosphate nick-end labeling (*TUNEL*; *red*), nuclei shown by 4′,6-diamidino-2-phenylindole (*DAPI*) stain (*blue*) in treated arteries 3 days after injury. *Scale bar* = 100 μm. **B,** TUNEL index as determined by TUNEL-positive cells/nuclei. Measurements taken from $CaCl_2$-treated (*black bar*) and $CaPO_4$-treated (*white bars*) arteries harvested 24, 48, or 72 hours after surgery (n = 3). **P* < .05. The *error bars* show the standard error.

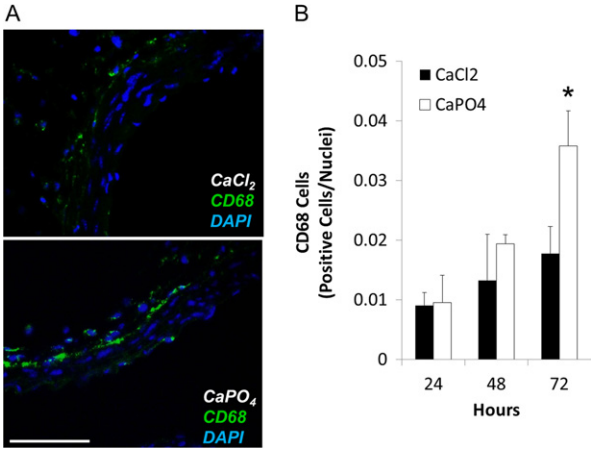

Fig 4. Inflammation accompanies calcium phosphate (*$CaPO_4$*)-induced aneurysm. Mice underwent abdominal aortic aneurysm induction with calcium chloride (*$CaCl_2$*) or $CaPO_4$ and were euthanized at indicated intervals as described in the Methods section. **A,** Representative images are shown of immunohistochemistry for macrophage marker CD68 (*green*) in $CaCl_2$-treated and $CaPO_4$-treated aorta 3 days after injury. Nuclei stained with 4′,6-diamidino-2-phenylindole (*DAPI; blue*). *Scale bar* = 100 μm. **B,** Macrophage infiltration as determined by CD68-positive cells/nuclei in treated arteries 24, 48, and 72 hours after treatment (n = 3). **P* < .05. The *error bars* show the standard error.

was evaluated by TUNEL staining at each interval. $CaPO_4$ injury induced significantly more apoptosis than $CaCl_2$ injury at 2 and 3 days after injury (Fig 3, *A* and *B*, respectively). Most of the apoptotic cells were noted in the media and localized to cells that were positive for SMA (Supplemental Fig 1, online only).

$CaPO_4$-induced aneurysm is associated with inflammation and medial calcification. A prevalent feature of human and experimental aneurysms is significant inflammatory infiltrate. We have previously reported a relationship between apoptosis of SMCs and the inflammatory response(s) leading to the infiltration of macrophages and other inflammatory cells to the aortic wall.[28] At this notion, $CaPO_4$-treated arteries were stained for the presence of macrophages, as identified by the marker CD68. $CaPO_4$-treated arteries harvested 3 days after injury showed significant macrophage infiltration (Fig 4, *A*). The graph in Fig 4, *B* shows macrophage infiltration as determined by CD68-positive cells divided by total nuclei. Supplemental Fig 2 (online only) depicts additional inflammatory markers in day 3 $CaPO_4$-treated arteries. Macrophage marker Mac3, T-lymphocyte marker CD3, and the inflammatory cytokine MCP-1 evidenced a significant inflammatory response.

Using cleaved (activated) caspase 3 as a marker for apoptosis, we evaluated the spatial relationship between apoptosis and inflammation. Monocytes and macrophages, marked by MOMA, localized mostly in the adventitia (Supplemental Fig 3, *A* online only). Using cleaved or activated caspase 3 as a marker for apoptosis, we found that most of the monocytes and macrophages at this interval were not apoptotic; however, they tended to concentrate in areas proximal to apoptotic cells (Supplemental Fig 3, online only).

Significant calcification in $CaPO_4$-treated arteries was easily noted visually and tactilely at the time of artery harvest. Cross-sections of the aortas receiving treatment with $CaCl_2$ or $CaPO_4$ injury were stained with Alizarin Red according to manufacturer's protocol. $CaPO_4$ injury caused pronounced medial calcification appearing ~48 hours after injury and maximizing at ~7 days (Fig 5, *A* and *B*).

DISCUSSION

Animal models of AAAs have been used in a range of experiments to explore various aspects of AAA pathogenesis as well as potential methods of AAA treatment. Here, we report the creation of a mouse experimental AAA model with rapid and robust aneurysmal dilation through sequential adventitial application of $CaCl_2$ and PBS. This modified $CaCl_2$ model, or the $CaPO_4$ model, displayed similar pathologic and histologic characteristics as the previously described $CaCl_2$ model but at a higher magnitude.

We postulate that adventitial insult in the form of $CaCl_2$ application causes a series of tissue degenerative events, at least partly through formation of $CaPO_4$ crystals. Supporting this argument is our finding that $CaCl_2$ did not cause a significant degree of apoptosis or necrosis when

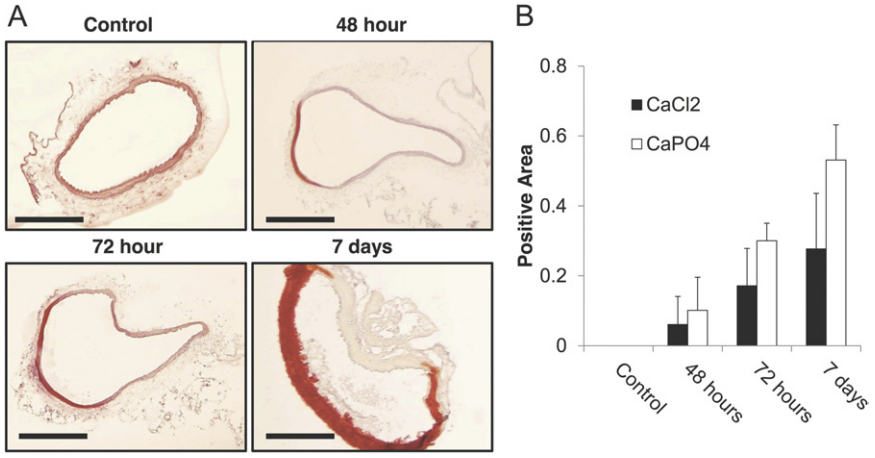

Fig 5. Calcium phosphate (*$CaPO_4$*)-induced aneurysm samples contain medial calcification. **A,** Arterial sections were stained with Alizarin Red for calcium deposit detection. Calcium appears *red* on a *pink* and *yellow* background. The control sections were harvested from animals treated with saline only. Sections were harvested at 48 hours, 72 hours, and at 7 days after $CaPO_4$ treatment. *Scale bar* = 200 μm for all images. **B,** Quantification of calcium content in arterial sections harvested from arteries with the conventional calcium chloride (*$CaCl_2$*) or the $CaPO_4$ model. Data are expressed as a ratio of the total calcified media divided by the total medial area of each arterial section (n = 4). The *error bars* show the standard error.

applied to cultured mouse aortic SMCs. In contrast, cultured mouse aortic SMCs responded to $CaPO_4$ with massive apoptosis, findings consistent with reports from other groups.[20,21,29]

Although the creation of an aneurysm phenotype with $CaCl_2$ or $CaPO_4$ is artificial, atherosclerotic calcification has been shown to consist mainly of $CaPO_4$ crystals, which is typically seen in the intimal and medial layer of the diseased human aorta.[18,19,30] We observed medial calcification in the arterial segments that sustained the $CaCl_2$ or $CaPO_4$ insult. Although tactile and immunohistochemical methods show substantial calcification in these arteries, the biologic mechanisms underlying this ectopic calcification have yet to be identified. Thus, future studies may lend insight to these processes through identification of calcification-regulating genes such as osteopontin.

Interestingly, robust apoptosis and calcification was observed in the medial layer of the aorta starting at ~2 days after surgery, at which time the elastin fibers appeared grossly intact.

A potential causal relationship between apoptosis and calcification has been conceptualized by Proudfoot et al,[31] who propose a model in which SMC death may form apoptotic bodies in the arterial wall, which in turn may serve as a nucleus for vascular calcification.[32] In our time course studies, we noted the time line of apoptotic induction in the arterial wall, which began at ~24 hours, was closely followed by the detection of calcium deposition at ~48 hours after injury. However, the link between SMC apoptosis and medial calcification has yet to be directly tested. Aortic calcification has been reported in human AAAs,[33] but the precise contribution calcification may make toward aneurysm progression is still controversial.

One important limitation within this study lies in the formation of the $CaPO_4$ crystals. Although mixing $CaCl_2$ with PBS generates these crystals, this method provides no means of controlling the formation of $CaPO_4$ crystals or of measuring the final concentration or composition of these crystals, especially in vivo. In preliminary studies, we tested the periaortic application of several forms of $CaPO_4$, including hydroxyapatite, nanocrystal, and basic $CaPO_4$. However, each of these forms of $CaPO_4$ failed to induce aneurysm formation in vivo and produced little if any apoptosis in vitro. One possible explanation for this significant difference among the types of $CaPO_4$ crystal is that the size variation, particularly compared with the naturally formed crystals, may not be appropriate for the endocytosis or autophagocytosis of these crystals to induce apoptosis.[34,35] To address a few questions surrounding the role of these $CaPO_4$ crystals, methods of interfering with crystal formation or the chemical reaction(s), or both, that take place might provide mechanistic insights. Although the scope of this study does not allow such an experiment, future work must explore these methods to fully understand the role of $CaPO_4$ crystals in this newly described model. Furthermore, a better understanding of the role of calcification in aneurysms is necessary to fully understand the potential effect of this study.

CONCLUSIONS

We have shown that the creation of a $CaPO_4$ mouse AAA model through the modification of the conventional $CaCl_2$ model significantly accelerates aneurysm formation. $CaPO_4$ treatment also induced significant enhancement of apoptosis both in vitro and in vivo. Calcification and macrophage infiltration were also prominent features of the

$CaPO_4$ aneurysm, sharing spatial and temporal similarities to the apoptosis within the medial layer. This model, with its rapid and robust dilation, can be utilized as a new model for mouse experimental AAAs.

AUTHOR CONTRIBUTIONS

Conception and design: DY, KK, BL
Analysis and interpretation: DY, SM, CS, JL, SS, KK, BL
Data collection: DY, SM, CS, JL, SS
Writing the article: DY, SM, BL
Critical revision of the article: DY, SM, KK, BL
Final approval of the article: DY, SM, CS, JL, SS, KK, BL
Statistical analysis: DY, SM
Obtained funding: DY, KK, BL
Overall responsibility: BL
DY and SM contributed equally to this article.

REFERENCES

1. Kent KC, Zwolak RM, Jaff MR, Hollenbeck ST, Thompson RW, Schermerhorn ML, et al. Screening for abdominal aortic aneurysm: a consensus statement. J Vasc Surg 2004;39:267-9.
2. Bengtsson H, Sonesson B, Bergqvist D. Incidence and prevalence of abdominal aortic aneurysms, estimated by necropsy studies and population screening by ultrasound. Ann N Y Acad Sci 1996;800:1-24.
3. Daugherty A, Cassis LA. Mouse models of abdominal aortic aneurysms. Arterioscler Thromb Vasc Biol 2004;24:429-34.
4. Brophy CM, Tilson JE, Braverman IM, Tilson MD. Age of onset, pattern of distribution, and histology of aneurysm development in a genetically predisposed mouse model. J Vasc Surg 1988;8:45-8.
5. Silence J, Collen D, Lijnen HR. Reduced atherosclerotic plaque but enhanced aneurysm formation in mice with inactivation of the tissue inhibitor of metalloproteinase-1 (timp-1) gene. Circ Res 2002;90:897-903.
6. Kuhlencordt PJ, Gyurko R, Han F, Scherrer-Crosbie M, Aretz TH, Hajjar R, et al. Accelerated atherosclerosis, aortic aneurysm formation, and ischemic heart disease in apolipoprotein e/endothelial nitric oxide synthase double-knockout mice. Circulation 2001;104:448-54.
7. Nishijo N, Sugiyama F, Kimoto K, Taniguchi K, Murakami K, Suzuki S, et al. Salt-sensitive aortic aneurysm and rupture in hypertensive transgenic mice that overproduce angiotensin II. Lab Invest 1998;78:1059-66.
8. Anidjar S, Salzmann JL, Gentric D, Lagneau P, Camilleri JP, Michel JB. Elastase-induced experimental aneurysms in rats. Circulation 1990;82:973-81.
9. Curci JA, Thompson RW. Variable induction of experimental abdominal aortic aneurysms with different preparations of porcine pancreatic elastase. J Vasc Surg 1999;29:385.
10. Chiou AC, Chiu B, Pearce WH. Murine aortic aneurysm produced by periarterial application of calcium chloride. J Surg Res 2001;99:371-6.
11. Daugherty A, Manning MW, Cassis LA. Angiotensin II promotes atherosclerotic lesions and aneurysms in apolipoprotein e-deficient mice. J Clin Invest 2000;105:1605-12.
12. Gertz SD, Kurgan A, Eisenberg D. Aneurysm of the rabbit common carotid artery induced by periarterial application of calcium chloride in vivo. J Clin Invest 1988;81:649-56.
13. Freestone T, Turner RJ, Higman DJ, Lever MJ, Powell JT. Influence of hypercholesterolemia and adventitial inflammation on the development of aortic aneurysm in rabbits. Arterioscler Thromb Vasc Biol 1997;17:10-7.
14. Longo GM, Xiong W, Greiner TC, Zhao Y, Fiotti N, Baxter BT. Matrix metalloproteinases 2 and 9 work in concert to produce aortic aneurysms. J Clin Invest 2002;110:625-32.
15. Yoshimura K, Aoki H, Ikeda Y, Fujii K, Akiyama N, Furutani A, et al. Regression of abdominal aortic aneurysm by inhibition of c-jun n-terminal kinase. Nat Med 2005;11:1330-8.
16. Urry DW. Neutral sites for calcium ion binding to elastin and collagen: a charge neutralization theory for calcification and its relationship to atherosclerosis. Proc Natl Acad Sci U S A 1971;68:810-4.
17. Boström K, Watson KE, Stanford WP, Demer LL. Atherosclerotic calcification: relation to developmental osteogenesis. Am J Cardiol 1995;75:88B-91B.
18. Weissen-Plenz G, Nitschke Y, Rutsch F. Mechanisms of arterial calcification: spotlight on the inhibitors. Adv Clin Chem 2008;46:263-93.
19. Villa-Bellosta R, Sorribas V. Calcium phosphate deposition with normal phosphate concentration. Circ J 2011;75:2705-10.
20. Ewence AE, Bootman M, Roderick HL, Skepper JN, McCarthy G, Epple M, et al. Calcium phosphate crystals induce cell death in human vascular smooth muscle cells: a potential mechanism in atherosclerotic plaque destabilization. Circ Res 2008;103:e28-34.
21. Pazár B, Ea HK, Narayan S, Kolly L, Bagnoud N, Chobaz V, et al. Basic calcium phosphate crystals induce monocyte/macrophage IL-11β secretion through the NLRP3 inflammasome in vitro. J Immunol 2011;186:2495-502.
22. Graham FL, van der Eb AJ. A new technique for the assay of infectivity of human adenovirus 5 DNA. Virology 1973;52:456-67.
23. Jordan M, Wurm F. Transfection of adherent and suspended cells by calcium phosphate. Methods 2004;33:136-43.
24. Wilson SP, Liu F, Wilson RE, Housley PR. Optimization of calcium phosphate transfection for bovine chromaffin cells: relationship to calcium phosphate precipitate formation. Anal Biochem 1995;226:212-20.
25. Kitamoto S, Sukhova GK, Sun J, Yang M, Libby P, Love V, et al. Cathepsin L deficiency reduces diet-induced atherosclerosis in low-density lipoprotein receptor–knockout mice. Circulation 2007;115:2065-75.
26. Tang XN, Berman AE, Swanson RA, Yenari MA. Digitally quantifying cerebral hemorrhage using Photoshop and Image J. J Neurosci Methods 2010;190:240-3.
27. Clowes AW, Clowes MM, Fingerle J, Reidy MA. Kinetics of cellular proliferation after arterial injury. V. Role of acute distension in the induction of smooth muscle proliferation. Lab Invest 1989;60:360-4.
28. Yamanouchi D, Morgan S, Kato K, Lengfeld J, Zhang F, Liu B. Effects of caspase inhibitor on angiotensin II-induced abdominal aortic aneurysm in apolipoprotein e-deficient mice. Arterioscler Thromb Vasc Biol 2010;30:702-7.
29. Trion A, van der Laarse A. Vascular smooth muscle cells and calcification in atherosclerosis. Am Heart J 2004;147:808-14.
30. Hunt JL, Fairman R, Mitchell ME, Carpenter JP, Golden M, Khalapyan T, et al. Bone formation in carotid plaques: a clinicopathological study. Stroke 2002;33:1214-9.
31. Proudfoot D, Skepper JN, Hegyi L, Bennett MR, Shanahan CM, Weissberg PL. Apoptosis regulates human vascular calcification in vitro: evidence for initiation of vascular calcification by apoptotic bodies. Circ Res 2000;87:1055-62.
32. Reynolds JL, Joannides AJ, Skepper JN, McNair R, Schurgers LJ, Proudfoot D, et al. Human vascular smooth muscle cells undergo vesicle-mediated calcification in response to changes in extracellular calcium and phosphate concentrations: a potential mechanism for accelerated vascular calcification in ESRD. J Am Soc Nephrol 2004;15:2857-67.
33. Matsushita M, Nishikimi N, Sakurai T, Nimura Y. Relationship between aortic calcification and atherosclerotic disease in patients with abdominal aortic aneurysm. Int Angiol 2000;19:276-9.
34. Sarkar S, Korolchuk V, Renna M, Winslow A, Rubinsztein DC. Methodological considerations for assessing autophagy modulators: A study with calcium phosphate precipitates. Autophagy 2009;5:307-13.
35. Gao W, Ding WX, Stolz DB, Yin XM. Induction of macroautophagy by exogenously introduced calcium. Autophagy 2008;4:754-61.

Submitted Sep 16, 2011; accepted Jan 4, 2012.

Additional material for this article may be found online at www.jvascsurg.org.